NEW STRATEGIES FOR HYDROSILYLATION OF PROPARGYL ALCOHOLS, OLEFIN POLYMERIZATION AND ON-CHIP ORGANIC SYNTHESIS

by

UDAYA SREE DAKARAPU

Presented to the Faculty of the Graduate School of

The University of Texas at Arlington in Partial Fulfillment

of the Requirements

for the Degree of

DOCTOR OF PHILOSOPHY

THE UNIVERSITY OF TEXAS AT ARLINGTON

August 2020

Acknowledgements

I would like to convey my sincere thanks and gratitude to my research supervisor, Professor Junha Jeon, for his guidance and support over the past 5 years in achieving my dream. He warmly welcomed me to his research group even though I was away from college for a quite a long time after my Masters Degree. I still remember the way he taught me the basics during my initial period in his lab. I learned many reactions and purification techniques and improved my spectroscopic knowledge under his guidance. His guidance helped me throughout every stage of my journey. I am really grateful for his support during my struggle in the program. I am very much inspired with his planning and execution (research and writing). I am very fortunate to have him as my mentor.

I pay my sincere thanks to my committee members, Professors Frank W. Foss Jr, Carl J. Lovely, and Robin Macaluso, for their continuous feedback and suggestions on my research progress. I would like to thank Dr.'s Lovely, Bugarin, and Foss for allowing me to borrow some chemicals from their labs, which avoided delay in my research. I want to express my gratitude to to all my research collaborators, Dr. Gyu Leem, Dr. Hyejin Moon, Matin and Searona Kim.

I would like to say special thanks to our post-doctoral fellow Dr. Yuanda Hua (2013-2016) and Dr. Apparao Bokka. I really appreciate their helping nature and willingness to teach new graduate students. I owe a great debt of gratitude to my brother from UTA Dr. Apparao Bokka for his endless support and knowledge. I would like to extend my gratitude to my fellow graduate students, Dr. Parham Asgari, Dr. Thirupathaiah Avullala and Hiep.

I am thankful to Jill, Debbie, Jim, Jason, Beth, and Natalie for their support at various levels in my program at UTA. My sincere thanks to Dr.'s Brian Edwards, Roy Mc Dougald, and Chuck Savage for their trainings and helped in various instruments. Many thanks to Dr.'s William Cleaver, Cynthia Griffith and Heidi Conrad for their support as Lab Coordinators.

I am grateful to my parents and brother Ravi for their unconditional love and affection. I would like to thank my husband Uday who adopted my dream, compromised and supported in many things for my ambition. I am truly blessed to have an understandable son Mahijith for his endless love and support. I am truly obliged to him for all the love and encouragement he gave me during my studies.

July 22, 2020

Abstract

NEW STRATEGIES FOR HYDROSILYLATION OF PROPARGYL ALCOHOLS, OLEFIN POLYMERIZATION AND ON-CHIP ORGANIC SYNTHESIS

Udaya Sree Dakarapu, Ph.D

The University of Texas at Arlington, 2020

Supervising Professor: Junha Jeon

The research described in this dissertation is on three different projects namely i) design and synthesis of traceless hydrosilyl acetal-directed, *exo-syn* hydrosilylation of propargyl alcohols to produce α-hydroxy (*E*)-vinylsilanes, ii) alkali metal lewis base-catalyzed, complexation-induced hydrogen atom transfer (LBCI-HAT) olefin polymerization and iii) on-chip organic synthesis enabled by engine-and-cargo on an electrowetting-on-dielectric digital microfluidic (EWOD) device.

The first chapter is focused on the design and synthesis of traceless hydrosilyl acetal-directed, *exo-syn* hydrosilylation of propargyl alcohols to produce α-hydroxy (*E*)-vinylsilanes. Transition metal-catalyzed regioselective intramolecular hydrosilylation of propargylic alcohols utilizing easily accessible, inexpensive, and readily installable hydrosilyl acetals as a directing

group to achieve high reactivity and high regioselectivity has been developed. Specifically, the current strategy involves iridium-catalyzed hydrosilylation of progargyl ester, followed by rhodium-catalyzed intramolecular alkyne hydrosilylation through a 6-*exo*-*syn* cyclization. This method successfully produces a range of cyclic α-(*E*)-vinylsilanes (i.e., dioxasilinanes) in moderate to excellent yields (only one regioisomer) and showed good functional group tolerance. Steric and electronic impacts of hydrosilyl acetals on the cyclization in terms of reactivity and regioselectivity to generate cyclic α-(*E*)-vinylsilanes are studied. Cyclic α-(*E*)-vinylsilanes (dioxasilinanes) upon further nucleophilic ring opening produces α-hydroxy (*E*)-vinylsilanes. The versatility of this strategy is demonstrated in a complex molecular setting with substituted-ethynylesterdiol by formation of dioxasilinane followed by its derivatizations. This protocol provides a new route to access α-(*E*)-vinylsilanes.

In second chapter, focus is on alkali metal Lewis base-catalyzed, complexation-induced hydrogen atom transfer (LBCI-HAT) olefin polymerization. This strategy introduces transition metal-free, LBCI-HAT olefin polymerization process to the field of the production of large polymeric architectures. Lewis base-catalyzed, complexation-induced hydrogen atom transfer (LBCI-HAT) from potassiated hypercoordinate hydridosilicon species to an olefin is an environmentally sustainable, versatile synthetic tool for preparation of high-value small molecules in highly selective fashion. The approach is operationally simple, practical, and its sustainable nature of the (controlled) LBCI-HAT polymerization proceeds rapidly under aerobic conditions and at room temperature. This approach also showed a wide scope including traditionally challenging electron-donating styrene monomers. This study, concerning redox-neutral, branch-selective hydrosilylation, has revealed mechanistically unsolved 'hydrogen-hydride transfer duality' in hypercoordinate hydridosilicon chemistry–referring to a mode of a competing single (SET) or two-electron transfer. The mechanism the LBCI-HAT radical olefin

polymerization has been investigated by in situ, time-resolved FT-NIR spectroscopy. This development permits the LBCI-HAT as a single catalytic platform for both small and large molecule synthesis in a highly controlled fashion.

In third chapter, focus is on on-chip organic synthesis using an electrowetting-on-dielectric (EWOD) digital microfluidic device. Despite of number of chemical/biological applications using EWOD digital microfluidic device, its application to organic reactions is limited. The major limitation is associated with the typical solvents used for synthetic organic chemistry that are not operable on EWOD device. In order to address this limitation a novel technique of an "engine-and-cargo" system is utilized that enables use of non-movable fluid (e.g., organic solvents) on an EWOD device. With esterification as the model reaction, on-chip chemical reactions were successfully demonstrated. Conversion data obtained from on-chip reactions were used in the demonstration of reaction characterization and optimization such as reaction kinetics, solvent screening, and catalyst loading. As the first step toward on-chip combinatorial synthesis, parallel esterifications of three different alcohols are demonstrated. Results from this study clearly show that EWOD digital microfluidic platform is a promising candidate for a micro scale chemical reaction. In addition to this, research is also carried out for in-line organic workup as a key move towards development of multi-step synthesis on an EWOD platform. Acid-base workup is chosen as a model system to demonstrate the compatibility of general organic workup procedure and was successfully demonstrated. Furthermore, in-line crystallization is observed during the operation that demonstrates the capability of EWOD to carry solid particles. This approach also successfully demonstrated the utility of solvent swapping without any further modification in the architecture of EWOD platform.

Table of Contents

Acknowledgements……iii

Abstract……v

List of illustrations……...x

List of Tables……xii

Chapter 1: Synthesis of α-Hydroxy Vinylsilanes via Traceless Hydrosilyl Acetal-Directed Catalytic Exo-Syn Hydrosilylation of Propargyl Alcohols

1.1 Introduction 1

1.1 Importance of Silicon and Organosilanes……..... 2

1.2 Importance of alkenyl silanes 2

1.3 Introduction of Alkyne hydrosilylation..... 4

1.4 Background and importance of stereo and regio-selectivity in alkyne hydrosilylation..... 5

1.5 Challenge in exoselective hydrosilylation of propargyl alcohols..... 9

1.6 Denmark's directing group strategy hydrosilylation of propargyl alcohols..... 10

1.7 Our designed directing group for hydrosilylation of propargyl alcohols..... 11

1.8 Proposed design for a traceless acetal-directed hydrosilylation of propargyl alcohols.....12

1.9 Chemoselective Iridium-catalyzed ester hydrosilylation..... 12

1.10 Regio and stereoselective Rhodium-catalyzed alkyne hydrosilylation 13

1.11 Initial studies..... 13

1.12 Kinetic studies..... 17

1.13 One mmol scale reaction feasibilty..... 21

1.14 Scope of various hydrosilylacetals for alkyne hydrosilylation..... 21

1.15 Scope of various substrates for alkyne hydrosilylation..... 22

1.16 Pyridine substrate for alkyne hydrosilylation..... 24

1.17 Indole substrate for alkyne hydrosilylation..... 25

1.18 Failed substrates for alkyne hydrosilylation..... 26

1.19 Ruthenium-catalyzed alkyne hydrosilylation..... 26

1.20 Synthesis of diene..... 27

1.21 Synthesis of enyne..... 27

1.22 Importance of ethinylesterdiol..... 28

1.23 Synthesis of phenyl-substituted ethinylesterdiol..... 28

1.24 Feasibility of various substituted ethinylesterdiol for alkyne hydrosilylation..... 29

1.25 Late-stage functionalization of phenyl-substituted ethinylesterdiol..... 30

1.26 Synthetic applications of dioxasilinanes..... 30

1.27 Summary of exo-syn hydrosilylation of propargyl alcohols..... 31

Chapter 2: Alkali Metal Lewis Base-Catalyzed, Complexation-Induced Hydrogen Atom Transfer (LBCI-HAT) Olefin Polymerization

2.1Introduction..... 33

2.2 Living free radical polymerization (LRP) 33

2.3 Atom-transfer radical polymerization (ATRP) 34

2.4 Background of LBCI-HAT polymerization 35

2.5 Our approach of LBCI-HAT radical olefin polymerization..... 36

2.6 Preliminary studies..... 37

2.7 Substrate scope for LBCI-HAT polymerization..... 39

2.8 Failed substrates for LBCI-HAT polymerization..... 40

2.9 Scope of copolymerization in LBCI-HAT polymerization..... 40

2.10 Conceptual mechanism for LBCI-HAT radical olefin polymerization..... 41

2.11 Kinetic study of LBCI-HAT. 44

2.12 FT-NIR studies of LBCI-HAT..... 44

2.13 Vinyl arene substituent and crown ether effects on LBCI-HAT..... 45

2.14 Crown ether effect with ethylsilane on LBCI-HAT..... 47

2.15 Crown ether effect with phenylsilane on LBCI-HAT..... 48

2.16 Kinetics of silane-ligand on LBCI-HAT..... 49

2.17 Metal cation effect on LBCI-HAT..... 51

2.18 Summary of LBCI-HAT polymerization..... 54

Chapter 3: On-chip organic synthesis in an electrowetting-on-dielectric digital microfluidic device

3A. Engine-and-cargo system in an electrowetting-on-dielectric digital microfluidic device

3.1 Introduction..... 56

3.2 Background research..... 58

3.3 Engine-and-cargo system..... 59

3.4 Esterification Reaction..... 60

3.5 Experimental data..... 62

3.6 Test Protocols..... 63

3.7 Results and Discussion..... 67

3.8 Kinetics study..... 67

3.9 Solvent Screening..... 70

3.10 Catalyst loading optimization..... 71

3.11 Parallel esterification reactions..... 73

3.12 Summary for engine-and-cargo strategy..... 75

3B. In-line workup on EWOD-DMF device

3.13 Introduction..... 75

3.14 Acid-Base workup..... 79

3.15 Experimental data..... 80

3.16 Test Protocols..... 82

3.17. Result and Discussion..... 83

3.18 Acid-base reaction..... 89

3.19 Neutralization..... 91

3.20 Assessment on the in-line workup performance..... 93

3.21 The relationship of yield and the agitation time in on-chip workup..... 94

3.22 Summary of in-line workup on EWOD device..... 95

3.23 Summary of on-chip organic synthesis..... 96

Appendix A List of Abbreviations 98

Appendix B General Experimental Procedure 100

Appendix C Spectral Data of Compounds 122

References.....163

Biographical Information 178

List of Illustrations

Figure 1.1 Examples of organosilanes with Industrial applications……..……..... 3

Figure 1.2 Importance of vinylsilanes……...……...……...…… 4

Figure 1.3 Intermolecular alkyne hydrosilylation…….....…….. 5

Figure 1.4 Intramolecular alkyne hydrosilylation……..……..... 5

Figure 1.5 Trost's intermolecular alkyne hydrosilylation……...……..... 6

Figure 1.6 Takeuchi's intermolecular alkyne hydrosilylation……...……..... 6

Figure 1.7 Directing group strategy intermolecular alkyne hydrosilylation……..……..... 7

Figure 1.8 Tamooka's intramolecular alkyne hydrosilylation……..……...…..……..... 8

Figure 1.9 Catalyst controlled strategy in intramolecular alkyne hydrosilylation…….…..... 8

Figure 1.10 Trost's directing group strategy……..……..……..……..... 9

Figure 1.11 Denmark's directing group strategy ……..……..…..……..... 9

Figure 1.12 Challenge in exoselective hydrosilylation of propargyl alcohols……....…..... 10

Figure 1.13 Denmark's directing group strategy in hydrosilylation of propargyl alcohols…….. 11

Figure 1.14 Design of two-atom tether for alkyne hydrosilylation……..…….…..….... 12

Figure 1.15 Proposed design for a traceless acetal-directed hydrosilylation of propargyl alcohols……..…… 12

Figure 1.16 Ir-Catalyzed ester hydrosilylation of propargyl alcohols……..……..... 13

Figure 1.17 Rh-Catalyzed alkyne hydrosilylation……..…….…..... 13

Figure 1.18 Initial studies- reaction temperature optimization…….... 14

Figure 1.19 Initial studies- catalyst loading optimization……..……..…..... 15

Figure 1.20 Exo-syn Vs Exo-anti alkyne hydrosilylation……..……..……..... 15

Figure 1.21 Ligand screening for alkyne hydrosilylation……..……..... 16

Figure 1.22 Structures of ligands……..……..…..... 17

Figure 1.23 Kinetic studies……..……..... 18

Figure 1.24 Feasability of 1mmol scale alkyne hydrosilylation……..……..... 21

Figure 1.25 Scope of various hydrosilylacetals……..……..... 22

Figure 1.26 Substrate scope of alkyne hydrosilyaltion ……...……..... 23

Figure 1.27 Pyridine substrate for alkyne hydrosilyaltion……..……..... 25

Figure 1.28 Indole substrate for alkyne hydrosilyaltion……..……..... 25

Figure 1.29 Failed substrates for alkyne hydrosilyaltion ……..……..... 26

Figure 1.30 Metal catalyzed alkyne hydrosilyaltion……..……..…..... 26

Figure 1.31 Synthesis of diene……..……...……..... 27

Figure 1.32 Synthesis of enyne……...……..... 28

Figure 1.33 Ethinylesterdiol (EE) ……...……..... 28

Figure 1.34 Synthesis of phenyl-substituted ethinylesterdiol……..……..... 29

Figure 1.35 Feasibility of various-substituted ethinylesterdiol for alkyne hydrosilylation……..……..... 30

Figure 1.36 Late-stage functionalization of phenyl-substituted ethinylesterdiol……..……...……..... 30

Figure 1.37 Derivitization of phenyl-substituted ethinylesterdiol……...……..... 31

Figure 2.1 LBCI-HAT polymerization…….……..…….....…....……..……..…..... 37

Figure 2.2 Preliminary results……..…….....……..……..... 38

Figure 2.3 Effect of concentration on polymerization……..…….....……..... 39

Figure 2.4 Substrate scope for LBCI-HAT polymerization……..……...……..... 39

Figure 2.5 Failed substrates for LBCI-HAT polymerization……..…….....…….... 40

Figure 2.6 Copolymerization scope for LBCI-HAT polymerization……..…….…..... 41

Figure 2.7 Conceptual mechanism of LBCI-HAT radical polymerization …….…..... 43

Figure 2.8 Vinylarene substituent effect and crown ether effect on LBCI-HAT……...…..... 46

Figure 2.9 Crown ether effect with ethylsilane on LBCI-HAT……...…..... 47

Figure 2.10 Crown ether effect with phenylsilane on LBCI-HAT……..…...…….…..... 49

Figure 2.11 Silane-ligand effect on LBCI-HAT……..……..……....…..... 51

Figure 2.12 Metal cation effect with ethylsilane on LBCI-HAT……..……...……..... 52

Figure 2.13 Metal cation effect with phenylsilane on LBCI-HAT……..……..... 53

Figure 3.1 Formation of engine-and-cargo system……..……..……....…..... 60

Figure 3.2 Model esterification reaction of menthol……..…….....…..... 61

Figure 3.3 EWOD digital microfluidic device……..……..……..... 62

Figure 3.4 Engine-and-cargo system formation……..……..……..…....…..... 64

Figure 3.5 Esterification steps on an EWOD device……..……..……...…..... 66

Figure 3.6 Efficiency of engine-and-cargo system……..……..……....…..... 68

Figure 3.7 Kinetic study of on-chip esterification……..……..……..... 70

Figure 3.8 Solvent screening ……..……..……....……..…….. 71

Figure 3.9 Catalyst loading optimization…….……..…….....…..... 72

Figure 3.10 Parallel esterification reactions……..……..…….....……..... 74

Figure 3.11 Experimental setup of EWOD device……..……..……..……..... 80

Figure 3.12 Solvent optimization……..……..…….....…...……....……..... 82

Figure 3.13 EWOD layout for in-line workup……..……..…….....……..... 83

Figure 3.14 Mixing scheme of two-phase droplet on EWOD device……..…..... 87

Figure 3.15 Separation scheme of two-phase droplet on EWOD device……..... 89

Figure 3.16 Acid-base reaction on EWOD device……..…….……..…….....…..... 90

Figure 3.17 Neutralization on EWOD device……..……..…….....…..... 92

Figure 3.18 In-line workup performance……..……...……..……..... 94

Figure 3.19 Yield and agitation relationship……..……..……..... 95

List of Tables

Table 1.1 Initial studies- reaction temperature optimization…….……...…....….14

Table 1.2 Initial studies- catalyst loading optimization…….……...….15

Table 1.3 Initial studies- ligand screening…….……...….17

Table 1.4 Kinetic study –Slopes of various ligand……..……..…….....…..... 19

Table 1.5 Kinetic study – rate study of various ligands w/r to PPh_3……..……..... 20

Table 3.1 Summary of voltage and frequency conditions of all reagents participating in this study. ……..……....……..……....……....……..... 84

Note

Portions of this thesis have been taken, with permission, from the following publications:

- On-chip organic synthesis enabled using an engine-and-cargo system in an electrowetting-on-dielectric digital microfluidic device. Torabinia, M.; Asgari, P., **Dakarapu, U. S**., Jeon, J. Moon, H. *Lab on a chip.* **2019,** *19*, 3054−3064. https://doi.org/10.1039/C9LC00428A

- In-line organic chemistry workup and solvent-swap in an electrowetting-on-dielectric digital microfluidic device. Torabinia, M.; **Dakarapu, U. S**.; Asgari, P.; Jeon, J., Moon, H. *Analytical chemistry.* **2020.** *(Submitted)*

Additional work performed while pursuing my Ph.D. that does not appear in this thesis has been published in:

- Lewis Base Activation of Silyl Acetals: Iridium –Catalyzed Reductive Horner-Wadsworth-Emmons Olefination. **Dakarapu, U. S.;** Bokka, A.; Asgari, P.; Trog, G., Hua, Y.; Nguyen, H. H.; Rahman, N.; Jeon, J. *Org. Lett*. **2015,** *17*, 5792-5795. https://doi.org/10.1021/acs.orglett.5b02901
- Reductive arene ortho-silanolization of aromatic esters with hydridosilyl acetals.. Hua, Y., Asgari, P., **Dakarapu, U. S**., Jeon, J. *Chem. Commun.* **2015**, *51*(18), 3778-3781. https://doi.org/10.1039/C4CC09850A

- Aryne cycloaddition reactions of benzodioxasilines as aryne precursors generated by catalytic reductive ortho-C-H silylation of phenols with traceless acetal directing groups. Asgari, P., **Dakarapu, U. S**., Nguyen, H. H & Jeon, J. *Tetrahedron.* **2017**, *73*(29), 4052-4061. https://doi.org/10.1016/j.tet.2016.12.002

Chapter 1

Synthesis of α-Hydroxy Vinylsilanes via Traceless Hydrosilyl Acetal-Directed Catalytic Exo-Syn Hydrosilylation of Propargyl Alcohols

1 Introduction

1.1 Importance of Silicon and Organosilanes

Silicon chemistry is an important and rapidly developing field of research in chemistry. Silicon is the second most abundant element (ca. 30% by mass) in the earth's crust and the eighth most abundant element in the universe. Due to the similarity of silicon to carbon, researchers are motivated to investigate the possibility of the replacement of carbon with silicon,[1] to modify the biological and chemical behavior of molecules. Organosilanes are important building blocks and are extensively used for C−C and C−O bond formations. Organosilanes can undergo variety of transformations (Si to C, Si to F, Si to O, N, Cl, Br, I). Organosilanes are widely employed in organic synthesis (e.g., as silicon-based blocking agents,[2,3] as reducing agents,[4] as cross-coupling reactions[5-7] and in silicon-based anion relay chemistry[8]), medicinal applications,[9,10] and materials science (e.g., coating materials, silicon polymers,[11,12] silicone-based surfactants, fluids, molding products, release coatings, and pressure sensitive adhesive[13,14]). Although the bond strength of carbon-silicon is considered to be relatively strong, there are few natural molecules containing silicon-carbon bonds. Organosilanes are environmentally benign, relatively inexpensive, stable, and a wide range of silyl precursors is commercially available. Organosilanes are essential synthetic moieties because they can serve as latent functional groups by Lewis base activation, and organosilanes by-products are relatively non-toxic.[15-18] In addition, organosilanes are being used in variety of fields including drug discovery,[19] biomedical agents,[20] electronics and photonics.[21]

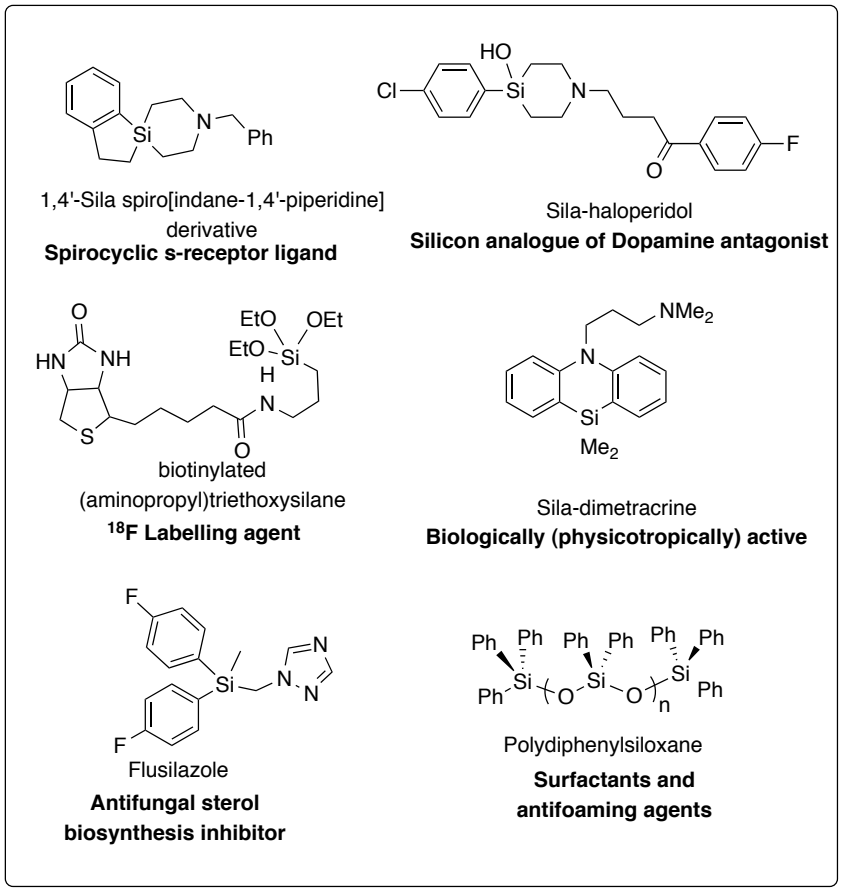

Figure 1.1 Examples of organosilanes with Industrial application

1.2 Importance of alkenylsilanes

Alkenylsilanes are stable and virtually nontoxic, and they serve as important synthetic building blocks for preparation of bioactive small molecules and materials.[15-17] Both the alkene and silyl moiety within vinylsilanes can be, independently or together, converted into several important functional groups. These include stereoselective electrophilic substitution,[22,23] cycloaddition,[24] ene reaction,[25] oxidation,[26-28] sigmatropic rearrangement,[29,30] and a variety of organometallic reactions (e.g., Heck reaction,[31] Denmark-Hiyama cross-coupling,[32] Murai reductive *ortho*-alkylation,[33] hydroesterification,[34] and olefin metathesis).[35-37]

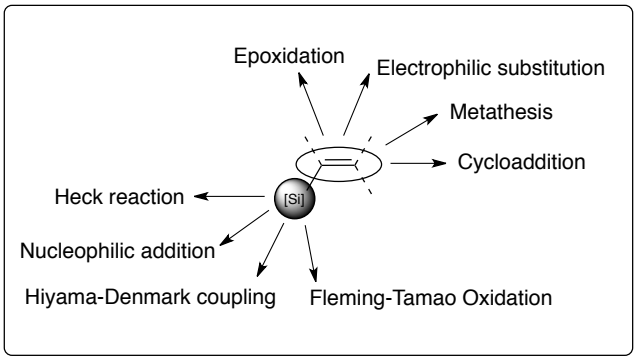

Figure 1.2 Importance of vinylsilanes

1.3 Introduction of Alkyne hydrosilylation

Hydrosilylation is defined as the addition of silicon-hydrogen (Si–H) bonds across an unsaturated substrate moiety (alkenes, alkynes, carbonyls, and imines) and results in a new silicon-carbon (Si–C) or silicon heteroatom (Si–O/N) bond. Hydrosilylation of alkynes/alkenes and carbonyls has been utilized for syntheses of diverse organosilanes.[38] In specific, alkyne hydrosilylation (Figure 1.1) is an important tool to synthesize alkenyl silanes,[38] which can be used as silicon-containing synthetic intermediates, functionalized materials,[38-40] and pharmaceutically useful molecules.[40-42] Hydrosilyaltion of alkynes is the most straightforward and atom-economical approach towards stereo- and regio-selective synthesis of alkenylsilanes. Alkyne hydrosilylation is mainly categorized into two types, 1) intermolecular alkyne hydrosilyaltion and 2) intramolecular hydrosilyaltion.

1.3a Intermolecular Alkyne hydrosilylation

Depending on the mode of addition of silicon-hydrogen (Si–H) bonds/hydrosilane across an alkyne carbon-carbon triple bond, the reaction can yield a mixture of four isomeric alkenylsilanes. Among the four isomeric alkenylsilanes two are result of addition of hydrosilane to the same face of triple bond (syn addition process) forming (*E*)-alkenylsilanes, the other two are result of trans-addition (anti addition) forming (*Z*)-alkenylsilanes.

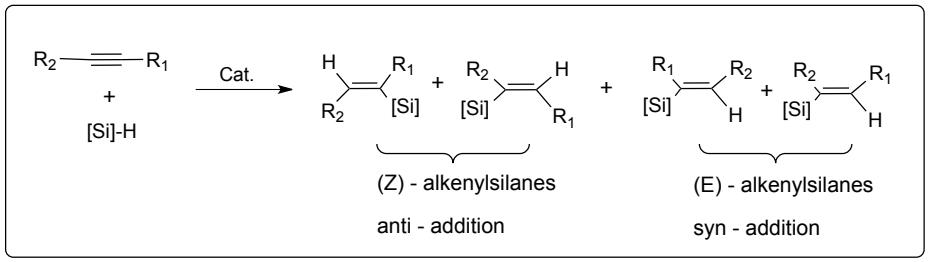

Figure 1.3 Intermolecular alkyne hydrosilylation

1.3b Intramolecular alkyne hydrosilylation

Depending on the mode of cyclization of silicon-hydrogen (Si–H) bonds across an alkyne triple bond, a mixture of upto three isomeric alkenylsilanes can be furnished. Among the three isomeric alkenylsilanes two are result of anti addition forming exo-anti and endo-anti alkenylsilanes, the other is a result of syn addition forming exo-syn alkenylsilane.

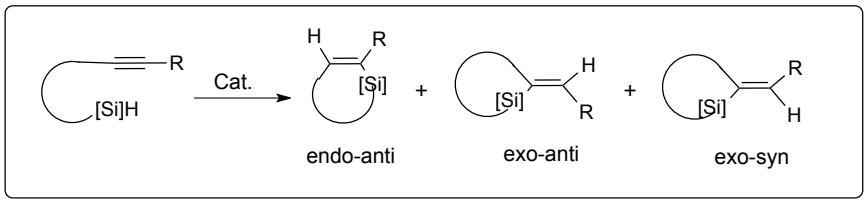

Figure 1.4 Intramolecular alkyne hydrosilylation

1.4 Background and importance of stereo- and regioselectivity in alkyne hydrosilylation

Stereo- and regiochemical outcome of alkyne hydrosilylation depends on several factors, including the catalytic system (metal and ligands), the substituents on both the alkyne and the hydrosilane used, and the reaction parameters such as solvent, temperature, and catalyst loading or even on the order of addition of the reagents. Several researchers have designed and executed the alkyne hydrosilylations in a regio- and stereocontrolled fashion using a number of transition metal catalysts. Despite the significant advances on transition metal-catalyzed alkyne hydrosilylation to access such synthetic building blocks in a regio and stereoselective fashion, α-regioselective hydrosilylation still remains challenging.

Our research is focused on the hydrosilylation of propargyl alcohols to generate α-hydroxy vinylsilanes. Propargyl alcohols are chosen as substrates to address challenges associated with selectivity.

1.4a Trost's intermolecular alkyne hydrosilylation

Trost and Ball have demonstrated intermolecular hydrosilylation of internal alkynes including propargylic alcohols in the presence of $[\{Cp^*Ru(MeCN)_3\}PF_6]$ (Cp* = pentamethylcyclopentadiene).[43] Regioselectivity is achieved as a result of *anti*-addition of hydrosilane to alkyne forming (Z)-alkenyl silanes. β-silyl selective products are observed as major product. Interestingly, tertiary propargyl alcohol system is not studied in this work.

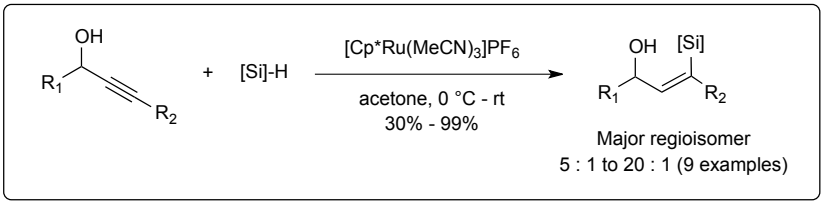

Figure 1.5 Trost intermolecular alkyne hydrosilylation

1.4b Takeuchi's intermolecular alkyne hydrosilylation

Takeuchi work utilized $[Rh(COD)_2]BF_4/2PPh_3$ as a useful tool for the synthesis of (E)-alkenyl silanes via *syn*-addition of hydrosilane to alkyne.[44] β-Silyl selective products are observed as a major regioisomer with good yields. Primary and secondary propargyl alcohol systems were primarily studied in this work.

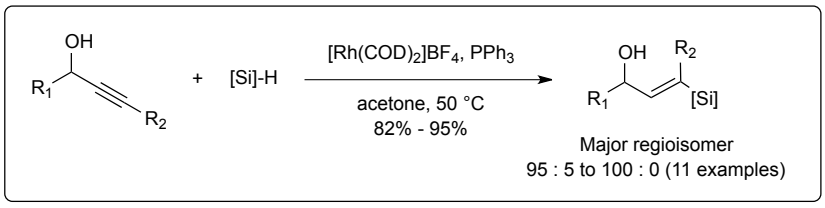

Figure 1.6 Takeuchi's intermolecular alkyne hydrosilylation

1.4c Directing group strategy Tamooka's intermolecular alkyne hydrosilylation

Alkyne hydrosilylation performed on unsymmetrical alkynes results in formation of a mixture of regioisomers leading to poor selectivity. With the introduction of a directing group into substrates regioselectivity can be controlled. Due to the presence of directing group proximal selectivity increases when compared to the distal position in intermolecular hydrosilylation. This strategy was utilized by Tomooka to achieve excellent proximal selectivity.[45] This strategy provides a method to achieve challenging α-selective hydrosilylation products.

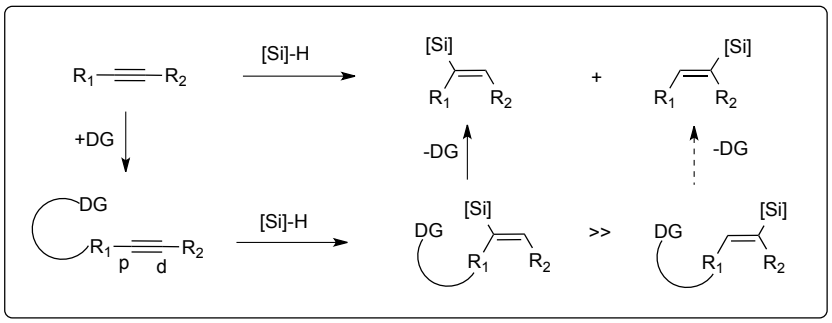

Figure 1.7 Directing group strategy intermolecular alkyne hydrosilylation

1.4c1 Tomooka's intermolecular alkyne hydrosilylation

Tomooka[45] demonstrated proximal α-selective hydrosilylation of protected propargyl alcohol and homopropargylic alcohol systems utilizing dimethylvinylsilyl (DMVS) group as a directing group. A DMVS group, a substructure of Karstedt catalyst was used as an excellent directing group to achieve α- and *syn*-selective alkyne hydrosilylation of primary and secondary propargylic alcohols in excellent yields. After the hydrosilylation the DMVS directing group was removed under basic conditions (e.g., TBAF). However, this Platinum-catalyzed strategy has a challenge associated with the selective removal of one alkoxy silane (i.e., DMVS ether) group over the other alkyl silane (i.e., newly introduced vinylsilane). Sterically hindered hydrosilane

like triisopropylsilane is used in this strategy to tolerate the basic conditions used. Unfortunately, tertiary propargylic alcohol subtrates were not demonstrated.

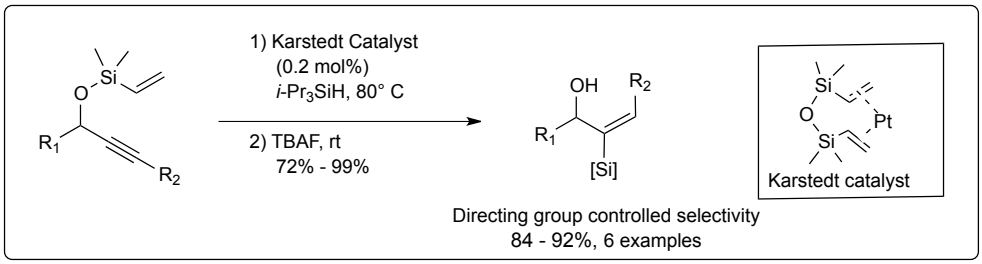

Figure 1.8 Tamooka's intramolecular alkyne hydrosilylation

1.4c2 Catalyst-controlled strategy in intramolecular alkyne hydrosilylation

Fürstner approach to achieve intramolecular alkyne hydrosilylation is based on a catalyst-controlled strategy.[46] $[Cp^*RuCl]_4$ was used as catalyst that provides a directing effect originating from [Ru–Cl] bond. The ability of polarized [Ru–Cl] bond to engage in hydrogen bonding with the protic substituent helps activate and locks the alkyne in the coordination sphere to generate the α-selective *anti*-addition products. Inter-ligand interactions control and dictate the selectivity in propargylic alcohols with excellent yields and a wide range of substrate scope.

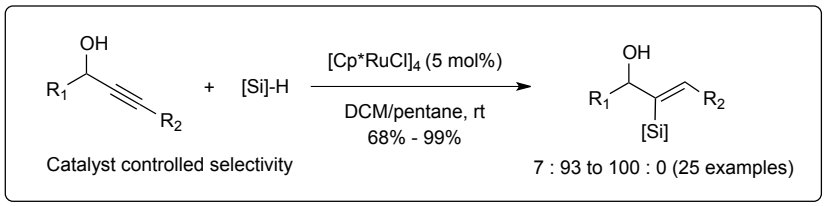

Figure 1.9 Catalyst controlled strategy in intramolecular alkyne hydrosilylation

1.4c3 Trost's directing group strategy for homopropargyl alcohols

Trost has also demonstrated intramolecular hydrosilylation of internal alkynes including homopropargylic and bishomopropargylic alcohols in the presence of $[\{Cp^*Ru(MeCN)_3\}PF_6]$.[47] β-silyl, endo-dig selective *anti*-hydrosilylation products were observed as a major regioisomer in good yields.

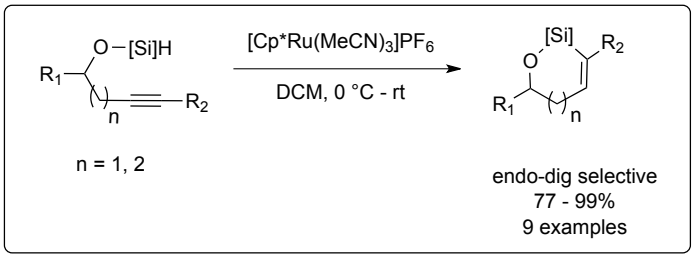

Figure 1.10 Trost's directing group strategy

1.4c4 Denmark's intramolecular alkyne hydrosilylation

Denmark have achieved a highly regio- and stereoselective intramolecular hydrosilylation of homopropargyl alcohols with ruthenium catalyst.[48] 3-pentynyloxysilane (or) alkynyl silyl ether underwent intramolecular hydrosilylation in presence of ruthenium complexes varying the products depending on the chosen ruthenium complex. Alkynyl silyl ether with ruthenium arene complexes {$[RuCl_2(benzene)_2]_2$ (a) and $[RuCl_2(p\text{-cymene})_2]_2$ (b)} gave the exo-, anti hydrosilylation product as major, along with a small amount of exo-syn hydrosilylation product. On the other hand, ruthenium hydride complex {$[RuHCl(CO)(P\textit{i}\text{-}Pr_3)]_2$ (c)} afforded the exo-syn hydrosilylation product exclusively in 75% yield.

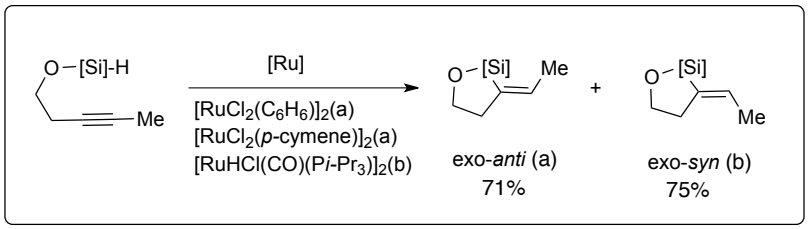

Figure 1.11 Denmark's directing group strategy

1.5 Challenges in exo-selective hydrosilylation of propargyl alcohols

Although there have been significant advances in alkyne hydrosilylation of homopropargyl and bishomopropargyl alcoholic derivatives. α-Regioselective hydrosilylation of propargyl alcohol derivatives to access α-hydroxy vinylsilanes still remains to be solved.

Propargyl alcohol derivatives can generate oxasiletanes via 4-exo-dig cyclization or oxasilole via 5-endo-dig cyclization. Oxasiletanes are oxasilacyclobutanes, which are not stable due to ring strain, undergo polymerization. Due to this instability of oxasiletanes, oxasiloles via 5-endo-dig cyclization is observed as major product. Ojima has observed the instability of putative oxasilacyclobutanes while investigation on silyl ethers of propargylic alcohol derivatives.[49] This supports the idea that the challenge associated with hydrosilylation of propargylic alcohol derivatives resides in the size of the ring formed after cyclization.

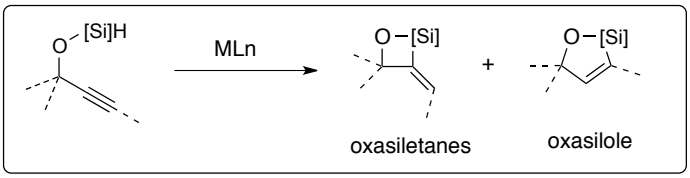

Figure 1.12 Challenge in exoselective hydrosilylation of propargyl alcohols

1.6 Denmark's directing group strategy in hydrosilylation of propargyl alcohols

Denmark has developed a highly regio- and stereoselective intramolecular hydrosilylation reaction of propargyl alcohols using a two-atom disiloxane tether to produce exo-cyclized 6-membered disiloxane products.[50] A two-atom tether is needed to connect the oxygen of the propargyl alcohol with the silyl hydride to address the ring strain challenge. The tetramethyldisiloxane tether is installed as a directing group on propargyl alcohol, which further undergoes exo-cyclization. Isomeric products are achieved via two different catalytic systems. A Platinum catalyst provided the exo-*syn* disiloxane where as a Ruthenium catalyst provided the exo-*anti* disiloxane. The formed disiloxanes were subjected to palladium catalyzed cross-coupling in order to remove disiloxane directing group. However this approach suffers from inefficient installation of the disiloxane-directing group. The directing group installation utilizes ca. 26 equivalents of tetramethyldisiloxane reagent, which has poor atom economy and provides

alkynyloxydisiloxane in moderate yield. Other limitations are associated with the narrow substrate scope of the reaction and purification of the alkynyloxydisiloxane.

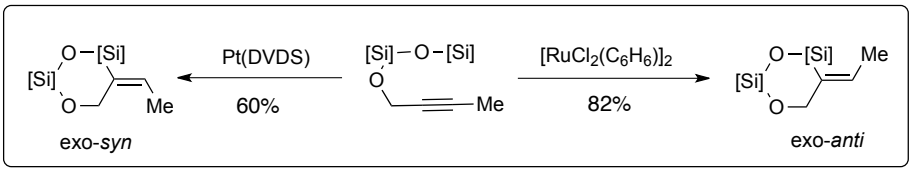

Figure 1.13 Denmark's directing group strategy in hydrosilylation of propargyl alcohols

1.7 Our designed directing group for hydrosilylation of propargyl alcohols

In order to address the challenges associated with regio- and stereoselectivity, directing group issues and excessive reagent issues, a traceless two-atom tether (X-Y = C-O, X=C & Y=O) on propargyl alcohol was designed. This two-atom tether is designed as a complementary to Denmark's tether (X-Y = Si-O, X = Si and Y = O) to address the limitations observed. Our approach involves the installation of an acetal directing group, followed by catalytic exo-selective hydrosilylation of propargyl esters to provide a range of cyclic α-(E)-vinylsilanes via dioxasilinanes. Our approach involves a directing group that is inexpensive, readily accessible, widely available and easy to install, does not require any requisite purification. Removal of directing group is performed at the end to afford α-hydroxy (E)- vinylsilanes. A highly fluorinated Rh(I)/$P(C_6F_5)_3$ catalyst was employed to provide α-selective hydrosilylation of propargyl alcohol derivatives with faster kinetics. Hydrosilyl acetal directing group can conceptually deliver a silicon moiety and hydrogen in a regio- and stereoselective fashion via 6-exo-dig cyclization to primary, secondary, and tertiary propargylic alcohols to furnish 6-membered dioxasilinanes for further downstream reactions.

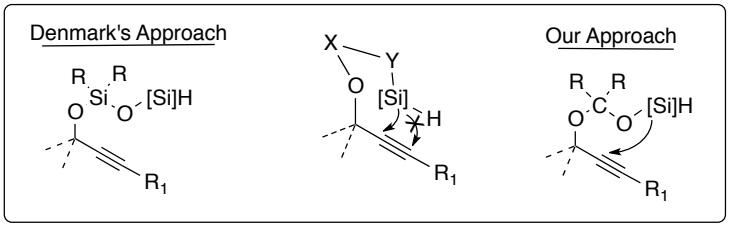

Figure 1.14 Design of two atom tether for alkyne hydrosilylation

1.8 Proposed design for a traceless acetal-directed hydrosilylation of propargyl alcohols

Our proposed approach of traceless acetal- directed hydrosilylation of propargyl alcohols comprises of two-step reaction sequence, one-pot chemoselective iridium-catalyzed ester hydrosilylation, regio- and stereoselective alkyne hydrosilylation followed traceless directing group removal to generate α-hydroxy-(E)-vinylsilanes.

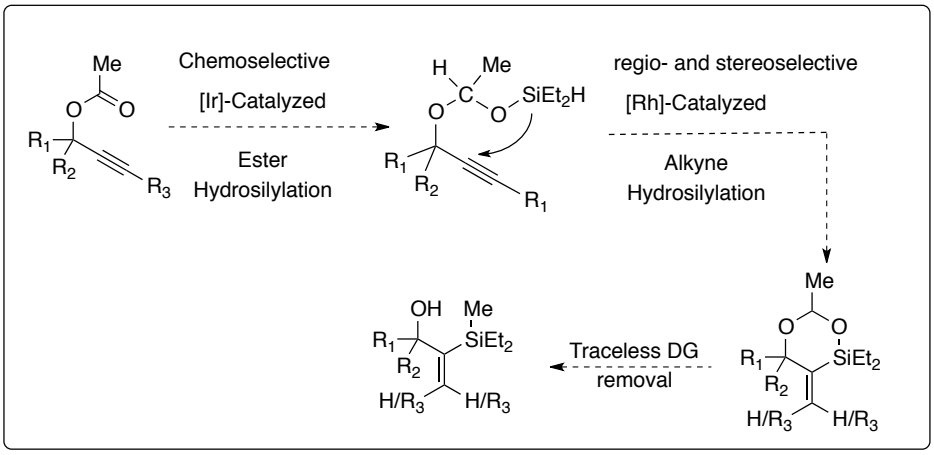

Figure 1.15 Proposed design for a traceless acetal-directed hydrosilylation of propargyl alcohols

1.9 Chemoselective iridium-catalyzed ester hydrosilylation

Ester hydrosilylation has been demonstrated in our group previous research.[51-53] In the previous work, ester hydrosilylation hass performed to generate a hydrosilylacetal as an aldehyde equivalent and followed by further modifications. We aimed to develop chemoselective ester hydrosilylation of the propargyl esters, not alkyne hydrosilylation which are well-established.

Chemoselective hydrosilylation of ester over the alkyne is achieved with the use of iridium-catalyzed hydrosilylation. A variety of esters can be synthesized from propargyl alcohols efficiently and subjected to ester hydrosilylation. Propargylic esters are treated with diethylsilane in the presence of iridium catalyst to generate hydrosilyl acetals in excellent yields.

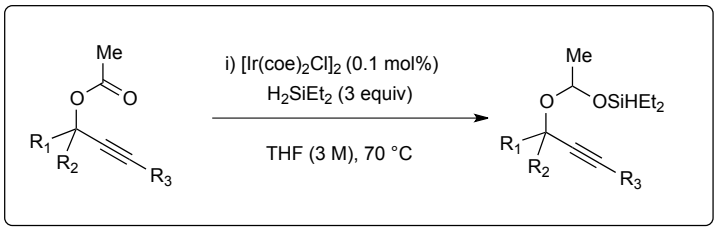

Figure 1.16 Ir-Catalyzed ester hydrosilylation of propargyl alcohols

1.10 Regio- and stereoselective rhodium-catalyzed alkyne hydrosilylation

The main focus of this research was to achieve regio- and stereoselective rhodium-catalyzed alkyne hydrosilylation of hydrosilyl acetals to synthesize a range of dioxasilinanes, leading to cyclic α-(E)-vinylsilanes (Figure 1.17).

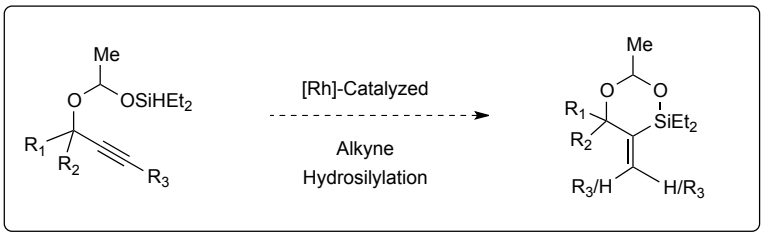

Figure 1.17 Rh-Catalyzed alkyne hydrosilylation

1.11 Initial studies

1.11.1 Initial studies - reaction temperature optimization

Rhodium-catalyzed alkyne hydrosilylation was performed on the hydrosilylacetal generated from propargylic acetate with a previously successful $[Rh(nbd)Cl]_2$ and $^{(CF_3)_2}$TpNa(THF) catalytic system. Two different temperatures are monitored for reaction

progress. Unon elevated temperature of 100 °C the reaction completed in 10 minutes with 89% NMR yield of dioxasilinanes (Figure 1.18). A room temperature reaction completed in 40 minutes with 94% NMR yield of dioxasilinanes. Room temperature reactions are generally easier to operate and the result was better by having improved yield compared to elevated temperature (Table 1.1). Rhodium-catalyzed alkyne hydrosilylation has succesfully provided a single regioisomer.

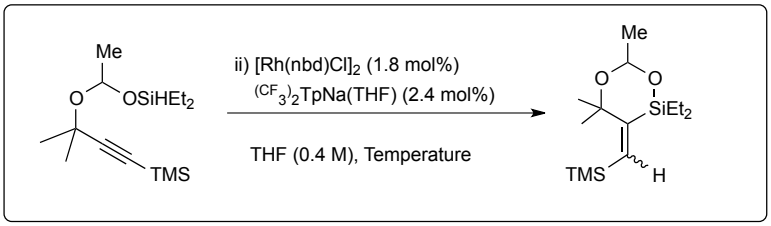

Figure 1.18 Initial studies- reaction temperature optimization

Entry	Temperature (°C)	Reaction time (min)	NMR yield (%)[a]
1	rt	40	94
2	100	10	89

[a] mesitylene as internal standard

Table 1.1 Initial studies - reaction temperature optimization

1.11.2 Initial studies - catalyst loading optimization

Rhodium-catalyzed alkyne hydrosilylation was performed on the hydrosilylacetal generated from propargylic ester with $[Rh(nbd)Cl]_2$ and $^{(CF_3)}{}_2TpNa(THF)$ catalyst system varying rhodium catalyst loading from 1.8 mol% to 0.2 mol% gradually. A catalyst loading of 0.1 mol% was evaluated, as the reaction timing is longer the optimal catalyst loading is considered to be 0.2 mol% without compromising yield of the dioxasilinane. Comparision is reported with respect to NMR yields in table 1.2. High catalyst loading is a drawback in some of the reactions even

with good selectivities and good functional group tolerance. In this approach low catalyst loading is an advantage.

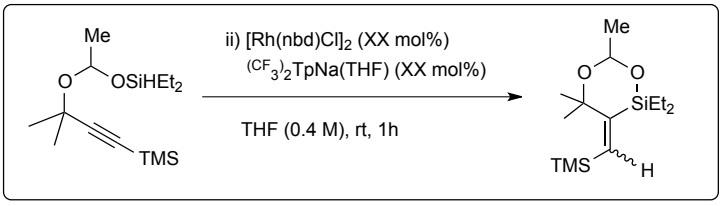

Figure 1.19 Initial studies- catalyst loading optimization

Entry	$[Rh(nbd)Cl]_2$ (XX mol%)	$Tp^{(CF_3)_2}Na(THF)$ (XX mol%)	NMR yield (%)[a]
1	1.8	2.4	94
2	0.2	0.4	90

[a] mesitylene as internal standard

Table 1.2 Initial studies- catalyst loading optimization

1.11.3 Initial studies: Exo-syn vs Exo-anti alkyne hydrosilylation

With the optimized conditions for alkyne hydrosilylation identified and resulted in formation of one regioisomer in excellent yield. Stereochemistry was confirmed with 1D-NOE NMR studies. 1-Dimensional nuclear overhauser effect (1D-NOE) is a specific type of spectroscopy works through space transfer of nuclear spin polarization. Irradition at the resonant frequency of the proton of interst promotes to B-state, this spin polarization is transferred through space to protons that are close in space, therby enhances the signal of neighbouring proton by increasing population. In my study, vinylic proton in dioxasilinane was selectively irradiated and interactions with neighbouring protons suhc as ethyl protons and TMS protons were observed. For further confirmation, TMS protons were selectively irradiated and interacting neighbouring protons such as geminal dimethyl protons and vinylic proton in dioxasilinane were observed. This confirms that the addition of hydrosilane on the triple bond occurred through an

exo-*syn* mode. With these information in hand, we sought the optimized reaction conditions to provide excellent stereo- and regioselective alkyne hydrosilylation leading to dioxasilinanes.

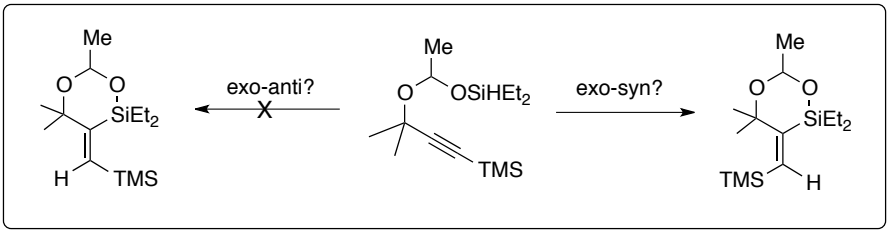

Figure 1.20 Exo-syn Vs Exo-anti alkyne hydrosilylation

1.11.4 Initial studies- Ligand screening

A survey of range of supporting ligands comprising phosphines, pentamethylcyclopentadienyl (Cp*), and tris(pyrazolyl)borates (Tp) (Figure 1.23) with varying electronic and steric capabilities in the presence of rhodium precatalysts were examined in the alkyne hydrosilylation at room temperature (Table 1.3). Rhodium catalysts assembled through the combination of the Rh(I) precatalyst and supporting ligand examined provided (*E*)-vinylsilane **2a** as major adduct (entries 1-11). Among them, highly fluorinated $P(C_6F_5)_3$ produced **2a** in excellent yield (92%) in shorter reaction time/ faster kinetics with complete regio- and stereoselectivity (*E* only, entry 2).

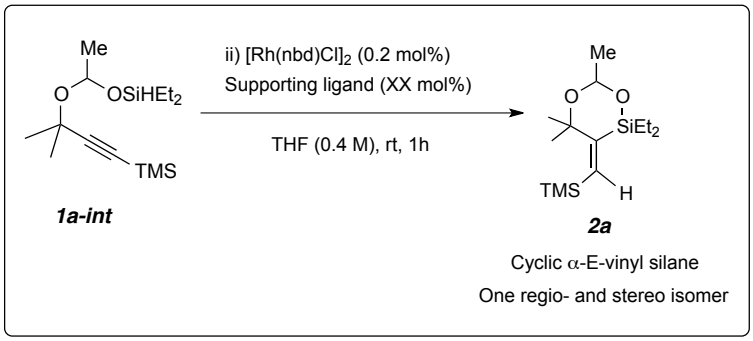

Figure 1.21 Ligand screening for alkyne hydrosilylation

Entry	Supporting ligand	Yield (%)[b]	α:β[c]	E:Z[d]
1	PPh_3	81	only α	only *E*
2	$P(C_6F_5)_3$	92	only α	only *E*
3	$P(4\text{-}MeOPh)_3$	84	only α	only *E*
4	PPh_2Et	83	only α	only *E*
5	JohnPhos	84	only α	only *E*
6	PCy_3	78	only α	only *E*
7	$P(OPh)_3$	77	only α	only *E*
8	$[RhCp^*Cl_2]_2$	90	only α	only *E*
9	$Tp^{(CH_3)_2}K$	82	only α	only *E*
10	$Tp^{CF_3,Ph}Na(THF)$	88	only α	only *E*
11	$Tp^{(CF_3)_2}Na(THF)$	85	only α	only *E*

[a]Conditions: **1a** (0.20 mmol), supporting ligand (0.6 mol % for phosphine ligands, 0.2 mol% for Tp ligands,), THF (0.4 M). [b]Determined by ^{1}H NMR spectroscopy utilizing an internal standard (mesitylene). [c]Determined by GC/MS analysis and ^{1}H NMR spectroscopy. [d]NOESY experiment.

Table 1.3 Initial studies- ligand screening

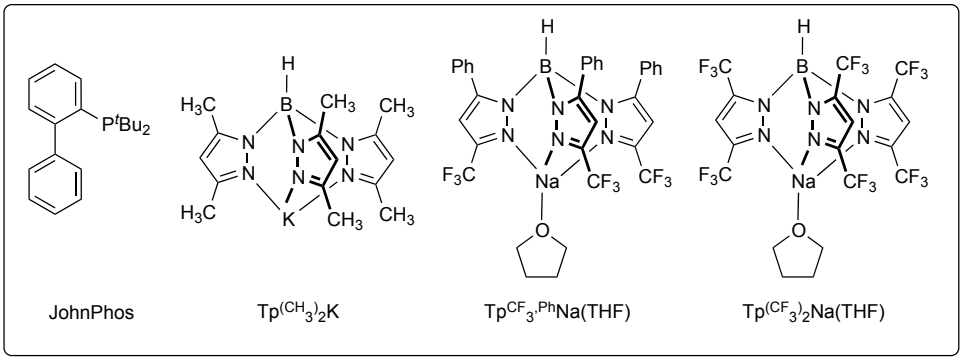

Figure 1.22 Structures of ligands

1.12 Kinetic studies

In order to better understand the efficiency of the reaction with highly fluorinated phosphine $P(C_6F_5)_3$ ligand, *in situ* reaction monitoring by ^{1}H NMR spectroscopy was performed. The graph in Figure 1.24 is an overlay of two graphs, namely percentage NMR yield against time

and log natural $\ln[M_o/M_t]$ against time. Top graph is the conversion graph representing the percentage of formation of product monitored with ^{1}H NMR utilizing mesitylene as an internal standard.

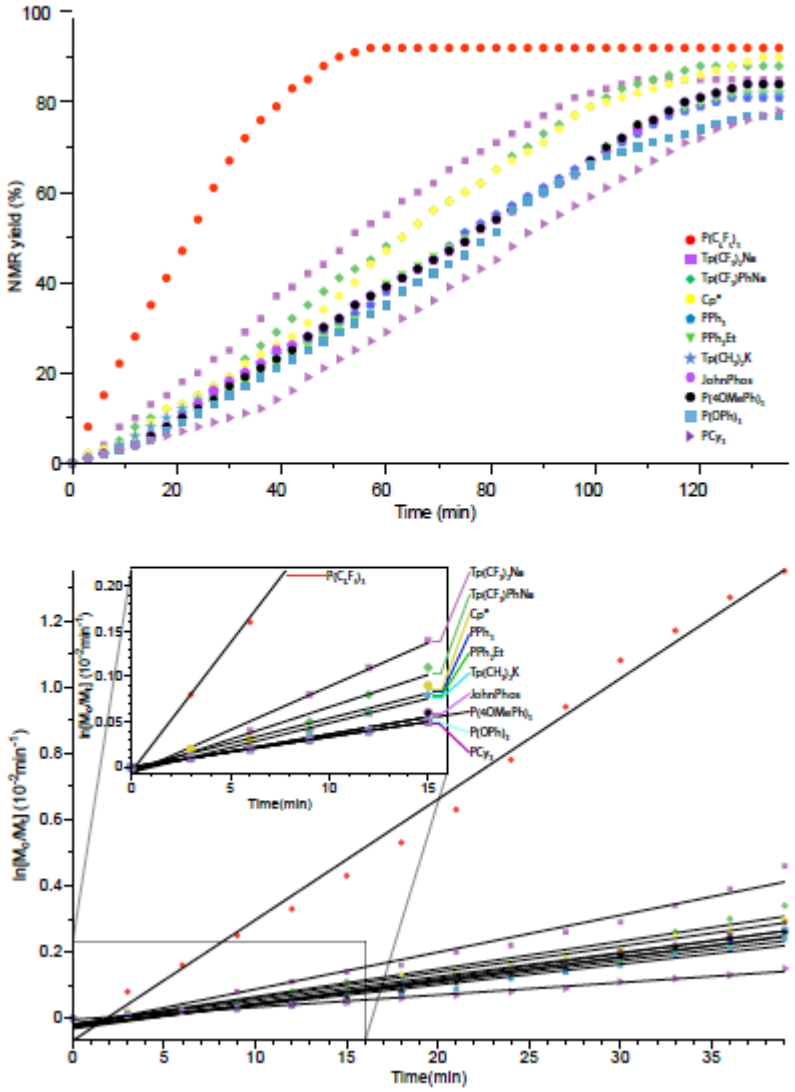

Kinetic profiles of hydrosilylation of various ligands in Table 1.3. Datasets obtained by *in situ* ^{1}H NMR spectroscopy in C_6D_6, 20 °C utilizing an internal standard (mesitylene): **1a** (0.20 mmol), supporting ligand (0.6 mol % for phosphine ligands, 0.2 mol% for Tp ligands,), THF (0.4 M). $[RhCp^*Cl_2]_2$ (0.2 mol %) used.

Figure 1.23 Kinetic studies

Conversion graphs shows that among all the catalytic systems, electron-poor catalyst systems [e.g., $P(C_6F_5)_3$, $Tp^{(CF_3)_2}Na(THF)$, $Tp^{(CF_3)_2\,Ph}Na(THF)$] exhibited fast reaction kinetics and achieved complete conversion in shorter time periods. Bottom plot is log natural $\ln[M_o/M_t]$ {M_0 is initial concentration, M_t is concentration at a given time} against time.

The resulting graph is a line with the tangential slope at any place on the line representing the instantaneous rate at that moment of time. Slopes of various ligands are tabulated in Table 1.4 with a descending order of the slopes of various ligands. Slope of highly fluorinated phosphorous ligand $P(C_6F_5)_3$ coordinated with Rh(1) species demonstrates faster kinetics relative to other ligands tested.

Ligand	Slope
$P(C_6F_5)_3$	0.036443
$Tp^{(CF_3)_2}Na$	0.011172
$Tp^{(CF_3)\,Ph}Na$	0.008351
$[RhCp^*Cl_2]_2$	0.007835
JohnPhos	0.007560
$Tp(CH_3)_2K$	0.007216
PPh_3	0.007069
$P(4OMePh)_3$	0.006982
PPh_2Et	0.006556
$P(OPh)_3$	0.006219
PCy_3	0.003722

Table 1.4 Kinetic study –Slopes of various ligand

Measurements of the rates obtained for various ligands are tabulated and compared with respect to PPh_3. Electron-withdrawing substituents led to increasing catalytic activity, the most rapid

with $P(C_6F_5)_3$ was a factor of 2.2 times faster than with PPh_3. An analysis of $t_{1/2}$ also clearly demonstrated that highly fluorinated electron poor phosphorous ligand $P(C_6F_5)_3$ coordinated with Rh(1) species has faster kinetics compared to other electron rich and electron poor ligands. Highly fluorinated phosphorous ligand $P(C_6F_5)_3$ has a $t_{1/2}$ of 21 minutes the shortest half life among the examined ligands and PCy_3 has the longest $t_{1/2}$ of 84 minutes. Mechanistically sigma/pi bonding characteristics of the electron poor ligands leads to weaker Rh-ligand bonding which in turn facilitates the rate determining ligand displacement by the alkyne substrate. The result suggests that the electrophilic rhodium center coordinated with highly fluorinated phosphine ligand substantially increases Rh–π interaction, allowing a fast kinetics.

Entry	Supporting ligand	$t_{1/2}$ (min)	$t_{completion}$ (min)	Relative rate w/r PPh_3 ($t_{completion}$)
1	$P(C_6F_5)_3$	21	57	2.2
2	$Tp^{(CF_3)_2}Na(THF)$	51	108	1.2
3	$Tp^{CF_3,Ph}Na(THF)$	57	120	1.07
4	$[RhCp^*Cl_2]_2$	60	126	1.02
5	PPh_3	69	129	1
6	PPh_2Et	72	123	1.04
7	$Tp^{(CH_3)_2}K$	75	129	1
8	JohnPhos	78	126	1.02
9	$P(4\text{-}MeOPh)_3$	78	120	1.07
10	$P(OPh)_3$	81	129	1
11	PCy_3	84	135	0.95

Table 1.5 Kinetic study – rate study of various ligands w/r to PPh_3

1.13 One mmol scale reaction feasibilty

Traceless acetal- directed hydrosilylation of propargyl alcohols is examined for one mmol scale feasibility. One mmol scale reaction succeeded in providing dioxasilinanes in a very good yield of 83% .

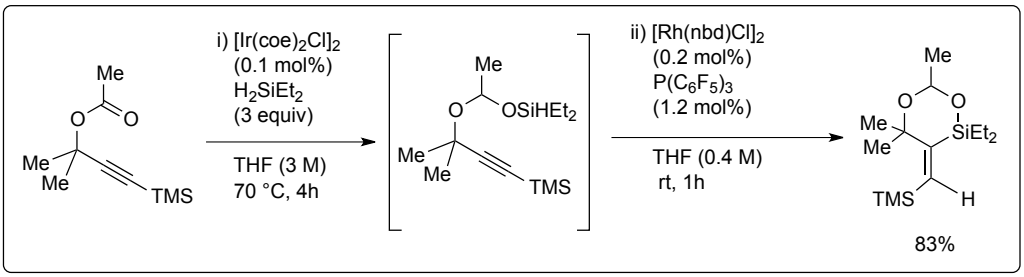

Figure 1.24 Feasability of 1mmol scale alkyne hydrosilylation

1.14 Scope of various hydrosilylacetals for alkyne hydrosilylation

With the optimized conditions in hand, the impact of acetal tethers on the cyclization was studied (Figure 1.25). Sterically and electronically tuned hydrosilyl acetals (**1a**-**1f**) were accessed via Ir-catalyzed ester hydrosilylation, and were examined. Sterically more accessible esters **1a**-**1d** (R = H, Me, α-chloro, ^{i}Pr) smoothly underwent the sequential Ir and Rh catalysis involving ester and alkyne hydrosilylations, respectively, to furnish **1a**-**1d** (83-94%). Significantly slower kinetics (12 h) were observed in ester hydrosilylation of sterically demanding ester **1e** (R = ^{t}Bu), but the rate of alkyne hydrosilylation was comparable with substrates **1a**-**1d** (ca. 0.5 h). Electron-deficient trifluoromethyl ester **1f** underwent both ester and alkyne hydrosilylations with slower rates (48 h and 1 h, respectively), but the overall reaction was efficient to produce **2f** (76% yield).

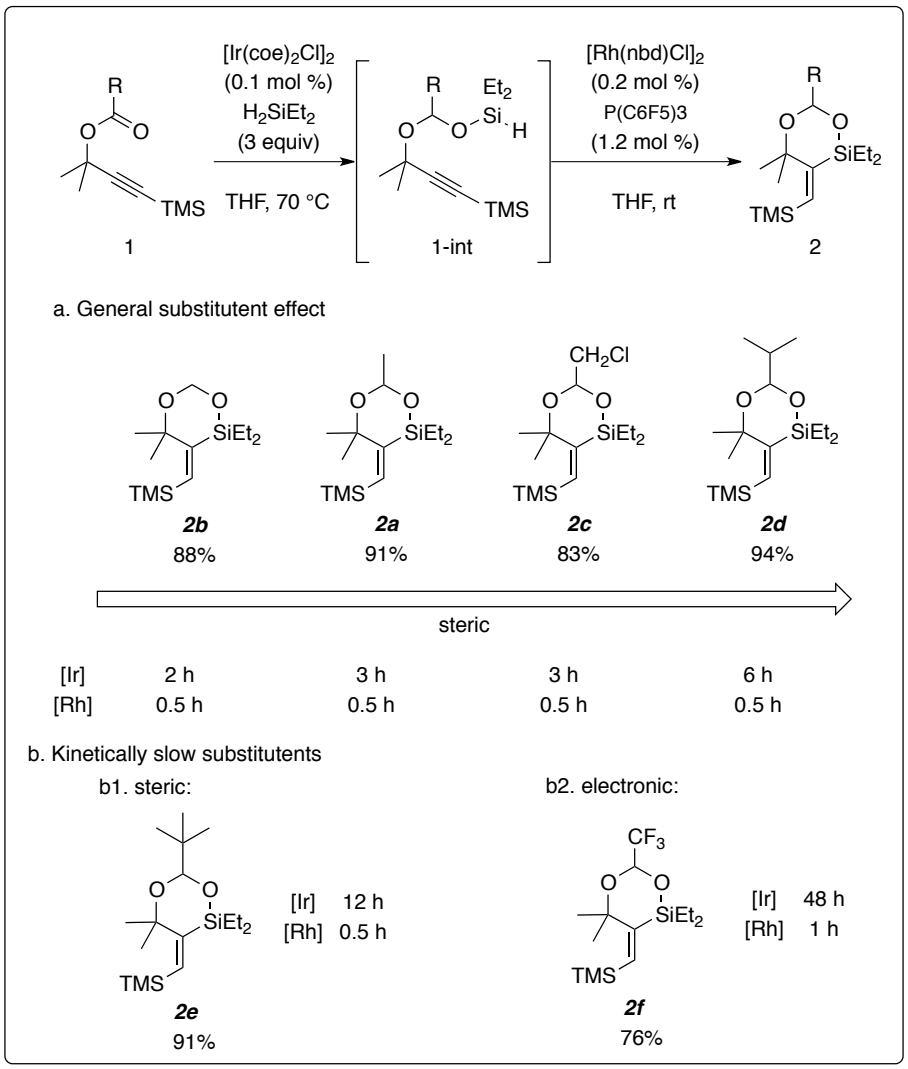

Figure 1.25 Scope of various hydrosilylacetals

1.15 Scope of various substrates for alkyne hydrosilylation

The scope of propargyl acetates was studied with structurally diverse hydrosilyl acetals (Figure 1.26) to achieve regio and stereoselectivity. Under the sequential Ir- and Rh-catalyzed hydrosilylation conditions trimethylsilyl-substituted primary, secondary, and tertiary propargyl acetates furnished (*E*)-dioxasilinanes (**2a**, **2g**-**2i**).

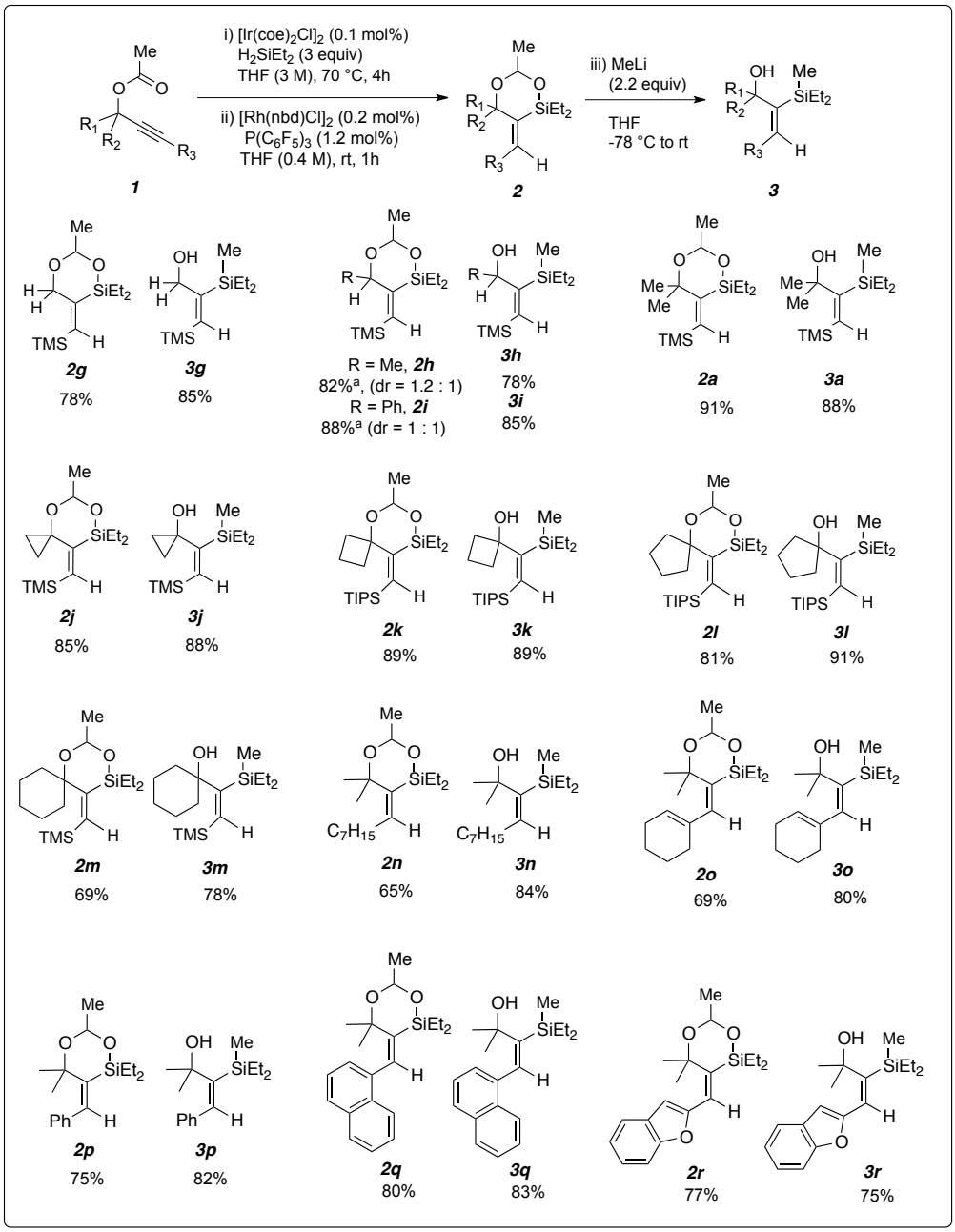

Figure 1.26 Substrate scope of alkyne hydrosilyaltion

Tertiary propargyl acetates reacted more efficiently vis-à-vis primary and secondary propargyl acetates. Cycloalkynol derivatives (**1j-1m)** ring size ascending from three membered to six membered, tolerated the reaction conditions generating (*E*)-dioxasilinanes (**2j-2m**). Further alkyl and cyclohexenyl-substituted propargyl alcohols are compatible with reaction conditions

and gave the corresponding (*E*)-dioxasilinanes (**2n**, **2o**) in good yields. Propargyl acetates bearing aromatic group including phenyl and naphthyl are efficient in providing the corresponding (*E*)-dioxasilinanes (**2p**, **2q**). Benzofuran propargylic acetate substrate **1r** was also compatible with the conditions to produce **2r**.

The traceless nature of this reaction was demonstrated by addition of nucleophile (e.g., MeLi) to (*E*)-dioxasilinanes **2**, which provided α-(*E*)-vinylsilanes (**3a**, **3g-3r**). Nucleophilic ring-opening reactions remove the acetal-directing group and uncover hydroxy groups in the same vessel rendering the traceless directing nature. A variety of nucleophiles (e.g., alkyl, hydride, vinyl, allyl, heterocycles, alcohols) can be used to produce a range of vinylsilanes. Overall, this protocol exhibited a reasonably wide functional group compatibility and established traceless acetal-directed, catalytic *exo-syn* hydrosilylation of propargyl esters **1** to provide a viable synthesis of α-(*E*)-vinylsilanes **(3)** with good yield and exclusive α-regioselectivity and (*E*)-stereoselectivity. In any of the cases the other regio and stereoisomer are not observed.

1.16 Pyridine substrate for alkyne hydrosilylation

The reactions with propargyl acetates bearing heterocycle pyridine [3-pyridyl (**1s**), 2-pyridyl (**1s**^{1})] were studied. Pyridine substrate required optimization in Rh-catalyzed alkyne hydrosilylation reaction sequence. The optimized condition for Rh-catalyzed alkyne hydrosilylation reaction were found to be a shorter reaction time and higher temperature, specifically 100 °C for 15 min. Interestingly 2-pyridyl (**1s**^{1}) was found to be efficient to provide the corresponding (*E*)-dioxasilinane (**2s**^{1}) compared to that of 3-pyridyl (**1s**). This anomaly can be attributed to the presence of the heteroatom in closer proximity can engage in alkyne hydrosilylation effectively compared to the farther one. (*E*)-dioxasilinanes are comparatively less

stable, hence proceeded further without purification were subjected to nucleophilic addition with (MeLi) provided α-(*E*)-vinylsilanes (**3s[1]**) in good yield (70%).

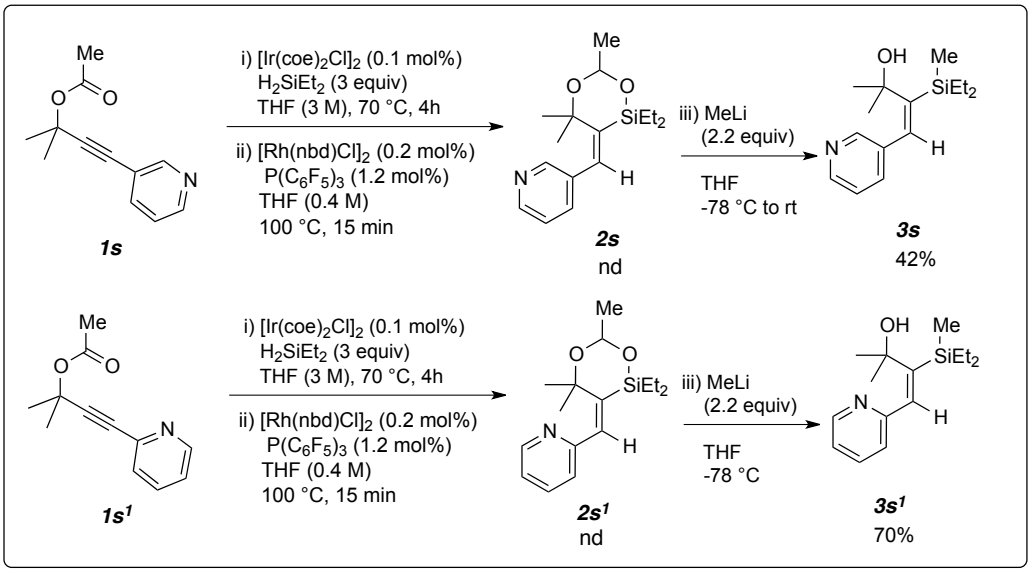

Figure 1.27 Pyridine substrate for alkyne hydrosilyaltion

1.17 Indole substrate for alkyne hydrosilylation

Propargyl acetates bearing an indole moiety was studied. Indole propargylic acetate substrate **1t** is compatible with the conditions. Interestingly, indole propargylic acetate substrate **1t** upon nucleophilic ring opening at lower temperature provided a spirocyclic compound **3t** in good yield (71%). Similar fact is observed in the case of enyne substrate (**2o**) (see Figure 1.26) in our study. Literature search justified the formation of spirocyclic compound under basic conditions.[54]

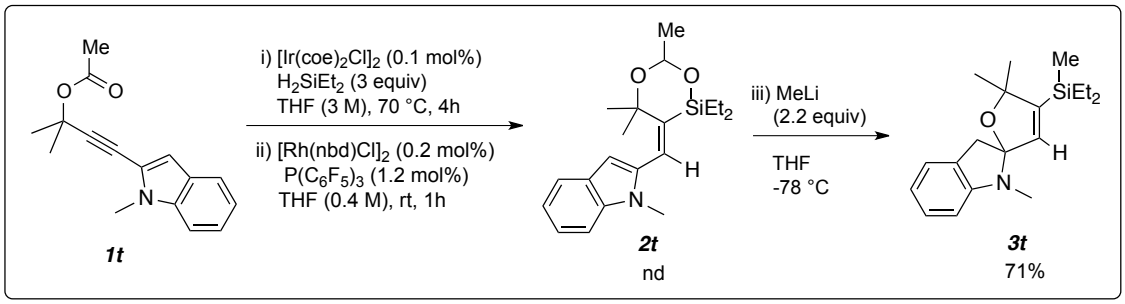

Figure 1.28 Indole substrate for alkyne hydrosilyaltion

1.18 Failed substrates for alkyne hydrosilylation

Reactions with propargyl acetates bearing thiophenyl, benzyl and bromo groups (**1u- 1w)** were studied. These reactions did not proceed as expected due to the functional group compatability with Ir-catalyzed ester hydrosilylation.

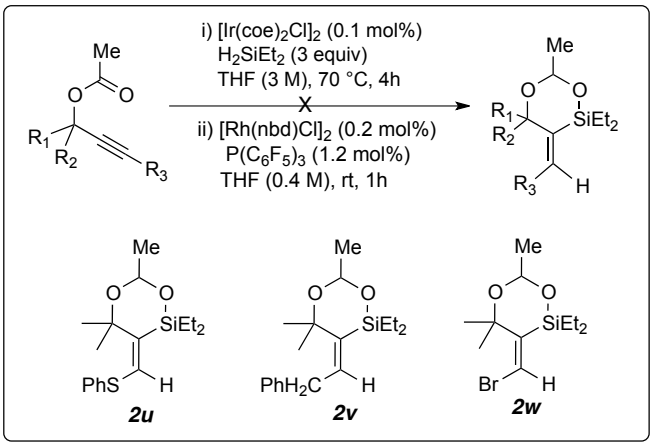

Figure 1.29 Failed substrates for alkyne hydrosilyaltion

1.19 Ruthenium-catalysed alkyne hydrosilylation

Denmark has achieved exo-*syn* and exo-*anti* selectivity for homopropargylic systems by altering the catalyst used.

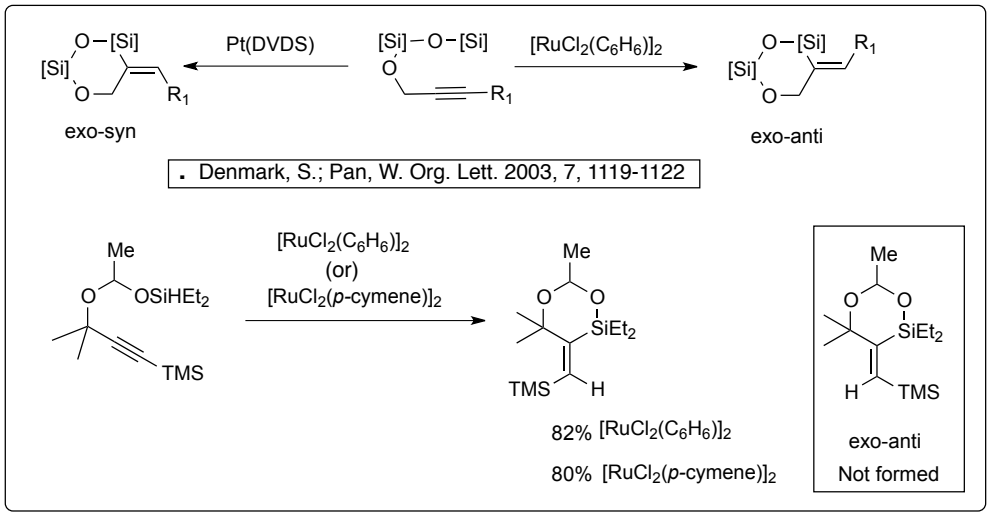

Figure 1.30 Metal catalyzed alkyne hydrosilyaltion

Attempts to achieve different selectivity utilizing the ruthenium arene complex were not successful, instead provided *exo-syn* selectivity. ^{1}D-NOE NMR studies were performed on the resulting product to confirm the selectivity, *exo-anti* selectivity was not observed.

1.20 Synthesis of diene

Dual cyclization of propargyl bis-esters generated dienes (Figure 1.31). Propargyl bis-acetate **1x** underwent consecutive ester and alkyne hydrosilylations to give conjugated 1,3-diene (*E,E*)-**2x** in 88% yield. The subsequent nucleophilic addition to **2x** furnished functionalized conjugated bis-silyl 1,3-diene **3x** in 83% yield.

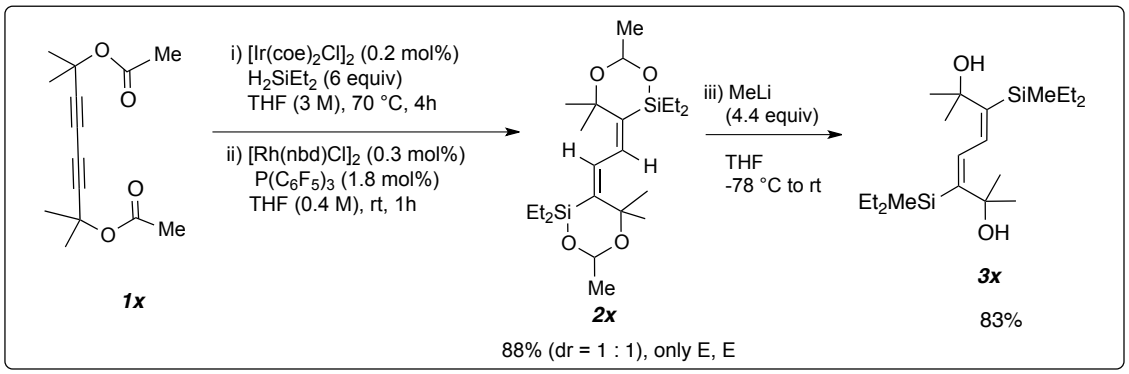

Figure 1.31 Synthesis of diene

1.21 Synthesis of enyne

Mono cyclization of trimethylsilyl protected diyne ester, in order to generate enynes (Figure 1.32) was studied. Propargyl acetate **1y** underwent consecutive ester and alkyne hydrosilylations to give conjugated 1,3-enyne (*E*)-**2y** in 70 % yield. Upon nucleophile addition to **2y** furnished functionalized conjugated 1,3-enyne **3y**. Propargyl bis alcohol is mono-protected with trimethylsilyl group, as the acetyl group was responsive toward alkyne hydrosilylation under the kinetically controlled conditions, enynes **3y** was generated in good yield (72%).

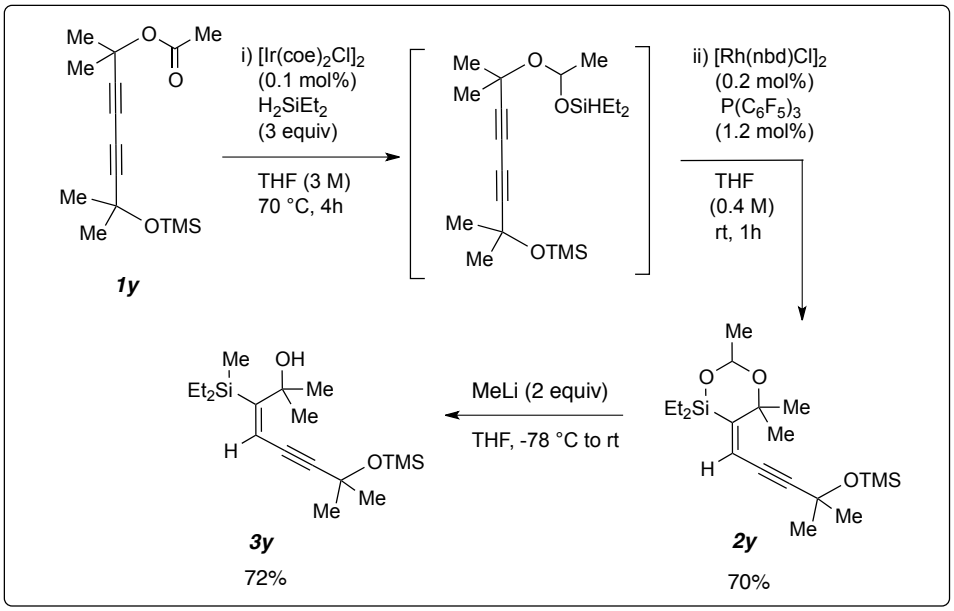

Figure 1.32 Synthesis of enyne

1.22 Importance of ethinylestradiol

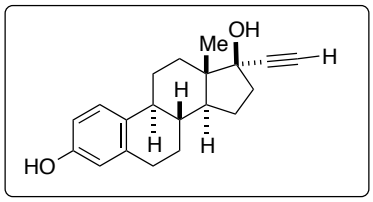

Figure 1.33 Ethinylestradiol (EE)

Ethinylesterdiol (EE) is a standalone oral estrogen medication used in birth control pills. EE is the first oral synthetic estrogen. EE has greatly improved bioavailability compared to estradiol. EE is used to treat hypogonadism, osteoporosis, prostate cancer in men and breast cancer in women. EE is widely marketed throughout the world in combination with progestins. Importance of ethinylesterdiol (EE) made it a potential substrate of interest to demonstrate the versatility of this method.

1.23 Synthesis of phenyl-substituted ethinylesterdiol

Phenyl substituted-17α-ethynylestradiol is synthesized from estrone. Estrone alcohol group is benzyl-protected, followed by alkyne addition generated substituted alcohol. Esterification of alcohol generated the desired phenyl substituted-17α-ethynylestradiol ester (**1z**) in quantitative yield.

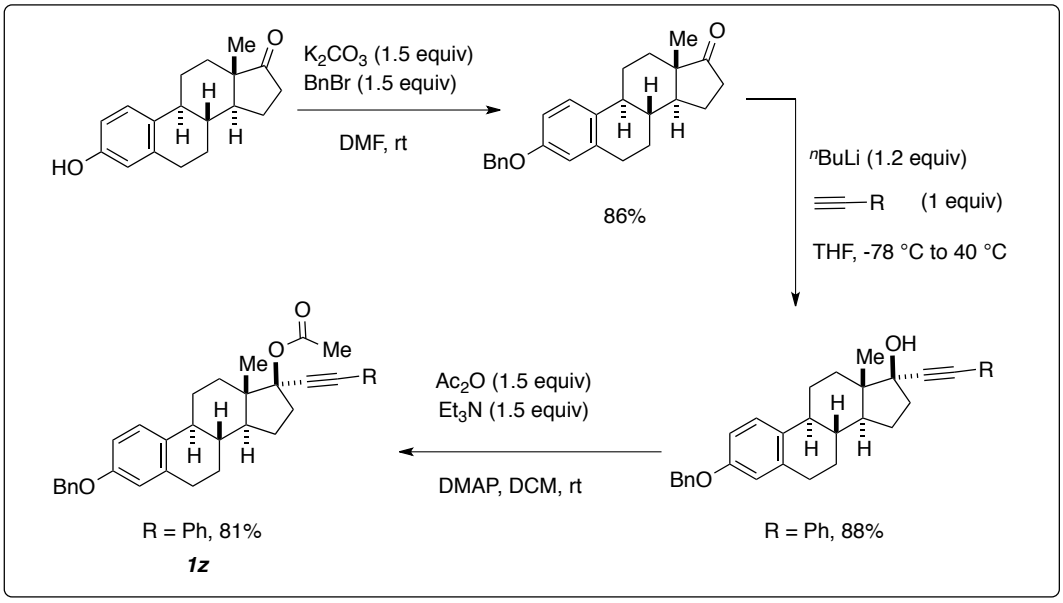

Figure 1.34 Synthesis of phenyl-substituted ethinylesterdiol

1.24 Feasibility of various substituted ethinylesterdiol for alkyne hydrosilylation

Substituted ethinylesterdiol esters are tested for hydrosilyl acetal directed exo-syn hydrosilyaltion. Among the esters tested (R = H, TMS, Ph), no reaction is observed in the case of TMS substituted ester (**1z-TMS**) and unsubstituted ester (**1z-H**) has shown progress but suffered from poor reactivity. Phenyl substituted ethinylesterdiol ester has successfully generated (*E*)-dioxasilinanes (**2z**) in excellent yield (86%).

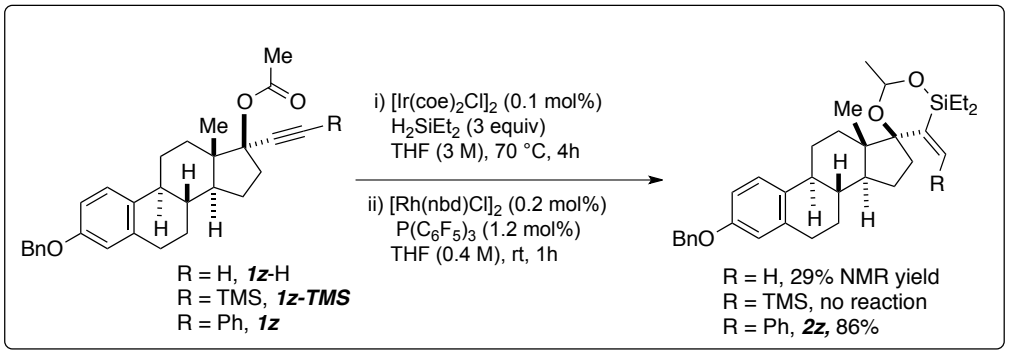

Figure 1.35 Feasibility of various-substituted ethinylesterdiol for alkyne hydrosilylation

1.25 Late-stage functionalization of phenyl-substituted ethinylesterdiol

In order to show the versatility of this method a complex molecular setting of Phenyl substituted-17α-ethynylestradiol was successfully demonstrated by generating (*E*)-dioxasilinanes (**2z**) in excellent yield. Nucleophilic ring-opening with methyl lithium has provided vinyl silane (**3z**) in excellent yield (91%). Late-stage hydrosilylation of phenyl-substituted esterdiol acetate is demonstrated for traceless hydrosilyl acetal-directed, *exo-syn* hydrosilylation to produce α-hydroxy (*E*)-vinylsilanes.

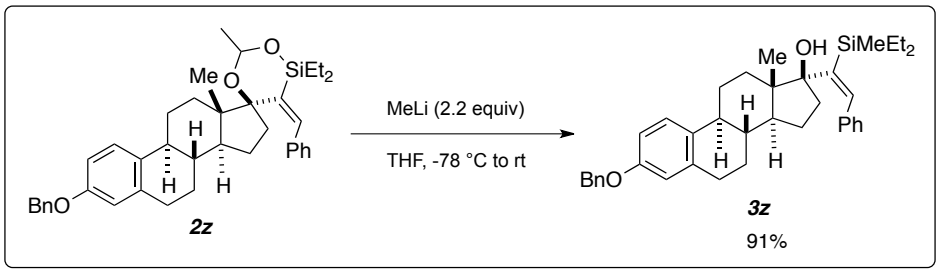

Figure 1.36 Late-stage functionalization of phenyl-substituted ethinylesterdiol

1.26 Synthetic applications of dioxasilinanes

Synthetic applications of dioxasilinanes are in progress. Attempts made to perform transformations of dioxasilinanes did give desired products, but not effectively. Optimizations of

these reactions are still in progress with phenyl substituted ethinylesterdiol dioxasilinane and with other dioxasilinanes from the substrate table.

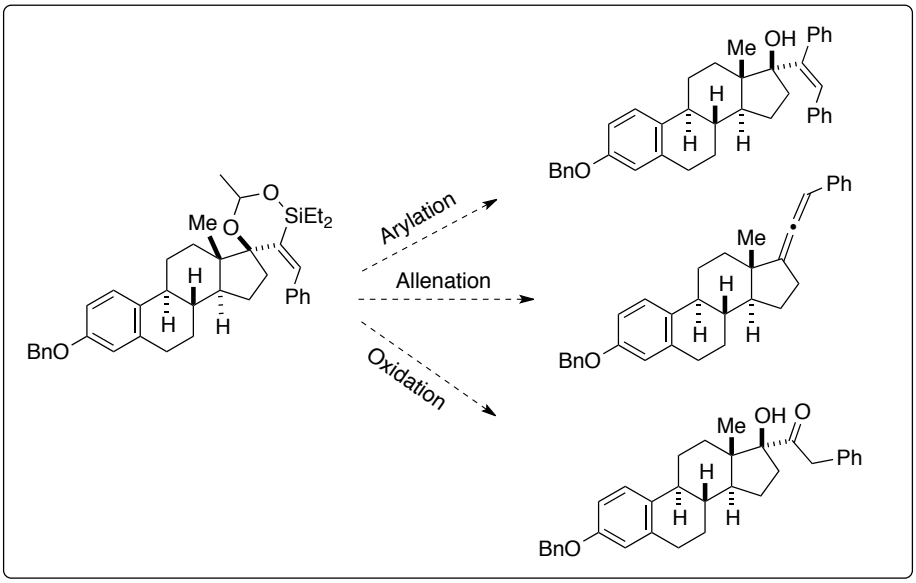

Figure 1.37 Derivitization of phenyl-substituted ethinylesterdiol

1.27 Summary of chapter one

In summary, design and synthesis of the traceless acetal-directing group for highly regio- and stereoselective catalytic hydrosilylation of propargyl alcohols to produce hydroxy *(E)*-vinylsilanes via dioxasilinanes has been demonstrated. Steric and electronic impacts of hydrosilyl acetals on the cyclization were investigated in terms of reactivity and regioselectivity. This catalytic protocol exhibited a reasonably wide scope, and the strategy was applied to efficient syntheses of conjugated bis-silyl 1,3-diene and 1,3-enyne. The versatility of this method was demonstrated in a complex molecular setting of phenyl substituted-17α-ethynylestradiol acetate to furnish α-vinylsilane containing estradiol.

Chapter 2

Alkali Metal Lewis Base-Catalyzed, Complexation-Induced Hydrogen Atom Transfer (LBCI-HAT) Olefin Polymerization

2.1 Introduction

Polymers are versatile materials composed of repeating structural units forming a macromolecule. Polymer industry is a multi-billion-dollar business, and still growing at a rate faster than most other industries. In the past decade, polymers have not only got industrial attention but also gained academic interest. Based on their origin major class of polymers are natural polymers and synthetic polymers. Synthetic polymers have a wide range of practical applications[54] from consumer plastics, automobile components, drug delivery devices and electronics for daily life to biomedical and materials research for future.

2.2 Living free radical polymerization (LRP)

Based on the mechanism of polymerization is classified to ionic polymerization and free radical polymerization. About 50% of the world production of polymers is based on free-radical polymerization, which is widely used because it is a robust process, able to produce a range of material with unique functions. Living free radical polymerization is one of the most widely used polymerization processes in both academic and industrial research laboratories. This successful adoption of LRP is due to the fact that LRP systems combine simplicity of preparation and versatile capabilities for macromolecular engineering. However, polymers obtained via radical polymerization techniques are highly variable, as the radical reaction can undergo a number of side reactions with side products clearly represent a waste of the raw material. Free-radical polymerization is a process in which the propagating species is a long-chain free radical, usually initiated by the attack of free radicals derived from unstable materials called initiators. Free-radical polymerization is a process in which the propagating species is a long-chain free radical, usually initiated by the attack of free radicals derived from unstable materials called initiators. A

living radical polymerization (LRP) is a free-radical polymerization that aims at displaying living character—that is, it does not terminate or transfer and is able to continue polymerization once the initial feed is exhausted by addition of more monomer. However, termination reactions are inherent to a radical process, and modern LRP techniques seek to minimize such reactions, therefore providing control over the molecular weight and the molecular weight distribution of a polymeric material. Furthermore, the better LRP techniques incorporate many of the desirable features of traditional free-radical polymerization, such as compatibility with a wide range of monomers, tolerance of many functionalities, and facile reaction conditions. The control of molecular weight and molecular weight distribution has enabled access to complex architectures and site-specific functionality that were previously impossible to achieve via free-radical polymerization. The major LRP techniques include nitroxide-mediated polymerization (NMP), reversible addition-fragmentation transfer polymerization (RAFT) and atom-transfer radical polymerization (ATRP).

2.3 Atom-transfer radical polymerization (ATRP)

Conventional free-radical polymerization is a very useful method for large-scale production of a variety of polymers. More than 70% of the vinyl polymers have been industrially produced by free-radical polymerization. Conventional free-radical polymerization has a problem of controlling the molecular weight and polydispersity of the polymer. Unlike ionic polymerization, interaction between radical chains is very fast, and one chain easily reacts with other growing chains. Thus, unwanted chain termination occurs, causing polymers with very broad polydispersity with uncontrolled molecular weights to be obtained. ATRP allows the synthesis of well-defined (co)polymers with controlled degrees of polymerization (DPs), molecular weight distributions, functionality, microstructures, and architectures.

2.4 Background of LBCI-HAT-radical olefin polymerization

2.4.1 Hydrogen atom transfer (HAT)

Hydrogen atom transfer (HAT) is one of the most fundamentally important chemical processes in chemistry and biology.[55,56] Hydrogen atom transfer (HAT) is a process where two elemental particles, a proton and an electron undergo concerted migration from a donor to acceptor molecule. Stereo-selective and regio-selective catalytic processes have been explored using transition metal catalysts (e.g., Co, Mn, Fe) [55,57,58] and in the active sites of metalloenzymes (e.g., cytochrome P450s and non-heme Fe and Cu oxidases).[59,60] However, the shortcoming of the transition metal catalyst is being toxic and expensive reagent.[61-63] In chemical synthesis, HAT is closely related to free radical chemistry, often called hydrogen atom abstraction, and typically involves in the termination step of radical reactions between group 14 metal(oid) hydrides and carbon-centered radicals.[61] Especially, First-row transition metal hydrides bearing relatively weak metal-hydride (M–H) bonds (ca. 40-70 kcal/mol) allow a facile generation of carbon-centered radicals from olefins by HAT.[64,65] Despite substantial advances in this field, the wide and sustainable application of current thermal radical chemistry are hindered by the need for a stoichiometric amount of toxic reducing agents (e.g., organotin hydrides), excess solvent, and operational inconvenience.

Organosilicon hydrides have displayed an impressive range of applications, including hydrogen storage source,[66] silicon-based materials,[67] biomedically relevant agents, [54] and medical applications.[55] An inexpensive, environmentally benign alternative to generate more sustainable hydrogen source is organosilicon hydrides. Usage of organo silicon hydrides for HAT eliminates the limitations associated with transition metal hydrides.

2.4.2 LBCI-HAT polymerization

Lewis base catalysts have been recently developed as an efficient catalysts for HAT processes.[68,69] Besides being inexpensive, nontoxic and sustainable non-precious metal Lewis base complexes have been reported as HAT source affinity catalysts.[70] Recent studies have reported hypercoordinate hydridosilicon species for Lewis-catalyst cross-dehydrogenative C–H silylation of heteroarenes. Among them, the most recent study, Hydrogen atom transfer studies via Lewis base-catalyzed, complexation-induced HAT (LBCI-HAT) from pentacoordinate hydridosilicate species, has been reported.[71-75] This study concerns a redox-neutral process, which focuses on hydrogen atom transfer from pentacoordinate hydridosilicate species to unsaturated moieties via LBCI-HAT. However, the mechanism and kinetics for this process is currently unclear.

2.5 Our approach of LBCI-HAT radical olefin polymerization

A desirable synthetic method would be to use inexpensive and environmentally benign reagents and operationally simple techniques for producing high-value chemicals in a selective manner. This need for the design of sustainable materials, from production to disposal, is counterbalanced by the ever-increasing requirements for polymer products to have well-defined properties, structures and functionalities to serve modern applications.

A sustainable Lewis base (LB)-catalyzed, complexation-induced hydrogen atom transfer (LBCI-HAT) olefin polymerization is developed utilizing alkali metal lewis base catalyst. This catalytic process exploits organosilicon hydrides and readily available earth abundant, alkali metals base catalysts to yield styrene polymerization in a highly selective manner. This approach proceeds via unexplored HAT providing a variety of polystyrene polymers bearing silane-end group. LBCI-HAT-radical polymerization technique provides new routes for polymer synthesis

and polymer post-functionalization. This system utilizes earth abundant alkali metal Lewis base catalyst as radical initiators for HAT instead of use of transition metals. This method demonstrated the kinetics of radical polymerization under mild reaction conditions. Substituted styrenes varying electron-withdrawing and electron-donating substitutents, crown ethers, metal and ligand effect on Lewis base are studied.

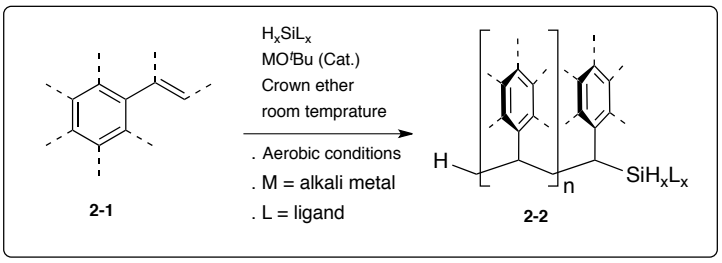

Figure 2.1 LBCI-HAT polymerization

2.6 Preliminary studies

2.6a Initial results for LBCI-HAT polymerization

In previous research from our group,[75] the LBCI-HAT-radical polymerization of para-substituted styrene with electron-withdrawing group (4-chlorostyrene, **2-1a**) spontaneously underwent complete conversion to provide polymer readily in presence of potassium tert-butoxide and hydrosilane. While that with electron-donating groups (4-methoxystyrene, **2-1b**) did not readily proceed to polymerization. This is consistent with previous studies in the literature, where the controlled radical polymerization reactions (e.g., ATRP) of electron-donating group containing vinylarenes show a substantially slower polymerization rate than that with electron-withdrawing group containing vinylarenes.

Initial results for LBCI-HAT-initiated polymerization of 4-Chlorostyrene(**2-1a)** provided the polystyrenes **2-2a** (M_n 27,600; PDI 2.64) in complete conversion (Figure 2.2). The more

exiting result was that an addition of 18-crown-6 (10 mol%) permitted the polymerization of 4-methoxystrene (**2-1b)** to afford **2-2b** (M_n 10,400; PDI 1.46) in complete conversion (Figure 2.2). Polydispersity index (PDI) is used as a measure of breadth of molecular weight distribution. PDI is defined as M_w/M_n where M_w and M_n are weight average and number average molecular weights repectively. Polymer sample with higher PDI is believed to have broader molecular weight distribution. Electron-withdrawing group containing vinylarenes can have broader molecular weight distribution, similar to polystyrenes **2-2a.**

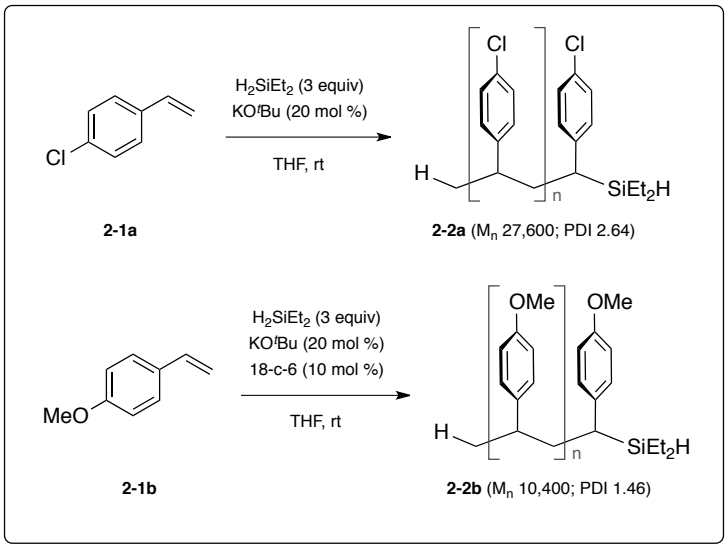

Figure 2.2 Preliminary results

2.6b Effect of concentration on polymerization

Furthermore, effect of concentration of hydrosilane and KO*t*Bu on polymerization (Mn, Mw and PDI) was examined and preliminary results suggest that the by lowering the Lewis base concentration, narrower PDIs can be obtained. Effect of silane concentration changes was minimal. (Figure 2.3)

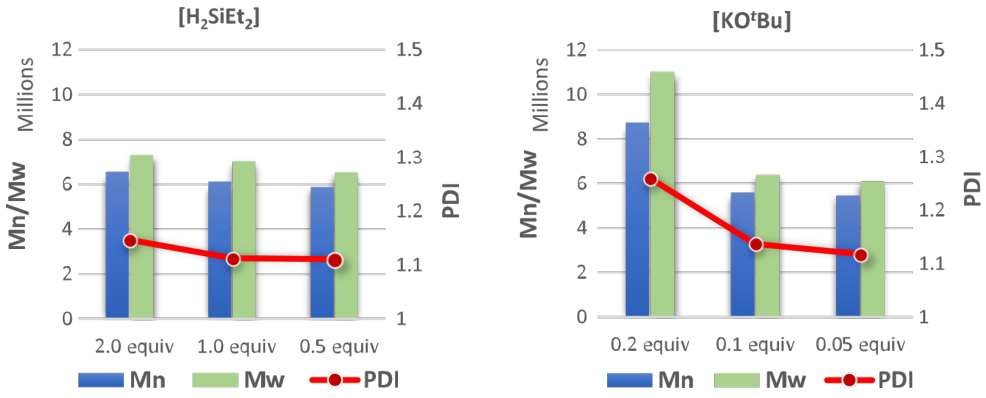

Figure 2.3 Effect of concentration on polymerization

2.7 Substrate scope for LBCI-HAT polymerization

LBCI-HAT-radical polymerization is studied with structurally diverse styrenes. Polymers are successfully synthesized from various styrenes varying the substituents with electron-rich, electron-neutral and electron-poor substituents.

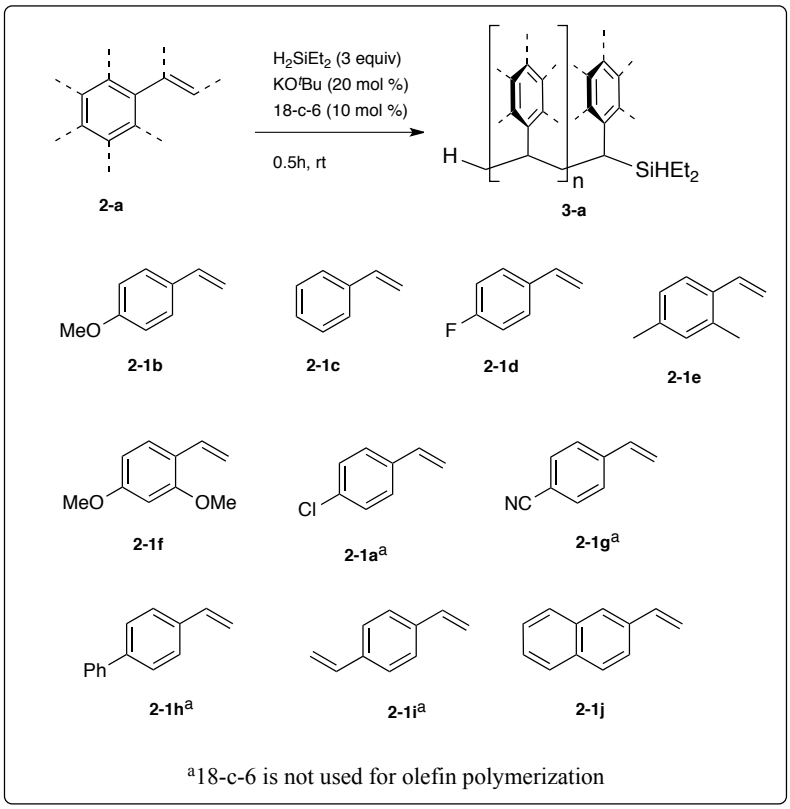

Figure 2.4 Substrate scope for LBCI-HAT polymerization

Electron-poor styrene substrates (**2-1a, 2-1g to 2-1i)** readily polymerized in the presence of hydrosilane and KO*t*Bu. Electron-neutral styrene substrates and electron-rich styrene substrates (**2-1b to 2-1f, 2-1j)** polymerized with addition of 18-crown-6 along with hydrosilane and KO*t*Bu. Polymers

2.8 Failed substrates for LBCI-HAT polymerization

LBCI-HAT-initiated polymerization studied on vinyl pyridine substrates (**2-1k, 2-1l)** and internal alkynes (**2-1m, 2-1n)** was not successful. Polymers are not observed even with the addition of 18-crown-6. Increasing the amount of KO*t*Bu from catalytic amount (20 mol%) to stoichiometric amount (1 equivalent) was not helpful to provide polymers. Attempt of increasing the temperature (room temperature to 100 °C) and decreasing/increasing the concentration of the reaction did not succeed in providing the polymers.

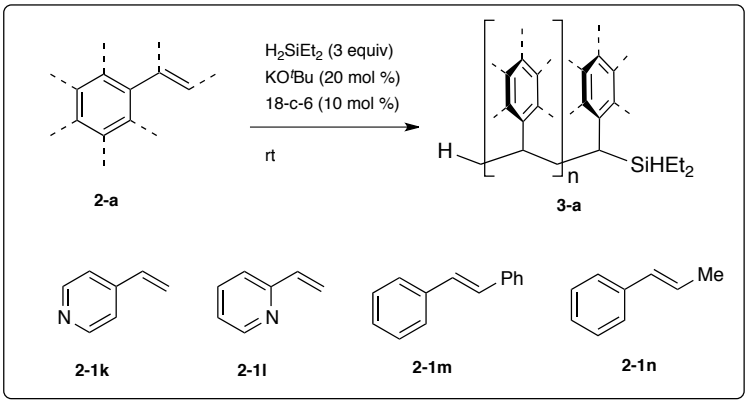

Figure 2.5 Failed substrates for LBCI-HAT polymerization

2.9 Scope of copolymerization in LBCI-HAT polymerization

LBCI-HAT olefin polymerization is susceptible of generating various types of polystyrene polymers. To determine the extent of copolymerization in LBCI-HAT olefin polymerization, a mixture of substituted styrenes (**2-1o, 2-1r)** are tested. Mixture of styrenes in 1:1 ratio is tested for copolymerization with and without 18-crown-6. Combinations of electron-

rich styrene and electron-poor styrenes are considered to envision the reaction mechanism in detail. The main purpose of this study is to study if the generated radical from readily polymerizable substrate like 4-chlorostyrene will be able to initiate the other substrate or not. Reaction kinetics study on copolymers generated is under progress.

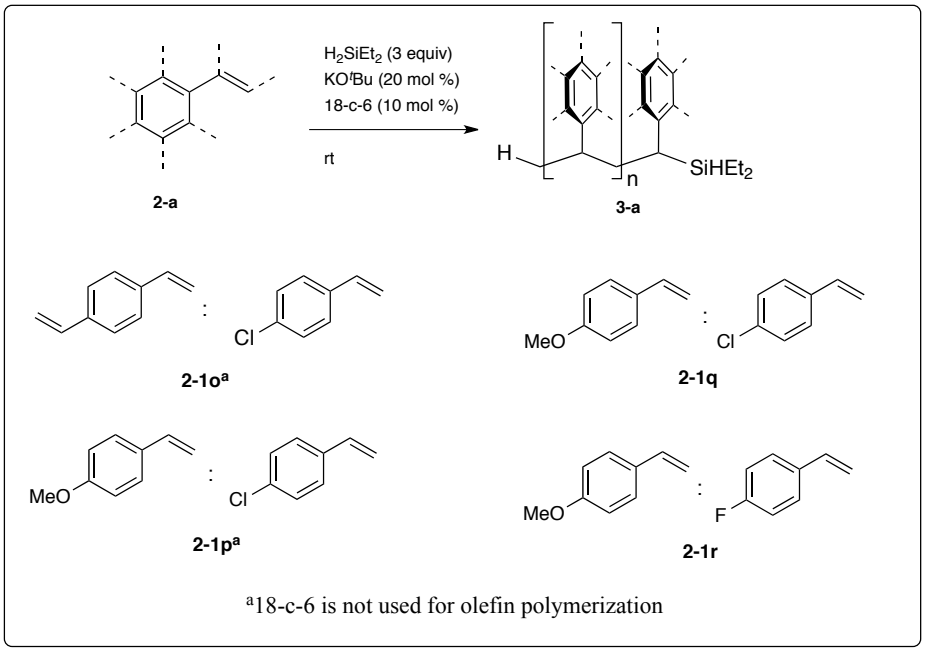

Figure 2.6 Copolymerization scope for LBCI-HAT polymerization

2.10 Conceptual mechanism for LBCI-HAT radical olefin polymerization

Mechanism of LBCI-HAT radical olefin polymerization is proposed. a) In the first step assembly of HAT-initiator is takes place by reversible addition of 18-crown-6 ether-coordinated potassiated Lewis base onto hydrosilane $\mathbf{Si^{H}}$ forming penta-coordinated hydridosilicon species (**I**). Penta-coordinated hydridosilicon species (**I**) can fragment to liberate a new, 18-crown-6 ether-coordinated potassium hydride and can form a new silane $\mathbf{Si^{LB}}$. Formation of penta-coordinated hydridosilicon species was observed in previous research.[75] Generation of new silane $\mathbf{Si^{LB}}$ is considered as a pre-equilibrium process of assembling the HAT-initiator. b) LBCI-HAT

initiation step proceeds via addition of styrene substrate to penta-coordinated hydridosilicon species (**I**). HAT is facilated by styrene dual π-M and n-M donor (substrate)/acceptor (pentacoordinate silicate) interaction. This interaction permits LBCI-HAT to form an initial radical-radical anion pair **2.** Modes of substrate-hypercoordinate silicate interaction, anatomy of polarized Si–H bond cleavage and the donor (substrate)/acceptor (pentacoordinate silicate) interaction dictates the ligand transfer of metal pentacoordinate silicate to give the intimate radical–radical anion pair **2.** c) Initial radical-radical anion pair **2** can be in equilibrium to form benzylic radical **pm**$^{\cdot}$, silyl radical **Si**$^{\cdot}$ and **K[(18-c-6)]LB.** The new radical **pm**$^{\cdot}$ initiates polymerization by reacting with mononers forming **pn**$^{\cdot}$ and then with silyl radical **Si**$^{\cdot}$ forming radical **p1**$^{\cdot}$ with silane end group. Radical **p1**$^{\cdot}$ further reinitiates by reacting with mononers and propagates further forming silane end group **p2**$^{\cdot}$ d) termination and regeneration of catalyst is the last step for any polymerization reactions. Termination can proceed via combination of two **pn**$^{\cdot}$ radicals or via two **p2**$^{\cdot}$ radicals or a combination of **pn**$^{\cdot}$ radical and **p2**$^{\cdot}$ radical. Combination of **pn**$^{\cdot}$ radicals provide the polymer **3** having one functionalizable silane end group whereas combination of **p2**$^{\cdot}$ radicals generate the polymer **4** having two functionalizable silane end groups. Investigations to prove this mechanism are under progress. From the identification of end groups as silane end groups the conceptual mechanism would have proof/evidence.

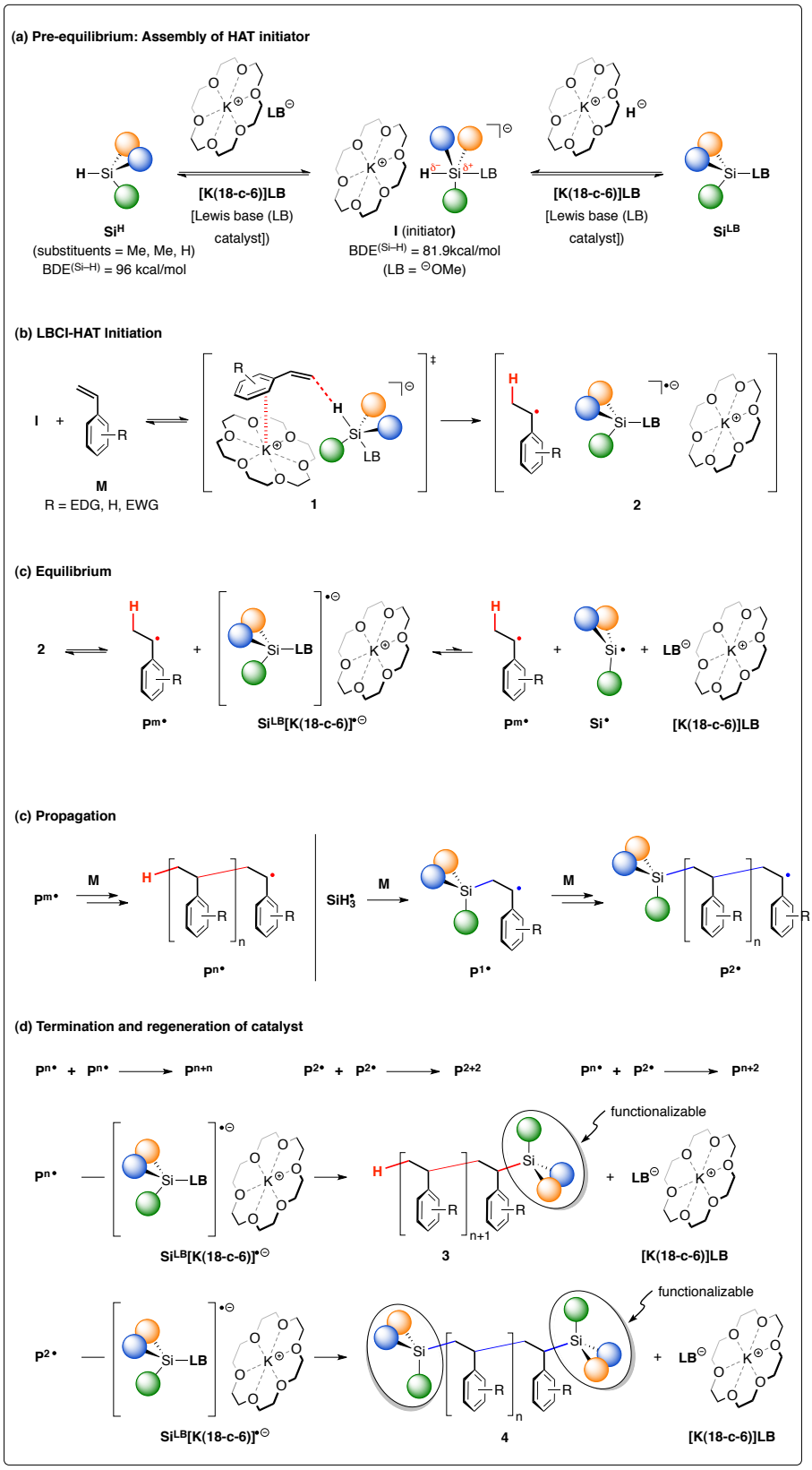

Figure 2.7 Conceptual mechanism of LBCI-HAT radical polymerization

2.11 Kinetic study of LBCI-HAT

To provide insight towards the LBCI-HAT radical polymerization strategy various kinetic studies are performed. Various factors such as substituents on styrene, silane ligand effect, crown ether effect (18-c-6, 15-c-5 and 12-c-4), metal cation effects (KO^{t}Bu and LiO^{t}Bu) were investigated. Initial optimization with 4-methoxtstyrene and styrene as model substrates provided the insight on olefin polymerization.[74] Metal cations played crucial role in LBCI-HAT radical polymerization pathway. Rate of polymerization is clearly enhanced with the KO^{t}Bu as lewis base and the reaction kinetics are further explored by calculating first-order kinetics for monomer conversion. In association with potassium tertiary butoxide as the base, coordinating ligand crown ether 18-c-6 clearly standed out and other crown ether effects are studied.

2.12 FT-NIR studies of LBCI-HAT

LBCI-HAT radical polymerization kinetic behavior of vinylarenes under different conditions was followed by in situ FT-NIR (fourier transform near-infrared) spectroscopy. FT-NIR spectroscopy allows the time-resolved measurement of styrene monomer conversion in radical polymerization. FT-NIR has proven to be an efficient characterization method for real-time monitoring of monomer conversion[81-84]. Spectrum was characterized by the disappearance of the signal at 6133 cm^{-1} and 6136 cm^{-1}, corresponding to carbon-carbon double bond (C=C) stretching vibration of 4-methoxystyrene and styrene vinyl groups respectively, which confirms a successful polymerization. When converting from monomer to polymer, it was confirmed that the intensity of certain peaks is decreased or disappearance with time depending on the monomer. This proved that the polymerization was successful and showed how the key factor variations effect the polymerization. The conversion of monomer was determined via FT-NIR from the integration of the IR signal between 6050-6250 cm^{-1} originating from the C=C double

bond stretching of vinyl groups. The intensity of styrene was monitored via, the NIR absorption at 6136 cm^{-1} whereas for 4-methoxy styrene NIR absorption at 6133 cm^{-1} was monitored.

The values of log natural of ($[M_0]/[M_t]$) {M_0 is initial concentration, M_t is concentration at a given time} against time, obtained by linear fitting of the first order kinetic plots of monomer with NIR specific peak intensity. First-order kinetic plots of ln ($[M_0]/[M_t]$) vs time for LBCI-HAT radical polymerization were investigated under the same conditions. Conversions and first-order kinetic plots were calculated through equations 1 and 2.

$$\text{Conversion yield (\%)}: \frac{I_0 - I_t}{I_0} \times 100\ (\%) \tag{1}$$

$$\ln\ ([M_0]/[M_t]): \ln \frac{I_0}{I_t} \tag{2}$$

Where I is the intensity at a specific peak according to vinylarene. I_0 is initial intensity and I_t is intensity value over time, which is an important experimental parameter commonly used to prove the monomer conversion of polymerization.

2.13 Vinyl arene substituent and crown ether effects on LBCI-HAT

The rate of polymerization varies depending on whether the substituent on vinyl arene is an electron-donating or electron-withdrawing group. Conversion graphs and first-order kinetic plots of ln ($[M_0]/[M_t]$) vs time for LBCI-HAT radical polymerization of two samples styrene and 4-methoxy styrene were studied and displayed in figure 2.8. The results clearly demonstrate the importance of crown ether presence in the LBCI-HAT radical polymerization (Figure 2.8c, d). A relatively fast polymerization was observed in the presence of crown ether (Figure 2.8c, d). Crown ether acted as a cage to hold the metal cation. Comparison of first order plots of 4-methoxystyrene with styrene showed slower kinetics for the LBCI-HAT to that of styrene

(Figure 2.8a, b). EDG-substituted styrene undergoes polymerization at a slower rate than compared to that of un-substituted styrene.

4-Methoxystyrene's slower polymerization rate can be attributed to active species in the LBCI-HAT system. Presence of para methoxy group on styrene favors the dissociation of C=C bond at the propagating end owing to its electron-donating effect, leading to the formation of the active species in the LBCI-HAT system, which resulted in slow polymerization. A presence of EDG on styrene increases the bond dissociation energy of the carbon-carbon bond at the propagating chain end of styrene, as a result slowing the polymerization.

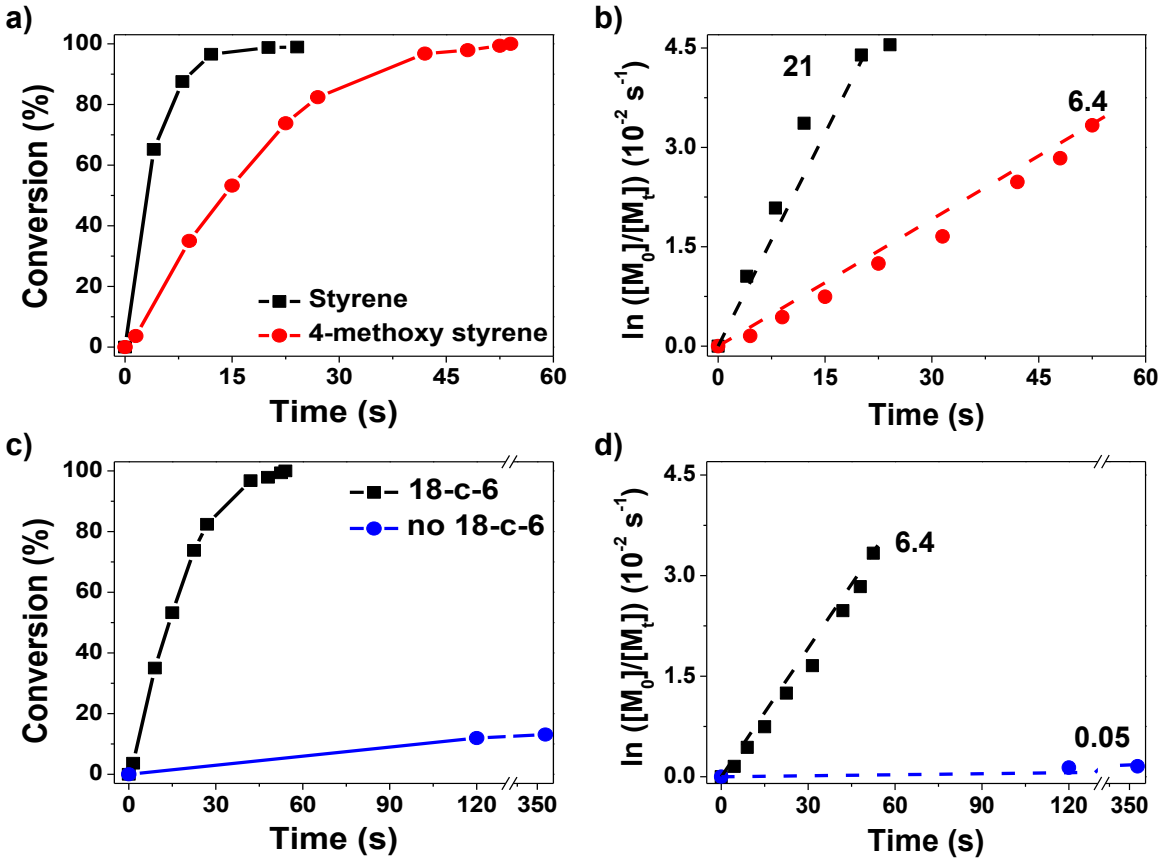

Different substituents on styrene plot for (a, b) styrene and 4-methoxystyrene, and (c, d) crown effect for 4-methoxystyrene: (a, c) Conversion plot, and (b,d) First-order kinetic plots of ln ($[M_0]/[M_t]$) vs time for polymerization at 25 °C with the different conditions, the peak is between 6133 and 6136 cm^{-1} corresponding to C=C double bond stretching vibration of styrene vinyl group.

Figure 2.8 Vinylarene substituent effect and crown ether effect on LBCI-HAT

2.14 Crown ether effect with ethylsilane on LBCI-HAT

Presence of crown ether 18-c-6 having substantial effect on LBCI-HAT olefin polymerization is observed (Figure 2.8c, d). Then conversion and first-order kinetic plots of ln ($[M_0]/[M_t]$) vs time for LBCI-HAT radical polymerization plots for different crown ethers at identical concentrations (18-c-6, 15-c-5, 12-c-4) obtained through FT-NIR peak analysis. Effect of crown ether with diethylsilane on rate of polymerization is observed to be 18-c-6>15-c-5>12-c-4 (Figure 2.9a, b). Effect of crown ether with triethylsilane on rate of polymerization is observed to be 18-c-6>15-c-5=12-c-4. When 18-c-6 was used with triethylsilane in the polymerization, the polymerization rate was higher than that of other crown ethers. When 15-c-5 was used, triethylsilane did not undergo styrene polymerization.

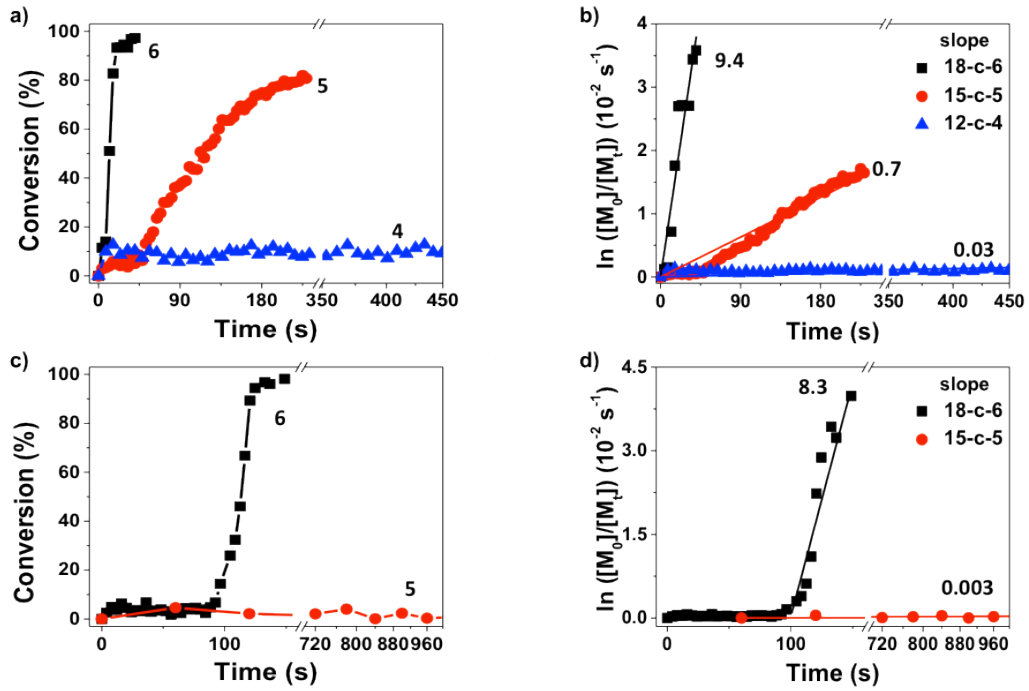

Polymerization of styrene using ethyl-silane with different crown ether for (a, b) H_2SiEt_2, and (c, d) $HSiEt_3$: (a, c) Conversion plot, and (b,d) First-order kinetic plots of ln ($[M_0]/[M_t]$) vs Time for polymerization at 25 °C with the different conditions, the peak is between 6136 cm^{-1} corresponding to C=C double bond stretching vibration of styrene vinyl group.

Figure 2.9 Crown ether effect with ethylsilane on LBCI-HAT

In case of 12-c-4, the ethyl group ligand was not polymerized. However, for triethylsilane, there was no significant change peak from 15-c-5, displayed in Figure 2.9c-d. The polymerization using triethylsilane (Figure 2.9c, d) has induction period (0–95s) in the beginning phase of the reaction due to evolution of hydrogen. This induction period has a variety of factors (catalyst loading, solvent, additives, and moisture, etc.). In particular, H_2 formation is associated with trace water consumption or radical initiation processes.[10] Nevertheless, the triethylsilane showed excellent reproducibility under the same conditions.

2.15 Crown ether effect with phenylsilane on LBCI-HAT

Conversion and first-order kinetic plots of ln ($[M_0]/[M_t]$) vs time for LBCI-HAT radical polymerization plots of styrene with different crown ethers (18-c-6, 15-c-5, 12-c-4) in combination of phenylsilanes are obtained through FT-NIR peak analysis. Effect of crown ether with phenylsilanes on rate of polymerization is observed with phenylsilane, diphenylsilane and triphenylsilane. Compared with the ethylsilane, the phenyl silane was relatively slow in polymerization rate in the presence of crown ether. Phenyl silane as a whole, was relatively well polymerized at 18-c-6 and 15-c-5, and showed little polymerization at 12-c-4 (Figure 2.10). Monophenyl silane polymerized faster with 18-c-6 than with15-c-5 (Figure 2.10a, b). Diphenyl silane polymerized with the order as follows18-c-6>15-c-5>12-c-4 (Figure 2.10c, d). Triphenylsilane with crown ethers has almost no polymerization effect (10–20%) (Figure 2.10e, f). Triphenyl silane low polymerization can be attributed to its bulkiness.

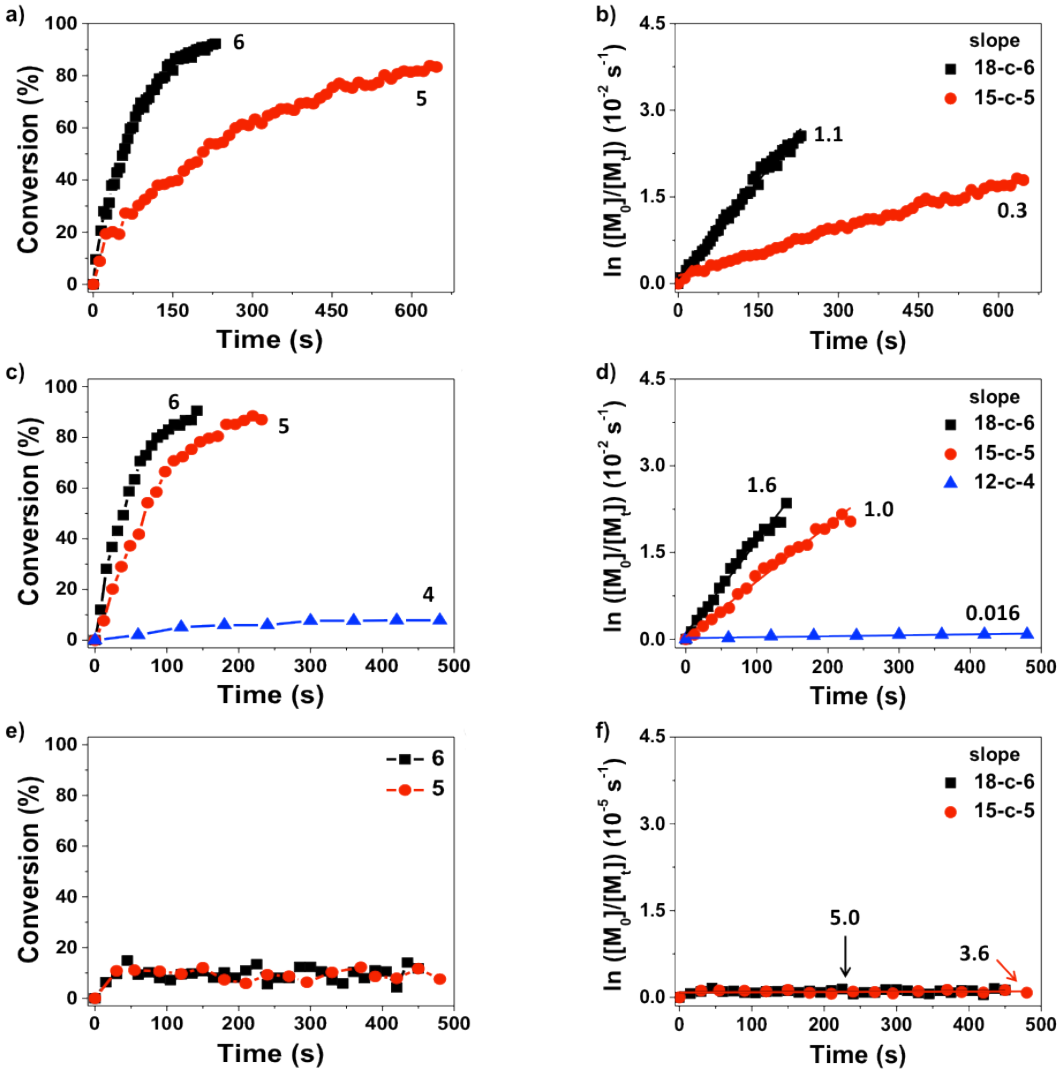

Polymerization of styrene using phenyl-silane with different crown ether for (a, b) H_3SiPh_1, (c, d) H_2SiPh_2, and (e, f) $HSiPh_3$: (a, c, e) Conversion plot, and (b, d, f) First-order kinetic plots of ln ($[M_0]/[M_t]$) vs Time for polymerization at 25 °C with the different conditions, the peak is between λ= 6136 cm^{-1} corresponding to C=C double bond stretching vibration of styrene vinyl group.

Figure 2.10 Crown ether effect with phenylsilane on LBCI-HAT

2.16 Kinetics of silane-ligand on LBCI-HAT radical polymerization

The ligand on silane in the LBCI-HAT radical polymerization system plays an important role. The ligand on silane affects in Si–H binding capacity that alters the electron density, resulting the bond dissociation energy to be weak or strong. Ligand effect of silane using ethyl and phenyl functional groups in combination with crown ethers is studied. The ethyl group is more reactive than the phenyl group, and phenyl is richer in electrons and bulky than the ethyl

group. Figure 2.11 displays conversion graphs for polymerization for the five samples, H_2SiEt_2, $HSiEt_3$, H_3SiPh_1, H_2SiPh_2, and $HSiPh_3$, obtained through FT-NIR peak analysis. First-order kinetic plots of ln ($[M_0]/[M_t]$) vs time for polymerization are also plotted in figure 2.11, clearly showing the polymerization rate.

With 18-c-6 the order of polymerization is observed to be H_2SiEt_2>$HSiEt_3$> H_3SiPh_2>H_2SiPh_1>$HSiPh_3$ (Figure 2.11a, b). When comparing the ligand effect of silanes (Figure 2.11a, b), the ethyl group showed faster polymerization rate than the phenyl group, and the graph also showed a sharp shape proved that the polymerization rate was fast. For diphenylsilane, which expected to be less polymerized than phenylsilane, polymerized faster than phenylsilane. This effect might be due to the structural stability; structural effect is superior that competition occurs. It is relatively structurally stable compared to other ligands, and thus breaks down Si–H bonds easily, resulting in rapid polymerization.

With 15-c-5 the order of polymerization rate is observed to be H_3SiPh_2>H_2SiEt_2> H_2SiPh_1>$HSiPh_3$> $HSiEt_3$(Figure 2.11c, d). It is important to note that the diphenylsilane was found to be unusual. Further confirmation of this behavior testing is under progress. The conversion of monohydrosilane ($HSiEt_3$ and $HSiPh_3$) did not change significantly during the polymerization because of relatively slow termination (Figure 2.11c, d). In other words, the degree of in situ cleavage C=C bond stretching of vinyl groups for $HSiEt_3$ and $HSiPh_3$ were significantly smaller than compared to other sample and the contribution of the persistent radical effect was very small.

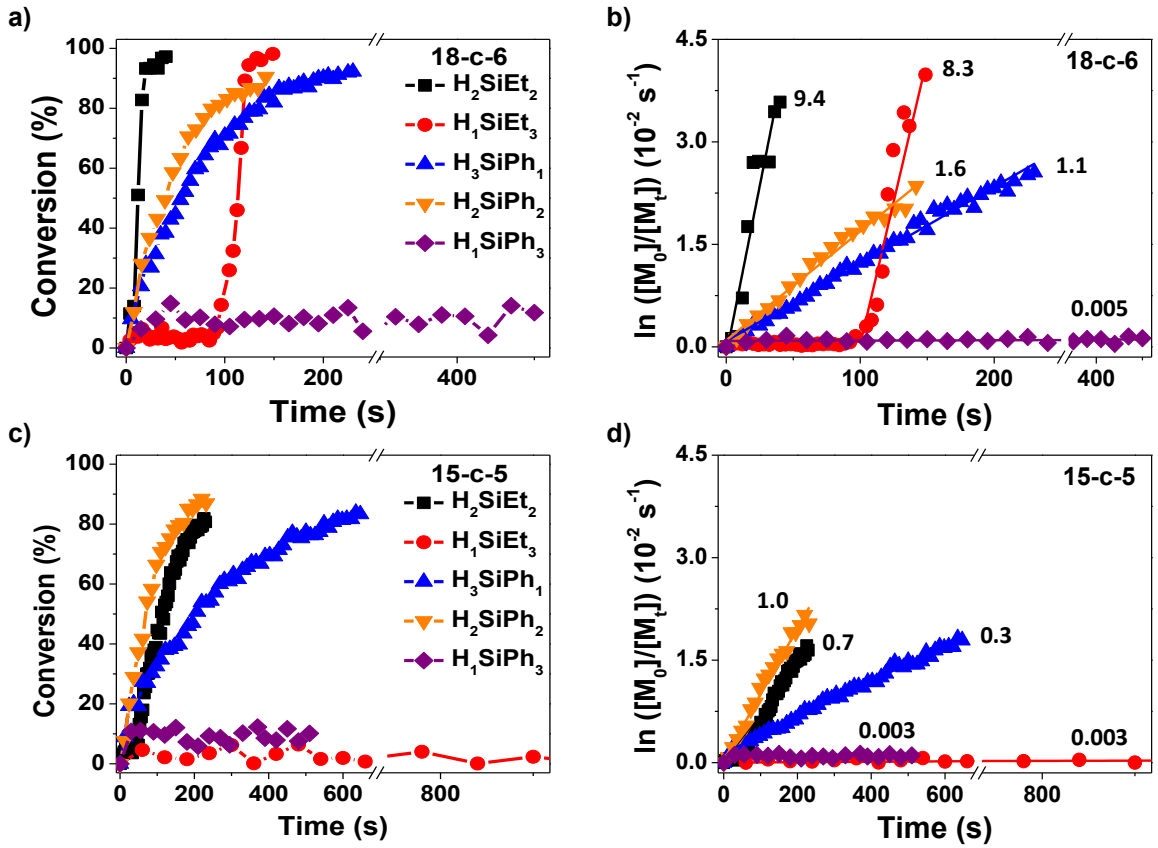

LBCI-HAT polymerization of styrene with different ligand of silane: (a, c) Conversion plot, and (b,d) First-order kinetic plots of ln ($[M_0]/[M_t]$) vs Time for polymerization at 25 °C with the different conditions, the peak is between λ= 6136 cm^{-1} corresponding to C=C double bond stretching vibration of styrene vinyl group.

Figure 2.11 Silane-ligand effect on LBCI-HAT

2.17 Metal cation effect on LBCI-HAT

Metal cations play an important role in facilitating and controlling the reaction pathway for LBCI-HAT radical polymerization. When K^+ (large cation) was used, the reaction rate was faster than that of Li^+, which is a relatively small cation indicating that larger cation promotes the polymerization reaction. Smaller lithium cation was relatively unable to catalyze the reation to the extent of potassium (Figure 2.12, 2.13). These metal cations interacted with crown ether and showed the greatest effect combined with 18-c-6. Conversion plots and first-order kinetic plots of ln ($[M_0]/[M_t]$) vs time for ethylsilanes and phenylsilanes with Li*O*t*Bu are plotted (Figure 2.12, 2.13). In all of the plots (Figure 2.12, 2.13) it is observed that Li*O*t*Bu as a Lewis base is not

effective either with ethylsilanes or phenylsilanes. The rate of polymerization is consisitently low in all the instances.

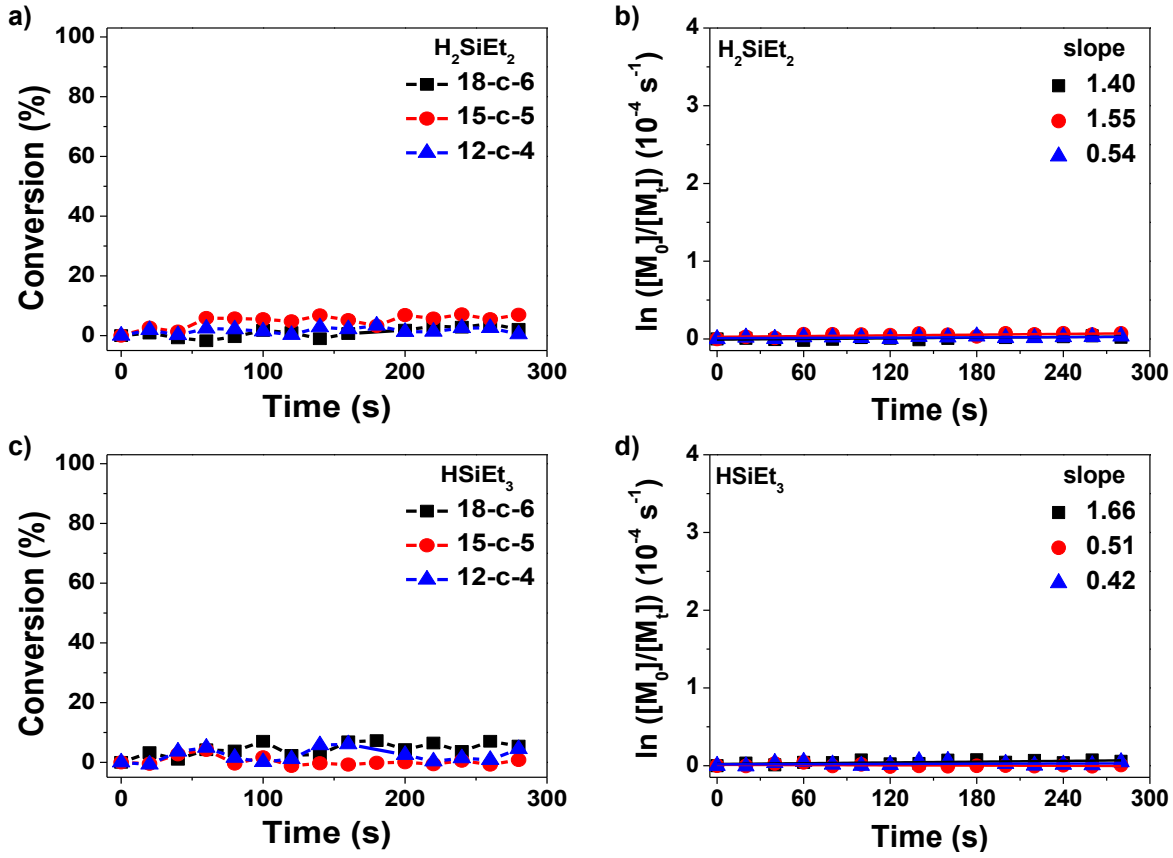

LBCI-HAT polymerization of styrene using Li*O*tBu: (a, c) Conversion plot, and (b, d) First-order kinetic plots of ln ($[M_0]/[M_t]$) vs Time for polymerization at 25 °C with the different conditions, the peak is between λ= 6136 cm^{-1} corresponding to C=C double bond stretching vibration of styrene vinyl group.

Figure 2.12 Metal cation effect with ethylsilane on LBCI-HAT

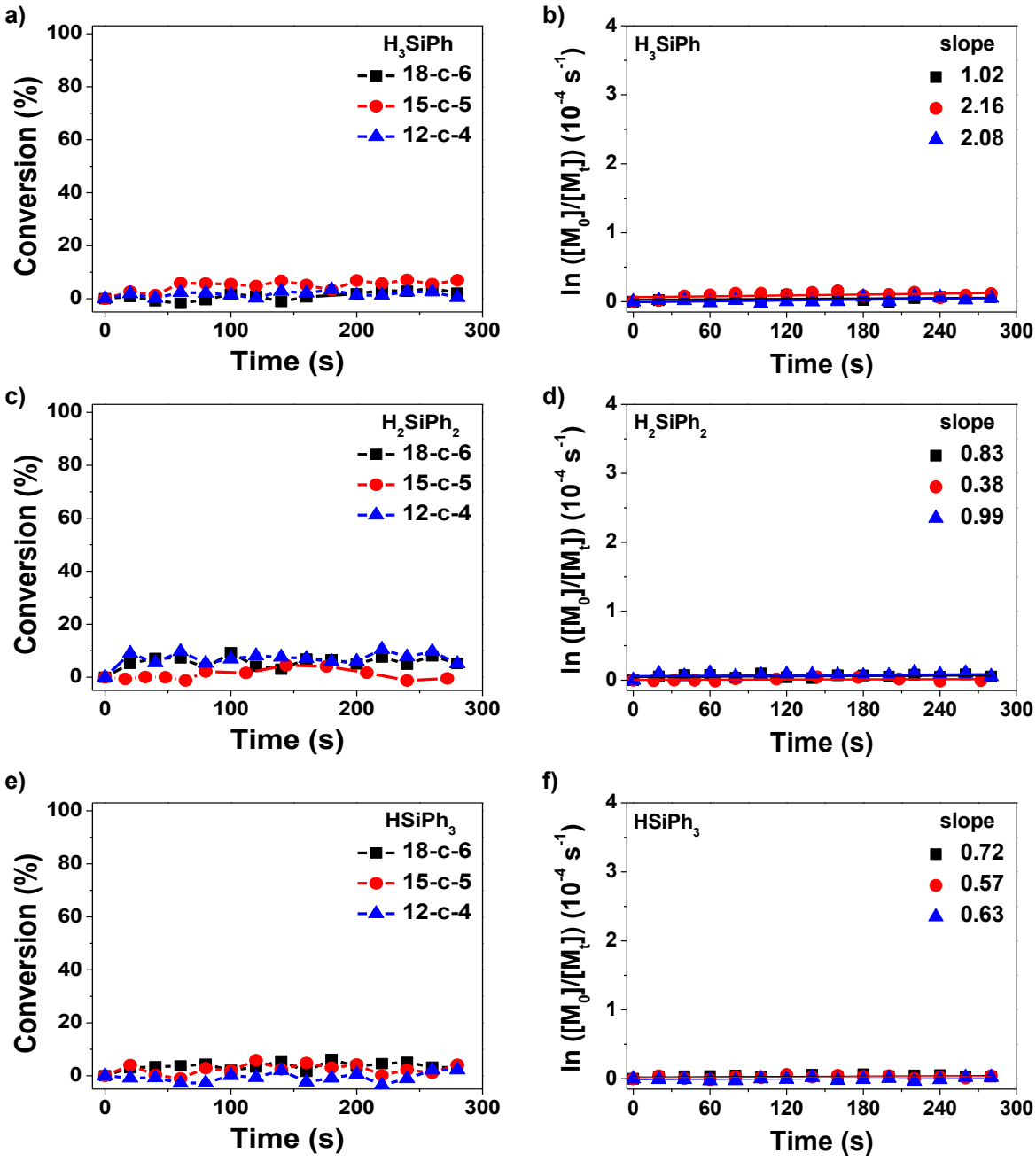

Polymerization of styrene using LiO*t*Bu with phenyl-silane for (a, b) H_3SiPh_1, (c, d) H_2SiPh_2, and (e, f) $HSiPh_3$: (a, c, e) Conversion plot, and (b, d, f) First-order kinetic plots of ln ($[M_0]/[M_t]$) vs Time for polymerization at 25 °C with the different conditions, the peak is between λ= 6136 cm^{-1} corresponding to C=C double bond stretching vibration of styrene vinyl group.

Figure 2.13 Metal cation effect with phenylsilane on LBCI-HAT

2.18 Summary of LBCI-HAT polymerization

This protocol provides a new sustainable catalytic route for olefin polymerization utilizing inexpensive readily available earth abundant alkali metal lewis base catalyst. This study provides the mechanism and kinetic behavior for LBCI-HAT olefin polymerization. This demonstrates the key to radical polymerization of various vinylarene polymers by adjusting and controlling various key factors to investigate and control the polymerization rate. Key factors examined include metal cation effect, crown ether effect, silane-ligand effect and their combinations. The radical polymerization was monitored in real-time via FT-NIR and the values were derived to investigate the kinetics. In real-time the conversion of various styrene monomers to polymers is studied. Investigation of identifying the end groups is under progress, which can be a very important for functional transformation to generate various different polymers containing functionalizable end groups. Furthermore, it is expected that polymerization of block copolymers, crosslink polymers and network polymers can be possible by knowing the ending group.

Chapter 3

On-chip organic synthesis in an electrowetting-on-dielectric digital microfluidic device

- On-chip organic synthesis enabled using an engine-and-cargo system in an electrowetting-on-dielectric digital microfluidic device. Torabinia, M.; Asgari, P., **Dakarapu, U. S**., Jeon, J. Moon, H. *Lab Chip* **2019,** *19*, 3054−3064. https://doi.org/10.1039/C9LC00428A

- In-line organic chemistry workup and solvent-swap in an electrowetting-on-dielectric digital microfluidic device. Torabinia, M.; **Dakarapu, U. S**.; Asgari, P.; Jeon, J., Moon, H. *Anal. Chem.* **2020.** *(Submitted)*

3A. **Engine-and-cargo system in an electrowetting-on-dielectric digital microfluidic device**

3.1 Introduction

Micro-scale chemical reaction technology allows for the precise control of quantified reagents and efficient heat and mass transfer. Because of a large interface-to-volume ratio– particularly in case of the exothermic reaction and mixing, reduced consumption of toxic or expensive agents, improved reaction profiles, and enhanced selectivity compared to macro-scale reactions.[85-87] The first generation of micro-scale chemical reaction processes was initiated by establishing continuous micro-channel flow systems where chemical reactions were carried out. The Lob group[88] performed fluorination of toluene in micro-channel reactors made of silicon, and mono-fluorinated products were obtained with higher yield, compared to a batch system. Miller's group[89] showed rapid formation of amides via carbonylative cross-coupling of aryl halides with benzyl amine using a reaction channel, and the micro-reactions developed allowed higher gains in yields over this time period than conventional batch reactions. Other examples include Suzuki cross-coupling,[90] Wittig olefination reaction,[91] nitration of benzene, and tripeptide synthesis.[92] Despite of successful demonstration from prior studies, micro-channel-based approaches suffer from several limitations. For example, clogging of the channels by products or byproducts may cause the difficulty of maintaining a constant hydrodynamic pressure, thus stable flow. Requirement of complex flow network and cross-contamination due to unwanted diffusion through channels are also concerned. Moreover, solvent-swapping processes pose very challenging problems in micro-channel reactors. Another drawback of micro-channel reactors presents in combinatorial chemistry, a powerful tool for lead compound discovery and optimization of new drugs and materials.[122] Since combinatorial synthesis through either batch or

flow reactors requires as many reactors as the number of all possible combinations of reactants, a reactor system tends to be large.

Electrowetting-on-dielectric (EWOD) digital microfluidic device (DMF) continues to revolutionize Big Pharma and medical device industries and provide pharmaceutical companies an information-driven discovery platform, there is going to be a substantial demand for the development of the fully-automated and unceasing lab-on-chip work cycle. The key to an automated and efficient synthesis is not only the parallel arrangement of reactions but also simple and adaptive workup techniques to bypass energy-consuming and tedious purification steps. A DMF platform using EWOD principle can be an alternative and/or complement a micro-channel reactor. An EWOD digital microfluidic platform eliminates the necessity of predetermined channel network and mechanical pumps and valves. Since it is a droplet-based flow, it can prevent cross-mixing and cross-contamination. Each droplet plays as a batch reactor, which brings the feasibility of performing multi-step reactions that may involve with solvents swapping and combinatorial synthesis.[93-95] While these unique features and advantages of EWOD digital microfluidic device were employed to develop a range of applications for biotechnology protocols,[96] they have not been explored yet to develop organic synthesis platforms. It is attributed that most biological fluids are aqueous solutions of which EWOD microfluidic functionalities (e.g. transporting, merging, mixing, and dispensing) are well established,[95] whereas typical chemical reactions require organic solvents whose EWOD microfluidic functionalities are not well understood yet.

3.2 Background research

The Chatterjee group[97] experimentally assessed the movability of organic solvents and

solutions in the EWOD system. In this study, many organic solvents such as cyclohexane, carbon tetrachloride, chloroform, and toluene cannot be electrically actuated or displaced in EWOD devices. Recently, Torabinia[98] reported an electromechanical model that can predict the movability of a fluid by EWOD device. This study showed that both the magnitude and the frequency of the operation voltage needed to be tuned, to obtain maximum force in an EWOD device. Their model was able to produce the virtually same results as Chatterjee reported.[97] Nevertheless, a couple of efforts were made to operate non-movable fluids in EWOD DMF. Inspired by Brassard,[99] Li's[100] work demonstrated manipulations of oil, organic, and gaseous chemicals in the aqueous shell. However, such configuration fails to host the fluids having a lower surface tension compared to the aqueous solutions. For instance, most of organic solvents have much lower surface tension ($\sim 20\, mNm^{-1}$) than that of water, which does not allow them to be encapsulated in an aqueous shell. In addition, additional capillary tube settings were needed to create core-shell droplets, leading to unfavorable complexities of device design and fabrications. Another approach was to use dielectrophoretic (DEP) force to operate non-movable fluids; Fan[101] reported the manipulation of a silicone oil droplet by DEP force in a typical EWOD device. However, exerting DEP force required extremely higher voltage than the EWOD operation does. In addition, fluids must have some specific dielectric properties to be manipulated by DEP force. In fact, according to Torabinia research most of essential organic solvents for chemical reactions are not movable, even in the range of frequency at which DEP force is dominant. These hindrances limit the scope of possible chemical reactions in EWOD device. As addressing abovementioned challenges, this work introduces a novel strategy of *"engine-and-cargo"* which enables an EWOD device to handle electrically non-responsive fluids such as organic solvents. Since esters are widely popular in plants and animals and have a

broad range of use in industry and pharmaceutical laboratories[102,103] esterification reaction is chosen as a model reaction, and demonstrated the capability of an EWOD device to perform on-chip organic synthesis. Using conversion data obtained from on-chip reactions, studies on characterization and optimization of the reactions were conducted. In addition, as the first step toward combinatorial organic synthesis, parallel esterification reactions of three different types of alcohols were attempted.

3.3 Engine-and-cargo system

An engine-and-cargo system harnesses a compound droplet of two immiscible liquids. An engine refers to the liquid that has the electrowetting properties; a cargo is the other one without electrowetting properties, thus non-movable in an EWOD device. Figure 3.1 shows the formation and operation of an engine-and-cargo system in an EWOD device. In this example, ionic liquid ([bmim]PF_6) works as the engine and toluene is carried as the cargo. As shown in Figure 3.1a, ionic liquid has electrowetting properties so that it moves as response to the applied voltage on electrodes underneath it, whereas toluene stays unresponsive under any magnitude and frequency of voltages.[97] When the ionic liquid droplet approaches to the toluene droplet, it is encapsulated by toluene spontaneously to minimize the surface free energy and forms a compound droplet (Figure 3.1b). Note that surface tension of ionic liquid (~ 40 mN/m) is higher than that of toluene (~ 20 mN/m). Figure 1c illustrates the motion of the engine-and-cargo system, arising from the electrowetting force exerted on the engine that carries the cargo by viscous drag force. Evidently, the designed engine-and-cargo system enables the use of toluene and other non-movable liquids in a typical EWOD device without any modification of device structures or architectures. In the later section of this study, it is reported that all the basic fluidic functions of an EWOD digital microfluidic device including dispensing, transporting, merging,

and splitting of droplets are achieved with electrically non-responsive fluids. This technique has the potential to make substantial advances on biological and chemical protocols processed on EWOD digital microfluidic device.

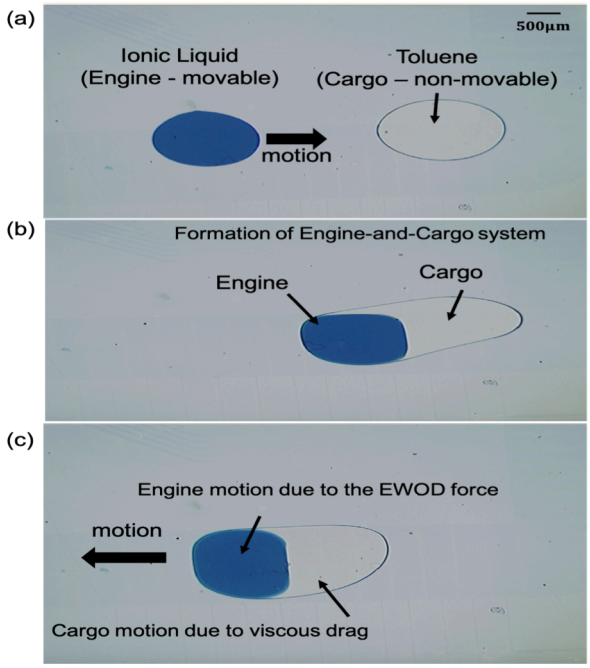

The formation of the engine-and-cargo system of an ionic liquid([bmim]PF_6) as the engine (movable) and toluene as the cargo (non-movable). (a) Actuation of Engine towards the Cargo. (b) Encapsulation and formation of Engine-and-Cargo. (c) the motion of an engine droplet by electrowetting operation leads motion of an entire compound droplet, thus fluidic functionalities of cargo droplet Images from the top view of the EWOD device. Blue dye was added to the ionic liquid for the better visualization purpose only.

Figure 3.1 Formation of engine-and-cargo system

3.4 Esterification Reaction

Esters are one of the most important classes of organic molecules that are widely used in synthesis of fine chemicals, drugs, food preservatives, perfumes, plasticizers, and pharmaceuticals.[104-106] In a biological aspect, acetylation is one of important protein modification methods in cell biology that has an impact on gene expression and metabolism.[107] There are high demands of rapid, simple, and environmentally friendly protocols for the micro-scale

esterification of alcohols for facile production of a wide variety of esters for medicinal and biological applications.[108-109]

In this study, esterification of alcohols with acetic anhydride is chosen as our model reaction to demonstrate the on-chip organic synthesis capabilities of an EWOD digital microfluidic device. Total 60 tests varying different esterification reaction conditions, secondary alcohols substrates, and acetic anhydride were carried out on-chip. The esterification of menthol, one of 13 reactions that we performed in this study is shown in Figure 3.2. A traditional macroscale esterification (e.g., flask-based protocol) involves aliquoting, introducing, and mixing reagents, followed by quenching the reaction at controlled time. Instead, on EWOD chip, generating reagents droplets, transporting, and merging droplets can initiate a reaction, and at the end of the processes merging the reacting droplet with the quenching agent droplet quenches the reaction.

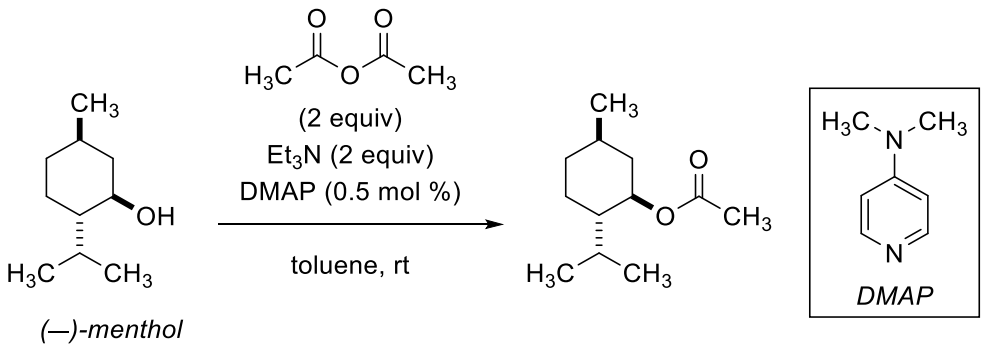

Model esterification reaction using menthol, acetic anhydride (Ac_2O), trimethylamine (Et_3N), and DMAP in the presence of specific solvent. Menthol (5 μmol), Et_3N (10 μmol), and DMAP (0.5 mol %) were dissolved into 1 μL of solvent. Ac_2O (10 μmol) was dissolved in corresponding solvent.

Figure 3.2 Model esterification reaction of menthol

3.5 Experimental data

3.5a Device fabrication and experimental setup

All EWOD microfluidic devices used in this study were fabricated in the Shimadzu Institute Nanotechnology Research Center of the University of Texas at Arlington. Actuation electrodes in the bottom plate of an EWOD device were fabricated by photolithography followed by wet etching of an indium tin oxide (ITO) layer (100 nm) coated on a glass wafer. The dielectric layer (SU-8, 6µm) and the hydrophobic layer (Teflon, 350 nm) were spin-coated and oven baked. The gap between top and bottom plates of devices was kept at 100 µm throughout the entire workflow. The side view schematic of a sandwiched droplet in an EWOD device is shown in Fig.1 (a). The details of the fabrication steps and device assembly can be found in the supplementary material. The EWOD operation voltages were provided by Agilent arbitrary waveform generator and the TEGAM high voltage amplifier (model 23400). Desired sequence of turning on/off electrodes were applied through LabVIEW program. Droplet motions were recorded using Hirox KH-1300 digital microscope system. Later, images were extracted from videos and processed using Editor PIXESTYLE and ImageJ software. Fig. 1(b) shows the experimental setup of an EWOD chip operation.

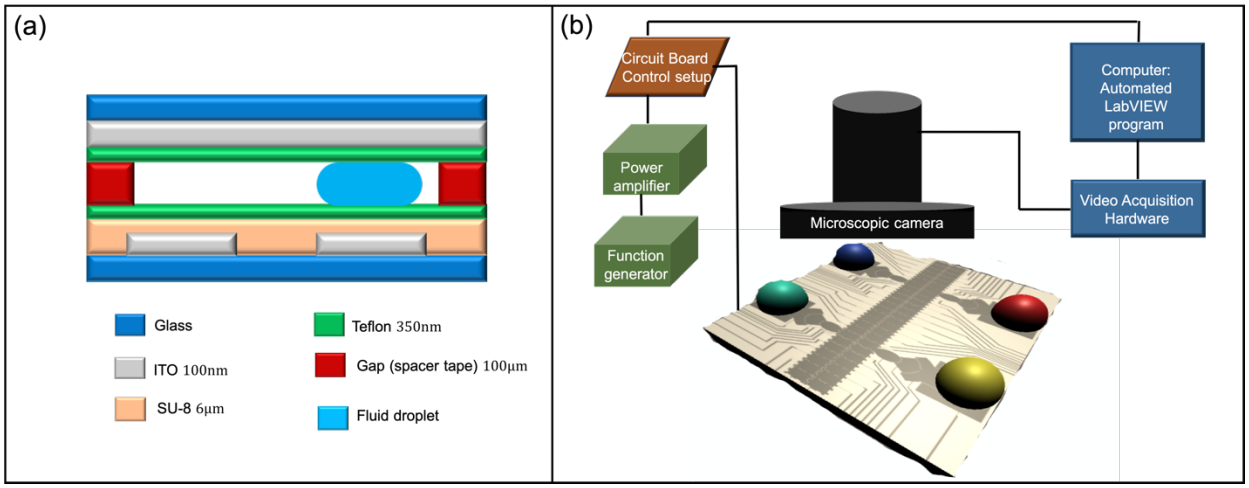

(a) The side view schematic of a sandwiched droplet in an EWOD digital microfluidic device, and the surrounding medium is air all throughout the experiment. (b) The experimental setup of an EWOD chip operation.

Figure 3.3 EWOD digital microfluidic device

3.5b Materials

(–)-Menthol (99%), phenol, ≥99.5% (GC), Benzyl alcohol anhydrous, 99.8%, trimethylamine, acetic anhydride, 4-(dimethylamino) pyridine (DMAP) (≥ 90%) were purchased from SIGMA-ALDRICH (USA). Toluene (Certified ACS), 1,4-dioxane, dimethylformamide, 1,1-dichloroethane (DCE), dichloromethane, (>99.8%) and 1-butyl-3-methylimidazolium hexafluorophosphate ([bmim]PF_6) (98+%) obtained from Fisher Scientific. Assorted food and egg dye purchased form Walmart (USA). All chemicals were analytical grade and used as received. Before each test, reagents were placed in designated reservoirs. Among the esterification reagents listed alcohol (i.e., menthol), trimethylamine, and DMAP were identified as non-movable fluids on the EWOD platform. A solution of these 3 reagents were prepared and placed at 'cargo' reservoir, where they were sitting together with the 'engine' fluid (i.e., ionic liquid). On the other hand, acetic anhydride (acylating reactant) and sodium bicarbonate (quenching agent) are movable in the EWOD platform due to their electrowetting properties, so that they were operated without the help of engine droplets.

3.6 Test Protocols

3.6a Formation of an engine-and-cargo droplet

Each test began with forming an engine-and-cargo compound droplet. Figure 4 shows the sequence of formation of an engine-and-cargo droplet from the reservoir. First, EWOD forces let an engine liquid droplet dispensed from its reservoir puddle (Figure 3.4a,b) while the cargo puddles remained non-responsive to the sequence of activation voltages. As the engine droplet was dispensed and moved further away from the reservoir, cargo solution elongated and created a neck due to the viscous drag force between the engine droplet and the cargo solution (Figure 3.4c). Afterwards, the hydrodynamic instability at the cargo neck eventually let it pinch-off as shown in figure 3.4c, 3.4d. The completely detached droplet from the reservoir was an engine-

and-cargo droplet (Figure 3.4d).

To quantify the volume of dispensed cargo solution, footprint area of cargo is measured using ImageJ software and multiplied the area with the gap between the top and the bottom plates of the EWOD chip (100 μm) to obtain the volume of droplet.

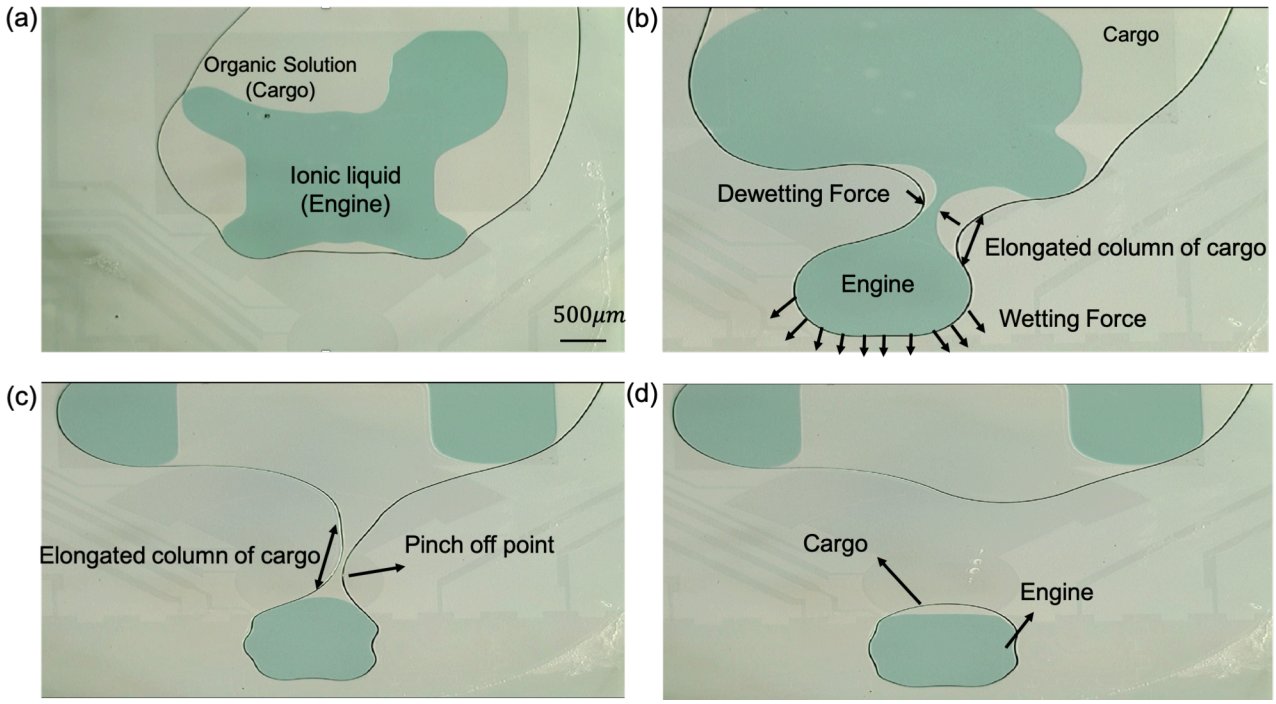

A sequence of formation of an engine-and-cargo system from the reservoir. (a)The initial state, (b) The viscous drag between the engine and cargo fluids stretched the cargo fluid, (c) The engine droplet was dispensed and it pulled the cargo further so that a neck formed in the cargo and the hydrodynamic instability grew, and (d) the cargo neck eventually pinched off and formed an engine-and-cargo system.

Figure 3.4 Engine-and-cargo system formation

3.6b On-chip reactions

General procedure of each on-chip reaction test protocol is summarized in Figures 3.5a-f. First, an engine-and-cargo droplet was dispensed (Figure 3.5a). Then, a droplet of the other solute solution was dispensed from the reservoir and it was merged with the previously dispensed engine-and-cargo droplet (Figure 3.5b). As they merged, the esterification began and

continued to proceed (Figure 3.5c). A droplet of a quenching agent was dispensed from the reservoir and delivered to the reacting droplet at the prescribed reaction time (Figure 3.5d). This allowed that the esterification reaction stopped at the prescribed reaction time (Figure 3.5e). Then, the reaction mixture (organic layer) was carefully drawn out using a syringe and diluted with DCM in a GC vial, which was subjected to the GC-MS mass spectrometry analysis to measure a conversion of the reaction (Figure 3.5f).

While demonstrating capability of an EWOD device to carry out organic reactions, three reaction parameters–reaction time, type of solvents, and catalyst concentration–of on-chip esterification reaction of secondary alcohols with acetic anhydride were independently evaluated, summarized in Figure 3.5g.

For the kinetic study, other reaction parameters (e.g., catalyst concentration, solvent) were fixed and the reaction were monitored from 10 seconds to 90 seconds. For the solvent screening, catalyst concentration and reaction time were fixed and four different solvents (toluene, dioxane, dimethylformamide, DCE) were tested. For optimization of catalysis loading, solvent and reaction time were fixed and the concentration of catalysis was varied from 0.1 to 1.5 mol %.

As demonstrating the capability of EWOD device to conduct combinatorial synthesis, we performed esterification of three substrates including menthol, benzyl alcohol, and phenol with acid anhydride under basic conditions. The reactivity difference of these three substrates was examined over the first 30 seconds of each reaction. As a proof-of-the-concept, each reaction was performed on a different chip (not simultaneously on a single chip). However, this does not limit the capability of an EWOD device to host combinatorial synthesis.

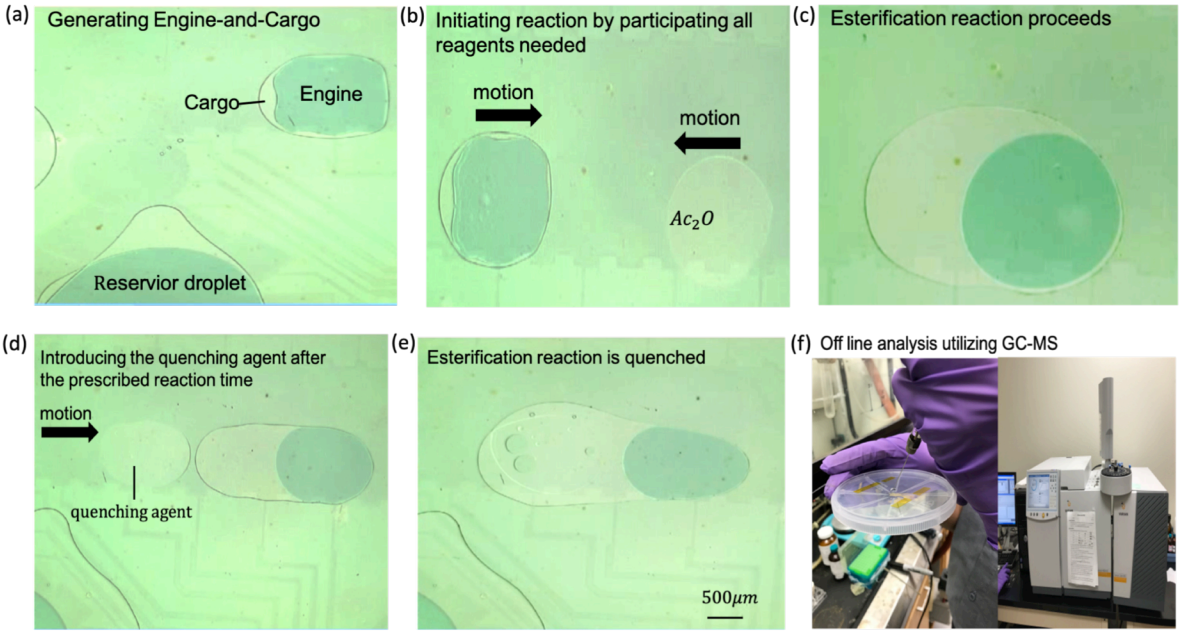

(g) Design of Experiment

Configuration / Reaction Characterization	Engine	Cargo solution			Other reactant		Quenching agent	Reaction time (s)
		Catalyst (Loading)	Reactant	Solvent	Reactant	Solvent		
Kinetic Study	[bmim]PF_6	DMAP (0.5 mol%)	menthol, Et_3N	toluene	Ac_2O	toluene	$NaHCO_3$	10 , 20 , 30 , 40, 50, 60, 70, 80, 90
Solvent Screening	[bmim]PF_6	DMAP (0.5 mol %)	menthol, Et_3N	toluene, dioxane, DMF, DCE	Ac_2O	toluene, dioxane, DMF, DCE	$NaHCO_3$	30
Optimize Catalyst Loading	[bmim]PF_6	0.1 %, 0.5 1.0 1.5 mol %	menthol, Et_3N	toluene	Ac_2O	toluene	$NaHCO_3$	30
Parallel esterification reactions	[bmim]PF_6	DMAP (0.5 mol %)	menthol, benzyl alcohol, phenol, Et_3N	toluene	Ac_2O	toluene	$NaHCO_3$	30

(a-f) Sequential snap shots illustrating the steps of esterification on an EWOD device. (a) An engine-and cargo compound droplet is dispensed from the reservoir. (b) The other reagent solution is dispensed and merged with the engine-and-cargo droplet. (c) Esterification proceeds. (d) A quenching agent is dispensed from the reservoir and transferred to the reacting droplet. (e) As the quenching agent droplet and the reacting droplet merge, reaction is quenched and stops. (f) After quenching, the reaction mixture is drawn out using a syringe and is diluted with DCM within the GC vials. The diluted sample is placed in the GC-MS machine. (g)Design of experiment summarizes conditions of all reactions tested in this study.

Figure 3.5 Esterification steps on an EWOD device

3.7. Result and Discussion

3.7a Qualification of an engine-and-cargo system

According to Ren,[111] most of chemical and biological applications of lab-on-chip devices require volume inconsistency to remain below ±5%. To assess the cargo volume inconsistency, Dr.Moon's Lab generated 26 engine-and-cargo droplets consecutively and characterized cargo volumes. During the tests, the cargo reservoir was kept refilled as it depleted. As it is evident from Figure 3.6a, after 3 dispensing of droplets with the average volume (black dots), the fourth droplet (red dots) was dispensed with larger volume than the average. This is attributed to volume changes of the reservoir puddle after several dispensing of engine-and-cargo droplets. Guan[112] reported that in an EWOD device a volume of a dispensed droplet has the dependency on a volume of the reservoir puddle. With excluding the red dots, the inconsistency is as low as ±3%. Based on this result, we tried not to deplete the cargo reservoir. In addition, droplets with the larger cargo volume than the average were discarded before it proceeded to the reaction so that the dispensed cargo volume was maintained, consistent throughout all esterification tests. The engine fluid is not a reagent for esterification while it stays in the reacting droplet during the course of the reaction. It needs to be established that the presence of engine fluid would not interfere the reaction. Moreover, in this study, adding color dye to the engine fluid is desirable for clear visualization of experiments. To identify reaction compatibility of the engine and color dye, we investigated three off-chip reactions; (1) the model esterification, (2) the esterification in the presence the ionic liquid, and (3) the esterification in the presence of ionic liquid and the green food dye. As shown in Figure 3.6b, GC-MS spectrometry confirmed that use of the engine with the green dye did not interfere the esterification reaction at all.

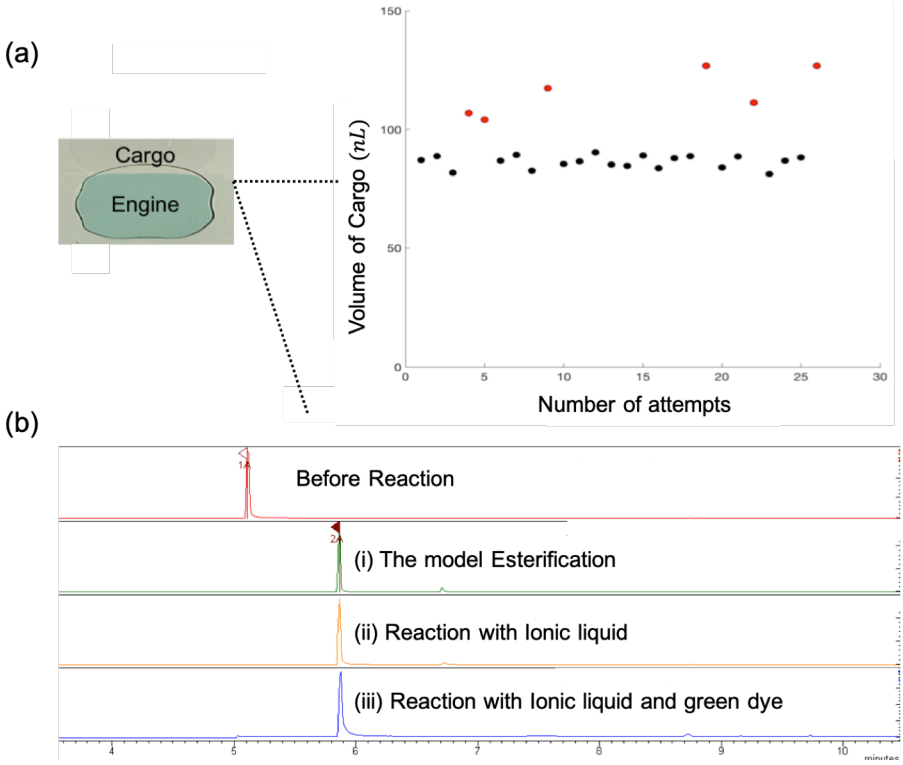

(a) The cargo volume of 26 engine-and-cargo droplets consecutively dispensed from a reservoir. By excluding outliers (red dots), volume inconsistency was kept as low as ±3 %, and (b) GC-MS spectrometry results of 3 off-chip reactions. This confirms that the presence of the engine and the food dye does not interfere esterification reactions.

Figure 3.6 Efficiency of engine-and-cargo system

3.7b Optimization of the reaction

To achieve an efficient reaction, reaction conditions often need to be investigated thoroughly. Typically, optimized reaction conditions can be determined by conversion data from a number of reactions with varying reaction parameters.[113-115] Unquestionably, such reaction optimization is a tedious process that requires substantial resources including time and efforts, and it generates chemical wastes. An EWOD digital microfluidic technology is particularly useful to address this issue; an EWOD device can readily provide arrays of droplets, where each

droplet carries unique reaction conditions and many newly generated droplets can be individually controlled.[116] These features make an EWOD device suitable for the high-throughput screening platform. In this study, we performed 60 on-chip reactions and the conversion data from these reactions were used to optimize the esterification reaction as followed.

3.8 Kinetics study

Study of the kinetics of a reaction is an essential part of the reaction optimization, because it provides insights into the reaction mechanism.[117,118] Kinetics study typically associates with a quenching process in which a quenching agent is added to the reaction mixture to stop the reaction at a desired time and conversion measurement is followed. However, quenching a reaction in a macroscale is not a well-controlled process because of the time for applying a quenching agent and its homogeneous diffusion throughout an entire reactor. These factors are, indeed, negligible in microscale reactions, simply more efficient fluid handling of microfluidic means and short diffusion length. Consequentially, more precise conversions and yields data can be obtained in a microscale reaction.

To this end, we quenched reactions at nine different times (i.e., 10-90 s at 10 s intervals). As shown in Figure 3.7, a conversion from reactants to products increased as the reaction proceeds, similar to the measurement from typical lab-scale reactions (Supporting Information, Fig. S2). This confirms that EWOD chip is capable to carry out accurate quenching of reactions. A notable difference between on-chip and off-chip reactions was reaction kinetics; substantially improved kinetics of the on-chip reactions was observed. For example, while the lab-scale reaction reached to 95% conversion in 40 min, the on-chip reaction reached to 97 % conversion only in 90 s. Procopiou [119] and other researchers [120] reported that to achieve at least 50% yield from the esterification of secondary alcohols requires 30 to 150 min under the conditions of Ac_2O at room

temperature. Overall, an EWOD microfluidics are a versatile microscale organic chemical reaction platform, which can deliver significantly enhanced reaction kinetics with precise reaction control.

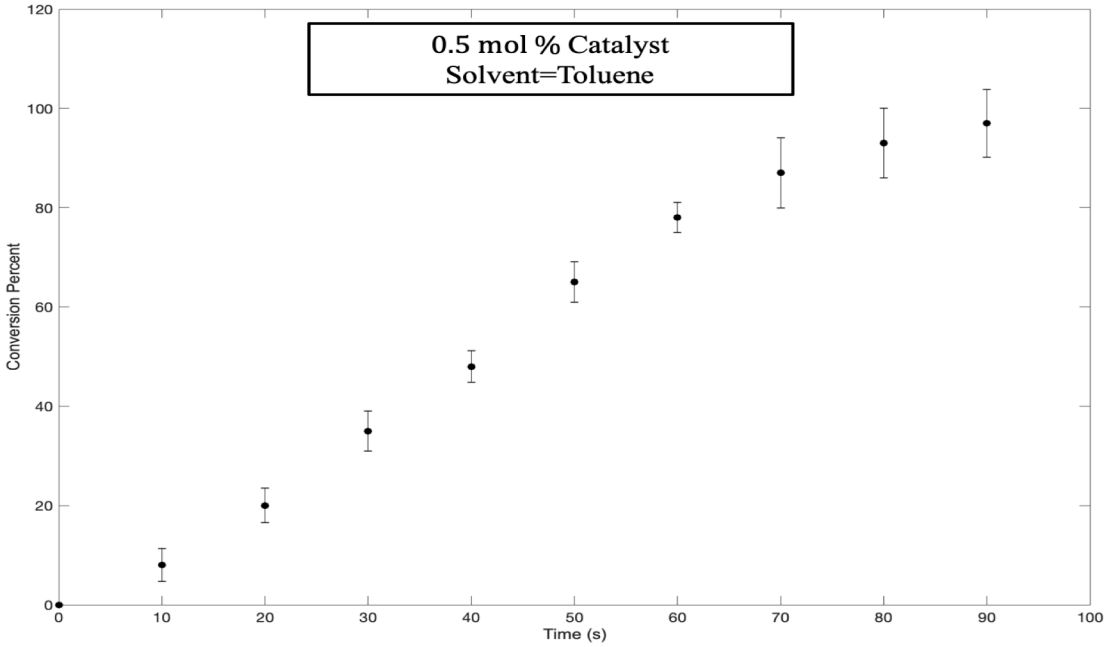

The conversion percent of on-chip esterification of menthol for different reaction times. For all reactions, toluene was used as solvent and concentration of catalyst (DMAP) was kept at 0.5 mol %. Dots and error bars are the average conversions and standard deviations from 3 reactions per each, respectively.

Figure 3.7 Kinetic study of on-chip esterification

3.9 Solvent Screening

Impact of solvent on EWOD microfluidics platform, where catalyst concentration and reaction time are fixed at 0.5 mol % and 30 s, respectively are studied. A conversion rate for esterification of menthol with Ac_2O in four different solvents is shown in figure 3.8 where SPI indicates solvent polarity index. Esterification of menthol in DCE (SPI, 3.7), dioxane (SPI, 4.8), and toluene (SPI, 2.4) resulted in 5 times more conversion compared to the reaction in

dimethylformamide (SPI, 6.4). [121] This suggested that esterification with non-polar solvent gives higher yield than with polar counterpart, which well agrees with reports from others.[122]

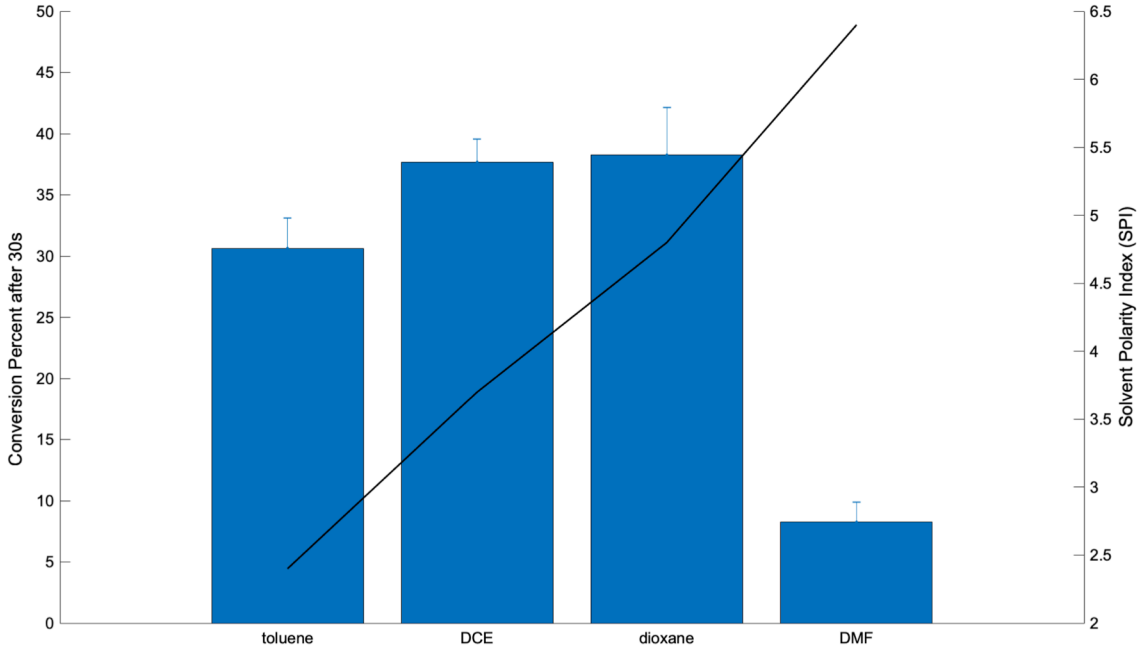

Comparison of the conversion of esterification of menthol in the presence of different solvents including toluene, dioxane, dimethylformamide, and DCE, at first 30 s. The concentration of catalyst was kept at 0.5 mol% throughout all the solvent screening experiments. Columns and error bars are the average conversions and standard deviations from 3 reactions per each, respectively. The secondary y-axis indicates Solvent Polarity Index (SPI). As it is evident esterification with non-polar solvent gives higher yield than with polar counterpart

Figure 3.8 Solvent screening

3.10 Catalyst loading optimization

DMAP has been an efficient catalyst for traditional flask-based acylation reactions.[122] In this study, use of DMAP as a promising catalyst for esterification of the less reactive alcohols (i.e., secondary alcohols) on EWOD microfluidics platform is demonstrated. To investigate the optimal loading of DMAP, four different concentrations (0.1, 0.5, 1.0, and 1.5 mol%) were examined.

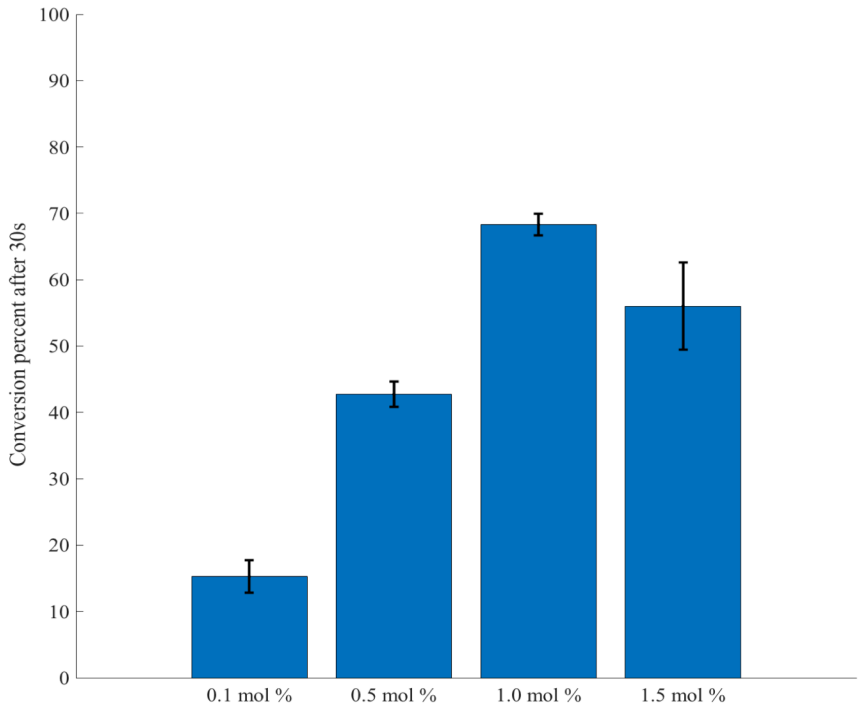

Comparison the conversion percent of esterification of menthol with the concentration of DMAP. For the catalyst loading optimization study, the type of solvent (toluene) and the reaction time (30 s) were fixed for all tests. Columns and error bars are the average conversions and standard deviations from 3 reactions per each, respectively.

Figure 3.9 Catalyst loading optimization

As seen from figure 3.9, the higher concentration of DMAP resulted in better yield. However, loading of 1.5 mol % of DMAP slightly diminished yield. It is likely attributed to solubility of DMAP in toluene, impacting on reaction kinetics. For instance, at the higher concentration of DMAP, pyridinium salt precipitates, which might lead to off-cycle of the catalyst. Sakakura[123] reported similar result in a flask chemistry. Overall, these studies infer that new reaction development exploiting EWOD-based platform needs careful optimization on each reaction parameter.

3.11 Parallel esterification reactions

Over the past decades, microscale combinational synthesis has been actively sought.[124-127] Kikutani[128] demonstrated 2×2 combinatorial synthesis of amides through a parallel micro-flow reactor system in a single glass microchip. This approach is mainly based on micro unit operations (MUOs) in pressure driven multi-phase laminar flow networks. Theberge[129] proposed a droplet-based microfluidic platform for combinatorial library synthesis of potential drug candidates, where a 7×3 library of potential enzyme inhibitors was used. In both cases the design and architecture of the device are quite complicated. For examples, Kikutani[128] utilized three parallel plates to prevent the cross-contamination that caused the complexity in the fabrication process.

On the other hand, an EWOD digital microfluidic device intrinsically has multiplexing capability so that achieving M×N combinations of reactants can be easily done without any complicate modification of a device. Moreover, each droplet can form an independent microreactor; therefore, cross-contamination and crosstalk can be minimized or eliminated, and reaction conditions constituting each combination of reactants can be individually controlled or altered. As a small step toward the EWOD device for combinatorial syntheses, we performed parallel esterification reactions of three different substrates on a single device. Each droplet was independently generated and manipulated; all other reaction conditions, e.g., solvent, catalyst concentration, and reaction time, were predetermined (Figure 3.5g).

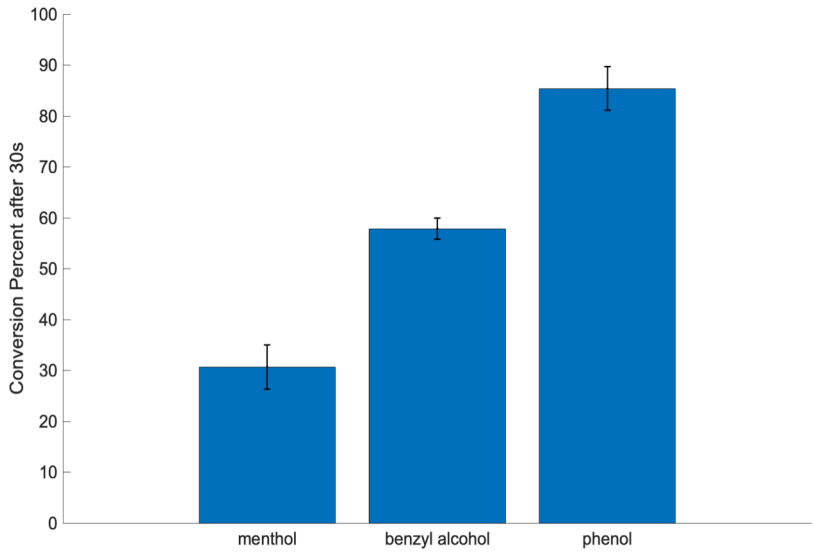

Eterification of phenol, benzyl alcohols, and menthol in presence of toluene, during the first 30s of the reaction.

Figure 3.10 Parallel esterification reactions

As shown in Figure 3.10, phenol underwent the esterification in the high yield (85%), compared to benzyl alcohols and menthol in the first 30 s of the reactions. This result is consistent with well-known reactivity of acylation of alcohols and phenols. Structurally, phenol possesses more acidic hydrogen, yet a less nucleophilic oxygen donor than the alcohols. This feature leads to mechanistically different reaction pathways; phenols first undergo facile deprotonation by either DMAP or auxiliary base (e.g., Et_3N) and the resulting oxyanion attacks acylpyridinium ion generated from a reaction of Ac_2O and DMAP.[123,130] This differs from nucleophilic attack of alcohol to acylpyridinium followed by deprotonation. As expected, sterically less encumbered benzyl alcohol is more reactive toward acylation vis-à-vis menthol.[131,132] Overall, our result shows that an EWOD device is capable of hosting a library of reagents and permitting combinatorial organic synthesis with organic solvents. Notably, this technology will be a

valuable tool for rapidly elucidating of the reactivity difference of reagents or substrates and providing mechanistic insights into a range of organic transformations.

3.12 Summary for engine-and-cargo strategy

This work demonstrated that an EWOD digital microfluidic platform is an alternative or a complementary tool to microreactors based on continuous channel flow for organic synthesis. In this study, we introduced the "engine-and-cargo" strategy that addressed the shortcoming of an EWOD device; the novel technique makes an EWOD device capable of handling electrically non-responsive fluids, particularly organic solvents, where organic fluids are not generally electrically movable. With the engine-and-cargo approach, esterification involving alcohols and phenols with acetic anhydride in the presence of base and DMAP were successfully carried out on EWOD devices. The study on reaction kinetics established benefits from an EWOD device on account of rapid and precise quenching of reactions. Furthermore, rapid reaction optimization was realized on a EWOD device, examining two parameters including solvents and catalyst loading. Finally, we demonstrated the 3×1 combinatorial synthesis of esters with three substrates in a rapid fashion.

3B. In-line workup on EWOD-DMF device

3.13 Introduction

After the emergence of micro-reaction technology and the advancement of micro-reactor platforms in the 90s, miniaturization of multi-step chemical synthesis has drawn extensive attention. The integration of multi-step chemical reactions into micro-reaction machinery demands inter-stage workup processes, meaning that each reaction (i.e., stage) generally associates with workup purification at the end of the process, prior to the next reaction.[133]

Workup techniques in chemical reactions generally include but not limited to, quenching a reaction mixture, liquid-liquid extraction (LLE), distillation, evaporation, and crystallization. For example, in an effort of preparation of active pharmaceutical ingredients (APIs), there are inevitable workup steps where reagents and by-products need to be removed or solvent must be changed prior to moving to the downstream processes.

Among workup techniques, LLE is often a practical choice in a chemistry laboratory because LLE runs at the lower temperatures and consumes less energy than distillation. Along with the higher mass transfer in micro-scale, LLE has encouraged its miniaturization, both in the field of continuous microchannel flow and digital microfluidic platform. Sahoo et al.[133] demonstrated a continuous-flow multistep reaction where the separation steps were added through an external "separator." Despite the novel design of the separator proposed in their system and in other similar works,[134-136] the complexity in the architecture, just made for a "separator component", leads to the uncertainty concerning the system-level integration. Moreover, the low yield performance of LLE in flow chemistry setup has been an ongoing barrier attributing to the saturation of liquid-liquid interfaces. Even successful plug-and-play miniaturized devices in flow chemistry still do not fully meet the requirements for some essential lab-scale techniques, such as evaporation, solvent-swap, and crystallization because these steps involved with precipitation which consequently causes the obstruction (i.e., clogging) of continuous microchannels. Note that overcoming these problems in microchannel flow is very challenging, often impossible without compromising the intricacy of the design and fabrication.

A digital microfluidic platform using the electrowetting-on-dielectric (EWOD) principle as an alternative and/or a complement to the continuous micro-channels system, eliminate the obligation of predestined channel networks and mechanical pumps and valves. A droplet-based flow type in an EWOD device expands even further the benefits of miniaturizing LLE, by offering the large arrays of digitized droplets and the one-to-one fashion of mating the droplets. Researchers have made excessive use of these novel characteristics of the EWOD to downscale the extraction system e.g. LLE[137-139] and solid-phase extraction[140,141] on the digital microfluidic platform.

In an EWOD digital microfluidic device, each droplet acts as a batch reactor, which promises the feasibility of performing multi-step reactions that may involve solvent-swapping and combinatorial synthesis. Nonetheless the EWOD device has been employed for just few organic reactions[142-144] because a critical limitation caused by the incompatibility of most common organic solvents with EWOD devices. Note that EWOD has been a great platform for polar liquids such as water, but not been able to handle non-polar solvents, and all the reactions reported on EWOD chips utilized solvent fluids that are movable by EWOD actuation. We have recently demonstrated a more realistic organic synthesis on the EWOD, introducing an "engine-and-cargo" concept that enables the use of non-movable, non-polar organic fluids on an EWOD device.[145] The establishment of the engine-and-cargo system in the report has expanded the scope of chemical reactions harnessing the EWOD device. For instance, any standalone reactions, i.e., reaction1 and reaction 2 shown in Fig. 3 (a), can be integrated on an EWOD device regardless of the organic solvents participating in the reactions.

To fully host the multi-step synthesis, one crucial element is the inter-stage workup

process. Because in-line workup on the EWOD, allows the continuity of a chemistry workflow from starting material to the final product. There is a paucity of literature in multi-step chemical reactions on EWOD, especially involving the inter-stage workup process. The synthesis of radiotracer [18 F] FDG is one of the few (if any) examples representing a multistep synthesis followed by distillation on the EWOD device.[145] Of note, all solvents in this synthesis were movable by EWOD actuation. Over the last two decades, on-chip distillation and miniaturized distillation columns have been reported.[146,147] However, they have not been used widely in multistep synthesis; mainly due to the demand for change in device architecture and design and the higher requirement of energy for distillation.

In this report, in-line organic workup as a step towards promoting multi-step synthesis on an EWOD device is developed. Acid-base workup as a model system was successfully demonstrated the consecutive steps that include acid-base reaction, neutralization, and crystallization. Moreover, in-line solvent-swap crystallizations of benzoic acid and benzophenone manifest the capacity of an EWOD device to host reactions that require solvent evaporation followed by crystallization of compounds. Furthermore, we identified the optimal device operation for each workup reagent as it underwent every stage of the protocol. Besides, a specific mixing and phase separation schemes employed and discussed in this study.

As EWOD digital microfluidic devices continue to revolutionize the hi-tech medical technologies and provide the pharmaceutical companies a discovery platform to aid the clinical judgment at a very early stage, there is going to be a substantial demand for the development of the fully-automated and continues on-chip workflow. The union of the in-line workup/in-line solvent-swap crystallization and on-chip “engine-and-cargo” organic synthesis reported

previously,[145] will pave the way to the fully-automated combinatorial drug discoveries on an EWOD device, without a change in device architecture and design.

3.14 Acid-Base workup

Acid-base workup, practical and common product isolation technique in the pharmaceutical and food industries, is typically applied to isolate organic compounds from each other, relying on their acid-base properties. Biofuel, biochemical, petrochemical, and substances produced by biological processes, for instance, fermentation and algae, usually require acid-base workup as the first move in product isolation; on the grounds that many of these compounds have high boiling leading to the high energy requirement for distillation. This study is to demonstrate on-chip isolation of benzoic acid as a product of interest from a model post-reaction mixture comprising the acid and neutral organic compound, benzophenone. A model reaction mixture contains benzoic acid and benzophenone in THF undergoes three sequential workup steps to regenerate pure benzoic acid. The entire workflow for our proposed acid-base workup is presented in Fig 3.

Traditional macroscale acid-base workup (e.g., flask-based protocol) requires a dry flask, a stir bar, a septum, and some other apparatus (i.e., syringes and needles, inert gas chamber, and filter paper) followed by aliquoting, adding, and mixing reagents. Instead, on the EWOD chip, an in-line acid-base workup can be initiated by generating reagents droplets, transporting, and mixing droplets, go along with the separation of phases and ending with droplet evaporation and crystallization of product of interest.

3.15 Experimental data

3.15a Device fabrication and experimental setup

All EWOD microfluidic devices used in this study were fabricated in the Shimadzu Institute Nanotechnology Research Center of the University of Texas at Arlington. Actuation electrodes in the bottom plate of an EWOD device were fabricated by photolithography followed by wet etching of an indium tin oxide (ITO) layer (100 nm) coated on a glass wafer. The dielectric layer (SU-8, 6μm) and the hydrophobic layer (Teflon, 350 nm) were spin-coated and oven baked. The gap between top and bottom plates of devices was kept at 100 μm throughout the entire workflow. The side view schematic of a sandwiched droplet in an EWOD device is shown in Figure 3.11a. The details of the fabrication steps and device assembly can be found in the supplementary material.

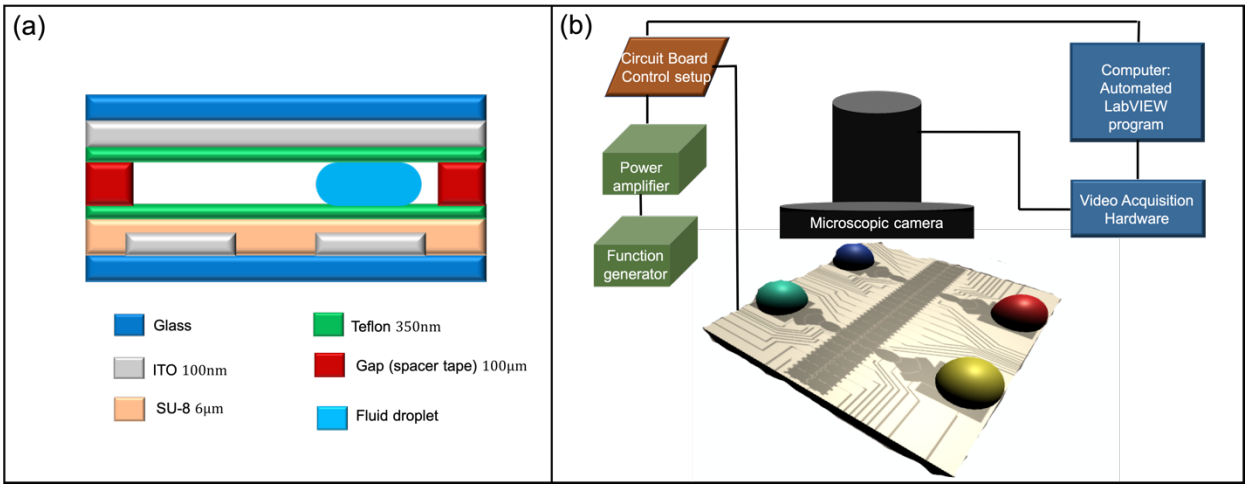

(a) The side view schematic of a sandwiched droplet in an EWOD digital microfluidic device, and the surrounding medium is air all throughout the experiment. (b) The experimental setup of an EWOD chip operation.

Figure 3.11 Experimental setup of EWOD device

The EWOD operation voltages were provided by Agilent arbitrary waveform generator and the TEGAM high voltage amplifier (model 23400). Desired sequence of turning on/off

electrodes were applied through LabVIEW program. Droplet motions were recorded using Hirox KH-1300 digital microscope system. Later, images were extracted from videos and processed using Editor PIXESTYLE and ImageJ software. Figure 3.11b shows the experimental setup of an EWOD chip operation.

3.15b Materials

Benzoic Acid [≥99.5%], Tetrahydrofuran (THF) [anhydrous, 99.9%, inhibitor-free], Ethyl acetate [anhydrous, 99.8%], Diethyl ether [anhydrous, ACS reagent, 99.8%], and dichloromethane [(>99.8%)] were obtained from Fisher Scientific. Toluene (Certified ACS), Benzophenone [purified by sublimation, ≥99%], Sodium hydroxide, BioXtra, 98% (acidimetric), pellets (anhydrous), and Hydrochloric acid, ACS reagent, were purchased from SIGMA-ALDRICH (USA). All the chemicals were of analytical grade and used as received.

Diethyl ether was a primary choice of the organic phase; however, the volatility of this organic solvent did not allow us sufficient time to complete the entire workup procedures. As it is evident from Figure 3.12, as mixing started, diethyl ether (organic layer) was shrinking due to the evaporation. Figure 3.12 discloses a fact that although some organic reagents are the primary choice to conduct based on solubility properties, the miniaturized system sacrificed their on-chip utility; mainly due to evaporation and movability concerns. Of note, with the emergence of a novel system of Engine-and-Cargo vanished the hindrances concerning movability. The experimental video manifesting the evaporation issue can be found in the supplementary material.

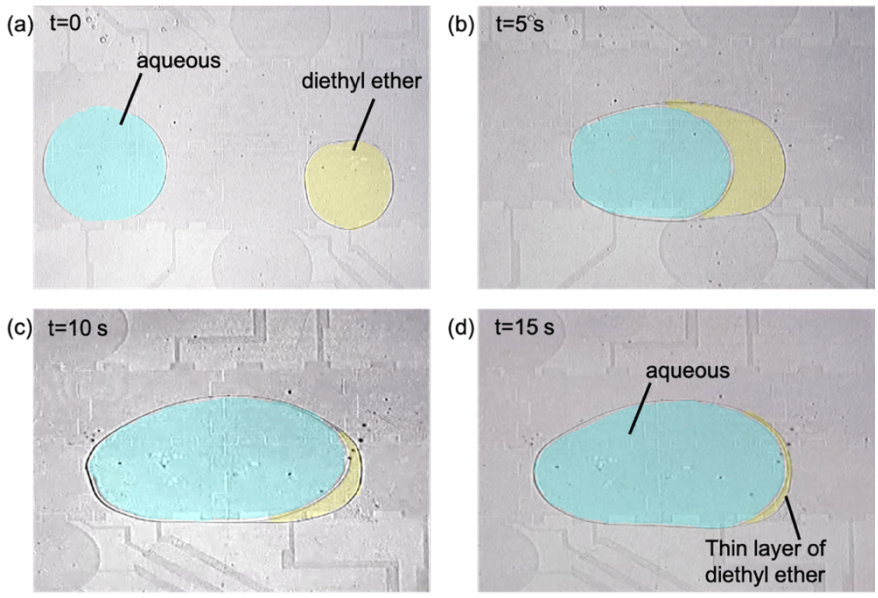

(a-d) Sequential snapshots depicting that as mixing started, diethyl ether began shrinking due to its high vapor pressure. The organic and aqueous droplets artificially coloured for better visualization purposes only.

Figure 3.12 Solvent optimization

3.16 Test Protocols

A total of 15 tests of 5 different conditions of acid-base workup were carried out on-chip. The four primary reagents participating in our proposed in-line workup were placed in designated reservoirs as shown in Figure 3.13c. Furthermore, there are two designated locations on chip (~ 4 to 6 EWOD electrode), ring 1 and ring 2 in Figure 3.13c, to complete the mixing and the phase separation; as to be discussed later, they are the essential stages both in acid-base reaction and neutralization. Additionally, there is an evaporation and crystallization site, ring 3 in Figure 3.13c, where it will be hosting in-line solvent-swap crystallizations. The following sections 4.1-4 describe the details of the on-chip workup protocol.

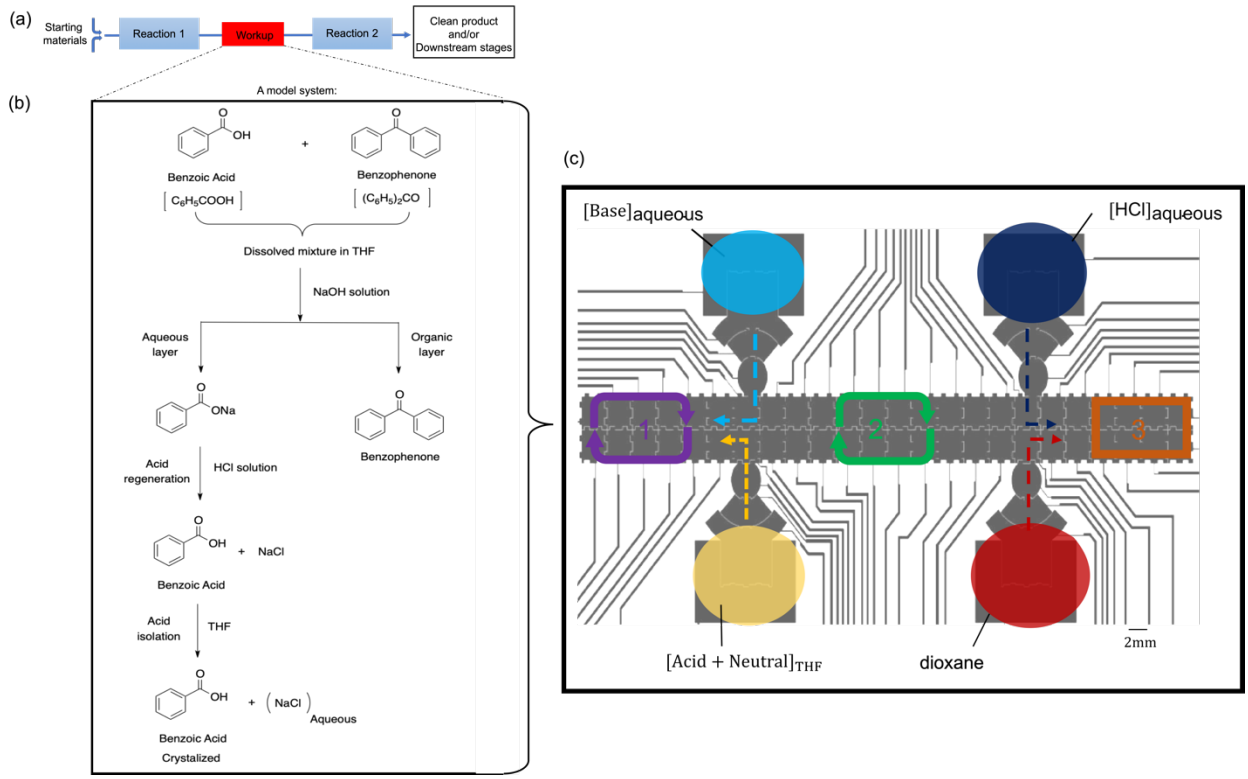

(a) The entire workflow for a multi-step synthesis. (b) A model reaction mixture contains benzoic acid and benzophenone in THF undergoes three sequential workup steps to regenerate pure benzoic acid; acid-base reaction with aqueous NaOH/droplet separation, neutralization with aqueous HCl/droplet separation, and evaporation/crystallization. (c) the EWOD chip electrode layout and the placement of reagents on the chip at the beginning of each test.

Figure 3.13 EWOD layout for in-line workup

3.17 Result and Discussion

3.17a Device Operation Throughout Workup Process

The fluidic functionalities (generating, transporting, mixing, and splitting) of EWOD have long been established.[149] Such capabilities presented the EWOD device to be the proper choice to conduct many applications.[150-152] Despite the available studies, there is no consensus report on the optimal way for the EWOD to be operated throughout a certain lab-on-chip application. Previously, we presented an electromechanical model predicting an optimal voltage and frequency for any fluid to be moved on an EWOD digital microfluidic device.[153] It is quite

interesting that this optimal voltage and frequency is changing as a liquid droplet undergoes the different stages of a certain process.

EWOD Operation								
Operations / Solvent and Reagent	Generating		Transporting		Mixing		Phase Separation	
	Voltage	Frequency	Voltage	Frequency	Voltage	Frequency	Voltage	Frequency
DI water (reference solvent)	110 V_{rms}	1 kHz	100 V_{rms}	1 kHz	100 V_{rms}	1 kHz	From THF: 120 V_{rms}	From THF: 1 kHz
NaOH (aq)	100 V_{rms}	5.3 kHz	90 V_{rms}	1 kHz	90 V_{rms}	1 kHz	From THF: 110 V_{rms}	From THF: 1 kHz
THF (contain reaction mixture)	90 V_{rms}	75 Hz	90 V_{rms}	75 Hz	90 V_{rms}	75 Hz	From NaOH (aq): 110 V_{rms}	From NaOH (aq): 500 Hz
THF (bare solvent)	100 V_{rms}	10 Hz	100 V_{rms}	10 Hz	100 V_{rms}	10 Hz	From HCl: 90 V_{rms}	From HCl: 75 Hz
HCl (aq)	90 V_{rms}	10 kHz	80 V_{rms}	1 kHz	80 V_{rms}	1 kHz	From THF: 90 V_{rms}	From THF: 1 kHz
dioxane	100 V_{rms}	1 Hz	100 V_{rms}	1 Hz	80 V_{rms}	40 Hz	Not Tested	

Table 3.1 Summary of voltage and frequency conditions of all reagents participating in this study.

Table 3.1 summarizes the optimal voltages and frequencies of all the reagents participating in this workup. Deionized (DI) water was included in the table as a reference liquid since it is the most frequently used fluids in EWOD devices. Table 3.1 shows that the optimal required voltage was the highest while a reagent droplet experienced phase separation and generating, respectively. Such a trend can be well perceived as phase separation and generation of a droplet

on the EWOD device requires more electrowetting force to overcome the interfacial surface tension. This trend of voltage operation was true for each reagent in this workup.

In our previous work, we demonstrated the frequency-dependent behavior of the EWOD force. Table1 shows the frequency at which the peak of the net force occurs shifts as a reagent droplet undergoes the different stages of workup; representing the distinct optimal EWOD forces for each different stage. Additionally, Table1 shows that for a certain EWOD functionality (i.e., generating) at which the peak of the net force occurs varies as the type of reagent changes. Such behavior is well understood from our earlier work where we showed the dependency of EWOD force on fluid properties.

Interestingly, comparing the voltage operation for HCl(aq), NaOH(aq), and DI water, in all cases of fluidic functionality, shows the lowest to the highest need of EWOD force, respectively. The ionic conductivity of HCl(aq) and NaOH(aq) solutions leading to an increase in the ion density at the solid-liquid interface; Consequently, lowering the required voltage magnitude. Noteworthy, comparing the frequency of the same three liquids shows a shift to the higher value. This trend is consistent with our previous finding on the effect of conductivity on the peak frequency at which the highest net force occurs. Similarly, Chatterjee[154] and Chen[155] investigated the association of liquid conductivity with the force in the EWOD device.

It can be seen from Table that the optimal frequency for THF and dioxane was at the very lower spectrum of the frequency range, which agrees with our model as well as the experimental observation of Chatterjee.[154] Besides, comparing THF (bare solution) and THF (contain reaction mixture) confirms the effect of conductivity on the frequency shift.

3.17b Formation, mixing, and separation of two-phase droplet

To achieve a successful LLE system on an EWOD device, there is a need to form a two-phase droplet, mix, and separate the two-phase of immiscible liquids. To form a two-phase droplet-THF and deionized water were used. After merging two phases, multiphase droplets were spontaneously created and remained at the phase equilibrium state with the minimum free energy configuration.

Mixing has been recognized as one of the most common challenges in microfluidics, dominated by laminar flow of low Reynolds Number (Re). While there are attempts to enhance mixing for the conventional continuous flow in microchannels, EWOD digital microfluidic device appeared to be an effective way to tackle such shortcoming by offering droplet-to-droplet scheme of mixing. Fowler[156] introduced a mixing fashion by encapsulating one phase into another phase (rather the side-by-side configuration); maximizing the contact area between two phases and reducing the diffusion length significantly. Additionally, in an EWOD device, upon the actuation of voltage, there is a flow circulating inside the droplet as the result of Laplace pressure variations at the liquid-air interface. Such an intrinsic characteristic of the EWOD device diminishes and/or eliminates the saturation of mass transfer at the liquid-liquid interface. However, in case of the two-phase droplet, due to the different viscosity of the liquids and also different actuation behaviors, upon the actuation of voltage and the movement of both phases, the multiphase droplet changes its configuration from fully encapsulated to partially engulfed or side-by-side; leading to decrease the contact area between two droplets. Therefore, in order to take advantage of both features, maximizing contact area (minimized the diffusion length) and the flow circulation at liquid-liquid interface, we employed a combination of both reported a mixing scheme. Figure 3.14 illustrates the mixing scheme which was practiced for this workup

process where the organic phase moved and around while the aqueous phase kept fix. This mixing scheme was utilized for both Acid-Base Reaction and Neutralization.

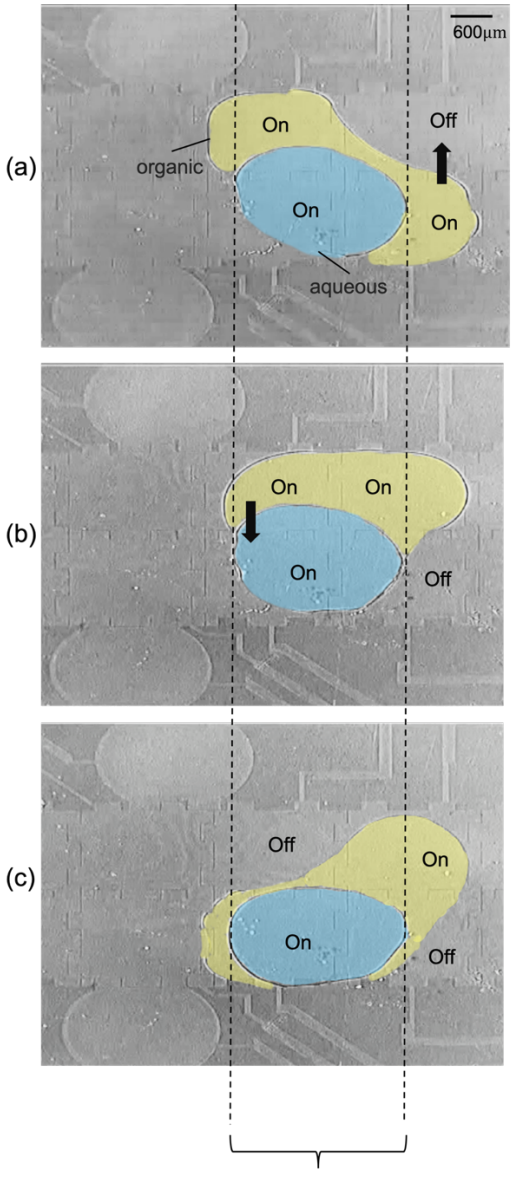

(a-c) Sequential snapshots demonstrating the steps of a mixing scheme that is employed for the workup. The organic and aqueous droplets artificially coloured for better visualization purposes only. The organic phase moved around while the aqueous phase kept fix; allowing to maximizing contact area as well as limiting the interface saturation.

Figure 3.14 Mixing scheme of two-phase droplet on EWOD device

Merging and splitting the single-phase droplet on an EWOD device has long been established. However, there is a lack of objective data addressing the phase separation on an EWOD device. Recently, The Moon group demonstrated the separation of the immiscible phases of multiphase in the EWOD device where Nahar[157] introduced two different techniques to control the deformation of the phases, leading to a successful separation and minimization of the residue formation (less than 2% in both techniques). Herein, we employed the second method of multiphase separation to achieve the essential stages (of formation and separation) within the workflow for the acid-base workup.

In this method of phase separation, Figure 3.15, we relied on applying the different actuation scheme as the voltage magnitude was constant for both aqueous and organic phases. After the mixing was complete and in the beginning of phase separation scheme, the two middle electrodes were turned on, illustrated in Figure 3.15a. In next step, one middle electrode was turned off and the electrode at its side turned on; leading to actuation of yellow (organic) phase, Figure 3.15b. During this transition, yellow phase moved further and elongated which caused the occurrence of hydrodynamic instability followed by pinching off and separation of phases, Figure 3.15c. In this scheme of separation, blue (aqueous) phase was kept in in its initial position so that its meniscus was forced to conform to the electrode shape and deformation was minimized. Nahar[157] demonstrated that in case of using square electrode, having one phase fixed in contrast to the conventional droplet splitting method (moving both phases in the opposite direction), resulted in a significant decrease of the residue formation (by 90%); owing to reducing the deformation.

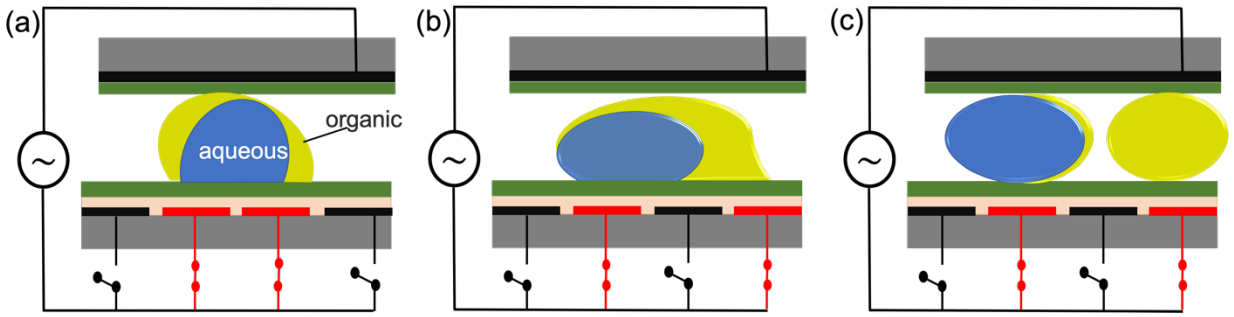

The sequence of actuation schemes tested in the separation stage of the workup. The activated electrodes are colored in red while the grounded electrodes are colored in black (a) illustrates the multiphase droplet placement at the beginning. (b) The multiphase droplet profile upon the on and off pattern of actuation. (c) Elongation and hydrodynamic instability of the organic phase followed by pinching off and separation of phases.

Figure 3.15 Separation scheme of two-phase droplet on EWOD device

3.18 Acid-base reaction

Figure 3.16 shows sequential snapshots illustrating the steps associated with an acid-base reaction on the EWOD device. As demonstrated in Figure 3.16a and Figure 3.16b, a droplet of THF containing benzophenone and benzoic acid from one end and an aqueous droplet of sodium hydroxide from the other end, were actuated to form a two-phase droplet. As mixing was taking place, the acid-base reaction proceeded (Figure 3.16c). Specifically, this reaction produced sodium benzoate salt–which is water-soluble, hence diffused into aqueous droplet–and benzophenone–which is organic-soluble, hence remained in THF droplet. To proceed further with the in-line acid-base workup, a two-phase droplet needs to be separated. As illustrated in Figure 3.16d, providing two electrowetting forces in opposite directions resulted in a pinch-off point right in the middle. Finally, because of a consequential hydrodynamic instability, the organic and aqueous droplets were separated where the aqueous droplet contained sodium benzoate salt and the THF droplet included benzophenone (Figure 3.16e).

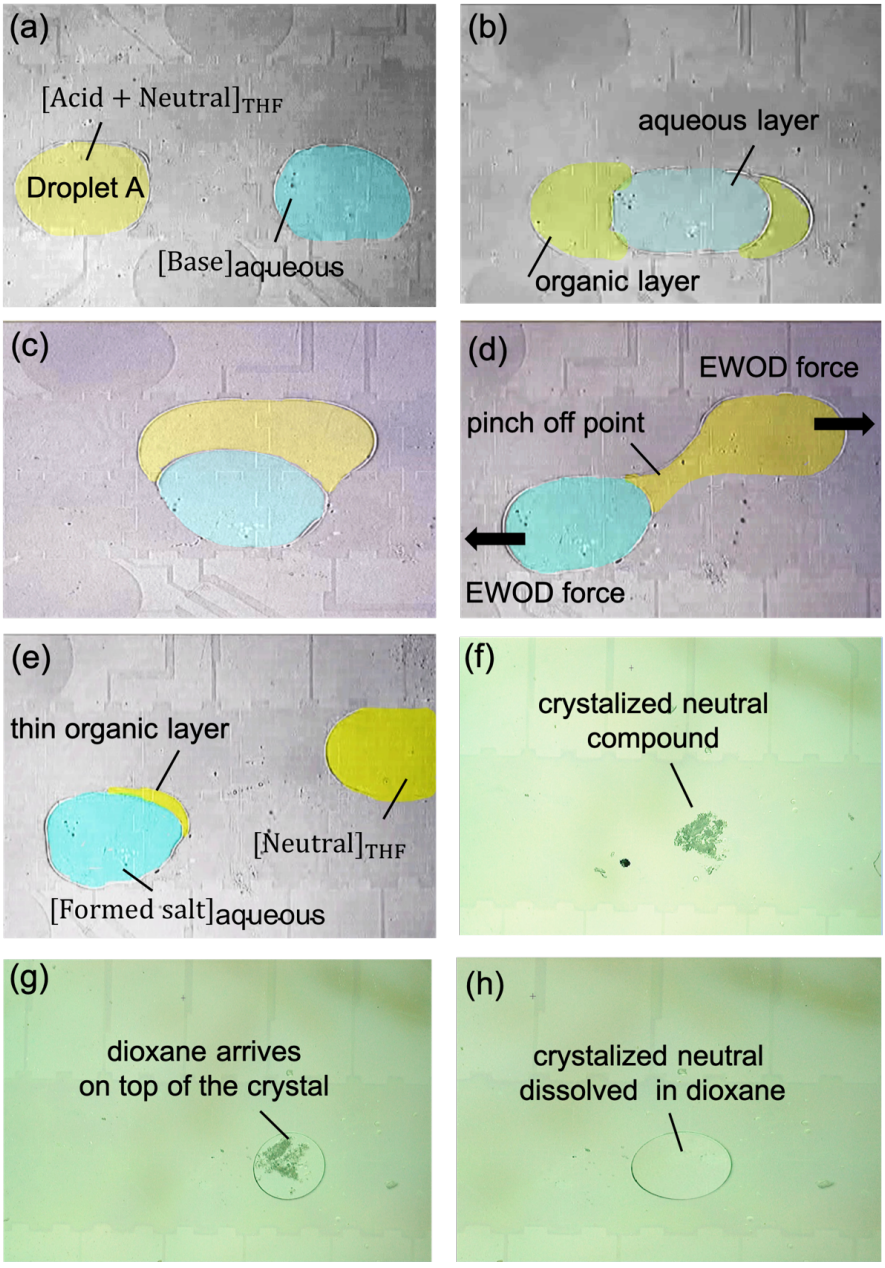

(a-f) Sequential snapshots illustrating the steps of acid-base reaction on an EWOD device. The organic and aqueous droplets artificially coloured for better visualization purposes only. (a) An organic (THF) droplet containing benzophenone and benzoic acid and an aqueous droplet of sodium hydroxide were introduced on an EWOD chip. (b) Two droplets were actuated to form a two-phase droplet. (c) As mixing was taking place, the acid-base reaction proceeded. (d) Electrowetting force in the opposite direction was applied to separate the two-phase droplet. (e) The organic and aqueous droplets were separated where the aqueous droplet contained sodium benzoate salt and the THF droplet included benzophenone. (f) Evaporation of THF allowed the neutral benzophenone to crystalize on an EWOD chip. (g) The solvent-swap reagent (dioxane) was transferred to the crystalized benzophenone. (h) Neutral benzophenone was fully dissolved in dioxane for further downstream reactions.

Figure 3.16 Acid-base reaction on EWOD device

To spotlight the capability of the EWOD device for running the evaporation without a change in device architecture and design, we let THF evaporated, and as a result, the benzophenone crystallized on an EWOD device surface, as depicted in Figure 3.16f. Furthermore, to underscore the capacity of an EWOD device to adapt solvent-swap operation, dioxane was transferred as the second choice of organic solvent, and let the crystalized neutral compound dissolve into it. The purpose of this operation is that the benzophenone dissolved in dioxane can be used for downstream chemical processes (Figure 3.16g and Figure 3.16h).

3.19 Neutralization

After the stage for the acid-base reaction is completed, the aqueous droplet was separated from organic droplet and it was moved to the stage for neutralization. As illustrated in Figure 3.17a, two droplets of aqueous HCl (1M) and aqueous sodium benzoate were actuated towards each other. After two droplets merged, the neutralization proceeded to produce benzoic acid and sodium chloride (Figure 3.17b). To extract the benzoic acid, a THF droplet was introduced and actuated into the aqueous droplet, depicted in Figure 3.17c. This made the benzoic acid to diffuse into the organic layer, and the application of electrowetting force in the opposite direction started to separate the two-phase droplet (Figure 3.17d). The two droplets were fully separated to give an organic and an aqueous droplet (Figure 3.17e). As presented in Figure 3.17f, THF evaporated, leading to crystallization of the benzoic acid on an EWOD device. To measure the concentration of the isolated benzoic acid, the droplet of THF solution (droplet B in Figure 3.17e) was drawn by a syringe and transferred to a GC-MS vial. Due to the low mass sensitivity, the nucleic magnetic resonance (NMR) spectroscopy was not used. Instead, we utilized GC-MS spectrometry for the quantitative analysis of the final extracted benzoic acid. Prior to performing

the GC-MS analysis, a calibration curve for the acid was obtained (see the supplementary material).

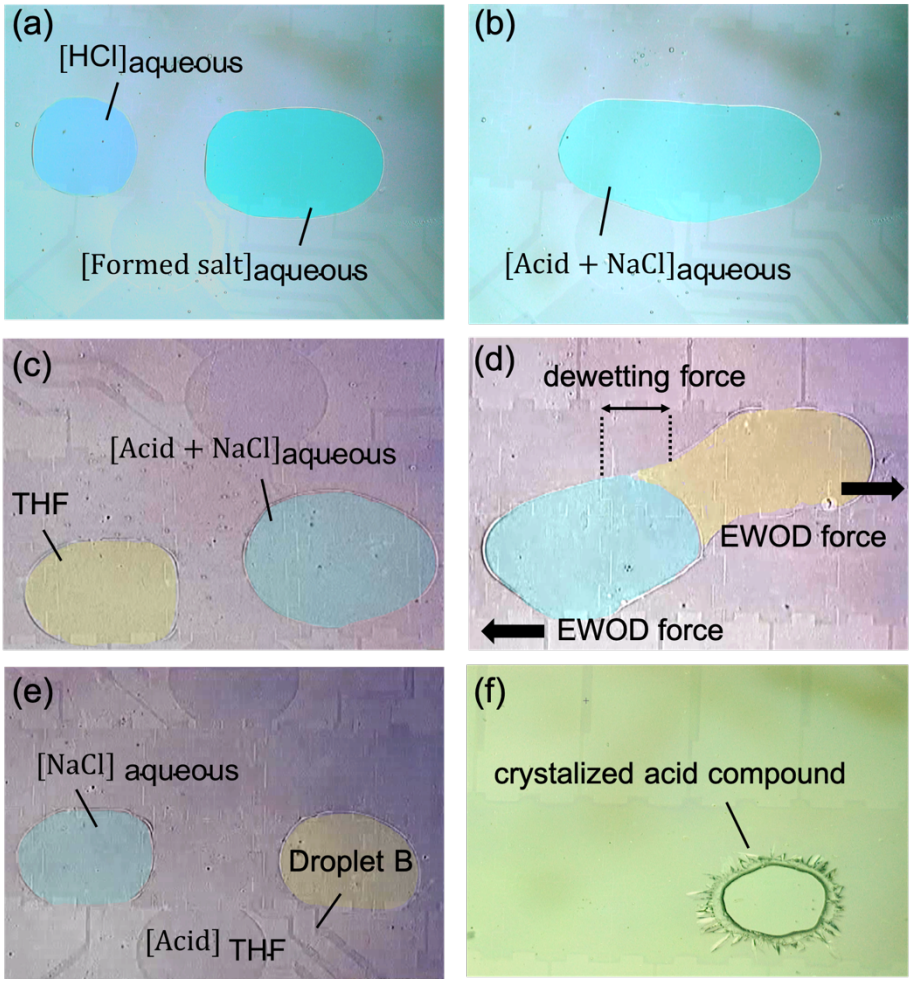

(a-f) Sequential snapshots illustrating the steps of neutralization reaction on an EWOD device. The organic and aqueous droplets artificially coloured for better visualization purposes only. (a) A concentrated HCl droplet and an aqueous droplet were introduced and actuated towards each other. (b) Two droplets were merged and the neutralization reaction proceeded. (c) The THF droplet was actuated into the aqueous droplet to extract benzoic acid into organic layer. (d) The application of electrowetting force in the opposite direction starts to separate the two-phase droplet. (e) The two droplets were fully separated to give an organic droplet and aqueous droplet. (f) THF evaporated and benzoic acid crystalized on an EWOD chip.

Figure 3.17 Neutralization on EWOD device

3.20 Assessment on the in-line workup performance

The performance of the in-line workup was assessed by comparing the concentration of the isolated benzoic acid through the workup processes to the concentration of benzoic acid in the mixture prior to the workup. With a variation of the initial concentration of benzoic acid, the comparison of the concentration changes of benzoic acid before and after workup was illustrated in Figure 3.18. The concentration of benzoic acid before workup (droplet A in Figure 3.16a) is plotted in blue, and the concentration of the acid after workup (droplet B in Figure 3.17e) is plotted in red. Since the volumes of the droplets at the beginning and the end of the workup process are virtually equal, concentration changes before and after workup can be a fair representation of the yield of the separation. Through this performance analysis, we can conclude that the higher initial concentration of benzoic acid resulted in higher yield after workup recovery. Because the reaction time and mixing (e.g. agitation) scheme were fixed for all tests, the notable increase in yield is attributed to the higher concentration gradients, which caused faster diffusion in the given time period.

In a work by Madikizela,[158] studying the factors affecting the adsorption of ketoprofen onto a molecularly imprinted polymer (MIP), he demonstrated that by increasing the initial concentration of ketoprofen (while keeping other parameters) the extraction efficiency increased significantly. Also, Erwa[159] studied the effect of initial concentration on the extraction percentage of chromium (VI). He concluded the sharp rise of extraction efficiency by increasing the initial concentration of chromium. In both works mentioned above, the researcher reported that after a certain concentration, the concentration raise did not change the extraction percentage and it became constant; owing to the saturation of acceptor phases.

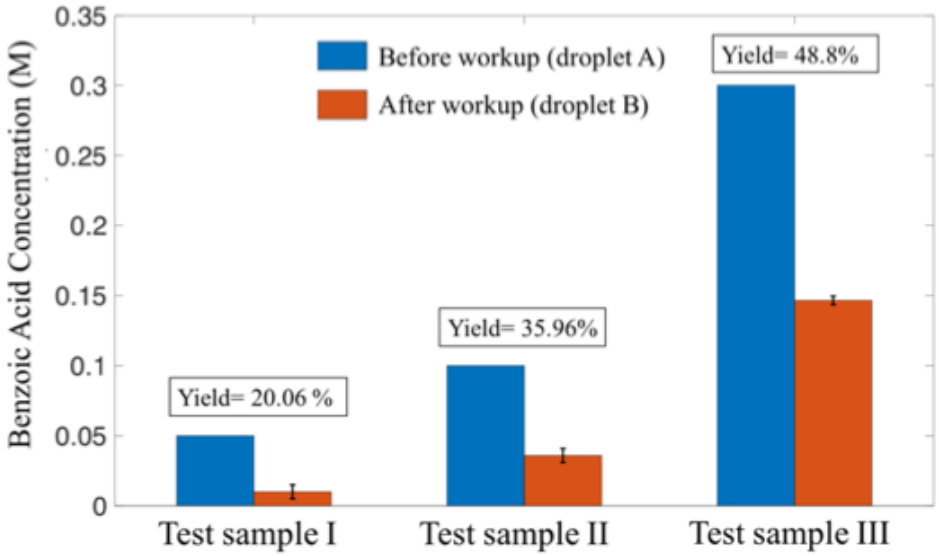

Assessment on the in-line workup performance on EWOD device. The blue bar indicates the initial concentration of benzoic acid before workup and the red bar shows the concentration of benzoic acid after the workup procedures. Yield of workup was obtained based on a fraction of concentration for each test. Columns and error bars are the average conversions and standard deviations from 3 reactions per each sample, respectively.

Figure 3.18 In-line workup performance

3.21 The relationship of yield and the agitation time in on-chip workup

In a conventional microfluidic channel, obtaining more than one equilibrium stage of the LEE system has been an ongoing obstacle. Traditional flow chemistry has taken advantage of serpentine and counter-current flows to overcome such an issue.[160] In contrast, in an EWOD device, a relatively stronger circulating flow is created within a droplet due to large Laplace pressure (i.e., capillary pressure) changes at liquid-air interface whenever EWOD actuation voltage is applied. Moreover, the direction of droplet motion can be randomly selected, which is equivalent to the serpentine microchannels. The experimental video presenting the aqueous-organic LLE system can be found in the supplementary material. To this end, the effect of agitation time to the on-chip workup yield was investigated. As shown in Figure 3.19, longer agitation time gave higher yield. Over time, the effect of the concentration gradient became less significant as the LLE system gets closer to the equilibrium. This result generally agrees with

literature precedents, which concern flask-based reactions. Moor[161] studied the extraction behavior of zirconium at both tracer and macro concentrations from aqueous solutions of nitric acid, hydrochloric acid, and oxalic acid into 2-thenoyltrifluoroacetone-xylene. He examined the efficiency of the extraction as a function of agitation time and concluded that the longer agitation time results in a linear increase in the extraction efficiency followed by a constant line; indicating the saturation of acceptor phases. Other researchers drew a similar conclusion.[162,163]

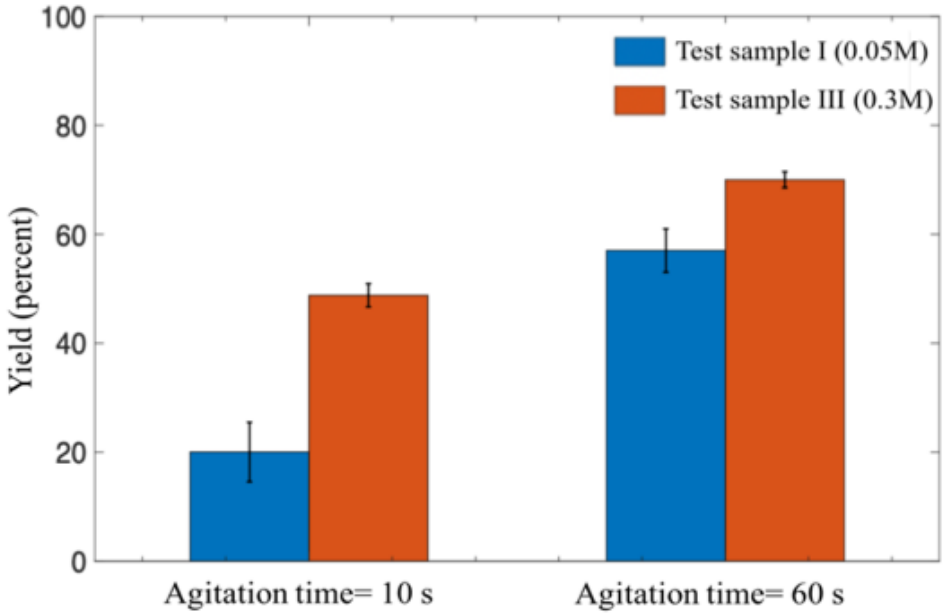

The relationship of yield and the agitation time in on-chip workup. Longer agitation time gave higher yield. Over time, the effect of the concentration gradient became less significant as the LLE system gets closer to the equilibrium. Columns and error bars are the average conversions and standard deviations from 3 reactions per each sample, respectively.

Figure 3.19 Yield and agitation relationship

3.22 Summary of in-line workup on EWOD device

In conclusion, we have demonstrated an in-line workup as a step towards promoting multi-step synthesis on an EWOD device. In this study, an acid-base workup was utilized as a model system, where the consecutive steps, including acid-base reaction, neutralization,

evaporation, and crystallization, were successfully operated. Moreover, in-line crystallization of benzoic acid and benzophenone manifested the capacity of an EWOD device to handle the solid particles, which are either added or formed during the reaction. Importantly, neither changes in device architecture nor disassembly were required to achieve workup and crystallization. We employed the novel techniques for mixing and phase separation, which is an essential part of the workup. Additionally, throughout the process, we identified the optimal EWOD voltage and frequency operation conditions for all the participating reagents. Finally, because the EWOD digital microfluidic device has robustness, chemical compatibility, and ease of use, we anticipate that it can be an alternative or a complementary tool to microreactors based on continuous channel flow for organic synthesis provide a broader range of chemistries and operating conditions.

3.23 Summary of on-chip organic synthesis

On-chip organic synthesis using an electrowetting-on-dielectric (EWOD) digital microfluidic device was successfully demonstrated. With esterification as the model reaction, on-chip chemical reactions were successfully demonstrated. Conversion data obtained from on-chip reactions using engine-and-cargo method were used in the demonstration of reaction characterization and optimization such as reaction kinetics, solvent screening, and catalyst loading. Results from this study clearly show that EWOD digital microfluidic platform is a promising candidate for a micro scale chemical reaction. In addition to this, research is also carried out for in-line organic workup as a key move towards development of multi-step synthesis on an EWOD platform. Acid-base workup is chosen as a model system to demonstrate the compatibility of general organic workup procedure and was successfully demonstrated. This

approach also successfully demonstrated the utility of solvent swapping without any further modification in the architecture of EWOD platform.

Appendix A: List of Abbreviations

δ: chemical shift (ppm)

μL: microliter

Ac: acetate

Ad: adamantyl

Ar: aryl group or substituent, general

Bn: benzyl

Bu: butyl

*t*Bu: tert-butyl

C: Celsius

calcd: calculated

cat.: catalyst, catalytic amount

COD: 1,5-cyclooctadiene

cf: compare

Cy: cyclohexyl

DCM: dichloromethane

Eq.: equation

equiv.: equivalent

Et: ethyl

g: gram

GCMS: gas chromatography mass spectrometry

h: hours

HRMS: high resolution mass spectrometry

Hz: hertz

IR: infrared spectroscopy

J: coupling constant, NMR spectroscopy

M: metal, general

M: molar

[M+]: molecular ion

Me: methyl

min.: minutes

mg: milligram

MHz: megahertz

mL: milliliter

mmol: millimole

MW: molecular weight

n/a: not applicable

NHC: *N*-heterocyclic carbene ligand

NMR: nuclear magnetic resonance spectroscopy

Appendix B: Experimental Procedures

Chapter 1

I. Materials and Methods

Reactions requiring anhydrous conditions were performed under an atmosphere of nitrogen or argon in flame or oven-dried glassware. Anhydrous toluene, dichloromethane (DCM), dimethylformamide (DMF) were distilled from CaH_2. Anhydrous tetrahydrofuran (THF) and diethyl ether (Et_2O) were distilled from sodium and benzophenone. Triethylamine and pyridine were distilled from KOH. DMF was stored over 4 Å molecular sieves. All other solvents and reagents from commercial sources were used as received. ^1H, ^2H, and ^{13}C NMR spectra were recorded on JEOL Eclipse Plus 500 (500 MHz) and JEOL ECX 300 (300 MHz) spectrometers. NMR spectra were recorded on a 500 or 300 MHz NMR spectrometer. ^1H NMR chemical shifts are referenced to benzene (7.16 ppm) and chloroform (7.26 ppm). ^{13}C NMR chemical shifts are referenced to C_6D_6 (128.06 ppm) and $CDCl_3$ (77.23 ppm). The following abbreviations are used to describe multiplets: s (singlet), d (doublet), t (triplet), q (quartet), pent (pentet), m (multiplet), nfom (nonfirst-order multiplet), and br (broad). The following format was used to report peaks: chemical shift in ppm [multiplicity, coupling constant(s) in Hz, integral, and assignment]. ^1H NMR assignments are indicated by structure environment (e.g., CH_aH_b). ^1H NMR and ^{13}C NMR were processed with the iNMR software program. Infrared (IR) spectra were recorded using neat (for liquid compound) or a thin film from a concentrated DCM solution. Absorptions are reported in $cm^{-1.}$ Only the most intense and/or diagnostic peaks are reported. MPLC refers to medium pressure liquid chromatography (25−200 psi) using hand-packed columns of silica gel (20−45 μm, spherical, 70 Å pore size), an HPLC pump, and a differential refractive index detector. High-resolution mass spectra (HRMS) were recorded in atmospheric-pressure chemical ionization and time-of-flight (APCI/TOF) mode. Samples were introduced as solutions in a

mixed solution of methanol and DCM. GC/MS data were recorded on a Varian 450-GC/Varian 240-MS System. The methods used are noted parenthetically: 5025015 refers to 2 min @ 50 °C – 20 °C/min – 3 min @ 250 °C (a 50 °C initial temperature that was held for 2 minutes followed by a 20 °C/min ramp to a final temperature of 250 °C that was held for 3 minutes for a total run time of 15 minutes). 5029017 refers to: 2 min @ 50 °C – 20 °C/min – 3 min @ 290 °C. 5029019 refers to: 2 min @ 50 °C – 20 °C/min – 5 min @ 290 °C. 5032021 refers to: 2 min @ 50 °C – 20 °C/min – 5 min @ 320 °C. Analytical TLC experiments were performed on an F254 plate with 250 μm thickness. Detection was performed by UV light or potassium phosphomolybdic acid, potassium permanganate, and *p*-anisaldehyde staining.

II. General Procedure for Preparation of Propargyl Acetates

A. Method 1: Preparation of propargyl alcohols via an addition reaction

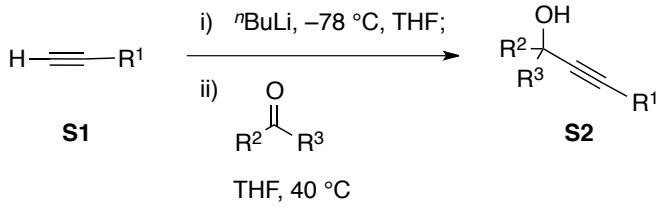

Alkynes **S1** (5.0 mmol) and THF (5 mL) were placed in a flame-dried round-bottom flask. A 2.5 M solution of ^{n}BuLi in hexanes (2.2 mL, 5.5 mmol) was added to the solution at –78 °C, and the suspension was stirred for 30 min at –78 °C. Carbonyls (5.5 mmol) in THF (5 mL) were added to the reaction mixture. The mixture was slowly warmed to room temperature (rt) and then continued stirred for 12 h at 40 °C. The reaction mixture was quenched with saturated aqueous NH_4Cl and extracted with Et_2O. The combined organic layers were washed with saturated aqueous $NaHCO_3$ and brine, dried over Na_2SO_4, and concentrated under reduced pressure to

afford propargyl alcohol **S2** as a colorless oil, which was used directly to the next acetylation reaction.

B. Method 2: Preparation of propargyl alcohols via Sonogashira coupling

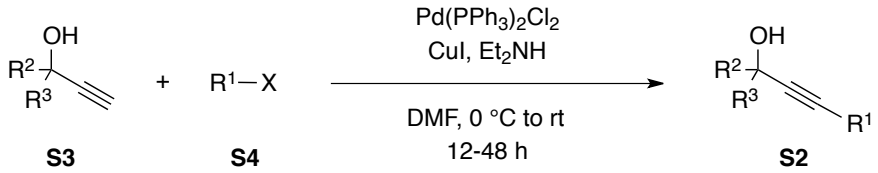

S3 **S4** **S2**

Palladium catalyst $Pd(PPh_3)_2Cl_2$ (35 mg, 10 mol %) and copper iodide (6 mg, 5 mol %) were placed to a flame-dried round-bottom flask. Alkenyl or aryl halide **S4** (5.0 mmol) in DMF (4 mL) was added to the mixture at 0 °C, and diethylamine (10.0 mmol) and alkynols **S3** (6 mmol) were added to the mixture. The reaction mixture was slowly warmed to room temperature (rt) and then continued stirred for 12-48 h. The solvent was evaporated under reduced pressure, and the residue was diluted with ethyl acetate (EtOAc). The organic layer was washed with saturated aqueous NH_4Cl and extracted with EtOAc. The combined organic layers were washed with brine, dried over Na_2SO_4, and concentrated under reduced pressure. The resultant was filtered through a pad of silica gel, and the filtrate was concentrated under reduced pressure to afford propargyl alcohol **S2** as a colorless oil, which was used directly to the next acetylation reaction.

C. Acetylation of alcohols:

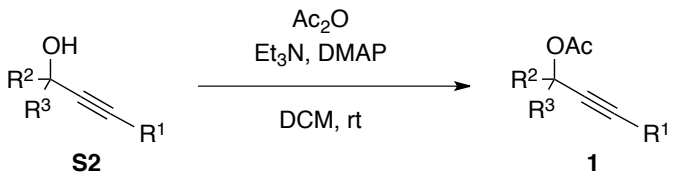

S2 **1**

Propargylic alcohol **S2**, CH_2Cl_2 (20 mL, 0.25 M), dimethylaminopyridine (DMAP, 61 mg, 10 mol %), and Et_3N (0.76 mL, 5.5 mmol) were placed in a flame-dried round bottom flask. Acetic anhydride (0.57 mL, 6 mmol) was added dropwise over 15 min. After being stirred at rt for 3 h, the reaction mixture was quenched by adding saturated aqueous $NaHCO_3$ and stirred for 10 min. The reaction mixture was extracted with Et_2O. The organic layer was washed with water, followed by saturated aqueous brine. The organic extract was combined and dried over anhydrous Na_2SO_4. The resulting solution was concentrated under reduced pressure to afford a brown oil, which was purified by column chromatography to give propargyl acetates **1**.

III. Reaction Optimization

A. Ligand Screening

Hydrosilyl acetal **1a-int** (0.2 mmol) was added to a nitrogen purged Norell® pressure NMR tube. $[Rh(nbd)Cl]_2$ (0.2 mg, 0.2 mol %), ligand (0.2 mol % for Tp ligands and 0.6 mol % for phosphine ligands) shown in Table S1, mesitylene (internal standard), THF (0.6 mL), and C_6D_6 (100 mL) were added to the NMR tube. The tube was capped, and the mixture was agitated occasionally. The reaction progress was monitored by ^1H NMR spectroscopy for 1h at room temperature.

Table S1.

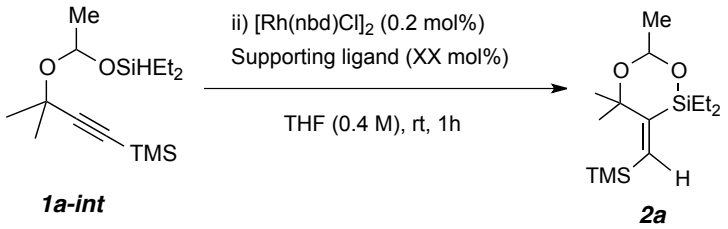

1a-int ***2a***

Entry	Supporting ligand	Yield (%)[b]	α:β[c]	E:Z[d]

1	PPh_3	81	only α	only *E*
2	$P(C_6F_5)_3$	92	only α [d]	only *E*
3	$P(4\text{-}MeOPh)_3$	84	only α	only *E*
4	PPh_2Et	83	only α	only *E*
5	JohnPhos	84	only α	only *E*
6	PCy_3	78	only α	only *E*
7	$P(OPh)_3$	77	only α	only *E*
8	Cp*[e]	90	only α	only *E*
9	$Tp^{(CH3)2}K$	82	only α	only *E*
10	$Tp^{CF3,Ph}Na(THF)$	88	only α	only *E*
11	$Tp^{(CF3)2}Na(THF)$	85	only α [d]	only *E*

[a]Conditions: **1a-int** (0.20 mmol), supporting ligand (1.2 mol % for phosphine ligands, 0.4 mol % for Tp ligands,), THF (0.4 M). [b]Determined by ^1H NMR spectroscopy utilizing an internal standard (mesitylene). [c]Determined by GC/MS analysis and ^1H NMR spectroscopy. [d]NOESY experiment. [e]$[RhCp^*Cl_2]_2$ was used. TMS = trimethylsilyl

---

B. Temperature Screening

Hydrosilyl acetal **1a-int** (0.2 mmol) was added to a nitrogen purged Norell® pressure NMR tube. $[Rh(nbd)Cl]_2$ (0.2 mg, 0.2 mol %), ligand (0.4 mol % for Tp ligands and 1.2 mol % for phosphine ligands) shown in Table S1, mesitylene (internal standard), THF (0.6 mL), and C_6D_6 (100 mL) were added to the NMR tube. The tube was capped, and the mixture was agitated occasionally. The reaction progress was monitored by ^1H NMR spectroscopy for 1h at temperature specified in Table S1.

C. Catalyst Loading Screening

Hydrosilyl acetal **1a-int** (0.2 mmol) was added to a nitrogen purged Norell® pressure NMR tube. $[Rh(nbd)Cl]_2$ (0.2 mg, 0.2 mol %), ligand (0.4 mol% for Tp ligands and 1.2 mol% for phosphine ligands) shown in Table S1, mesitylene (internal standard), THF (0.6 mL), and C_6D_6 (100 mL) were added to the NMR tube. The tube was capped, and the mixture was agitated occasionally. The reaction progress was monitored by ^1H NMR spectroscopy for 1h at temperature specified in Table S1.

IV. General Procedure for Propargyl acetates to Prepare Dioxasilinanes 6

Scheme S1. Preparation of Dioxasilinanes **2**

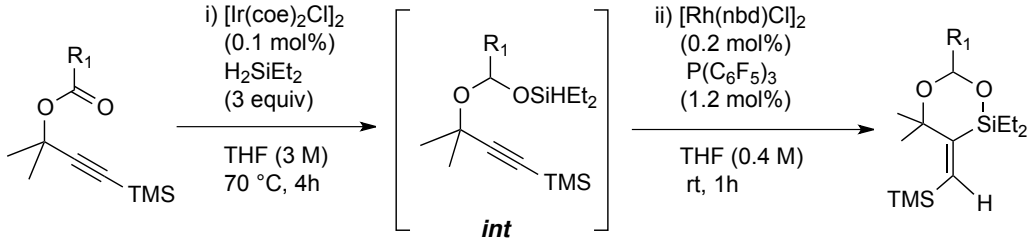

$[Ir(coe)_2Cl]_2$ (0.1 mol %) and propargyl acetates **1a** (0.2 mmol) were dissolved with THF (0.6 mL, 0.33 M). Diethylsilane (3 equiv) was added to the mixture. The septum on the vial was replaced by a screw cap with a Teflon liner. The reaction mixture was stirred for 12 h at rt or 3 h at 70 °C. The volatiles were removed *in vacuo* to afford the silyl acetals **1a-int**, which were directly used for a subsequent reaction without further purification.

$[Rh(nbd)Cl]_2$ (0.2 mg, 0.2 mol %) and $P(C_6F_5)_3$ (1.2 mg, 1.2 mol %) were dissolved with THF (0.5 mL, 0.4 M). The crude silyl acetals **1a-int** (0.2 mmol) were added to the mixture in one portion. The septum on the vial was replaced by a screw cap with a Teflon liner, and the mixture was stirred at rt. The reaction progress was monitored by GC-MS spectrometry. The volatiles were removed *in vacuo*, and the resulting mixture was dissolved with pentane, filtered

through a pad of Celite®, and concentrated *in vacuo* to afford the crude dioxasilinanes **2,** which were purified by MPLC (hexanes/EtOAc).

V. General Procedure for Hydrosilyl Acetals to Prepare Dioxasilinanes 2

Scheme S2. Preparation of Dioxasilinanes **2**

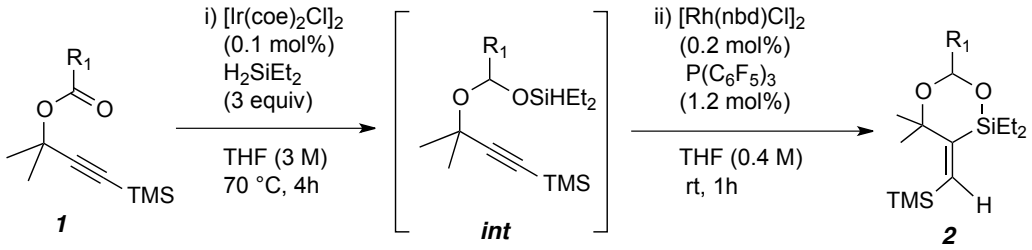

$[Ir(coe)_2Cl]_2$ (0.1 mol %) and propargyl ester **1** (0.2 mmol) were dissolved with THF (0.6 mL, 0.33 M) in a flame dried vial. Diethylsilane (3 equiv) was added to the mixture. The septum on the vial was replaced by a screw cap with a Teflon liner. The reaction mixture was stirred for 12 h at rt or 3 h at 70 °C. The volatiles were removed under reduced pressure to afford the silyl acetal **5**, which were directly used for a subsequent reaction without further purification.

$[Rh(nbd)Cl]_2$ (0.2 mg, 0.2 mol%) and $P(C_6F_5)_3$ (1.2 mg, 1.2 mol %) were dissolved with THF (0.5 mL, 0.4 M). The crude silyl acetals **1-int** (0.2 mmol) were added to the mixture in one portion. The septum on the vial was replaced by a screw cap with a Teflon liner, and the mixture was stirred at rt. The reaction progress was monitored by GC-MS spectrometry. The volatiles were removed *in vacuo*, and the resulting mixture was dissolved with pentane, filtered through a pad of Celite®, and concentrated under reduced pressure to afford the crude dioxasilinanes **2**, which was purified by MPLC

VI. General Procedure for Nucleophilic Ring opening of Dioxasilinanes 3

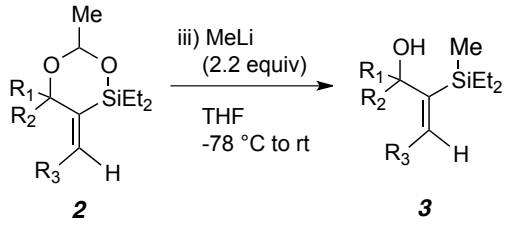

To a flame-dried vial a solution of dioxasilolane **2** (0.1 mmol) in THF (0.5 mL, 0.2 M) was added and mixture cooled to –78 °C. MeLi (137μL, 1.6 M in Et_2O, 2.2 equiv) was added slowly to the reaction mixture. After being stirred for 30 min at –78 °C, the reaction mixture was quenched with saturated aqueous NH_4Cl and extracted with Et_2O. The volatiles were removed to afford crude material, which was purified by MPLC (hexanes/EtOAc) to afford **3** as a colorless oil.

VII. Synthetic Applications

Scheme S3. Synthesis of Diene **3x**

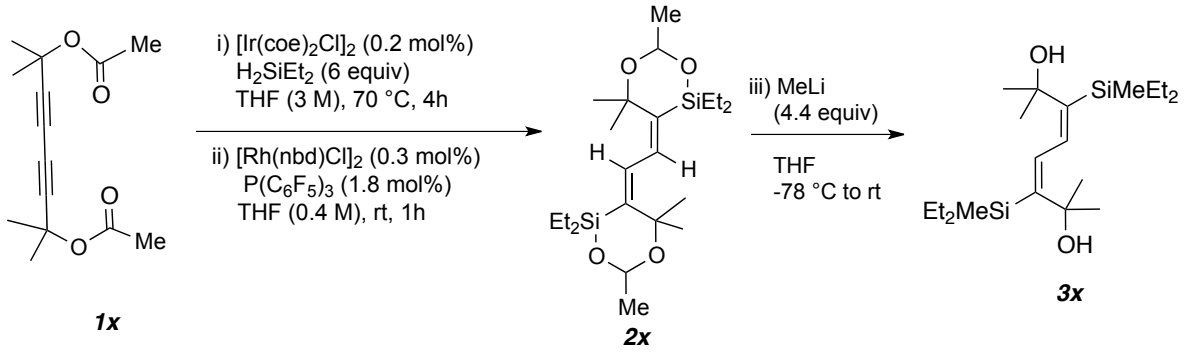

$[Ir(coe)_2Cl]_2$ (0.1 mol %) and dialkynyl ester **1x** (0.2 mmol) were dissolved with THF (0.6 mL, 0.33 M). Diethylsilane (3 equiv) was added to the mixture. The septum on the vial was replaced by a screw cap with a Teflon liner. The reaction mixture was stirred for 12 h at rt or 3 h at 70 °C.

The volatiles were removed *in vacuo* to afford the silyl acetal **int**, which were directly used for a subsequent reaction without further purification.

$[Rh(nbd)Cl]_2$ (0.3 mg, 0.3 mol %) and $P(C_6F_5)_3$ (1.8 mg, 1.8 mol %) were dissolved with THF (0.5 mL, 0.4 M). The crude silyl acetals **int** (0.2 mmol) were added to the mixture in one portion. The septum on the vial was replaced by a screw cap with a Teflon liner, and the mixture was stirred at rt. The reaction progress was monitored by GC-MS spectrometry. The volatiles were removed *in vacuo*, and the resulting mixture was dissolved with pentane, filtered through a pad of Celite®, and concentrated *in vacuo* to afford the crude dioxasilinanes **2x**, which were purified by MPLC (hexanes/EtOAc =100:1, 5 mL/min).

To a flame-dried vial a solution of dioxasilolane **3x** (0.1 mmol) in THF (0.5 mL, 0.2 M) was added and mixture cooled to –78 °C. MeLi (137μL, 1.6 M in Et_2O, 2.2 equiv) was added slowly to the reaction mixture. After being stirred for 30 min at –78 °C, the reaction mixture was quenched with saturated aqueous NH_4Cl and extracted with Et_2O. The volatiles were removed to afford crude material, which was purified by MPLC (hexanes/EtOAc = 5:1, 5 mL/min) to afford **17** as a colorless oil.

Scheme S4. Synthesis of Enyne **3y**

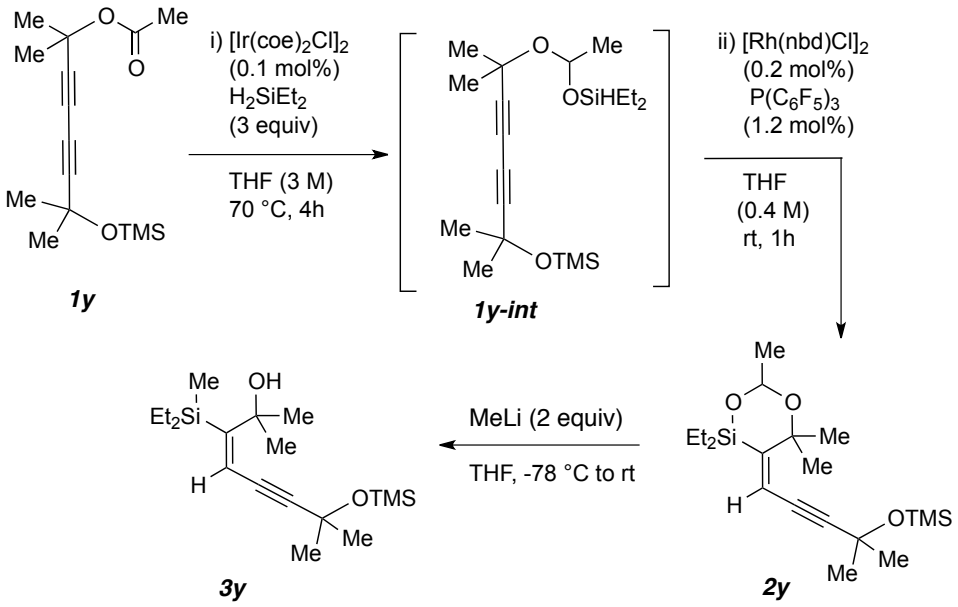

$[Ir(coe)_2Cl]_2$ (0.1 mol %) and dialkynyl ester **1y** (0.2 mmol) were dissolved with THF (0.6 mL, 0.33 M). Diethylsilane (3 equiv) was added to the mixture. The septum on the vial was replaced by a screw cap with a Teflon liner. The reaction mixture was stirred for 12 h at rt or 3 h at 70 °C. The volatiles were removed *in vacuo* to afford the silyl acetal **1y-int**, which were directly used for a subsequent reaction without further purification.

$[Rh(nbd)Cl]_2$ (0.2 mg, 0.2 mol %) and $P(C_6F_5)_3$ (1.2 mg, 1.2 mol %) were dissolved with THF (0.5 mL, 0.4 M). The crude silyl acetals **1y-int** (0.2 mmol) were added to the mixture in one portion. The septum on the vial was replaced by a screw cap with a Teflon liner, and the mixture was stirred at rt. The reaction progress was monitored by GC-MS spectrometry. The volatiles were removed *in vacuo*, and the resulting mixture was dissolved with pentane, filtered through a pad of Celite®, and concentrated *in vacuo* to afford the crude dioxasilinanes **2y**, which were purified by MPLC (hexanes/EtOAc =100:1, 5 mL/min).

To a flame-dried vial a solution of dioxasilolane **2y** (0.1 mmol) in THF (0.5 mL, 0.2 M) was added and mixture cooled to –78 °C. MeLi (137μL, 1.6 M in Et_2O, 2.2 equiv) was added slowly to the reaction mixture. After being stirred for 30 min at –78 °C, the reaction mixture was quenched with saturated aqueous NH_4Cl and extracted with Et_2O. The volatiles were removed to afford crude material, which was purified by MPLC (hexanes/EtOAc = 10:1, 5 mL/min) to afford **3y** as a colorless oil.

VIII. Derivitazation of phenyl-substituted ethinyl estradiol (EE)

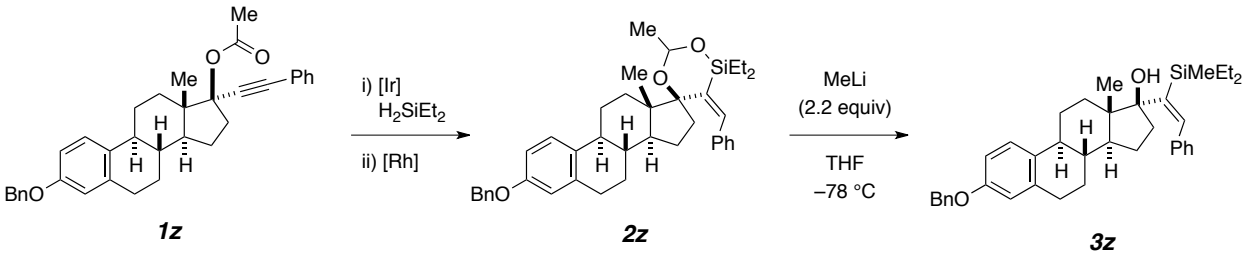

$[Ir(coe)_2Cl]_2$ (0.1 mol %) and EE **1z** (0.2 mmol) were dissolved with THF (0.6 mL, 0.33 M). Diethylsilane (3 equiv) was added to the mixture. The septum on the vial was replaced by a screw cap with a Teflon liner. The reaction mixture was stirred for 12 h at rt or 3 h at 70 °C. The volatiles were removed *in vacuo* to afford the silyl acetal **int**, which were directly used for a subsequent reaction without further purification.

$[Rh(nbd)Cl]_2$ (0.2 mg, 0.2 mol %) and $P(C_6F_5)_3$ (1.2 mg, 1.2 mol %) were dissolved with THF (0.5 mL, 0.4 M). The crude silyl acetals **int** (0.2 mmol) were added to the mixture in one portion. The septum on the vial was replaced by a screw cap with a Teflon liner, and the mixture was stirred at room temperature. The reaction progress was monitored by GC-MS spectrometry. The volatiles were removed *in vacuo*, and the resulting mixture was dissolved with pentane,

filtered through a pad of Celite®, and concentrated *in vacuo* to afford the crude dioxasilinanes **6**, which were purified by MPLC (hexanes/EtOAc = 40:1, 5 mL/min).

To a flame-dried vial a solution of dioxasilolane **2z** (0.1 mmol) in THF (0.5 mL, 0.2 M) was added and mixture cooled to –78 °C. MeLi (137μL, 1.6 M in Et_2O, 2.2 equiv) was added slowly to the reaction mixture. After being stirred for 30 min at –78 °C, the reaction mixture was quenched with saturated aqueous NH_4Cl and extracted with Et_2O. The volatiles were removed to afford crude material, which was purified by MPLC (hexanes/EtOAc = 10:1, 5 mL/min) to afford **11** as a colorless oil.

Chapter 2

Experimental Section

***Materials*.** Styrene (stabilized with TBC, >99.0 %) and lithium-*tert*-butoxide (Li*O*tBu, ca. 10% in Tetrahydrofuran, ca. 1mol/L) were purchased from TGI. 4-methoxystyrene (98.0 %, stabilized with 0.1% 4-tert-butylcatechol) and potassium-*tert*-butoxide (K*O*tBu) were purchased form Alfa Aesar. 18-crown-6-ether (18-c-6) was purchased from AK Scientific. 15-crown-5-ether (15-c-5), 12-crown-4-ether (12-c-4), triethylsilane ($HSiEt_3$, 98%), phenylsilane (H_3SiPh_1, 97%) and triphenylsilane ($HSiPh_3$, 99%) were purchased form BeanTown Chemical, Inc. Diethylsilane (H_2SiEt_2) was purchased from GELEST,Inc. Diphenylsilane (H_2SiPh_2, min, 97%) was purchased from STREM Chemicals, Inc.

Preparation of Metal Lewis-Base Hydrogen Atom Transfer Catalyst (LBCI-HAT). First, lewis base solution was prepared as follows: KOtBu (0.02 mmol) was dissolved in 10 mL

of 0.1 M THF solution. KOtBu solution was mixed for a seconds at room temperature. Three different of crown ethers (18-c-6, 15-c-5, and 12-c-4, 0.019 mmol), and monomers (0.8 mmol) were mixed in a screw cap vial with 1.4 ml THF. After mixing the resulting solution with lewis base, silane (0.54 mmol) with various ligands was injected using a micro syringe. Triphenylsilane was dissolved in 0.4 ml THF using 0.54 mmol and injected (equilibrium), as shown in Scheme S1-S4. All LBCI-HAT sample were prepared >2 ml of THF solvent using simple approach (Table S2). The polymerization of substituent styrene was performed in monomer:hydrosilane:lewis base:crown ether = 0.8:0.54:0.02:0.019 mole ratio, with 1.4 ml THF, at 25 °C. Briefly, the Lewis base with metal was prepared by dissolving in THF solvent, and then mixed with monomer, crown ether, and THF at room temperature for several seconds according to the mole ratio. Various key factors were prepared with equivalent mole ratios for each molecular weight. Finally, about 1 ml of silane with a specific ligand was injected using a micro syringe. When injected with a silane, hydrogen bubbles generated on the top of the solution surface and the reaction begins. In a moment, the color of the solution changed from transparent to orange or pink depending upon the key factors. The color change resulted in a transparent color upon contact with air (Figure SX). It suggests that the reaction involve anion or radical mediated processes.

FT-NIR measurements. FT-NIR allowed the time-resolved measurement of monomer conversion in radical polymerization. Spectrum was characterized by the disappearance of the signal at 6136 cm^{-1} for styrene, at 6133 cm^{-1} for 4-methoxystyrene corresponding to C=C double bond stretching vibration of vinyl group, which confirms a successful polymerization.[17-20] FT-NIR measurement performed with resolution 8 and 16 cm^{-1}, sample and baseline scan time 16 set. Analysis of peaks was 6210-6050 cm^{-1}. All real-time monitoring of monomer conversion

were performed using a Bruker MPA FT-NIR Spectrophotometer. The peak baseline and analysis values were calculated using an OPUS operator software.

I. General Procedure for Polymerization of electron-poor vinylarenes

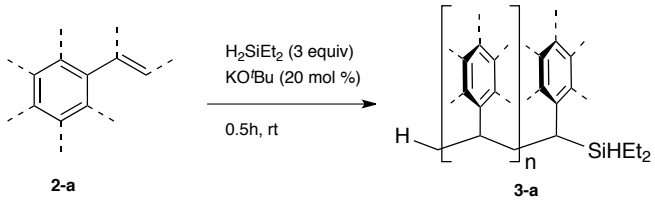

2-a 3-a

In a flame dried vial vinylarene substrate (0.2 mmol) is added. Freeze-pump-thaw process is performed for three times. KO^{t}Bu (1 M in THF) (20 mol %) and diethylsilane (3.5 equiv) were added to the mixture. Once the polymerization was completed, the polymer is dissolved in solvent (THF or Toluene) and precipitated by addition of methanol to the reaction mixture. After filtration, white solids were washed with cold methanol to provide polystyrenes.

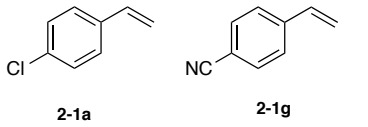

2-1a 2-1g

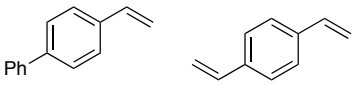

2-1h 2-1i

II. General Procedure for Polymerization of electron-rich and electron-neutral vinylarenes

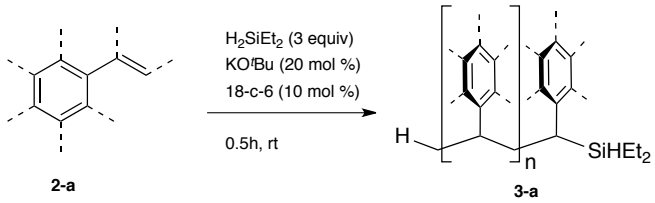

2-a 3-a

In a flame dried vial vinylarene substrate (0.2 mmol) and 18-crown-6 (10 mol %) are added. Freeze-pump-thaw process is performed for three times. KO^{t}Bu (1 M in THF) (20 mol %) and

diethylsilane (3.5 equiv) were added to the mixture. Once the polymerization was completed, the polymer is dissolved in solvent (THF or Toluene) and precipitated by addition of methanol to the reaction mixture. After filtration, white solids were washed with cold methanol to provide polystyrenes.

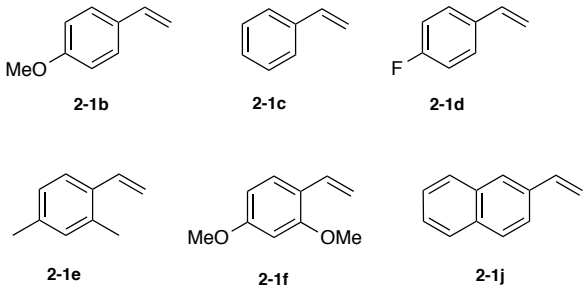

II. General Procedure for Copolymerization of vinylarenes

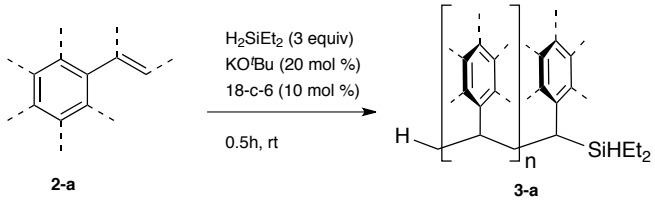

In a flame dried vial vinylarene substrate mixture in 1:1 ratio (0.2 mmol i.e., 0.1 mmol each) and 18-crown-6 (10 mol %) are added. Freeze-pump-thaw process is performed for three times. KO^tBu (1 M in THF) (20 mol %) and diethylsilane (3.5 equiv) were added to the mixture. Once the polymerization was completed, the polymer is dissolved in solvent (THF or Toluene) and precipitated by addition of methanol to the reaction mixture. After filtration, white solids were washed with cold methanol to provide polystyrenes.

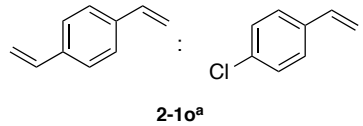

2-1o[a]

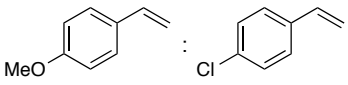

2-1q

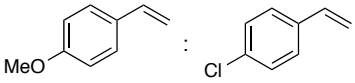

2-1p[a]

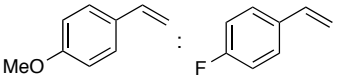

2-1r

[a]18-c-6 is not used for olefin polymerization

Chapter 3

I. EWOD device fabrication

First, using acetone, isopropanol, methanol and DI water the Indium tin oxide (ITO) coated wafer plates was cleaned followed by blow drying with N_2 and the dehydration process on a hotplate at 150 ℃ for 5 min. Then, utilizing a spin coater with the recipe of ramping the speed spin to 500 rpm with 100 rpm/s for 5 s; ramping with 900 rpm/s to 4000 rpm for 30 s, the hexamethyldisilazane (HMDS) was coated on the substrate to promote the adhesion of photoresist (PR). Moreover, the wafer baked at 150 ℃ for 90 s to evaporate the solvent present in the HMDS solution. Then, 1.2 μm uniform thickness of a positive PR (Microchem S1813, MicroChem Corp, Newton, MA, USA) was spin coated on the wafer utilizing the following recipe; Spin speed was ramped up to 500 rpm by 100 rpm/s for 5 s; ramping by 900 rpm/s to 3000 rpm for 30 s. To remove the excess solvent and to anneal the PR, soft bake was done at 115 ℃ for 60 s. The photolithography was done with the exposure does of 140 mJ/cm^2 using the backside-aligner (OAI 806MBA) followed by the post baked at 110 ℃ for 1 min. After that,

using a developer (Microchem, MF-319), the wafer was developed and dehydrated at 115 ℃ for 2 min. To etch the ITO layer, a solution consists of Hydrochloric acid (HCl), Nitric acid (HNO_3) and DI water (H_2O) (wt %- 20% HCl, 5% HNO_3, 75% H_2O or vol %- 8:1:15, HCl: HNO_3: H_2O) was used and the wafer was immersed in the solution at 55 ℃ for 2.5 min. Then, the wafer went through stripping PR (Remover 1165, Microchem) and dehydration at 150 ℃ for 2 min.

After that, 5μm uniform thickness of (SU-8 2005, Microchem) as dielectric layer was spin coated on the wafer with the subsequent recipe; Spin speed was ramped up to 500 rpm by 100 rpm/s for 5 s; ramping by 900 rpm/s to 2000 rpm for 30 s. To harden the dielectric layer, the wafer was baked at 70 ℃ for 1min, 100 ℃ for 3 min and cooled down at 70 ℃ and the room temperature for 1 min and 2 min respectively. After that, the exposure was done with a light does of 140 mJ/cm^2 followed by post baked at 70 ℃ for 1 min, 100 ℃ for 3 min and also hard baked at 150 ℃ for 5 min. Teflon AF1600S (Du Pont powder dissolved in Fluorinert FC-40 Sigma-Aldrich) as a hydrophobic layer was spin coated on top of the dielectric layer with the following recipe; Spin speed was ramped up to 1000 rpm by 300 rpm/s for 30 s, resulting in 300 nm thickness. Then, the wafer baked at 70 ℃ for 1 min, 100 ℃ for 1 min and 180 ℃ for 3 min. To suppress the chance of voltage-break down, another layer of Teflon was spin coated followed by annealing at 70 ℃ for 1 min, 100 ℃ for 3 min and 180 ℃ for 15 min. As a top plate, the ITO-coated glass went through the cleaning and dehydration process. Then, 300 nm layer of Teflon AF1600S was spin coated with aforementioned recipe. Then, the wafer annealed at 70 ℃ for 1 min, 100 ℃ for 3 min and 180 ℃ for 5 min.

II. General procedure for lab-scale reactions:

Menthol (31.2 mg, 0.2 mmol), Et_3N (56 μL, 0.4 mmol), and DMAP were dissolved in solvent (0.16 mL) in a vial. Acetic anhydride (38 μL, 0.4 mmol) was added to the mixture. The septum on the vial was replaced by a screw cap with a Teflon liner, and the reaction mixture was stirred at rt. The reaction progress was monitored by either GC-MS spectrometry or 1H-NMR spectroscopy. The reaction was quenched by addition of saturated aqueous $NaHCO_3$ solution. After being stirred for 10 min, the reaction mixture was extracted with Et_2O three times. The organic layer was washed with water followed by saturated aqueous brine and dried over anhydrous Na_2SO_4. The resulting solution was concentrated under reduced pressure to afford a brown oil. ^1H spectra were recorded on JOEL Eclipse Plus 500 (500 MHz) spectrometer with 10 second relaxation delay, yields are measured with Mesitylene as internal standard.

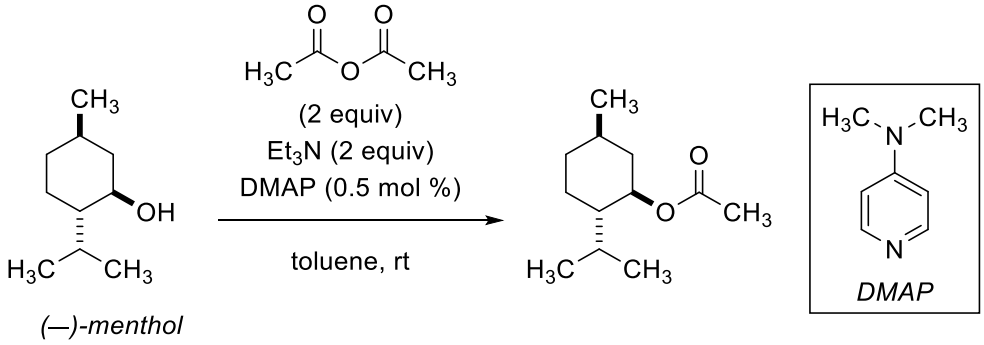

III. NMR studies:

Menthol (97.5 mg, 0.625 mmol), Et3N (126 μL, 1.25 mmol) and DMAP were placed in a Norell®pressure NMR tube and dissolved in Toluene-D8 (0.5 mL). Acetic anhydride (127 μL, 1.25 mmol) was added to the mixture and the tube was capped and agitated for 5 seconds. 1H spectra wererecorded on JOEL Eclipse Plus 500 (500 MHz) spectrometer with 10 second relaxation delay. ^{1}HNMR chemical shifts are referenced to Toluene-D8 (7.00 ppm).

^{1}H and ^{13}C NMR spectra were recorded on JOEL Eclipse Plus 500 (500 MHz) and JEOL ECX 300 (300 MHz) spectrometers. ^{1}H NMR chemical shifts are referenced to chloroform (7.26 ppm). ^{13}C NMR chemical shifts are referenced to $^{13}CDCl3$ (77.23 ppm). ^{1}H NMR and ^{13}C NMR were processed with the iNMR software program.

NMR Spectroscopy Result for Kinetic Study

Before running the kinetic study on the EWOD chip, we characterized the profile of the esterification reaction in lab-scale. In this regard, we utilized the NMR spectroscopy to

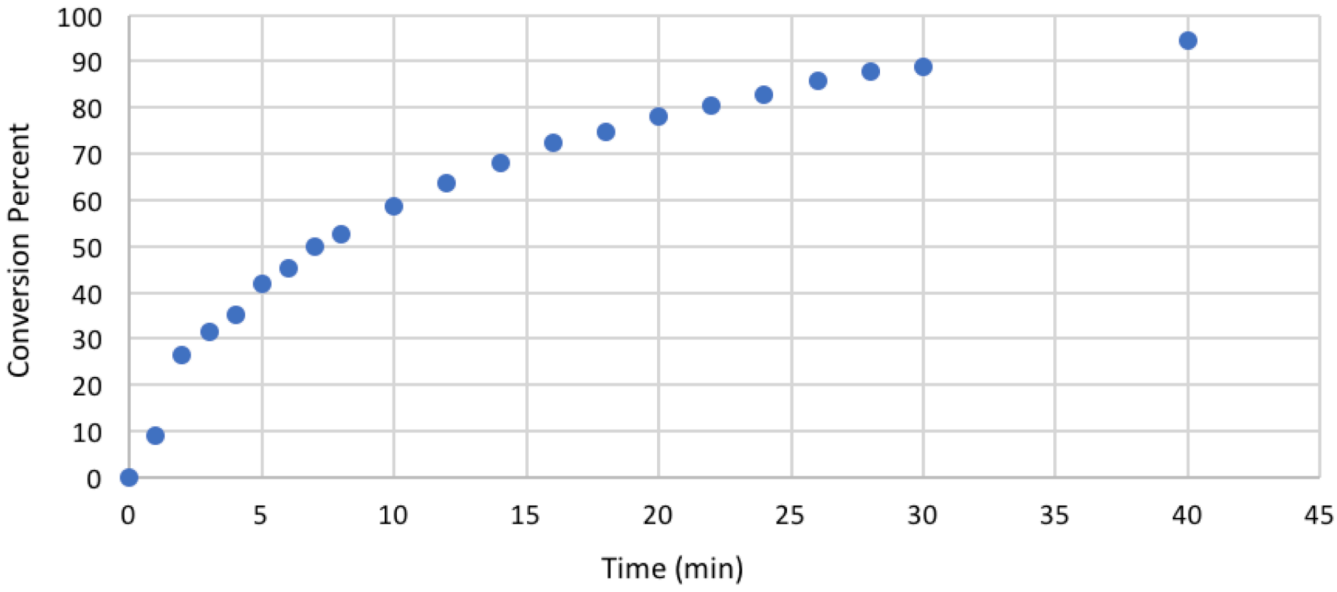

Figure S2: NMR spectroscopy result showing the profile of the esterification resulted from Lab-scale synthesis.

investigate the conversion of the starting material to the product. Fig. S2, shows the profile of esterification of menthol in lab-scale where the reaction reached 95% in 40 min.

IV. Mass Spectroscopy (GC-MS) for Kinetic Study on Chip

GC-MS analysis:

GC-MS data were recorded on a Varian 450-GC/Varian 240-MS System. The methods used are noted parenthetically: 5029017 refers to: 2 min @ 50 °C – 20 °C/min – 3 min @ 290 °C (a 50 °C initial temperature that was held for 2 minutes followed by a 20 °C/min ramp to a final temperature of 290 °C that was held for 3 minutes for a total run time of 17 minutes).

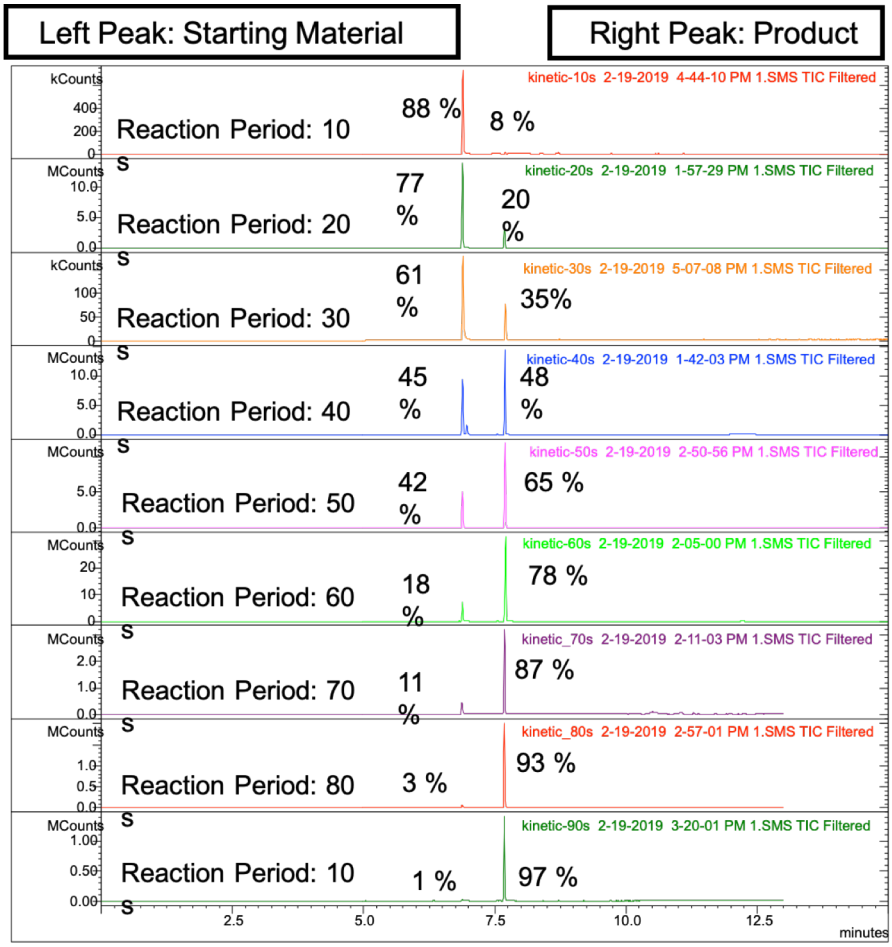

Figure S3: The mass spectroscopy (GC-MS) of each sample product, which was quenched at different time periods.

V. Mass Spectroscopy (GC-MS) for Catalyst Optimize Loading

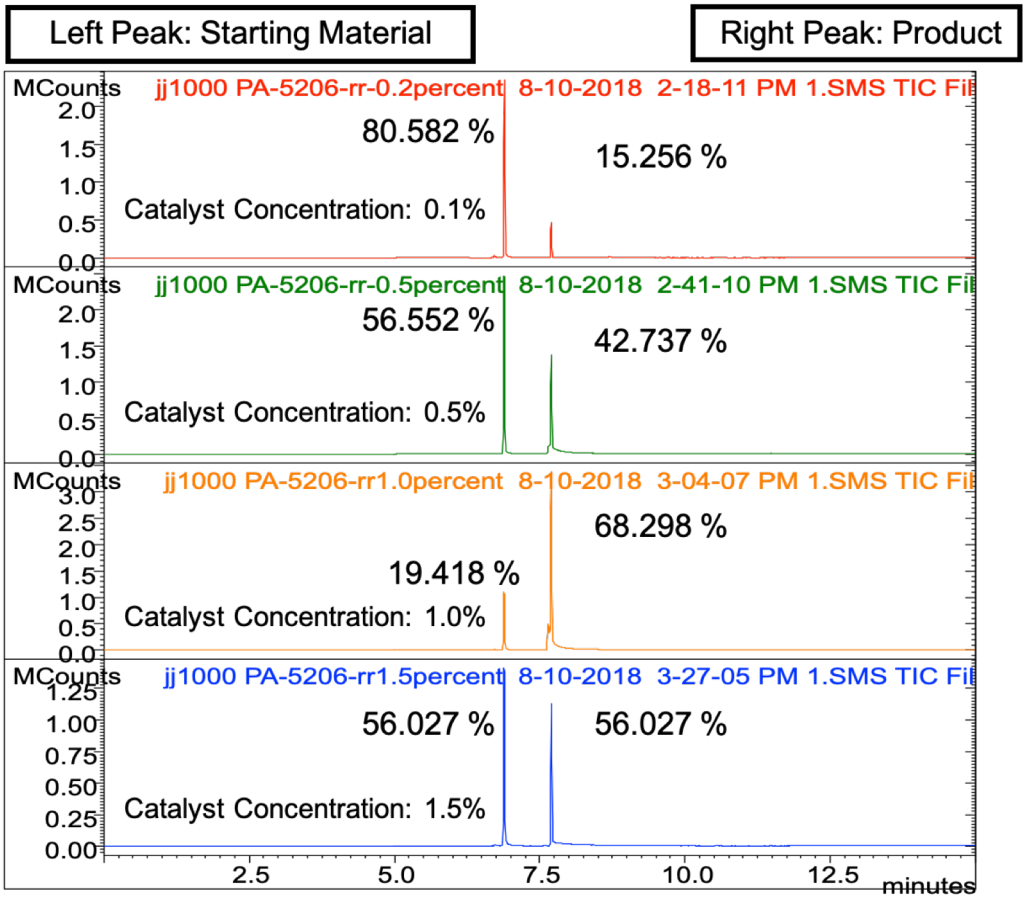

Figure S4: The progress of the mass spectroscopy (GC-MS) of different concentration of DMAP.

Appendix C

Spectral data of the compounds

2-Methyl-4-(trimethylsilyl)but-3-yn-2-yl acetate (1a)

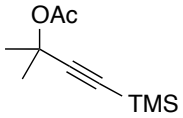

Yield: 5.0 mmol, 1045 mg, 95%

^{1}H NMR ($CDCl_3$, 500 MHz): δ 2.00 (s, 3H, C*H*$_3$C=O), 1.64 [s, 6H, C(C*H*$_3$)$_2$], and 0.15 [s, 9H, Si(C*H*$_3$)$_3$].

^{13}C NMR ($CDCl_3$, 125 MHz): δ 169.3, 106.5, 88.4, 72.5, 29.1, 22.20, and 0.06.

IR (neat): 2994 (w), 1745 (m), 1366 (m), 1219 (s), 1163 (s), 865 (m), and 761 (s) cm^{-1}.

TLC: R_f = 0.5 in 20:1 hexanes: EtOAc.

GC-MS (5032021): t^R = 3.167 min, *m/z* 198, 198 [M^+, 10], 199 [$(M+H)^+$, 50], 155[$(M–COCH_3)^+$, 100], and 138(30).

HRMS (**APCI/TOF**): Calcd for $(M+Na)^+$ $(C_{10}H_{18}NaO_2Si)^+$: 221.0968. Found: 221.0959.

2-Methyl-4-(trimethylsilyl)but-3-yn-2-yl formate (1b)

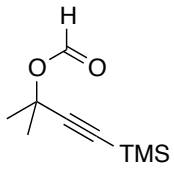

Yield: 754 mg, 82%

^{1}H NMR ($CDCl_3$, 500 MHz): δ 8.27 (s, 1H, *H*C=O), 1.66 [s, 6H, C(C*H*$_3$)$_2$], and 0.15 [s, 9H, Si(C*H*$_3$)$_3$].

^{13}C NMR ($CDCl_3$, 125 MHz): δ 160.8, 105.1, 91.1, 73.6, 29.8, and 0.04.

IR (neat): 2935 (w), 1732 (m), 1406(w), 1339(m), and 726 (s) cm^{-1}.

TLC: R_f = 0.6 in 10:1 hexanes: EtOAc.

GC-MS (5032021): t^R = 3.219 min, *m/z* 184, 184 [M^+, 50], 185 [$(M+H)^+$, 10], 155[$(M–HCO)^+$, 60], and 111 (100).

HRMS (**APCI/TOF**): Calcd for $(M+Na)^+$ $(C_9H_{16}NaO_2Si)^+$: 207.0812. Found: 207.0808.

2-Methyl-4-(trimethylsilyl)but-3-yn-2-yl 2-chloroacetate (1c)

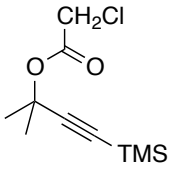

Yield: 858 mg, 74%

^{1}H NMR ($CDCl_3$, 500 MHz): δ 4.00 (s, 1H, $ClCH_2C$=O), 1.68 [s, 6H, $C(CH_3)_2$], and 0.15 [s, 9H, $Si(CH_3)_3$].

^{13}C NMR ($CDCl_3$, 125 MHz): δ 165.7, 100.5, 91.0, 75.2, 42.1, 29.4, and 0.4.

IR (neat): 3030 (w), 2930 (m), 1741 (w), 1230 (m), 820 (m), and 704 (s) cm^{-1}.

TLC: R_f = 0.4 in 10:1 hexanes: EtOAc.

GC-MS (5032021): t^R = 3.642 min, *m/z* 232, 232 [M^+, 50], 233 [$(M+H)^+$, 30], 155[$(M–COCH_2Cl)^+$, 80], and 159 (20).

HRMS (**APCI/TOF**): Calcd for $(M+Na)^+$ $(C_{10}H_{18}ClO_2Si)^+$: 233.0759. Found: 233.0758.

2-Methyl-4-(trimethylsilyl)but-3-yn-2-yl isobutyrate (1d)

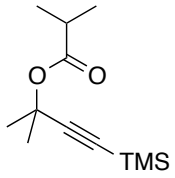

Yield: 881 mg, 78%

^{1}H NMR ($CDCl_3$, 500 MHz): δ 2.46 [sept, J = 6.9 Hz, 1H, $(CH_3)_2CHC$=O], 1.64 [s, 6H, $C(CH_3)_2$], 1.13 [d, J = 6.9 Hz, 6H, $(CH_3)_2CHC$=O], and 0.14 [s, 9H, $Si(CH_3)_3$].

^{13}C NMR ($CDCl_3$, 125 MHz): δ 175.0, 106.8, 87.7, 71.8, 34.2, 28.7, 18.6, and 0.32.

IR (neat): 2998 (w), 1730 (m), 1342 (m), 1251 (m), 1105 (m), and 750 (s) cm^{-1}.

TLC: R_f = 0.5 in 10:1 hexanes: EtOAc.

GC-MS (5032021): t^R = 3.499 min, *m/z* 226, 226 [M^+, 10], 227 [$(M+H)^+$, 10], 155[$(M–CO(CH_3)_2)^+$, 60], and 211 (100).

HRMS (**APCI/TOF**): Calcd for $(M+Na)^+$ $(C_{12}H_{23}O_2Si)^+$: 227.1462. Found: 227.1460.

2-Methyl-4-(trimethylsilyl)but-3-yn-2-yl pivalate (1e)

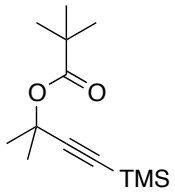

Yield: 828 mg, 69%

^{1}H NMR ($CDCl_3$, 500 MHz): δ 1.66 [s, 6H, $C(CH_3)_2$], 1.48 [s, 9H, $(CH_3)_3CC$=O], and 0.14 [s, 9H, $Si(CH_3)_3$].

^{13}C NMR ($CDCl_3$, 125 MHz): δ 151.2, 105.9, 88.3, 81.8, 73.5, 28.7, 27.5, and 0.37.

IR (neat): 2943 (w), 1711 (m), 1367 (m), 1236 (m), 1014 (m), and 675 (s) cm^{-1}.

TLC: R_f = 0.6 in 10:1 hexanes: EtOAc.

GC-MS (5032021): t^R = 4.329 min, *m/z* 240, 240 [M^+, 60], 241 [$(M+H)^+$, 30], 155[$(M–CO(CH_3)_3)^+$, 400], and 183 (100).

HRMS (**APCI/TOF**): Calcd for $(M+Na)^+$ ($C_{13}H_{24}NaO_2Si)^+$: 263.1438. Found: 263.1435.

2-Methyl-4-(trimethylsilyl)but-3-yn-2-yl 2,2,2-trifluoroacetate (1f)

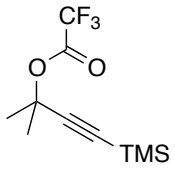

Yield: 996 mg, 79%

^{1}H NMR ($CDCl_3$, 500 MHz): δ 1.64 [s, 6H, $C(CH_3)_2$], and 0.14 [s, 9H, $Si(CH_3)_3$].

^{13}C NMR ($CDCl_3$, 125 MHz): δ 156.9, 127.1, 118.1, 110.5, 86.0, 65.4, 31.4, and 0.02.

IR (neat): 2936 (w), 1741 (m), 1507(m), 1395 (m), 1218 (m), 1196 (m), and 790 (s) cm^{-1}.

TLC: R_f = 0.3 in 10:1 hexanes: EtOAc.

GC-MS (5032021): t^R = 4.512 min, *m/z* 252, 252 [M^+, 50], 253 [$(M+H)^+$, 10], 233[$(M–F)^+$, 60], and 179 (30).

HRMS (**APCI/TOF**): Calcd for $(M+Na)^+$ ($C_{10}H_{15}F_3NaO_2Si)^+$: 275.0686. Found: 275.0682.

3-(Trimethylsilyl)prop-2-yn-1-yl acetate (1g)

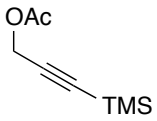

Yield: 774 mg, 91%

^{1}H NMR ($CDCl_3$, 500 MHz): δ 4.66 (s, 2H, C*H*$_2$COAc), 2.08 (s, 3H, C*H*$_3$C=O), and 0.16 [s, 9H, Si(C*H*$_3$)$_3$].

^{13}C NMR ($CDCl_3$, 125 MHz): δ 170.5, 99.2, 92.3, 53.0, 21.0, and 0.06.

IR (neat): 2931 (w), 1742 (m), 1366 (m), 1220 (s), 1163 (s), 862 (m), and 760 (s) cm^{-1}.

TLC: R_f = 0.5 in 20:1 hexanes: EtOAc.

GC-MS (5032021): t^R = 3.242 min, *m/z* 170, 170 [M^+, 10], 171 [$(M+H)^+$, 50], 126[$(M–COCH_3)^+$, 100], and 113 (10).

HRMS (**APCI/TOF**): Calcd for $(M+Na)^+$ $(C_8H_{14}NaO_2Si)^+$: 193.0655. Found: 193.0658.

4-(Trimethylsilyl)but-3-yn-2-yl acetate (1h)

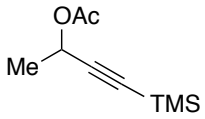

Yield: 828 mg, 90%

^{1}H NMR ($CDCl_3$, 500 MHz): δ 5.45 (q, *J* = 6.6 Hz, 1H, AcOC*H*Me), 2.07 (s, 3H, C*H*$_3$C=O), 1.46 (d, *J* = 6.6 Hz, 3H, AcOCHC*H*$_3$), and 0.16 [s, 9H, Si(C*H*$_3$)$_3$].

^{13}C NMR ($CDCl_3$, 125 MHz): δ 169.7, 103.4, 89.3, 60.5, 21.4, 21.0, and 0.3.

IR (neat): 3053 (w), 1749 (m), 1421 (m), 1264 (s), 1223 (s), 845 (m), and 764 (s) cm^{-1}.

TLC: R_f = 0.5 in 20:1 hexanes: EtOAc.

GC-MS (5032021): t^R = 3.233 min, *m/z* 184, 184 [M^+, 10], 185 [$(M+H)^+$, 50], 140[$(M–COCH_3)^+$, 100], and 127(20).

HRMS (**APCI/TOF**): Calcd for $(M+Na)^+$ $(C_9H_{16}NaO_2Si)^+$: 207.0812. Found: 207.0807.

1-Phenyl-3-(trimethylsilyl)prop-2-yn-1-yl acetate (1i)

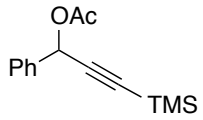

Yield: 1055 mg, 86%

^{1}H NMR ($CDCl_3$, 500 MHz): δ 7.53 (d, *J* = 7.5 Hz, 2H, Ar-*H*), 7.51 (m, 3H, Ar-*H*), 6.49 (s, 1H, AcOC*H*Ph), 2.10 (s, 3H, C*H*$_3$C=O), and 0.20 [s, 9H, Si(C*H*$_3$)$_3$].

^{13}C NMR ($CDCl_3$, 125 MHz): δ 170.1, 137.3, 129.2, 129.0, 128.2, 101.6, 92.8, 66.2, 21.5 and 0.13.

IR (neat): 2984 (w), 1740 (m), 1219 (s), 1163 (s), 865 (m), and 768 (s) cm^{-1}.

TLC: R_f = 0.5 in 20:1 hexanes: EtOAc.

GC-MS (5032021): t^R = 4.469 min, *m/z* 246, 246 [M^+, 10], 247 [$(M+H)^+$, 50], 202[$(M–COCH_3)^+$, 100], and 111(20).

HRMS (**APCI/TOF**): Calcd for $(M+Na)^+$ $(C_{14}H_{18}NaO_2Si)^+$: 269.0968. Found: 269.0965.

1-[(Trimethylsilyl)ethynyl]cyclopropyl acetate (1j)

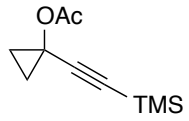

Yield: 910 mg, 93%

^{1}H NMR ($CDCl_3$, 500 MHz): δ 2.02 (s, 3H, C*H*$_3$C=O), 1.23-1.20 [nfom, 2H, C(C*H*$_2$)$_2$], 1.15-1.12 [nfom, 2H, C(C*H*$_2$)$_2$], and 0.13 [s, 9H, Si(C*H*$_3$)$_3$].

^{13}C NMR ($CDCl_3$, 125 MHz): δ 169.9, 106.0, 84.2, 48.7, 21.2, 18.8, 16.5, and 11.3.

IR (neat): 2964 (w), 1738 (m), 1376 (m), 1198 (s), 1163 (s), 865 (m), and 763 (s) cm^{-1}.

TLC: R_f = 0.5 in 10:1 hexanes: EtOAc.

GC-MS (5032021): t^R = 11.469 min, *m/z* 196, 196 [M^+, 10], 197 [$(M+H)^+$, 50], 153[$(M–COCH_3)^+$, 100], and 124 (10).

HRMS (**APCI/TOF**): Calcd for $(M+Na)^+$ ($C_{10}H_{16}NaO_2Si)^+$: 219.0812. Found: 219.0815.

1-((Trimethylsilyl)ethynyl)cyclobutyl acetate (1k)

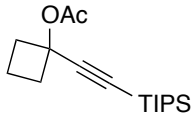

Yield: 1308 mg, 89%

^{1}H NMR ($CDCl_3$, 500 MHz): δ 2.54 [ddd, *J* = 6.1, 6.1, 3.3 Hz, 2H, C(C*H*$_2$)$_2$], 2.39 [ddd, *J* = 9.7, 9.7, 3.2 Hz, 2H, C(C*H*$_2$)$_2$], 1.99-1.93 [nfom, 1H, C(C*H*$_2$)$_2$] 1.86 [ddddd, *J* = 13.2, 9.8, 6.9, 3.5, 3.5 Hz, 1H, C(C*H*$_2$)$_2$], 2.01 (s, 3H, COC*H*$_3$), and 1.06 {m, 21H, Si[C*H*(C*H*$_3$)$_2$]$_3$}.

^{13}C NMR ($CDCl_3$, 125 MHz): δ 168.3, 107.4, 84.6, 71.5, 36.6, 20.8, 18.1, 14.2, and 10.7.

IR (neat): 2994 (w), 1745 (m), 1366 (m), 1219 (s), 1163 (s), 865 (m), and 761 (s) cm^{-1}.

TLC: R_f = 0.5 in 80:1 hexanes: EtOAc.

GC-MS (5032021): t^R = 3.912 min, *m/z* 294, 294 [M^+, 10], 295 [$(M+H)^+$, 50], 251[$(M–COCH_3)^+$, 50], and 137 (50).

HRMS (**APCI/TOF**): Calcd for $(M+Na)^+$ ($C_{17}H_{30}NaO_2Si)^+$: 317.1902. Found: 317.1897.

1-[(Triisoprpylsilyl)ethynyl]cyclopentyl acetate (1l)

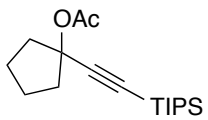

Yield: 1247 mg, 81%

^{1}H NMR ($CDCl_3$, 500 MHz): δ 2.18-2.15 [m, 4H, C(C*H*$_2$)$_4$], 1.74-1.72 [m, 4H, C(C*H*$_2$)$_4$], 2.0 (s, 3H, C*H*$_3$C=O), and 1.06 {m, 21H, Si[CH(C*H*$_3$)$_2$]$_3$}.

^{13}C NMR ($CDCl_3$, 125 MHz): δ 169.5, 108.4, 85.6, 81.1, 40.9, 23.6, 22.0, 18.9, 18.8, and 11.5.

IR (neat): 2994 (w), 1745 (m), 1366 (m), 1219 (s), 1163 (s), 865 (m), and 761 (s) cm^{-1}.

TLC: R_f = 0.5 in 80:1 hexanes: EtOAc.

GC-MS (5032021): t^R = 3.982 min, *m/z* 308, 309 [M^+, 100], 310 [$(M+H)^+$, 50], 293[$(M–CH_3)^+$, 100], and 151 (40).

HRMS (**APCI/TOF**): Calcd for $(M+Na)^+$ $(C_{18}H_{32}NaO_2Si)^+$: 331.2064. Found: 331.2060.

1-[(Trimethylsilyl)ethynyl]cyclohexyl acetate (1m)

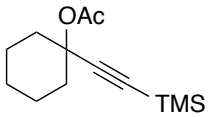

Yield: 1035 mg, 87%

^{1}H NMR ($CDCl_3$, 500 MHz): δ 2.11-2.09 [m, 2H, C(C*H*$_2$)$_5$], 2.01 (s, 3H, C*H*$_3$C=O), 1.82-1.76 [m, 2H, C(C*H*$_2$)$_5$], 1.61-1.57 [m, 4H, C(C*H*$_2$)$_5$], 1.54-1.48 [m, 1H, C(C*H*$_2$)$_5$], 1.32-1.26 [m, 1H, C(C*H*$_2$)$_5$], and 0.15 [s, 9H, Si(C*H*$_3$)$_3$]

^{13}C NMR ($CDCl_3$, 125 MHz): δ 168.9, 105.2, 90.7, 75.6, 36.9, 25.1, 22.6, 21.9, and 0.09.

IR (neat): 2994 (w), 1745 (m), 1366 (m), 1219 (s), 1163 (s), 865 (m), and 761 (s) cm^{-1}.

TLC: R_f = 0.5 in 80:1 hexanes: EtOAc.

GC-MS (5032021): t^R = 4.127 min, *m/z* 238, 238 [M^+, 100], 239 [$(M+H)^+$, 50], 195[$(M–COCH_3)^+$, 30], and 165 (40).

HRMS (**APCI/TOF**): Calcd for $(M+Na)^+$ $(C_{13}H_{23}O_2Si)^+$: 239.1462. Found: 239.1459.

2-Methylundec-3-yn-2-yl acetate (1n)

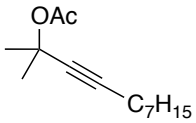

Yield: 940 mg, 84%

^{1}H NMR ($CDCl_3$, 500 MHz): δ 2.18 [t, *J* = 7.1 Hz, 2H, $CH_3(CH_2)_5CH_2CC$], 2.00 (s, 3H, CH_3C=O), 1.63 [s, 6H, $C(CH_3)_2$], 1.48 [pent, *J* = 7.3 Hz, 2H, $CH_3(CH_2)_4CH_2CH_2CC$], 1.38-1.23 [m, 8H, $CH_3(CH_2)_4CH_2CC$], and 0.88 [t, *J* = 7.1 Hz, 3H, $CH_3(CH_2)_6CC$].

^{13}C NMR ($CDCl_3$, 125 MHz): δ 169.5, 84.8, 81.5, 72.7, 31.4, 29.4, 28.6, 28.5, 22.6, 22.2, 18.8, and 14.1.

IR (neat): 3053 (w), 2931 (w), 1742 (m), 1342 (m), 1264 (m), 1105 (m), and 750 (s) cm^{-1}.

TLC: R_f = 0.5 in 10:1 hexanes: EtOAc.

GC-MS (5032021): t^R = 4.841 min, *m/z* 224, 224 [M^+, 50], 225 [$(M+H)^+$, 10], 181[$(M–COCH_3)^+$, 60], and 165 (100).

HRMS (**APCI/TOF**): Calcd for $(M+K)^+$ $(C_{14}H_{24}KO_2)^+$: 263.1408. Found: 263.1409.

4-(Cyclohex-2-en-1-yl)-2-methylbut-3-yn-2-yl acetate (1o)

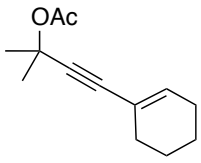

Yield: 890 mg, 86%

^{1}H NMR ($CDCl_3$, 500 MHz): δ 6.09 (dd, 1H, C=C*H*), 2.12-2.03 (m, 4H, (C*H*$_2$)$_4$C=C), 1.63-1.52 (m, 4H, (C*H*$_2$)$_4$C=C), 2.00 (s, 3H, C*H*$_3$C=O), and 1.66 [s, 6H, C(C*H*$_3$)$_2$].

^{13}C NMR ($CDCl_3$, 125 MHz): δ 169.4, 135.4, 120.1, 87.6, 85.7, 72.7, 29.2, 25.6, 22.3, 22.2, and 21.5.

IR (neat): 3053 (w), 2985 (m), 2942 (m), 1736 (w), 1444 (m), 1264 (m), and 734 (s) cm^{-1}.

TLC: R_f = 0.4 in 10:1 hexanes: EtOAc.

GC-MS (5032021): t^R = 5.757 min, *m/z* 206, 206 [M^+, 50], 205 [$(M-H)^+$, 10], 162[$(M–COCH_3)^+$, 100], and 150 (70).

HRMS (**APCI/TOF**): Calcd for $(M+Na)^+$ $(C_{13}H_{18}NaO_2)^+$: 229.1199. Found: 229.1193.

2-Methyl-4-phenylbut-3-yn-2-yl acetate (1p)

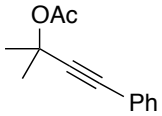

Yield: 858 mg, 85%

^{1}H NMR ($CDCl_3$, 500 MHz): δ 7.42 (m, Hz, 2H, Ar-*H*), 7.27 (m, 3H, Ar-*H*), 2.02 (s, 3H, C*H*$_3$C=O), and 1.73 [s, 6H, C(C*H*$_3$)$_2$].

^{13}C NMR ($CDCl_3$, 125 MHz): δ 169.2, 131.6, 128.1, 127.9, 122.4, 90.0, 83.7, 72.3, 28.8, and 21.9.

IR (neat): 2994 (w), 1745 (m), 1366 (m), 1219 (s), 1163 (s), 865 (m), and 761 (s) cm^{-1}.

TLC: R_f = 0.5 in 10:1 hexanes: EtOAc.

GC-MS (5032021): t^R = 6.469 min, *m/z* 202, 202 [M^+, 10], 203[$(M+H)^+$, 50], 160[$(M–COCH_3)^+$, 100], and 144 (60).

HRMS (**APCI/TOF**): Calcd for $(M+Na)^+$ $(C_{13}H_{14}KO_2)^+$: 241.0625. Found: 241.0622.

2-Methyl-4-(naphthalen-1-yl)but-3-yn-2-yl acetate (1q)

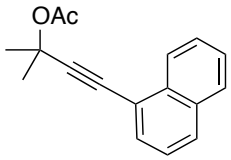

Yield: 1134 mg, 90%

^{1}H NMR ($CDCl_3$, 500 MHz): δ 8.35 (d, *J* = 8.2 Hz, 1H, Ar-*H*), 7.81 (m, 2H, Ar-*H*), 7.66 (d, *J* = 7.2 Hz, 1H, Ar-*H*), 7.58 (m, 1H, Ar-*H*), 7.50 (m, 1H, Ar-*H*), 7.39 (m, 2H, Ar-*H*), 2.09 (s, 3H, C*H*$_3$C=O), and 1.85 [s, 6H, C(C*H*$_3$)$_2$].

^{13}C NMR ($CDCl_3$, 125 MHz): δ 169.6, 133.7, 133.2, 130.7, 129.0, 128.3, 127.0, 126.5, 126.4, 125.2, 120.4, 95.3, 82.3, 72.7, 29.4, and 22.2.

IR (neat): 2986 (w), 1748 (m), 1264 (s), 1163 (s), 837 (m), and 730 (s) cm^{-1}.

TLC: R_f = 0.4 in 10:1 hexanes: EtOAc.

GC-MS (5032021): t^R = 5.408 min, *m/z* 252, 252 [M^+, 10], 253 [$(M+H)^+$, 50], 209[$(M–COCH_3)^+$, 100], and 124 (40).

HRMS (**APCI/TOF**): Calcd for $(M+Na)^+$ $(C_{17}H_{26}NaO_2)^+$: 275.1043. Found: 275.1041.

4-(Benzofuran-2-yl)-2-methylbut-3-yn-2-yl acetate (1r)

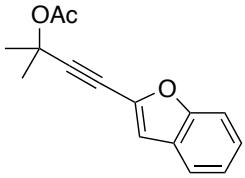

Yield: 1004 mg, 83%

^{1}H NMR ($CDCl_3$, 500 MHz): δ 7.54 (d, *J* = 7.5 Hz, 1H, Ar-*H*), 7.43 (d, *J* = 8.2 Hz, 1H, Ar-*H*), 7.31 (dd, *J* = 7.2, 8.2 Hz, 1H, Ar-*H*), 7.21 (dd, *J* = 7.5, 7.2 Hz, 1H, Ar-*H*), 6.94 (s, 1H, Ar-*H*), 2.06 (s, 3H, C*H*$_3$C=O), and 1.78 [s, 6H, C(C*H*$_3$)$_2$].

^{13}C NMR ($CDCl_3$, 125 MHz): δ 169.8, 155.3, 138.6, 128.0, 126.1, 123.7, 121.7, 112.5, 111.7, 96.5, 72.4, 29.2, and 22.4.

IR (neat): 2988 (w), 1742 (m), 1366 (m), 1234 (s), 1161 (s), 863 (m), and 759 (s) cm^{-1}.

TLC: R_f = 0.4 in 5:1 hexanes: EtOAc.

GC-MS (5032021): t^R = 6.669 min, *m/z* 242, 242 [M^+, 50], 243 [$(M+H)^+$, 10], 199[$(M–COCH_3)^+$, 60], and 182 (100).

HRMS (**APCI/TOF**): Calcd for $(M+Na)^+$ $(C_{15}H_{14}NaO_3)^+$: 265.0835. Found: 265.0835.

2-Methyl-4-(pyridin-3-yl)but-3-yn-2-yl acetate (1s^1)

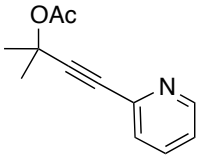

Yield: 842 mg, 83%

^{1}H NMR ($CDCl_3$, 500 MHz): δ 8.59-8.54 (d, *J* = 4.7 Hz 1H, Ar-*H*), 7.75-7.64 (dd, *J* = 7.9, 4.7 Hz, 1H, Ar-*H*), 7.52-7.42 (d, *J* = 7.9 Hz, 1H, Ar-*H*), 7.29-7.21 (dd, *J* = 7.9, 4.7 Hz, 1H, Ar-*H*), 2.03 (s, 3H, C*H*$_3$C=O), and 1.76 [s, 6H, C(C*H*$_3$)$_2$].

^{13}C NMR ($CDCl_3$, 125 MHz): δ 169.4, 149.0, 142.1, 137.1, 127.7, 123.2, 91.9, 82.5, 71.9, 28.8, and 22.0.

IR (neat): 2987 (m), 1747 (m), 1562 (w), 1444 (m), 1263 (m), 1133 (m), and 731 (s) cm^{-1}.

TLC: R_f = 0.5 in 3:1 hexanes: EtOAc.

GC-MS (5032021): t^R = 5.412 min, *m/z* 203, 203 [M^+, 50], 204 [$(M+H)^+$, 10], 160[$(M–COCH_3)^+$, 60], and 144 (100).

HRMS (**APCI/TOF**): Calcd for $(M+Na)^+$ $(C_{12}H_{13}NNaO_2)^+$: 226.0838. Found: 226.0835.

2-Methyl-4-(1-methyl-1*H*-indol-2-yl)but-3-yn-2-yl acetate (1t)

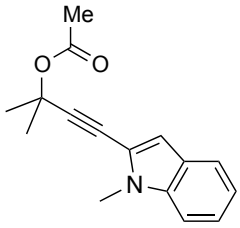

Yield: 1045 mg, 82%

^{1}H NMR ($CDCl_3$, 500 MHz): δ 7.56 (d, *J* = 7.5 Hz, 2H, Ar-*H*), 7.25 (d, *J* = 8.2 Hz, 1H, Ar-*H*), 7.10 (dd, *J* = 7.5, 8.2 Hz, 1H, Ar-*H*), 6.73 (s, 1H, Ar-*H*), 3.79 (s, 3H, N-C*H*$_3$), 2.06 (s, 3H, C*H*$_3$C=O), and 1.78 [s, 6H, C(C*H*$_3$)$_2$].

^{13}C NMR ($CDCl_3$, 125 MHz): δ 169.9, 138.6, 128.0, 123.1, 121.0, 120.7, 109.5, 107.3, 98.5, 72.3, 30.6, 29.1, and 22.1.

IR (neat): 3050 (m), 1686 (m), 1377 (m), 1296 (s), 1197 (s), 898 (m), and 753 (s) cm^{-1}.

TLC: R_f = 0.4 in 3:1 hexanes: EtOAc.

GC-MS (5032021): t^R = 8.669 min, *m/z* 255, 255 [M^+, 50], 256 [$(M+H)^+$, 10], 212[$(M–COCH_3)^+$, 60], and 195 (100).

HRMS (**APCI/TOF**): Calcd for $(M+Na)^+$ $(C_{15}H_{14}NaO_3)^+$: 279.1168. Found: 278.1165.

2,7-Dimethylocta-3,5-diyne-2,7-diyl diacetate (1x)

Yield: 5.0 mmol, 1100 mg, 88%

^{1}H NMR ($CDCl_3$, 500 MHz): δ 2.01 (s, 6H, C*H*$_3$C=O), and 1.64 [s, 12H, C(C*H*$_3$)$_2$].

^{13}C NMR ($CDCl_3$, 125 MHz): δ 169.5, 80.6, 71.9, 68.6, 28.8, and 22.0.

IR (neat): 2957 (m), 1776 (m), 1459 (w), 1240 (s), 1006 (m), and 741 (s) cm^{-1}.

TLC: R_f = 0.5 in 40:1 hexanes: EtOAc.

GC-MS (5032021): t^R = 4.983 min, *m/z* 250, 250 [M^+, 20], 249 [$(M–H)^+$, 60], 207[$(M–COCH_3)^+$, 100], 164[$(M–COCH_3)^+$, 80], and 152 (40).

HRMS (**APCI/TOF**): Calcd for $(M+Na)^+$ $(C_{14}H_{18}NaO_4)^+$: 273.1138. Found: 273.1138.

2,7-Dimethyl-7-[(trimethylsilyl)oxy]octa-3,5-diyn-2-yl acetate (1y)

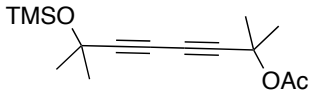

Yield: 5.0 mmol, 1120 mg, 80%

^{1}H NMR ($CDCl_3$, 500 MHz): δ 2.02 (s, 3H, C*H*$_3$C=O), 1.66 [s, 6H, C(C*H*$_3$)$_2$], 1.48 [s, 6H, C(C*H*$_3$)$_2$] and 0.18 [s, 9H, Si(C*H*$_3$)$_3$].

^{13}C NMR ($CDCl_3$, 125 MHz): δ 169.4, 84.5, 79.8, 71.9, 66.9, 32.7, 28.8, 21.9, and 1.9.

IR (neat): 2956 (m), 1776 (m), 1599 (w), 1460 (m), 1244 (m), 1088 (m), and 735 (s) cm^{-1}.

TLC: R_f = 0.4 in 40:1 hexanes: EtOAc.

GC-MS (5032021): t^R = 4.412 min, *m/z* 280, 280 [M^+, 50], 281 [$(M–H)^+$, 10], 237[$(M–COCH_3)^+$, 60], 164[$(M–TMS)^+$, 100], and 101 (80).

HRMS (**APCI/TOF**): Calcd for $(M+Na)^+$ $(C_{15}H_{24}NaO_3Si)^+$: 303.1422. Found: 303.1411.

(8*R*,9*S*,13*S*,14*S*,17*S*)-3-(Benzyloxy)-13-methyl-17-(phenylethynyl)-7,8,9,11,12,13,14,15,16,17-decahydro-6*H*-cyclopenta[*a*]phenanthren-17-yl acetate (1z)

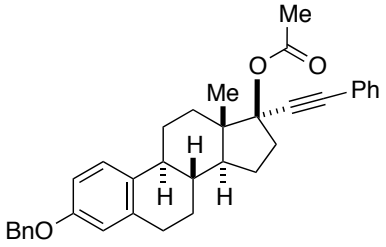

Yield: 5.0 mmol, 2091 mg, 83%

^{1}H NMR ($CDCl_3$, 500 MHz): δ 7.41 [d, *J* = 8.1 Hz, 2H, (OCH_2)Ar*H*], 7.37 [dd, *J* = 8.1 Hz, 1.7 Hz, 2H, Ph-*H*], 7.30 [d, *J* = 7.7 Hz, 1H, Ar*H*], 7.25-7.16 [m, 6H, Ar*H*], 7.05 (s, 1H, C=C*H*Ph), 6.77 [dd, *J* = 8.1 Hz, 1.7 Hz, 1H, Ar*H*], 6.67 [dd, *J* = 8.1 Hz, 1.7 Hz, 1H, Ar*H*], 5.02 [s, 2H, OC*H*$_2$Bn], 2.73-2.72 (m, 2H, C6-*H*), 2.48-2.46 (m, 1H, C7-*H*), 2.28-2.26 (m, 1H, C7-*H*), 2.08-2.06 (m, 1H, C8-*H*), 2.02 (s, 3H, C*H*$_3$C=O), 1.85-1.82 (m, 1H, C9-*H*), 1.55-1.44 (m, 2H, C15-*H*), 1.55-1.44 (m, 2H, C16-*H*), 1.25-1.24 (m, 2H, C11-*H*), 0.99-0.97 (m, 1H, C9-*H*), and 0.85 (s, 3H, C18-*H*).

^{13}C NMR ($CDCl_3$, 125 MHz): δ 169.7, 156.8, 138.1, 137.4, 132.8, 128.6, 127.9, 127.5, 126.5, 114.9, 112.4, 84.6, 83.5, 75.1, 70.1, 52.2, 47.9, 47.9, 43.5, 39.2, 37.5, 33.2, 29.8, 27.4, 26.4, 25.2, 23.4, 21.5, 20.2, 13.6, and 13.5.

IR (neat): 2980 (m), 2785(m), 1747 (s), 1381 (m), 1510(m), 1254 (s), 1071 (m), 983(s), and 795 (s) cm^{-1}.

TLC: R_f = 0.5 in 5:1 hexanes: EtOAc.

HRMS (**APCI/TOF**): Calcd for $(M+K)^+$ $(C_{35}H_{36}NKO_2)^+$: 543.2311. Found: 543.2309.

(*E*)-2,2-Diethyl-4,4,6-trimethyl-3-[(trimethylsilyl)methylene]-1,5,2-dioxasilinane (2a)

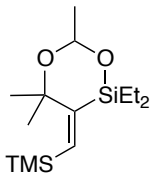

Yield: 0.2 mmol scale, 47 mg, 83%

^{1}H NMR ($CDCl_3$, 500 MHz): δ 5.82 (s, 1H, C=C*H*TMS), 5.35 (q, *J* = 5.0 Hz, 1H, OC*H*Me), 1.41 [s, 3H, OC(C*H*$_3$)$_2$], 1.39 [s, 3H, OC(C*H*$_3$)$_2$], 1.33 (d, *J* = 5.0 Hz, 3H, OCHC*H*$_3$), 0.96 (dd, *J* = 7.8, 1.2 Hz, 3H, SiCH$_2$C*H*$_3$), 0.95 (dd, *J* = 7.8, 1.3 Hz, 3H, SiCH$_2$C*H*$_3$), 0.73-0.61 (m, 4H, SiC*H*$_2$CH$_3$), and 0.18 [s, 9H, Si(C*H*$_3$)$_3$].

^{13}C NMR ($CDCl_3$, 125 MHz): δ 166.3, 139.6, 90.8, 81.9, 30.2, 25.7, 25.0, 8.63, 6.78, 6.58, 4.78, and 1.16.

IR (neat): 3110 (w), 2954 (m), 2876 (m), 1458 (m), 1248 (m), 1068 (s), 729 (s), and 698 (m) cm^{-1}.

TLC: R_f = 0.6 in 80:1 hexanes: EtOAc.

GC-MS (5032021): t^R = 5.412 min, *m/z* 286, 287 [$(M+H)^+$, 10], 286 [M^+, 8], 285 [$(M–H)^+$, 12], 257 [$(M–CH_2CH_3)^+$, 58], 242 [$(M–CH_3CHO)^+$, 100] and 155 (40).

HRMS (**APCI/TOF**): Calcd for $(M+H)^+$ $(C_{14}H_{31}O_2Si_2)^+$: 287.1857. Found: 287.1852.

(*E*)-2,2-Diethyl-4,4-dimethyl-3-[(trimethylsilyl)methylene]-1,5,2-dioxasilinane (2b)

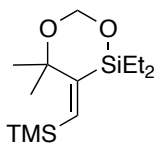

Yield: 0.2 mmol scale, 45 mg, 88%

^{1}H NMR (C_6D_6, 500 MHz): δ 5.92 (s, 1H, C=C*H*TMS), 5.18 (s, 2H, OCH_2), 1.41 [s, 3H, OC(CH_3)$_2$], 1.09 (dd, *J* = 7.9, 2.1 Hz, 6H, SiCH$_2$CH_3), 0.73-0.61 (m, 4H, SiCH_2CH$_3$), and 0.12 [s, 9H, Si(CH_3)$_3$].

^{13}C NMR (C_6D_6, 125 MHz): δ 169.2, 139.9, 86.7, 82.6, 28.4, 7.7, 7.6, and 1.8.

IR (neat): 2962 (w), 1519 (m), 1156 (m), 1075 (m), and 720 (s) cm^{-1}.

TLC: R_f = 0.6 in 80:1 hexanes: EtOAc.

GC-MS (5032021): t^R = 5.031 min, *m/z* 272, 273 [(M+H)$^+$, 40], 272 [M$^+$, 22], 271 [(M–H)$^+$, 50], 243 [(M–CH$_2$CH$_3$)$^+$, 55], and 242 [(M–CH$_2$O)$^+$, 10]

HRMS (**APCI/TOF**): Calcd for (M+Na)$^+$ ($C_{13}H_{28}NaO_2Si_2$)$^+$: 295.1520. Found: 295.1519.

(*E*)-6-(Chloromethyl)-2,2-diethyl-4,4-dimethyl-3-[(trimethylsilyl)methylene]-1,5,2-dioxasilinane (2c)

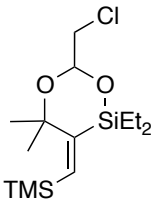

Yield: 53 mg, 83%

^{1}H NMR (C_6D_6, 500 MHz): δ 5.93 (s, 1H, C=C*H*TMS), 5.27 (t, *J* = 4.7 Hz, 1H, OC*H*CH$_2$Cl), 3.4 (d, *J* = 4.7 Hz, 2H, OCHCH_2), 1.46 [s, 3H, OC(CH_3)$_2$], 1.35 [s, 3H, OC(CH_3)$_2$], 1.04 (dd, *J* = 7.8, 2.1 Hz, 3H, SiCH$_2$CH_3), 1.00 (dd, *J* = 7.8, 2.1 Hz, 3H, SiCH$_2$CH_3), 0.76-0.62 (m, 4H, SiCH_2CH$_3$), and 0.09 [s, 9H, Si(CH_3)$_3$].

^{13}C NMR (C_6D_6, 125 MHz): δ 166.9, 140.2, 93.0, 82.7, 47.6, 30.3, 25.7, 8.9, 7.0, 6.8, 5.1, and 1.1.

IR (neat): 2935 (w), 2911 (w), 1411 (m), 1194 (m), 1133 (m), and 747 (s) cm^{-1}.

TLC: R_f = 0.4 in 80:1 hexanes: EtOAc.

GC-MS (5032021): t^R = 5.643 min, *m/z* 320, 321 [$(M+H)^+$, 100], 320 [M^+, 15], 319 [$(M–H)^+$, 30], 291 [$(M–CH_2CH_3)^+$, 50], 285 [$(M–Cl)^+$, 90] and 247 (21).

HRMS (**APCI/TOF**): Calcd for $(M+Na)^+$ $(C_{14}H_{30}ClO_2Si_2)^+$: 321.1467. Found: 321.1460.

(*E*)-2,2-Diethyl-6-isopropyl-4,4-dimethyl-3-[(trimethylsilyl)methylene]-1,5,2-dioxasilinane (2d)

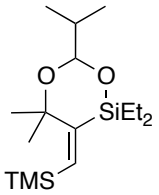

Yield: 60 mg, 94%

^{1}H NMR (C_6D_6, 500 MHz): δ 5.98 (s, 1H, C=C*H*TMS), 4.94 [d, *J* = 5.0 Hz, 1H, OC*H*CH(CH_3)$_2$], 1.97-1.85 [m, 1H, OCHC*H*(CH_3)$_2$],1.47 [s, 3H, OC(CH_3)$_2$], 1.38 [s, 3H, OC(CH_3)$_2$], 1.13-1.01 (m, 6H, CH(CH_3)$_2$), 1.13-1.01 (m, 6H, $SiCH_2CH_3$), 0.84-0.71 (m, 4H, $SiCH_2CH_3$), and 0.14 [s, 9H, Si(CH_3)$_3$].

^{13}C NMR (C_6D_6, 125 MHz): δ 139.6, 98.2, 97.7, 81.8, 35.8, 30.7, 29.1, 26.2, 17.5, 17.4, 7.3, 7.2, 5.4, and 1.4.

IR (neat): 2956 (w), 2912 (w), 1249 (m), 1072 (m), 1011 (m), 844 (s), and 747 (s) cm^{-1}

TLC: R_f = 0.5 in 80:1 hexanes: EtOAc.

GC-MS (5032021): t^R = 5.211 min, *m/z* 314, 315 [$(M+H)^+$, 70], 313 [$(M–H)^+$, 50], 285 [$(M–CH_2CH_3)^+$, 33], 299 [$(M–CH_3)^+$, 52] and 241 (29).

HRMS (**APCI/TOF**): Calcd for $(M+Na)^+$ $(C_{16}H_{34}NaO_2Si_2)^+$: 337.1990. Found: 337.1988.

(*E*)-2,2-Diethyl-4,6-dimethyl-3-[(trimethylsilyl)methylene]-1,5,2-dioxasilinane (2g)

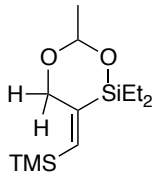

Yield: 40 mg, 78%

^{1}H NMR ($CDCl_3$, 500 MHz): 5.95 (s, 1H, C=C*H*TMS), 5.12 (q, *J* = 5.0 Hz, 1H, OC*H*Me), 4.73 [d, *J* = 5.0 Hz, 1H, OCH_2], 4.38 [d, *J* = 5.0 Hz, 1H, OCH_2], 1.35 (d, *J* = 5.0 Hz, 3H, OCHCH_3), 0.97-0.95(m, 6H, $SiCH_2CH_3$), 0.71-0.61 (m, 4H, $SiCH_2CH_3$), and 0.12 [s, 9H, $Si(CH_3)_3$].

^{13}C NMR ($CDCl_3$, 125 MHz): δ 155.1, 108.0, 94.9, 23.6, 17.3, 7.3, 6.9, 5.0, and 0.9.

IR (neat): 3108 (w), 2944 (m), 2871 (m), 1450 (m), 1239 (m), 1068 (s), and 723 (s) cm^{-1}.

TLC: R_f = 0.6 in 80:1 hexanes: EtOAc.

GC-MS (5032021): t^R = 4.562 min, *m/z* 258, 259 [$(M+H)^+$, 10], 258 [M^+, 12], 257 [$(M–H)^+$, 20], 229 [$(M–CH_2CH_3)^+$, 56], 214 [$(M–CH_3CHO)^+$, 100] and 127 (43).

HRMS (**APCI/TOF**): Calcd for $(M+Na)^+$ $(C_{15}H_{26}NaO_2Si_2)^+$: 281.1364. Found: 281.1360.

(*E*)-7,7-Diethyl-5-methyl-8-[(trimethylsilyl)methylene]-4,6-dioxa-7-silaspiro[2.5]octane (2j)

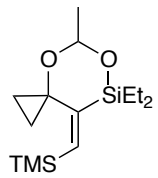

Yield: 48mg, 85%

^{1}H NMR ($CDCl_3$, 500 MHz): δ 5.64 (s, 1H, C=C*H*TMS), 5.26 (q, *J* = 5.0 Hz, 1H, OC*H*Me), 1.30 (d, *J* = 5.0 Hz, 3H, OCHCH_3), 1.15-1.09[nfom, 2H, C(CH_2)$_2$], 1.01-0.95[nfom, 2H,

C(C*H*$_2$)$_2$], 1.01-0.95(m, 6H, Si CH_2CH_3), 0.73-0.57 (m, 4H, $SiCH_2CH_3$), and 0.13 [s, 9H, Si(C*H*$_3$)$_3$].

^{13}C NMR ($CDCl_3$, 125 MHz): δ 162.1,135.9, 96.4, 66.0, 24.5, 17.8, 16.9, 7.4, 6.9, 6.0, and 1.4.

IR (neat): 2954 (m), 1388 (m), 1248 (m), 1087 (s), and 727 (s) cm^{-1}.

TLC: R_f = 0.5 in 80:1 hexanes: EtOAc.

GC-MS (5032021): t^R = 5.110 min, *m/z* 284, 285 [$(M+H)^+$, 40], 283 [$(M–H)^+$, 10], 240 [$(M–CH_3CHO)^+$, 100] and 211 (50).

HRMS (**APCI/TOF**): Calcd for $(M+Na)^+$ $(C_{14}H_{28}NaO_2Si_2)^+$: 307.1520. Found: 307.1518.

(*E*)-8,8-Diethyl-6-methyl-9-[(triisopropylsilyl)methylene]-5,7-dioxa-8-silaspiro[3.5]nonane (1k)

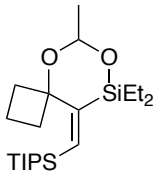

Yield: 53 mg, 89%

^{1}H NMR (C_6D_6, 500 MHz): δ 5.92 (s, 1H, C=C*H*TMS), 5.39 (q, *J* = 5.0 Hz, 1H, OC*H*Me), 2.54 [nfom, 1H, C(C*H*$_2$)$_2$], 2.33 [nfom, 1H, C(C*H*$_2$)$_2$], 2.23 [nfom, 1H, C(C*H*$_2$)$_2$], 2.13 [nfom, 2H, C(C*H*$_2$)$_2$], 1.50 (d, *J* = 5.0 Hz, 3H, OCHC*H*$_3$), 1.17-1.09 [m, 1H, C(C*H*$_2$)$_2$], 1.17-1.09 {m, 21H, Si[C*H*(C*H*$_3$)$_2$]$_3$}, 0.81-0.71(m, 6H, $SiCH_2CH_3$), and 0.71-0.61 (m, 4H, $SiCH_2CH_3$)

^{13}C NMR (C_6D_6, 125 MHz): δ 167.3, 134.3, 92.8, 87.2, 34.9, 31.8, 25.1, 19.5, 19.4, 14.7, 13.6, 8.3, 7.0, and 6.1.

IR (neat): 2951 (m), 2876 (m), 1558 (m), 1248 (s), 1015 (m), 836 (s), and 745 (m) cm^{-1}.

TLC: R_f = 0.6 in 80:1 hexanes: EtOAc.

GC-MS (5032021): t^R = 5.212 min, *m/z* 382, 383 [$(M+H)^+$, 30], 382 [M^+, 25], 381 [$(M–H)^+$, 58], 353 [$(M–CH_2CH_3)^+$, 46], and 338 [$(M–CH_3CHO)^+$, 80].

HRMS (**APCI/TOF**): Calcd for $(M+H)^+$ $(C_{15}H_{31}O_2Si_2)^+$: 299.1857. Found: 299.1853.

(*E*)-9,9-Diethyl-7-methyl-10-[(triisopropylsilyl)methylene]-6,8-dioxa-9-silaspiro[4.5]decane (1l)

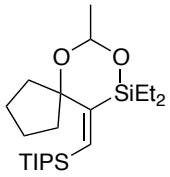

Yield: 51 mg, 81%

^{1}H NMR (C_6D_6, 500 MHz): δ 5.91 (s, 1H, C=C*H*TMS), 5.32 (q, *J* = 5.0 Hz, 1H, OC*H*Me), 2.27-2.23 [m, 1H, C(C*H*$_2$)$_4$], 2.15-2.11 [m, 1H, C(C*H*$_2$)$_4$], 1.95-1.90 [m, 2H, C(C*H*$_2$)$_4$], 1.71-1.62 [m, 4H, C(C*H*$_2$)$_4$],1.40 (d, *J* = 5.0 Hz, 3H, OCHC*H*$_3$), 1.17-1.11 (m, 6H, SiCH$_2$C*H*$_3$), 1.11 {m, 21H, Si[CH(C*H*$_3$)$_2$]$_3$}, and 0.71-0.61 (m, 4H, SiC*H*$_2$CH$_3$).

^{13}C NMR (C_6D_6, 125 MHz): δ 167.6, 134.6, 93.4, 91.2, 35.6, 25.4, 19.4, 13.5, 9.0, 7.1, and 5.7.

IR (neat): 2933 (m), 1390 (m), 1248 (m), 1086 (s), 842 (s), and 726 (m) cm^{-1}.

TLC: R_f = 0.6 in 80:1 hexanes: EtOAc.

GC-MS (5032021): t^R = 5.233 min, *m/z* 396, 397 [$(M+H)^+$, 60], 396 [M^+, 24], 395 [$(M–H)^+$, 80], 367 [$(M–CH_2CH_3)^+$, 20], and 352 [$(M–CH_3CHO)^+$, 50].

HRMS (**APCI/TOF**): Calcd for $(M+Na)^+$ $(C_{16}H_{32}KO_2Si_2)^+$: 351.1572. Found: 351.1570.

(*E*)-4,4-Diethyl-2-methyl-5-[(trimethylsilyl)methylene]-1,3-dioxa-4-silaspiro[5.5]undecane (2m)

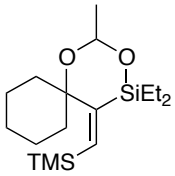

Yield: 45 mg, 69%

^{1}H NMR (C_6D_6, 500 MHz): δ 5.94 (s, 1H, C=C*H*TMS), 5.30 (q, *J* = 5.0 Hz, 1H, OC*H*Me), 2.10 [d, 1H, C(C*H*$_2$)$_5$], 1.95-1.84[m, 2H, C(C*H*$_2$)$_5$], 1.71-1.61 [m, 2H, C(C*H*$_2$)$_5$], 1.53-1.48 [m, 2H, C(C*H*$_2$)$_5$], 1.43 (d, *J* = 5.0 Hz, 3H, OCHC*H*$_3$), 1.41-1.23 [m, 3H, C(C*H*$_2$)$_5$], 1.10 (dd, *J* = 7.8, 1.3 Hz, 3H, SiCH$_2$C*H*$_3$), 1.08 (dd, *J* = 7.8, 1.3 Hz, 3H, SiCH$_2$C*H*$_3$), 0.81-0.68 (m, 4H, SiC*H*$_2$CH$_3$), and 0.19 [s, 9H, Si(C*H*$_3$)$_3$].

^{13}C NMR (C_6D_6, 125 MHz): δ 168.6, 139.2, 90.6, 82.9, 38.0, 32.2, 25.7, 25.4, 22.3, 22.2, 9.5, 7.1, 7.5, 5.8, and 1.9.

IR (neat): 2957 (m), 2926 (m), 1459 (m), 1236 (m), 1088 (s), 935 (s), and 698 (m) cm^{-1}.

TLC: R_f = 0.6 in 80:1 hexanes: EtOAc.

GC-MS (5032021): t^R = 5.331 min, *m/z* 326, 327 [$(M+H)^+$, 30], 326 [M^+, 18], 325 [$(M–H)^+$, 50], 297 [$(M–CH_2CH_3)^+$, 10], 282 [$(M–CH_3CHO)^+$, 90] and 253 (20).

HRMS (**APCI/TOF**): Calcd for $(M+Na)^+$ $(C_{17}H_{34}NaO_2Si_2)^+$: 349.1990. Found: 349.1995.

(*E*)-2,2-Diethyl-4,4,6-trimethyl-3-octylidene-1,5,2-dioxasilinane (2n)

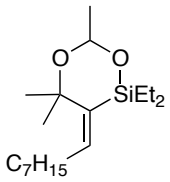

Yield: 41 mg, 65%

^{1}H NMR ($CDCl_3$, 500 MHz): δ 5.47(t, *J* = 7.3 Hz, 1H, C=C*H*C$_7$H$_{15}$), 5.34 (q, *J* = 5.0 Hz, 1H, OC*H*Me), 2.18-2.08 [m, 2H, CH$_3$(CH$_2$)$_5$C*H*$_2$CC], 1.46 [s, 3H, C(C*H*$_3$)$_2$], 1.41 [s, 3H, C(C*H*$_3$)$_2$], 1.31 (d, *J* = 5.0 Hz, 3H, OCHC*H*$_3$), 1.29-1.28 (m, 6H, CH$_3$(C*H*$_2$)$_6$CC], 0.98-0.93 (q, *J* = 7.1 Hz ,

6H, $SiCH_2CH_3$), 0.89-0.86 (t, J = 7.1 Hz , 4H, $SiCH_2CH_3$), and 0.70-0.59 [m, 3H, $CH_3(CH_2)_6CC$]

^{13}C NMR ($CDCl_3$, 125 MHz): δ 143.1, 139.4, 90.9, 80.2, 31.9, 30.7, 29.9, 29.4, 29.3, 25.5, 25.5, 22.7, 14.2, 9.1, 6.9, 6.6, and 4.9.

IR (neat): 3130 (w), 2939 (m), 2855 (m), 1460 (m), 1233 (m), 726 (s), and 693 (m) cm^{-1}.

TLC: R_f = 0.6 in 80:1 hexanes: EtOAc.

GC-MS (5032021): t^R = 6.532 min, *m/z* 312, 313 [$(M+H)^+$, 20], 312 [M^+, 12], 311 [$(M–H)^+$, 24], 283 [$(M–CH_2CH_3)^+$, 50], 268 [$(M–CH_3CHO)^+$, 100] and 226 (41).

HRMS (**APCI/TOF**): Calcd for $(M+Na)^+$ ($C_{18}H_{36}NaO_2Si)^+$: 335.2377. Found: 335.2375.

(*E*)-3-(Cyclohex-1-en-1-ylmethylene)-2,2-diethyl-4,4,6-trimethyl-1,5,2-dioxasilinane (2o)

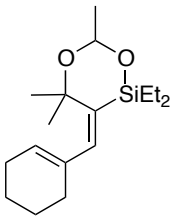

Yield: 47 mg, 79%

^{1}H NMR ($CDCl_3$, 500 MHz): δ 5.92 (d, 1.8 Hz 1H, C=C*H*TMS), 5.48 (ddd, J = 3.6, 1.8, 1.7 Hz, 1H, C=C*H*), 5.33 (q, J = 5.0 Hz, 1H, OC*H*Me), 2.09-2.01 (m, 2H, $(CH_2)_4C$=C), 1.98-1.91 (m, 2H, $(CH_2)_4C$=C), 1.68-1.60 (m, 2H, $(CH_2)_4C$=C), 1.60-1.53 (m, 2H, $(CH_2)_4C$=C), 1.46 [s, 3H, $C(CH_3)_2$], 1.42 [s, 3H, $C(CH_3)_2$], 1.32 (d, J = 5.0 Hz, 3H, $OCHCH_3$), 1.02-0.93(m, 6H, $SiCH_2CH_3$), and 0.71-0.61 (m, 4H, $SiCH_2CH_3$).

^{13}C NMR ($CDCl_3$, 125 MHz): δ 140.0, 137.1, 136.4, 124.0, 90.9, 80.7, 30.2, 28.9, 26.5, 25.2, 22.6, 22.0, 8.9, 6.8, 6.5, 6.2, and 4.9.

IR (neat): 3443 (w), 2956 (s), 2874 (m), 1506 (w), 1457 (m), 1233 (m), 1054 (s), 1009 (s), and 797 (m) cm^{-1}.

TLC: R_f = 0.4 in 80:1 hexanes: EtOAc.

GC-MS (5032021): t^R = 5.450 min, *m/z* 294, 295 [$(M+H)^+$, 10], 294 [M^+, 6], 293 [$(M–H)^+$, 20], 265 [$(M–CH_2CH_3)^+$, 80], 250 [$(M–CH_3CHO)^+$, 100] and 205 (40).

HRMS (**APCI/TOF**): Calcd for $(M+Na)^+$ $(C_{17}H_{30}NaO_2Si)^+$: 317.1907. Found: 317.1905.

(*E*)-3-Benzylidene-2,2-diethyl-4,4,6-trimethyl-1,5,2-dioxasilinane (1p)

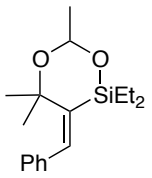

Yield: 44 mg, 75%

^{1}H NMR ($CDCl_3$, 500 MHz): δ 7.33-7.28 (dd, *J* = 7.7, 7.1 Hz, 2H, Ar-*H*), 7.26-7.21 (dd, *J* = 7.1, 7.1 Hz, 1H, Ar-*H*), 7.15-7.12 (d, *J* = 7.7 Hz, 2H, Ar-*H*), 6.72 (s, 1H, C=C*H*Ph), 5.37 (q, *J* = 5.0 Hz, 1H, OC*H*Me), 1.33 (d, *J* = 5.0 Hz, 3H, OCHC*H*$_3$), 1.28 [s, 3H, C(C*H*$_3$)$_2$], 1.23 [s, 3H, C(C*H*$_3$)$_2$], 1.09-1.04 (m, 6H, $SiCH_2CH_3$), and 0.84-0.69 (m, 4H, $SiCH_2CH_3$).

^{13}C NMR ($CDCl_3$, 125 MHz): δ 139.9, 137.3, 128.5, 128.3, 127.1, 91.4, 80.9, 30.5, 26.7, 25.4, 9.3, 7.2, 6.9, and 5.3.

IR (neat): 2964 (m), 2856 (m), 1438 (m), 1239 (m), 1078 (s), 726 (s), and 692 (m) cm^{-1}.

TLC: R_f = 0.5 in 80:1 hexanes: EtOAc.

GC-MS (5032021): t^R = 4.368 min, *m/z* 290, 291 [$(M+H)^+$, 10], 290 [M^+, 12], 289 [$(M–H)^+$, 20], 261 [$(M–CH_2CH_3)^+$, 60], 246 [$(M–CH_3CHO)^+$, 100] and 204 (40).

HRMS (**APCI/TOF**): Calcd for $(M+Na)^+$ $(C_{17}H_{26}NaO_2Si)^+$: 313.1594. Found: 313.1593.

(*E*)-2,2-Diethyl-4,4,6-trimethyl-3-(naphthalen-1-ylmethylene)-1,5,2-dioxasilinane (1q)

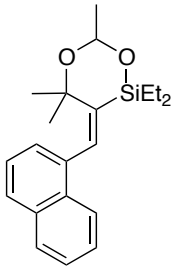

Yield: 55 mg, 80%

^{1}H NMR ($CDCl_3$, 500 MHz): δ 7.91-7.82 (m, 2H, Ar-*H*), 7.77 (d, *J* = 8.1 Hz, 1H, Ar-*H*), 7.48 (d, *J* = 7.0 Hz, 2H, Ar-*H*), 7.42 (dd, *J* = 8.1, 7.0 Hz, 2H, Ar-*H*), 6.95 (s, 1H, C=C*H*Ar), 5.42 (q, *J* = 5.0 Hz, 1H, OC*H*Me), 1.35 (d, *J* = 5.0 Hz, 3H, OCHC*H*$_3$), 1.17 [s, 3H, C(C*H*$_3$)$_2$], 1.11 [s, 3H, C(C*H*$_3$)$_2$], 1.17-1.13 (m, 6H, SiCH$_2$C*H*$_3$), and 0.94-0.81 (m, 4H, SiC*H*$_2$CH$_3$).

^{13}C NMR ($CDCl_3$, 125 MHz): δ 149.4, 136.9, 135.2, 133.2, 131.1, 130.8, 128.2, 127.3, 125.9, 125.8, 125.6, 124.8, 91.0, 80.5, 29.6, 25.9, 24.9, 9.0, 6.8, 6.6, and 4.9.

IR (neat): 2957 (m), 2926 (m), 1459 (m), 1236 (m), 1088 (s), 1007 (s), and 935 (m) cm^{-1}.

TLC: R_f = 0.5 in 80:1 hexanes: EtOAc.

GC-MS (5032021): t^R = 9.435 min, *m/z* 340, 341 [$(M+H)^+$, 40], 340 [M^+, 12], 339 [$(M–H)^+$, 50], 311 [$(M–CH_2CH_3)^+$, 56], 296 [$(M–CH_3CHO)^+$, 80] and 75 (100).

HRMS (**APCI/TOF**): Calcd for $(M+Na)^+$ $(C_{21}H_{29}O_2Si)^+$: 341.1931. Found: 341.1930.

(*E*)-3-(Benzofuran-2-ylmethylene)-2,2-diethyl-4,4,6-trimethyl-1,5,2-dioxasilinane (2r)

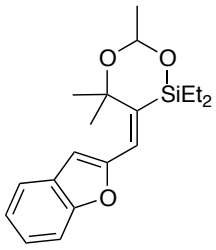

Yield: 51 mg, 77%

^{1}H NMR ($CDCl_3$, 500 MHz): δ 7.56 (d, *J* = 7.7 Hz, 1H, Ar-*H*), 7.48 (d, *J* = 8.2 Hz, 1H, Ar-*H*), 7.29 (dd, *J* = 7.2, 8.2 Hz, 1H, Ar-*H*), 7.22 (dd, *J* = 7.7, 7.2 Hz, 1H, Ar-*H*), 6.68 (s, 1H, Ar-*H*), 6.34 (s, 1H, C=C*H*Ar), 5.46 (q, *J* = 5.0 Hz, 1H, OC*H*Me), 1.75 [s, 3H, C(C*H*$_3$)$_2$], 1.71 [s, 3H, C(C*H*$_3$)$_2$], 1.38 (d, *J* = 5.0 Hz, 3H, OCHC*H*$_3$), 1.08-0.99(m, 6H, $SiCH_2CH_3$), and 0.85-0.73 (m, 4H, $SiCH_2CH_3$).

^{13}C NMR ($CDCl_3$, 125 MHz): δ 155.2, 153.4, 149.1, 128.4, 125.0, 123.3, 122.0, 121.3, 111.2, 109.2, 91.0, 81.7, 28.6, 25.3, 24.0, 9.3, 7.0, 6.6, and 4.7.

IR (neat): 2934 (m), 2876 (m), 1458 (m), 1237 (s), 1088 (s), and 731 (m) cm^{-1}.

TLC: R_f = 0.6 in 20:1 hexanes: EtOAc.

GC-MS (5032021): t^R = 8.459 min, *m/z* 330, 331 [$(M+H)^+$, 10], 330 [M^+, 2], 329 [$(M–H)^+$, 11], 301 [$(M–CH_2CH_3)^+$, 43], 286 [$(M–CH_3CHO)^+$, 90] and 235 (100).

HRMS (**APCI/TOF**): Calcd for $(M+Na)^+$ $(C_{19}H_{26}NaO_3Si)^+$: 353.1543. Found: 353.1540.

(1*E*,2*E*)-1,2-Bis(2,2-diethyl-4,4,6-trimethyl-1,5,2-dioxasilinan-3-ylidene)ethane (2x)

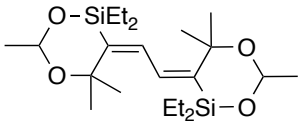

Yield: 0.2 mmol, 73 mg, 86%

^{1}H NMR ($CDCl_3$, 500 MHz): δ 6.24 (s, 2H, C=C*H*), 5.26 (q, *J* = 5.0 Hz, 2H, OC*H*Me), 1.41 [s, 6H, C(C*H*$_3$)$_2$], 1.36 [s, 6H, C(C*H*$_3$)$_2$], 1.23 (d, *J* = 5.0 Hz, 3H, OCHC*H*$_3$), 0.91-0.85(m, 6H, $SiCH_2CH_3$), and 0.71-0.61 (m, 4H, $SiCH_2CH_3$).

^{13}C NMR ($CDCl_3$, 125 MHz): δ 150.1, 130.2, 91.0, 80.1, 29.7, 29.6, 26.1, 25.9, 25.0, 8.9, 6.7, 6.4, and 4.6.

IR (neat): 2989 (m), 1367 (m), 1244 (m), 1132 (s), 960 (s), and 698 (m) cm^{-1}.

TLC: R_f = 0.5 in 100:1 hexanes: EtOAc.

HRMS (**APCI/TOF**): Calcd for $(M+K)^+$ $(C_{22}H_{42}KO_2Si_2)^+$: 465.2340. Found: 465.2339.

(4'*S*,8*R*,9*S*,13*S*,14*S*,*E*)-3'-Benzylidene-3-(benzyloxy)-2',2'-diethyl-6',13-dimethyl-6,7,8,9,11,12,13,14,15,16-decahydrospiro[cyclopenta[*a*]phenanthrene-17,4'-[1,5,2]dioxasilinane] (2z)

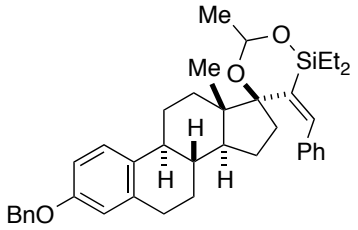

Yield: 0.2 mmol, 102 mg, 86%

^{1}H NMR (C_6D_6, 500 MHz): δ 7.26 [d, *J* = 8.1 Hz, 2H, (OCH_2)Ar*H*], 7.16 [d, *J* = 8.1 Hz, 1H, Ph-*H*], 7.11 [dd, *J* = 8.1, 1.7 Hz, 4H, Ar*H*], 7.06 [d, *J* = 8.1 Hz, 1H, Ar*H*], 6.96 [m, 4H, Ar*H*], 6.80 [dd, *J* = 8.1 Hz, 1.7 Hz, 1H, Ar*H*], 6.67 (s, 1H, C=C*H*Ph), 5.32 (q, *J* = 5.0 Hz, 1H, OC*H*Me), 4.74 [s, 2H, OCH_2Bn], 2.59 (m, 2H, C6-*H*), 2.30-2.23 (m, 1H, C7-*H*), 2.17-2.15 (m, 1H, C7-*H*), 1.97-1.95 (m, 1H, C8-*H*), 1.85-1.82 (m, 2H, C11-*H*), 1.67-1.65 (m, 1H, C9-*H*), 1.39 (d, *J* = 5.0 Hz, 3H, OCHCH_3), 1.30-1.28 (m, 2H, C12-*H*), 1.30-1.28 (m, 1H, C14-*H*), 1.17-1.15 (m, 6H, $SiCH_2CH_3$), 1.07-1.05 (m, 2H, C15-*H*), 0.85 (s, 3H, C18-*H*), 0.79-0.75 (s, 2H, C16-*H*), and 0.71-0.61 (m, 4H, $SiCH_2CH_3$).

^{13}C NMR (C_6D_6, 125 MHz): δ 157.1, 149.2, 140.1, 139.7, 138.9, 132.3, 128.4, 126.2, 126.1, 115.0, 112.6, 95.4, 93.9, 69.6, 49.9, 47.6, 43.4, 38.8, 37.7, 34.1, 29.8, 27.1, 26.6, 25.1, 23.4, 14.9, 9.5, 6.8, 6.7, and 4.8.

IR (neat): 3110 (w), 2984 (m), 2876 (m), 1381 (m), 1254 (m), 1071 (s), 962 (s), and 795 (m) cm^{-1}.

TLC: R_f = 0.6 in 40:1 hexanes: EtOAc.

HRMS (**APCI/TOF**): Calcd for $(M+H)^+$ $(C_{39}H_{49}O_3Si)^+$: 593.3405. Found: 593.3407.

(*E*)-3-[Diethyl(methyl)silyl]-2-methyl-4-(trimethylsilyl)but-3-en-2-ol (3a)

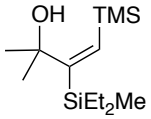

Yield: 0.2 mmol scale, 45 mg, 88%

^{1}H NMR (C_6D_6, 500 MHz): δ 6.20 (s, 1H, C=C*H*TMS), 1.17 [s, 6H, OC(C*H*$_3$)$_2$], 0.95 (dd, *J* = 7.8, 1.2 Hz, 3H, SiCH$_2$C*H*$_3$), 0.95 (dd, *J* = 7.8, 1.2 Hz, 3H, SiCH$_2$C*H*$_3$), 0.65-0.58 (m, 4H, SiC*H*$_2$CH$_3$), 0.32 [s, 9H, Si(C*H*$_3$)$_3$] and 0.11 (s, 3H, SiC*H*$_3$).

^{13}C NMR (C_6D_6, 125 MHz): δ 160.6, 141.9, 85.7, 30.9, 7.6, 6.9, 2.3, and -3.9.

IR (neat): 3300 (br), 2960 (w), 1249 (m), 1165 (s), 839 (s), and 634 (m) cm^{-1}.

TLC: R_f = 0.5 in 10:1 hexanes: EtOAc.

GC-MS (5032021): t^R = 4.329 min, *m/z* 258, 259 [(M+H)$^+$, 10], 258 [M$^+$, 22], 257 [(M–H)$^+$, 100], 220[(M–CH$_3$)$^+$, 50], 229 [(M–CH$_2$CH$_3$)$^+$, 56], and 127 (40).

HRMS (**APCI/TOF**): Calcd for (M+Na)$^+$ ($C_{13}H_{30}NaOSi_2$)$^+$: 281.1727. Found: 281.1725.

(*E*)-2-[Diethyl(methyl)silyl]-3-(trimethylsilyl)prop-2-en-1-ol (3g)

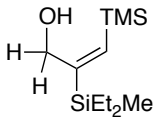

Yield: 39 mg, 85%

^{1}H NMR (C_6D_6, 500 MHz): δ 6.4 (s, 1H, C=C*H*TMS), 4.66 (s, 2H, C*H*$_2$COH), 0.95 (dd, *J* = 7.8, 1.4 Hz, 6H, SiCH$_2$C*H*$_3$), 0.64-0.60 (m, 4H, SiC*H*$_2$CH$_3$), 0.32 [s, 9H, Si(C*H*$_3$)$_3$] and 0.11 (s, 3H, SiC*H*$_3$).

^{13}C NMR (C_6D_6, 125 MHz): δ 160.6, 141.9, 85.7, 7.6, 6.9, 2.3, and -3.9.

IR (neat): 3290 (br), 2952 (w), 1240 (m), 1153 (s), 836 (s), and 639 (m) cm^{-1}.

TLC: R_f = 0.6 in 20:1 hexanes: EtOAc.

GC-MS (5032021): t^R = 3.502 min, *m/z* 230, 231 [$(M+H)^+$, 10], 230 [M^+, 23], 229 [$(M–H)^+$, 100], 216 [$(M–CH_3)^+$, 60], 202 [$(M–CH_2CH_3)^+$, 90], and 127 (40).

HRMS (**APCI/TOF**): Calcd for $(M+Na)^+$ $(C_{11}H_{26}NaOSi_2)^+$: 253.1414 Found: 253.1413.

(*E*)-3-[Diethyl(methyl)silyl]-4-(trimethylsilyl)but-3-en-2-ol (3h)

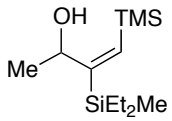

Yield: 37 mg, 75%

^{1}H NMR (C_6D_6, 500 MHz): 5.99 (s, 1H, C=C*H*TMS), 4.71 [q, *J* = 5.0 Hz, 1H, OCH(C*H*$_3$)], 1.28 [d, *J* = 5.0 Hz, 3H, OCH(C*H*$_3$)], 0.90 (dd, *J* = 7.8, 1.2 Hz, 6H, $SiCH_2CH_3$), 0.65-0.61 (m, 4H, $SiCH_2CH_3$), 0.12 [s, 9H, $Si(CH_3)_3$] and 0.11 (s, 3H, $SiCH_3$).

^{13}C NMR (C_6D_6, 125 MHz): δ 166.2, 142.9, 73.6, 23.9, 7.6, 6.5, 6.3, 0.9, and -4.4.

IR (neat): 2959 (br), 1249 (m), 1156 (s), 914 (s), 838 (s), and 759 (m) cm^{-1}.

TLC: R_f = 0.6 in 20:1 hexanes: EtOAc.

GC-MS (5032021): t^R = 4.301 min, *m/z* 244, 245 [$(M+H)^+$, 50], 244 [M^+, 40], 243 [$(M–H)^+$, 53], 229[$(M–CH_3)^+$, 80], 171 [$(M–TMS)^+$, 10], and 199 (20).

HRMS (**APCI/TOF**): Calcd for $(M+Na)^+$ $(C_{12}H_{28}NaOSi_2)^+$: 267.1571. Found: 267.1570.

(*E*)-2-[Diethyl(methyl)silyl]-1-phenyl-3-(trimethylsilyl)prop-2-en-1-ol (3i)

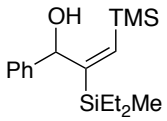

Yield: 52 mg, 85%

^{1}H NMR ($CDCl_3$, 500 MHz): δ 7.34 (d, *J* = 7.7 Hz, 2H, Ar-*H*), 7.30 (dd, *J* = 7.1, 7.1 Hz, 2H, Ar-*H*), 7.24 (d, *J* = 7.7 Hz, 1H, Ar-*H*), 6.28 (s, 1H, C=C*H*TMS), 5.61 [s, 1H, OC*H*Ph], 0.78-0.76 (m, 6H, $SiCH_2CH_3$), 0.54-0.33 (m, 2H, $SiCH_2CH_3$), 0.33-0.22 (m, 2H, $SiCH_2CH_3$), 0.18 [s, 9H, $Si(CH_3)_3$] and 0.11 (s, 3H, $SiCH_3$).

^{13}C NMR ($CDCl_3$, 125 MHz): δ 163.2, 145.9, 142.3, 128.1, 127.1, 126.2, 77.4, 7.5, 6.1, 6.0, 1.1, and -4.9.

IR (neat): 3298 (br), 2950 (w), 1246 (m), 1169(s), 834 (s), and 632 (m) cm^{-1}.

TLC: R_f = 0.6 in 20:1 hexanes: EtOAc.

GC-MS (5032021): t^R = 5.968 min, *m/z* 306, 307 [$(M+H)^+$, 40], 306 [M^+, 10], 305 [$(M–H)^+$, 90], 291[$(M–CH_3)^+$, 56], 277 [$(M–CH_2CH_3)^+$, 30], 289 [$(M–OH)^+$, 60] and 233 (50).

HRMS (**APCI/TOF**): Calcd for $(M+Na)^+$ $(C_{17}H_{30}NaOSi_2)^+$: 329.1727. Found: 329.1725.

(*E*)-1-{1-[Diethyl(methyl)silyl]-2- (trimethylsilyl)vinyl}cyclopropanol (3j)

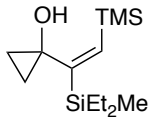

Yield: 45 mg, 88%

^{1}H NMR (C_6D_6, 500 MHz): δ 6.27 (s, 1H, C=C*H*TMS), 1.18 [s, 6H, $OC(CH_3)_2$], 1.33 (d, *J* = 5.0 Hz, 3H, $OCHCH_3$), 0.92 (dd, *J* = 7.8, 1.4 Hz, 6H, $SiCH_2CH_3$), 0.90-0.80 [nfom, 2H, $C(CH_2)_2$], 0.67-0.59 [nfom, 2H, $C(CH_2)_2$], 0.59-0.58 (m, 4H, $SiCH_2CH_3$), 0.15 [s, 9H, $Si(CH_3)_3$] and 0.09 (s, 3H, $SiCH_3$).

^{13}C NMR (C_6D_6, 125 MHz): δ 162.3, 146.5, 57.7, 14.8, 7.5, 6.0, 0.5, and -5.2.

IR (neat): 3302 (br), 2958 (w), 1248 (m), 1155 (s), 836 (s), and 759 (m) cm^{-1}.

TLC: R_f = 0.6 in 80:1 hexanes: EtOAc.

GC-MS (5032021): t^R = 4.341 min, *m/z* 256, 257 [$(M+H)^+$, 100], 256 [M^+, 10], 255 [$(M–H)^+$, 80], 241[$(M–CH_3)^+$, 20], 227 [$(M–CH_2CH_3)^+$, 30], 239 [$(M–OH)^+$, 15] and 183 (55).

HRMS (**APCI/TOF**): Calcd for $(M+Na)^+$ $(C_{13}H_{28}NaOSi_2)^+$: 279.1571. Found: 279.1568.

(*E*)-1-[1-(Diethyl(methyl)silyl-2-(triisopropylsilyl)vinyl]cyclobutanol(3k)

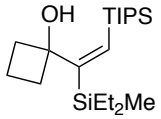

Yield: 48 mg, 89%

^{1}H NMR (C_6D_6, 500 MHz): δ 5.99 (s, 1H, C=C*H*TIPS), 2.38-2.36 [nfom, 2H, C(C*H*$_2$)$_2$], 2.03-1.99 [nfom, 1H, C(C*H*$_2$)$_2$], 1.84-1.80 [nfom, 2H, C(C*H*$_2$)$_2$], 1.70-1.63 [nfom, 1H, C(C*H*$_2$)$_2$], 1.10-1.09 {m, 21H, Si[C*H*(C*H*$_3$)$_2$]$_3$}, 0.95-0.92 (m, 6H, SiCH$_2$C*H*$_3$), 0.70-0.62 (m, 4H, SiC*H*$_2$CH$_3$) and 0.15 (s, 3H, SiC*H*$_3$).

^{13}C NMR (C_6D_6, 125 MHz): δ 166.8, 135.4, 80.2, 36.9, 19.4, 14.5, 13.4, 7.6, 7.0, and -4.0.

IR (neat): 3280 (br), 2956 (w), 1243 (m), 1162 (s), 832 (s), and 633 (m) cm^{-1}.

TLC: R_f = 0.6 in 80:1 hexanes: EtOAc.

GC-MS (5032021): t^R = 5.431 min, *m/z* 354, 355 [$(M+H)^+$, 100], 354 [M^+, 10], 353[$(M–H)^+$, 90], 339[$(M–CH_3)^+$, 32], 325 [$(M–CH_2CH_3)^+$, 50] and 197 (10).

HRMS (**APCI/TOF**): Calcd for $(M+H)^+$ $(C_{14}H_{31}OSi_2)^+$: 271.1908. Found: 271.1905.

(*E*)-1-{1-[Diethyl(methyl)silyl]-2-(triisopropylsilyl)vinyl}cyclopentanol(3l)

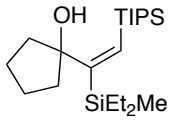

Yield: 52 mg, 91%

^{1}H NMR (C_6D_6, 500 MHz): δ 6.04 (s, 1H, C=C*H*TIPS), 1.80-1.78 [m, 1H, C(C*H*$_2$)$_4$], 2.15-2.11 [m, 1H, C(C*H*$_2$)$_4$], 1.95-1.90 [m, 2H, C(C*H*$_2$)$_4$], 1.71-1.62 [m, 4H, C(C*H*$_2$)$_4$], 1.11 {m, 21H, Si[CH(C*H*$_3$)$_2$]$_3$}, 0.94 (dd, J = 7.8, 1.4 Hz, 6H, SiCH$_2$C*H*$_3$), 0.61-0.57 (m, 4H, SiC*H*$_2$CH$_3$), and 0.05 (s, 3H, SiC*H*$_3$).

^{13}C NMR (C_6D_6, 125 MHz): δ 167.4, 134.8, 86.3, 41.1, 24.1, 19.5, 13.6, 7.6, 7.4, and -3.6.

IR (neat): 2980 (br), 1243 (m), 1155 (s), 829 (s), and 644 (m) cm^{-1}.

TLC: R_f = 0.6 in 80:1 hexanes: EtOAc.

GC-MS (5032021): t^R = 5.544 min, *m/z* 368, 369 [(M+H)$^+$, 80], 368 [M$^+$, 15], 367 [(M–H)$^+$, 50], 353[(M–CH$_3$)$^+$, 40], 351 [(M–OH)$^+$, 20] and 325 (10).

HRMS (**APCI/TOF**): Calcd for (M+H)$^+$ ($C_{15}H_{33}OSi_2$)$^+$: 285.2064. Found: 285.2061.

(*E*)-1-{1-[Diethyl(methyl)silyl]2-(trimethylsilyl)vinyl}cyclohexanol (3m)

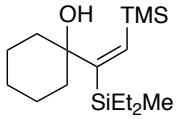

Yield: 46 mg, 78%

^{1}H NMR (C_6D_6, 500 MHz): δ 6.17 (s, 1H, C=C*H*TMS), 2.10 [m, 2H, C(C*H*$_2$)$_5$], 1.53-1.50[m, 4H, C(C*H*$_2$)$_5$], 1.50-1.48 [m, 2H, C(C*H*$_2$)$_5$], 1.41-1.333 [m, 2H, C(C*H*$_2$)$_5$], 0.19 [s, 9H, Si(C*H*$_3$)$_3$], 0.95 (dd, J = 7.8, 1.4 Hz, 6H, SiCH$_2$C*H*$_3$), 0.61-0.60 (m, 4H, SiC*H*$_2$CH$_3$), 0.27 [s, 9H, Si(C*H*$_3$)$_3$] and 0.10 (s, 3H, SiC*H*$_3$).

^{13}C NMR (C_6D_6, 125 MHz): δ 169.2, 142.8, 77.3, 37.3, 25.1, 22., 21.6, 7.7, 7.2, 2.5 and -3.4.

IR (neat): 2958 (br), 1246 (m), 1160 (s), 969 (s), 839 (s), and 759 (m) cm^{-1}.

TLC: R_f = 0.6 in 80:1 hexanes: EtOAc.

GC-MS (5032021): t^R = 5.602 min, *m/z* 382, 383 [$(M+H)^+$, 40], 382 [M^+, 20], 381 [$(M–H)^+$, 100], 367[$(M–CH_3)^+$, 30], 353 [$(M–CH_2CH_3)^+$, 51], and 365 [$(M–OH)^+$, 27]

HRMS (**APCI/TOF**): Calcd for $(M+K)^+$ $(C_{16}H_{34}KOSi_2)^+$: 337.1780. Found: 337.1778.

(*E*)-3-[Diethyl(methyl)silyl]-2-methylundec-3-en-2-ol (3n)

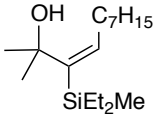

Yield: 48 mg, 84%

^{1}H NMR (C_6D_6, 500 MHz): δ 5.64 (t, *J* = 7.3 Hz, 1H, C=C*H*C_7H_{15}), 2.04-2.00 [m, 2H, $CH_3(CH_2)_5CH_2CC$], 1.26 [s, 6H, $C(CH_3)_2$], 1.27-1.18 [m, 8H, $CH_3(CH_2)_6CC$], 1.07 (dd, *J* = 7.8, 1.4 Hz, 6H, $SiCH_2CH_3$), 0.98-0.83 (m, 4H, $SiCH_2CH_3$), 0.98-0.83 [m, 8H, $CH_3(CH_2)_6CC$], 0.70-0.59 [m, 3H, $CH_3(CH_2)_6CC$] and 0.22 (s, 9H, $SiCH_3$).

^{13}C NMR (C_6D_6, 125 MHz): δ 148.2, 144.8, 73.3, 32.8, 32.4, 31.7, 29.7, 29.4, 22.7, 22, 21, 14.1, 7.9, 7.2, and -3.6.

IR (neat): 2956 (br), 1225 (m), 1168 (s), 1099 (s), 838 (s), and 759 (m) cm^{-1}.

TLC: R_f = 0.6 in 20:1 hexanes: EtOAc.

GC-MS (5032021): t^R = 6.392 min, *m/z* 284, 285 [$(M+H)^+$, 10], 284 [M^+, 8], 283 [$(M–H)^+$, 100], 273[$(M–CH_3)^+$, 30], 259 [$(M–CH_2CH_3)^+$, 40], and 89 (90).

HRMS (**APCI/TOF**): Calcd for $(M+H)^+$ $(C_{17}H_{37}OSi)^+$: 285.2644. Found: 285.2640.

(*E*)-4-(Cyclohex-1-en-1-yl)-3-[diethyl(methyl)silyl]-2-methylbut-3-en-2-ol (3o)

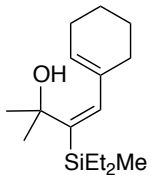

Yield: 43 mg, 80%

^{1}H NMR ($CDCl_3$, 500 MHz): δ 6.2 (s, 1H, C=C*H*cyclohexeneyl), 5.48 (ddd, *J* = 3.6, 1.8, 1.7 Hz, 1H, C=C*H*), 2.09-2.01 (m, 2H, (C*H*$_2$)$_4$C=C), 1.65-1.55 (m, 2H, (C*H*$_2$)$_4$C=C), 1.38-1.30 (m, 2H, (C*H*$_2$)$_4$C=C), 0.90-0.88 (m, 2H, (C*H*$_2$)$_4$C=C), 1.38 [s, 6H, OC(C*H*$_3$)$_2$], 0.92 (dd, *J* = 7.8, 1.4 Hz, 6H, SiCH$_2$C*H*$_3$), 0.65-0.61 (m, 4H, SiC*H*$_2$CH$_3$), and 0.09 (s, 3H, SiC*H*$_3$).

^{13}C NMR ($CDCl_3$, 125 MHz): δ 148.8, 140.4, 139.9, 123.5, 76.8, 32.1, 29.2, 25.2, 22.6, 22.0, 7.7, 7.0, and -3.4.

IR (neat): 2932 (br), 1449 (m), 1247 (s), 1084 (s), 837 (s), and 791 (m) cm^{-1}.

TLC: R_f = 0.6 in 10:1 hexanes: EtOAc.

GC-MS (5032021): t^R = 6.456 min, *m/z* 266, 267 [$(M+H)^+$, 30], 266 [M^+, 22], 265 [$(M–H)^+$, 100], 251 [$(M–CH_3)^+$, 90], 237 [$(M–CH_2CH_3)^+$, 45], and 180 (50).

HRMS (**APCI/TOF**): Calcd for $(M+Na)^+$ $(C_{16}H_{30}NaOSi)^+$: 289.2030. Found: 289.2035.

(*E*)-3-[Diethyl(methyl)silyl]-2-methyl-4-phenylbut-3-en-2-ol (3p)

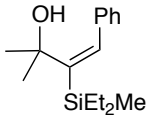

Yield: 43 mg, 82%

^{1}H NMR (C_6D_6, 500 MHz): δ 7.03 (m, Hz, 2H, Ar-*H*), 6.98 (m, 3H, Ar-*H*), 6.83 (s, 1H, C=C*H*Ph), 1.08 [s, 6H, OC(C*H*$_3$)$_2$], 1.06 (dd, *J* = 7.8, 1.4 Hz, 6H, SiCH$_2$C*H*$_3$), 0.82-0.80 (m, 4H, SiC*H*$_2$CH$_3$), and 0.24 (s, 3H, SiC*H*$_3$).

^{13}C NMR (C_6D_6, 125 MHz): δ 159.2, 140.8, 137.8, 126.2, 75.3, 32.1, 7.9, 7.2, and -3.6.

IR (neat): 2952 (br), 2870 (w), 1247 (m), 1111 (s), 847 (s), and 795 (m) cm^{-1}.

TLC: R_f = 0.5 in 20:1 hexanes: EtOAc.

GC-MS (5032021): t^R = 5.982 min, *m/z* 262, 263 [$(M+H)^+$, 18], 262 [M^+, 20], 261 [$(M–H)^+$, 100], 247[$(M–CH_3)^+$, 62], 233 [$(M–CH_2CH_3)^+$, 80], and 127 (20).

HRMS (**APCI/TOF**): Calcd for $(M+Na)^+$ $(C_{16}H_{26}NaOSi_2)^+$: 285.1645. Found: 285.1641.

(*E*)-3-[Diethyl(methyl)silyl]-2-methyl-4-(naphthalen-1-yl)but-3-en-2-ol (3q)

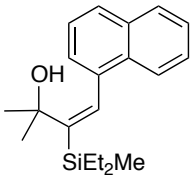

Yield: 52 mg, 83%

^{1}H NMR (C_6D_6, 500 MHz): δ 8.03 (d, *J* = 7.0 Hz, 1H, Ar-*H*), 7.57 (d, *J* = 8.1 Hz, 1H, Ar-*H*), 7.48 (d, *J* = 7.0 Hz, 1H, Ar-*H*), 7.30 (dd, *J* = 8.1, 7.0 Hz, 1H, Ar-*H*), 7.27 (dd, *J* = 8.1, 7.0 Hz, 1H, Ar-*H*), 7.13 (dd, *J* = 8.1, 7.0 Hz, 1H, Ar-*H*), 7.09 (dd, *J* = 8.1, 7.0 Hz, 1H, Ar-*H*), 7.00 (s, 1H, C=C*H*Ar), 0.98 [s, 6H, C(C*H*$_3$)$_2$], 0.95 (dd, *J* = 7.8, 1.4 Hz, 3H, SiCH$_2$C*H*$_3$), 0.86-0.81 (m, 4H, SiC*H*$_2$CH$_3$) and 0.29 (s, 3H, SiC*H*$_3$).

^{13}C NMR (C_6D_6, 125 MHz): δ 153.4, 139.8, 135.7, 127.9, 127.1, 127.0, 125.6, 125.4, 125.4, 125.1, 124.9, 124.5, 75.0, 31.2, 7.6, 6.8, and -4.0.

IR (neat): 2950 (br), 2872 (w), 1233 (m), 1118 (s), 1016 (s), 909 (s), and 784 (m) cm^{-1}.

TLC: R_f = 0.4 in 20:1 hexanes: EtOAc.

GC-MS (5032021): t^R = 6.413 min, *m/z* 312, 313 [$(M+H)^+$, 10], 312 [M^+, 25], 311 [$(M–H)^+$, 100], 297 [$(M–CH_3)^+$, 80], 283 [$(M–CH_2CH_3)^+$, 53], and 89 (50).

HRMS (**APCI/TOF**): Calcd for $(M+Na)^+$ $(C_{20}H_{28}NaOSi)^+$: 335.1842. Found: 335.1840.

(*E*)-4-(Benzofuran-2-yl)-3-[diethyl(methyl)silyl]-2-methylbut-3-en-2-ol (3r)

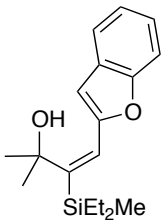

Yield: 45 mg, 75%

^{1}H NMR ($CDCl_3$, 500 MHz): δ 7.54 (d, *J* = 7.7 Hz, 1H, Ar-*H*), 7.48 (d, *J* = 8.2 Hz, 1H, Ar-*H*), 7.27 (dd, *J* = 7.2, 8.2 Hz, 1H, Ar-*H*), 7.25 (dd, *J* = 7.7, 7.2 Hz, 1H, Ar-*H*), 6.68 (s, 1H, Ar-*H*), 6.40 (s, 1H, C=C*H*Ar), 1.64 [s, 6H, $OC(CH_3)_2$], 0.99 (dd, *J* = 7.8, 1.4 Hz, 6H, $SiCH_2CH_3$), 0.75 (m, 4H, $SiCH_2CH_3$), and 0.19 (s, 3H, $SiCH_3$).

^{13}C NMR ($CDCl_3$, 125 MHz): δ 150, 148.8, 140.4, 139.9, 130, 128, 127, 126, 123.5, 120, 76.8, 32.1, 7.7, 7.0, and -3.4.

IR (neat): 2932 (br), 2863 (w), 1247 (m), 1160 (s), 837 (s), 791(s), and 699 (m) cm^{-1}.

TLC: R_f = 0.5 in 5:1 hexanes: EtOAc.

GC-MS (5032021): t^R = 6.407 min, *m/z* 302, 303 [$(M+H)^+$, 20], 302 [M^+, 12], 301 [$(M–H)^+$, 90], 287 [$(M–CH_3)^+$, 100], 273 [$(M–CH_2CH_3)^+$, 60], and 216 (80).

HRMS (**APCI/TOF**): Calcd for $(M+Na)^+$ $(C_{18}H_{26}NaO_2Si)^+$: 325.1651. Found: 325.1649.

(*E*)-3-[Diethyl(methyl)silyl]-2-methyl-4-(pyridin-3-yl)but-3-en-2-ol (3s^1)

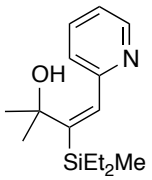

Yield: 37 mg, 70%

^{1}H NMR (C_6D_6, 500 MHz): δ 7.98 (d, *J* = 4.7 Hz 1H, Ar-*H*), 6.82 (dd, *J* = 7.9, 4.7 Hz, 1H, Ar-*H*), 6.65 (d, *J* = 7.9 Hz, 1H, Ar-*H*), 6.60 (s, 1H, C=C*H*Ar), 6.24 (dd, *J* = 7.9, 4.7 Hz, 1H, Ar-*H*), 1.65 [s, 6H, C(C*H*$_3$)$_2$], 0.99 (dd, *J* = 7.8, 1.4 Hz, 6H, SiCH$_2$C*H*$_3$), 0.74-0.68 (m, 4H, SiC*H*$_2$CH$_3$), and 0.18 (s, 3H, SiC*H*$_3$).

^{13}C NMR (C_6D_6, 125 MHz): δ 149.2, 139.2, 137.8, 133.1, 127.1, 127.2, 120.0, 69.3, 30.1, 7.9, 7.2, and -3.6.

IR (neat): 2954 (br), 2873 (w), 1448(m), 1254 (m), 1007 (s), 796 (s), and 739 (m) cm^{-1}.

TLC: R_f = 0.4 in 5:1 hexanes: EtOAc.

GC-MS (5032021): t^R = 7.850 min, *m/z* 263, 264 [(M+H)$^+$, 10], 263 [M$^+$, 6], 262 [(M–H)$^+$, 100], 248 [(M–CH$_3$)$^+$, 56], 234 [(M–CH$_2$CH$_3$)$^+$, 86], and 177 (60).

HRMS (**APCI/TOF**): Calcd for (M+Na)$^+$ ($C_{15}H_{25}KNOSi$)$^+$: 302.1309. Found: 302.1307.

4-(Diethyl(methyl)silyl)-1',5,5-trimethyl-5*H*-spiro[furan-2,2'-indoline] (3t)

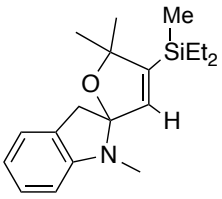

Yield: 45 mg, 71%

^{1}H NMR (C_6D_6, 500 MHz): δ 7.11 (dd, *J* = 7.2, 8.2 Hz, 1H, Ar-*H*), 7.00 (d, *J* = 8.2 Hz, 1H, Ar-*H*), 6.75 (dd, *J* = 7.2, 8.2 Hz, 1H, Ar-*H*), 6.35 (d, *J* = 7.7 Hz, 1H, Ar-*H*), 5.5 (s, 1H,

C=C*H*CNMe), 2.95 (s, 2H, NCHC*H*$_2$), 2.52 (s, 3H, N-C*H*$_3$), 1.26 [s, 3H, OC(C*H*$_3$)$_2$], 1.23 [s, 3H, OC(C*H*$_3$)$_2$], 0.85 (dd, *J* = 7.8, 1.4 Hz, 6H, SiCH$_2$C*H*$_3$), 0.46 (m, 4H, SiC*H*$_2$CH$_3$), and -0.04 (s, 3H, SiC*H*$_3$).

^{13}C NMR (C_6D_6, 125 MHz): δ 150.0, 149.9, 139.2, 126.9, 123.8, 117.5, 110.1, 105.9, 90.4, 43.1, 30.4, 28.1, 27.9, 7.3, 7.2, 5.7, 5.6, and -5.6.

IR (neat): 3045 (m), 2863 (w), 1547 (m), 1160 (s), 837 (s), 791(s), and 699 (m) cm^{-1}.

TLC: R_f = 0.4 in 3:1 hexanes: EtOAc.

HRMS (**APCI/TOF**): Calcd for $(M+Na)^+$ $(C_{19}H_{29}NNaO_2Si)^+$: 339.1918. Found: 339.1909.

(3*E*,5*E*)-3,6-Bis[diethyl(methyl)silyl]-2,7-dimethylocta-3,5-diene-2,7-diol (3x)

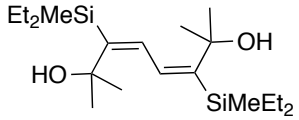

Yield: 0.2 mmol, 61 mg, 83%

^{1}H NMR (C_6D_6, 500 MHz): δ 6.65 (s, 2H, C=C*H*), 1.35 [s, 12H, OC(C*H*$_3$)$_2$], 1.02 (dd, *J* = 7.8, 1.2 Hz, 12H, SiCH$_2$C*H*$_3$), 0.82-0.76 (m, 8H, SiC*H*$_2$CH$_3$), and 0.22 (s, 6H, SiC*H*$_3$).

^{13}C NMR ($CDCl_3$, 125 MHz): δ 152.5, 132.7, 76.7, 31.4, 7.6, 6.9, 2.3, and -3.7.

IR (neat): 2956 (br), 1364(m), 1247 (m), 1133 (s), 822 (s), and 784 (m) cm^{-1}.

TLC: R_f = 0.4 in 5:1 hexanes: EtOAc.

GC-MS (5032021): t^R = 12.745 min, *m/z* 370, 371 [$(M+H)^+$, 10], 370 [M^+, 15], 369 [$(M–H)^+$, 100], 355 [$(M–CH_3)^+$, 60], 341 [$(M–CH_2CH_3)^+$, 90], and 285 (50).

HRMS (**APCI/TOF**): Calcd for $(M+Na)^+$ $(C_{20}H_{42}NaO_2Si)^+$: 393.2607. Found: 393.2698.

(*E*)-3-[Diethyl(methyl)silyl]-2,7-dimethyl-7-[(trimethylsilyl)oxy]oct-3-en-5-yn-2-ol] (3y)

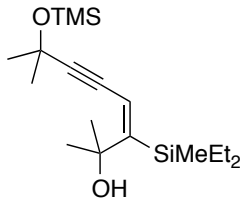

Yield: 0.2 mmol, 49 mg, 72%

^{1}H NMR ($CDCl_3$, 500 MHz): δ 5.70 (s, 1H, C=C*H*CC), 1.54 [s, 6H, OC(C*H*$_3$)$_2$], 1.53 [s, 6H, OC(C*H*$_3$)$_2$], 0.94 (dd, *J* = 7.8, 1.4 Hz, 6H, SiCH$_2$C*H*$_3$), 0.64-0.60 (m, 4H, SiC*H*$_2$CH$_3$), 0.17 [s, 9H, Si(C*H*$_3$)$_3$] and 0.09 (s, 3H, SiC*H*$_3$).

^{13}C NMR ($CDCl_3$, 125 MHz): δ 160.1, 117.2, 88.4, 80.3, 78.1, 70.7, 32.7, 29.6, 7.7, 6.6, 1.9, and -4.3.

IR (neat): 2980(br), 1254 (m), 1118 (s), 960 (s), and 630 (m) cm^{-1}.

TLC: R_f = 0.5 in 10:1 hexanes: EtOAc.

GC-MS (5032021): t^R = 5.875 min, *m/z* 340, 341 [$(M+H)^+$, 12], 340 [M^+, 18], 339 [$(M–H)^+$, 90], 325 [$(M–CH_3)^+$, 64], 311 [$(M–CH_2CH_3)^+$, 77], and 254 (100).

HRMS (**APCI/TOF**): Calcd for $(M+Na)^+$ $(C_{20}H_{42}NaO_2Si)^+$: 393.2607. Found: 393.2698.

(8*R*,9*S*,13*S*,14*S*,17*S*)-3-(Benzyloxy)-17-((*E*)-1-(diethyl(methyl)silyl)-2-phenylvinyl)-13-methyl-7,8,9,11,12,13,14,15,16,17-decahydro-6*H*-cyclopenta[*a*]phenanthren-17-ol (3z)

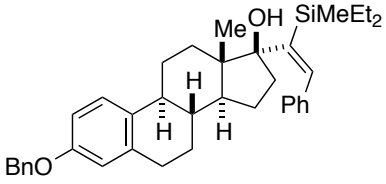

Yield: 0.2 mmol, 105 mg, 91%

^{1}H NMR ($CDCl_3$, 500 MHz): δ 7.41 [d, *J* = 8.1 Hz, 2H, (OCH_2)Ar*H*], 7.37 [dd, *J* = 8.1 Hz, 1.7 Hz 2H, Ph-*H*], 7.30 [d, *J* = 7.7 Hz, 1H, Ar*H*], 7.25-7.16 [m, 6H, Ar*H*], 7.05 (s, 1H, C=C*H*Ph), 6.77 [dd, *J* = 8.1 Hz, 1.7 Hz, 1H, Ar*H*], 6.67 [dd, *J* = 8.1 Hz, 1.7 Hz, 1H, Ar*H*], 5.02 [s, 2H, OC*H*$_2$Bn], 2.73-2.72 (m, 2H, C6-*H*), 2.48-2.46 (m, 1H, C7-*H*), 2.28-2.26 (m, 1H, C7-*H*), 2.08-2.06 (m, 1H, C8-*H*), 1.85-1.82 (m, 1H, C9-*H*), 1.55-1.44 (m, 2H, C15-*H*), 1.55-1.44 (m, 2H, C16-*H*), 1.25-1.24 (m, 2H, C11-*H*), 1.04-0.97 (m, 6H, $SiCH_2CH_3$), 0.85 (s, 3H, C18-*H*), 0.71-0.61 (m, 4H, $SiCH_2CH_3$), 0.39-0.37 (m, 1H, C9-*H*), and 0.20 (s, 3H, $SiCH_3$).

^{13}C NMR ($CDCl_3$, 125 MHz): δ 156.7, 150.9, 140.1, 139.2, 138.9, 138.0, 133.1, 129.1, 128.6, 127.9, 127.5, 127.4, 126.3, 125.9, 114.9, 112.3, 89.7, 70.1, 48.7, 43.7, 41.2, 39.5, 33.9, 29.9, 26.8, 26.7, 22.6, 14.3, 8.9, 8.4, 8.2, 7.6, and -2.1.

IR (neat): 3200(br), 2980 (w), 1256 (m), 1072 (s), 960 (s), and 795 (m) cm^{-1}.

TLC: R_f = 0.4 in 10:1 hexanes: EtOAc.

HRMS (**APCI/TOF**): Calcd for $(M+H)^+$ $(C_{39}H_{52}O_2Si)^+$: 580.3791. Found: 580.3790.

References:

1. Tacke, R.; Wannagat, U. Syntheses and properties of bioactive organo-silicon compounds. In *Bioactive Organo-Silicon Compounds*, Springer: **1979**, 1-75.
2. Greene, T.; Wuts, P. G. M. *Protecting Groups in Organic Synthesis*; 2nd ed.; Wiley: New York, **1991**.
3. Kocienski, P. I. *Protecting Groups*; Thieme: Stuttgart, **1994**.
4. Larson, G. L.; Fry, J. L. *Ionic and Organometallic-Catalyzed Organosilane Reductions.* Denmark, S. E. Ed.; John Wiley and Sons: **2008**, *71*, 1-737.
5. Denmark, S. E. Sweis, R. F. In *Metal-Catalyzed Cross-Coupling Reactions*; de Meijere, A., Diederich, F., Eds.; Wiley-VCH: New York, **2004**; Chapter 4.
6. Nakao, Y; Hiyama, T. Silicon-based cross-coupling reaction: an environmentally benign version. *Chem. Soc. Rev.* **2011**, *40*, 4893–4901.
7. Denmark, S. E. Palladium-catalyzed cross-coupling reactions of organosilanols and their salts: practical alternatives to boron-and tin-based methods. *Acc. Chem. Res.* **2008**, *41*, 1486-1499.
8. Smith, A. B., III; Wuest, W. M. Evolution of multi-component anion relay chemistry (ARC): construction of architecturally complex natural and unnatural products. *Chem. Commun.* **2008**, 5883-5895.
9. Bains, W.; Tacke, R. Silicon Chemistry as a Novel Source of Chemical Diversity in Drug Design**.** *Curr. Opin. Drug. Discovery Dev.* **2003**, *6*, 526-543.
10. Franz, A. K.; Wilson, S. O. Organosilicon Molecules with Medicinal Applications. *J. Med. Chem.* **2013**, *56*, 388-405.
11. Ojima, I. In *The Chemistry of Organic Silicon Compounds*; Patai, S; Rappoport, Z. Eds; John Wiley: New York, **1989**; Chapter 25, 1479–1526.
12. Brook, M. A. *Silicon in organic, organometallic, and polymer chemistry*. J. Wiley: **2000**.
13. Marciniec, B. Boron-Catalyzed Aromatic C–H Bond Silylation with Hydrosilanes. *Coord. Chem. Rev*. **2005**, *249*, 2374.
14. Atienza, C. C. H.; Diao, T.; Weller, K. J.; Nye, S. A.; Lewis, K. M.; Delis, J. G. P.; Boyer, J. L.; Roy, A. K.; Chirik, P. J. Bis(imino)pyridine Cobalt-Catalyzed Dehydrogenative Silylation of Alkenes: Scope, Mechanism, and Origins of Selective Allylsilane Formation. *J. Am. Chem. Soc.* **2014,** *136*, 12108-12118.

15. Fleming, I.; Barbero, A.; Walter, D. Stereochemical Control in Organic Synthesis Using Silicon-Containing Compounds. *Chem. Rev.* **1997,** *97*, 2063-2192.
16. Brook, M. A. *Silicon in organic, organometallic, and polymer chemistry*. J. Wiley: **1999**.
17. Nakao, Y.; Hiyama, T. Silicon-based cross-coupling reaction: an environmentally benign version. *Chem. Soc. Rev.* **2011,** *40*, 4893-4901.
18. Marciniec, B.; Maciejewski, H.; Pietraszuk, C.; Pawluc, P. *Hydrosilylation: A Comprehensive Review On Recent Advances*; Marciniec, B., Ed.; Springer: Berlin, **2009**, *1*, 3−51.
19. Sieburth, S. M.; Nittoli, T.; Mutahi, A. M.;Guo, L. Silanediols: A New Class of Potent Protease Inhibitors. *Angew. Chem., Int. Ed.* **1998,** *37*, 812-814.
20. Franz, A. K.; Wilson, S. O. Organosilicon Molecules with Medicinal Applications. *J. Med. Chem.* **2012,** *56*, 388-405.
21. Miller, R. D.; Michl. J. Polysilane high polymers. *Chem. Rev.* **1989,** *89*, 1359-1410.
22. Burke, S. D.; Deaton, D. N. Synthesis of (+)-dihydrocompactin and (+)-compactin via vinylsilane terminated cationic cyclization. *Tetrahedron lett.* **1991,** *32*, 4651-4654.
23. Lee, D.; Danishefsky, S. J. Cascade Resulting in the Reductive Ethynylation of Aldehydes: Dissection of Its Components. *J. Am. Chem. Soc.* **2010,** *132*, 4427-4430.
24. Young, D. G. J.; Gomez-Bengoa, E.; Hoveyda, A. H., Diastereoselective Intramolecular Cycloaddition of Vinylsilanes and Silyl Nitronates. Effective Control of Remote Acyclic Asymmetry. *The Journal of Organic Chemistry* **1999,** *64*, 692-693.
25. Mikami, K.; Loh, T. P.; Nakai, T. Carbonyl-ene reaction with vinylsilanes: silicon as a controlling element for regio-and stereochemistry. *J. Am. Chem. Soc.* **1990,** *112*, 6737-6738.
26. Han, Y.-K.; Paquette, L. A. Vinylsilane mediated stereoselective total synthesis of (.+-.)-gymnomitrol. *J. Org. Chem.* **1979,** *44*, 3731-3733.
27. Kato, K.; Mukaiyama, T. A convenient method for the direct preparation of ketones from vinylsilanes with molecular oxygen catalyzed by cobalt (II) complex. *Chem. Lett.* **1989,** *18*, 2233-2236.
28. Jones, G. R.; Landais, Y. The oxidation of the carbon-silicon bond. *Tetrahedron* **1996,** *52*, 7599-7662.

29. Kishi, N.; Imma, H.; Mikami, K.; Nakai, T. Novel SN2′-Type Reaction of β-(Silyl) allylic Ethers with Alkyllithiums: A Stereoselective Entry to (E)-Vinylic Silanes. *Synlett* **1992,** *1992*, 189-190.
30. Koichi, M.; Naoyuki, K.; Takeshi, N. Sigmatropic rearrangements of 2-(trimethylsilyl)allyl alcohol derivatives: Facile and general entries to functionalized vinylsilanes. *Chem. Lett.* **1982,** *11*, 1643-1646.
31. Weber, W. P.; Felix, R. A.; Willard, A. K.; Koenig, K. E. Reactions of vinyl silanes with palladium salts - vinyl heck reactions. *Tetrahedron Lett.* **1971,** *12*, 4701-4704.
32. Denmark, S.; Baird, J. D. Palladium-Catalyzed Cross-Coupling Reactions of Silanolates: A Paradigm Shift in Silicon-Based Cross-Coupling Reactions. *Chem. Eur.* **2006,** *12*, 4954-4963.
33. Murai, S.; Kakiuchi, F.; Sekine, S.; Tanaka, Y.; Kamatani, A.; Sonoda, M.; Chatani, N. Efficient catalytic addition of aromatic carbon-hydrogen bonds to olefins. *Nature* **1993,** *366*, 529.
34. Takeuchi, R.; Ishii, N.; Sugiura, M.; Sato, N. The highly regioselective carbonylation of vinylsilanes. *J. Org. Chem.* **1992,** *57*, 4189-4194.
35. Pietraszuk, C.; Fischer, H.; Kujawa, M.; Marciniec, B. Cross-metathesis of vinylsilanes with olefins in the presence of Grubbs' catalyst. *Tetrahedron Lett.* **2001,** *42*, 1175-1178.
36. Wang, Y.; Jimenez, M.; Hansen, A. S.; Raiber, E.-A.; Schreiber, S. L.; Young, D. W. Control of Olefin Geometry in Macrocyclic Ring-Closing Metathesis Using a Removable Silyl Group. *J. Am. Chem. Soc.* **2011,** *133*, 9196-9199.
37. Gallenkamp, D.; Fürstner, A. Stereoselective Synthesis of E,Z-Configured 1,3-Dienes by Ring-Closing Metathesis. Application to the Total Synthesis of Lactimidomycin. *J. Am. Chem. Soc.* **2011,** *133*, 9232-9235.
38. Hiyama, T.; Kusumoto, T. In *Comprehensive Organic Synthesis*; Trost, B. M.; Fleming, I. Eds.; Pergamon: Oxford, **1991**; Vol 8, pp. 763-792.
39. Yamamoto, K.; Hayashi, T. In *Transition Metals for Organic Synthesis*, 2nd ed.; Beller, M., Bolm, C., Eds.; Wiley-VCH: Weinheim, **2004**; pp 167-191.
40. Showell, G. A.; Mills, J. S. Exploitation of silicon medicinal chemistry in drug discovery. *Drug Discov. Today* **2003,** *8*, 551-556;

41. Gately, S.; West, R. Novel therapeutics with enhanced biological activity generated by the strategic introduction of silicon isosteres into known drug scaffolds. *Drug Dev. Res.* **2007,** *68*, 156-163.
42. Franz, A. K.; Wilson, S. O. Organosilicon Molecules with Medicinal Applications. *J. Med. Chem.* **2012,** *56*, 388-405.
43. Trost, B. M.; Ball, Z. T. Alkyne Hydrosilylation Catalyzed by a Cationic Ruthenium Complex: Efficient and General Trans Addition. *J. Am. Chem. Soc*. **2005**, *127*, 17644-17655
44. Takeuchi, R.; Nitta, S.; Watanabe, D. Complex-Catalyzed Hydrosilylation of 1-Alkynes and Tandem Hydrosilylation/Isomerization Reaction of Propargylic Alcohols to .beta.-Silyl Ketones. *J. Org. Chem*. **1995**, *60*, 3047
45. Kawasaki, Y.; Ishikawa, Y.; Igawa, K.; Tamooka, K. Directing Group-Controlled Hydrosilylation: Regioselective Functionalization of Alkyne. *J. Am. Chem. Soc*. **2011**, *133*, 20712-20715
46. Stephan, M. R,; Karin, R.; Dragos-A, R.; Furstner, A. Interligand Interactions Dictate the Regioselectivity of trans-Hydrometalations and Related Reactions Catalyzed by [Cp*RuCl]. Hydrogen Bonding to a Chloride Ligand as a Steering Principle in Catalysis. *J. Am. Chem. Soc*. **2015**, *137*, 5506-5519
47. Trost, B. M.; Ball, Z. T. Intramolecular endo-dig hydrosilylation catalyzed by ruthenium: evidence for a new mechanistic pathway. *J. Am. Chem. Soc*. **2003**, *125*, 30-31
48. Denmark, S.; Pan, W.; Intramolecular Anti-Hydrosilylation and Silicon-Assisted Cross-Coupling: Highly Regio- and Stereoselective Synthesis of Trisubstituted Homoallylic Alcohols. *Org. Lett*. **2002**, *4*, 4163-4166.
49. Ojima, I.; Vidal, E.; Tzamarioudaki, M.; Matsuda, I. Extremely regioselective intramolecular silylformylation of alkynes. *J. Am. Chem. Soc*. **1995**, *117*, 6797-6798.
50. Denmark, S.; Pan, W. Intramolecular Syn and Anti Hydrosilylation and Silicon-Assisted Cross-Coupling: Highly Regio- and Stereoselective Synthesis of Trisubstituted Allylic Alcohols. *Org. Lett*. **2003**, *5*, 1119-1122.

51. Dakarapu, U. S.; Bokka, A.; Asgari, P.; Trog, G., Hua, Y.; Nguyen, H. H.; Rahman, N.; Jeon, J. Lewis Base Activation of Silyl Acetals: Iridium –Catalyzed Reductive Horner-Wadsworth-Emmons Olefination. *Org. Lett*. **2015,** *17*, 5792-5795.
52. Hua, Y., Asgari, P., Dakarapu, U. S., Jeon, J. Reductive arene ortho-silanolization of aromatic esters with hydridosilyl acetals. *Chem. Commun.* **2015**, *51*(18), 3778-3781.
53. Asgari, P., Dakarapu, U. S., Nguyen, H. H & Jeon, J. Aryne cycloaddition reactions of benzodioxasilines as aryne precursors generated by catalytic reductive ortho-C-H silylation of phenols with traceless acetal directing groups. *Tetrahedron.* **2017**, *73*(29), 4052-4061.
54. Ting, R.; Adam, M. J.; Ruth, T. J.; Perrin, D. M. Arylfluoroborates and Alkylfluorosilicates as Potential PET Imaging Agents: High-Yielding Aqueous Biomolecular 18F-Labeling. *J. Am. Chem. Soc.* **2005,** *127*, 13094-13095.
55. Eisenberg, D. C.; Norton, J. R. Hydrogen-Atom Transfer Reactions of Transition-Metal Hydrides. *Isr. J. Chem.* **1991,** *31*, 55-66.
56. Kumar, M.; Sinha, A.; Francisco, J. S. Role of Double Hydrogen Atom Transfer Reactions in Atmospheric Chemistry. *Acc. Chem. Res.* **2016,** *49*, 877-883.
57. Mukaiyama, T.;Yamada, T. Recent Advances in Aerobic Oxygenation. *Bull. Chem. Soc. Jpn.* **1995,** *68*, 17-35.
58. Crossley, S. W.; Obradors, C.; Martinez, R. M.;Shenvi, R. A. Mn-, Fe-, and Co-Catalyzed Radical Hydrofunctionalizations of Olefins. *Chem. Rev.* **2016,** *116*, 8912-9000.
59. Mayer, J. M. Bioinspired Hydrogen Bond Motifs in Ligand Design: The Role of Noncovalent Interactions in Metal Ion Mediated Activation of Dioxygen. *Acc. Chem. Res.* **1998,** *31*, 441-450.
60. Guallar, V.; Baik, M.-H.; Lippard, S. J.;Friesner, R. A. Peripheral heme substituents control the hydrogen-atom abstraction chemistry in cytochromes P450. *Proc. Natl. Acad. Sci. U. S. A.* **2003,** *100*, 6998-7002.
61. S. W. Crossley, C. Obradors, R. M. Martinez, R. A. Shenvi, Mn-, Fe-, and Co-catalyzed radical hydrofunctionalizations of olefins. *Chem. Rev*. **2016**, *116*, 8912–9000.
62. T. Gunasekara, G. P. Abramo, A. Hansen, H. Neugebauer, M. Bursch, S. Grimme, J. R. Norton, TEMPO-Mediated Catalysis of the Sterically Hindered Hydrogen Atom Transfer

Reaction between $(C_5Ph_5)Cr(CO)_3H$ and a Trityl Radical. *J. Am. Chem. Soc*. **2019**, *141*, 1882−1886

63. Mayer, J. M. Hydrogen atom abstraction by metal-oxo complexes: understanding the analogy with organic radical reactions. *Acc. Chem. Res*. **1998**, *31*, 441–450

64. Simoes, J. M.;Beauchamp, J. Transition metal-hydrogen and metal-carbon bond strengths: the keys to catalysis. *Chem. Rev.* **1990,** *90*, 629-688.

65. Uddin, J.; Morales, C. M.; Maynard, J. H.;Landis, C. R. Computational Studies of Metal−Ligand Bond Enthalpies across the Transition Metal Series. *Organometallics* **2006,** *25*, 5566-5581.

66. Brunel, J. M. Polysilanes: The grail for a highly-neglected hydrogen storage source. *Int. J. Hydrogen Energy* **2017,** *42*, 23004-23009.

67. Peng, W.; Rupich, S. M.; Shafiq, N.; Gartstein, Y. N.; Malko, A. V.; Chabal, Y. J. Silicon Surface Modification and Characterization for Emergent Photovoltaic Applications Based on Energy Transfer. *Chem. Rev.* **2015,** *115*, 12764-12796.

68. Kummaria, A.; Pappurua, S.; Guptab, P. K.; Chakrabortya, De.; Verma, R. S. Metal-free Lewis pair catalyst synergy for fully alternating copolymerization of norbornene anhydride and epoxides: Biocompatible tests for derived polymers. *Mater. Today Commun.* **2019**, *19,* 306–314

69. Michael, L.; Graw, Mc.; Eugene Y.; Chen, X. Borane/silane frustrated Lewis pairs for polymerization of *b*-substituted Michael acceptors. *Tetrahedron* **2019**, *75*, 1475–1480

70. Li, Z-H.; Xue, L-P.; Qin, Q-P.; Zhang, J.; Wang, J-M.; Zhang, X-Y.; Zhao, A; zinc(II) coordination polymer material with Lewis basic pyridyl sites:Structure, photoluminescence, and heterogeneous catalysis. *J. Solid State Chem.* **2019***, 274*, 81–85

71. Liu, W.-B.; Schuman, D.; Yang, Y-F.; Toutov, A.; Liang, Y.; Klare, H.; Nesnas, N.; Oestreich, M.; Blackmond, D.; Virgil, S.; Banerjeell, S.; Zarell, R.; Grubbs, R.; Houk, K.N.; Stoltz, B. M. Potassium tert-Butoxide-Catalyzed Dehydrogenative C–H Silylation of Heteroaromatics: A Combined Experimental and Computational Mechanistic Study. *J. Am. Chem. Soc*. **2017**, *139*, 6867–6879

72. Toutov, A. A.; Liu. W. -B.; Betz. K.; Fedorov. A.; Stoltz, B.; Grubbs, R, -H. Silylation of CH bonds in aromatic heterocycles by an Earth-abundant metal catalyst. *Nature* **2015**, *518*, 80–84

73. Toutov, A. A.; Betz. K.; Schuman, D.; Liu. W. -B.; Fedorov. A.; Stoltz, B.; Grubbs, R, -H. Alkali metal-hydroxide-catalyzed C (sp)–H bond silylation. *J. Am. Chem. Soc*. **2017**, *139*, 1668–1674

74. Smith, A. J. Young, A.; Rohrbach, S.; O'Connor, E.; Alison, M.; Wang, H-S.; Poole, D.; Tuttle, T.; Murphy, J, -A. Electron-transfer and hydride-transfer pathways in the Stoltz–Grubbs reducing system (KOtBu/Et_3SiH). *Angew. Chem. Int. Ed*. **2017**, *56*, 13747–13751

75. Asgari, P.; Yuanda, H.; Apparao, B.; Chanachon, T.; Prasitwatcharakorn, W.; Karedath, A.; Chen, X.; Sardar, S.; Yum, K.; Leem, G.; Pierce, B-S.; Nam, K.; Gao, J.; Jeon, J. Catalytic hydrogen atom transfer from hydrosilanes to vinylarenes for hydrosilylation and polymerization. *Nat. Catal.* **2019,** *2*, 164–173

76. Schilli, C.; Lanzendörfer, M. G.; Müller, A. H. E. Benzyl and Cumyl Dithiocarbamates as Chain Transfer Agents in the RAFT Polymerization of N-Isopropylacrylamide. In Situ FT-NIR and MALDI−TOF MS Investigation. *Macromolecules*, **2002**, *35*, 6819–6827

77. Santos, A. F.; Silva, F. M.; Lenzi, M. K.; Pinto, J. C. Monitoring and Control of Polymerization Reactors Using NIR Spectroscopy. *Polym Plast. Technol. Eng*. **2005**, *44*, 1–61

78. Zetterlund, P. B.; Yamazoe, H.; Yamada, B. Free Radical Bulk Polymerization of Styrene: Simulation of Molecular Weight Distributions to High Conversion Using Experimentally Obtained Rate Coefficients. *Macromol. Theory Simul*. **2003**, *12*, 379–385

79. Cherfi, A.; Fe´votte, G. On-Line Conversion Monitoring of the Solution Polymerization of Methyl Methacrylate Using Near-Infrared Spectroscopy. *Macromol. Chem. Phys.* **2002***, 203,* 1188–1193

80. Couzijn, E. P.; Ehlers, A. W.; Schakel, M.; Lammertsma, K. Electronic structure and stability of pentaorganosilicates. *J. Am. Chem. Soc.* **2006**, *128*, 13634–13639

81. Kanabus-Kaminska, J.; Hawari, J.; Griller, D.; Chatgilialoglu, C. Reduction of silicon–hydrogen bond strengths. *J. Am. Chem. Soc*. **1987**, *109*, 5267–5268

82. GupperSergei, A.; Kazarian, G. Study of Solvent Diffusion and Solvent-Induced Crystallization in Syndiotactic Polystyrene Using FT-IR Spectroscopy and Imaging. *Macromolecules* **2005**, *38*, 2327–2332

83. Zetterlund, P. B.; Yamazoe, H.; Yamada, B.; Hill, D. J. T.; Pomery, P. J. High-Conversion Free-Radical Bulk Polymerization of Styrene: Termination Kinetics Studied by Electron Spin Resonance, Fourier Transform Near-Infrared Spectroscopy, and Gel Permeation Chromatography. *Macromolecules* **2001**, *34*, 7686-7691

84. Le, T. T.; Hill, D. J. Simultaneous FT-NIR and ESR analyses to yield propagation rate coefficients for polymerization of methyl methacrylate based monomers. *Polym Int.* **2003**, *52*, 1694–1700

85. Elvira, K. S.; Solvas, X. C.; Wootton, R.; Demello, A. J. The past, present and potential for microfluidic reactor technology in chemical synthesis. *Nat. Chem.*, **2013**, *5*, 905–915.

86. Biocomputer, O. Microreactors for chemical Sheila H Dewitt. **2013,** 350–356.

87. Mills, P. L.; Quiram, D. J.; Ryley, J. F. Microreactor technology and process miniaturization for catalytic reactions-A perspective on recent developments and emerging technologies. *Chem. Eng. Sci.* **2007,** *62*, 6992–7010.

88. Löb, P. ; Löwe, H.; Hessel, V. Fluorinations, chlorinations and brominations of organic compounds in micro reactors. *J. Fluor. Chem.*, **2004**, *125*, 1677–1694.

89. Miller, P. W.; Long, N. J.; De Mello, A. J.; Vilar, R.; Passchier, J.; Gee, A. Rapid formation of amides via carbonylative coupling reactions using a microfluidic device. *Chem. Commun.* **2006**, *5*, 546–548.

90. Greenway, G. M.; Haswell, S. J.; Morgan, D. O.; Skelton, V.; Styring, P. Use of a novel microreactor for high throughput continuous flow organic synthesis. *Sensors Actuators, B Chem.* **2000**, *63*, 153–158.

91. Skelton, V.; Greenway, G-M.; Haswell, S.; Styring, P.; Morgan, D.; Warrington, B.; Wong, S. Y. The preparation of a series of nitrostilbene ester compounds using micro reactor technology. *Analyst* **2001**, *126*, 7–10.

92. Watts, P.; Haswell, S. J.; Watts, P. The application of micro reactors for organic synthesis no. February **2002**.
93. Mariod, A. A.; Adam, H. F. Review: Gelatin, source, extraction and industrial applications. *Acta Sci. Pol. Technol. Aliment.* **2013**, *12*, 135–147.
94. Choi, K.; Ng, A. H. C.; Fobel, R.; Wheeler, A. R. Digital Microfluidics. *Annu. Rev. Anal. Chem.* **2012**, *5*, 413–440.
95. Cho, S. K.; Moon, H.; Kim, C. EWOD_droplet_management.pdf. **2003**, *12*, 70–80.
96. Berthier, J.; Mourier, V.; Sarrut, N.; Jary, D.; Caillat, P.; Peponnet. C. Some examples of micro-devices for biotechnology developed at the Department of Technologies for Life Science and Healthcare of the LETI. *x*, 1–17.
97. Chatterjee, D.; Hetayothin, B.; Wheeler, A. R.; King, D. J.; Garrell, R. L. Droplet-based microfluidics with nonaqueous solvents and solutions. *Lab Chip*. **2006**, *6*, 199–206.
98. Torabinia, M.; Farzbod, A.; Moon, H. Electromechanical model to predict the movability of liquids in an electrowetting-on-dielectric microfluidic device. *J. Appl. Phys.* **2018**, *123*, 154902.
99. Brassard, D.; Malic, L.; Normandin, F.; Tabrizian, M.; Veres, T. Water-oil core-shell droplets for electrowetting-based digital microfluidic devices. *Lab Chip* **2008**, *8*, 1342–1349.
100. Li, J.; Wang, Y.; Chen, H.; Wan, J. Electrowetting-on-dielectrics for manipulation of oil drops and gas bubbles in aqueous-shell compound drops. *Lab Chip* **2014**, *14*, 4334–4337.
101. Fan, S. K.; Hsieh, T. H.; Lin, D. Y. General digital microfluidic platform manipulating dielectric and conductive droplets by dielectrophoresis and electrowetting. *Lab Chip* **2009** , *9*, 1236–1242.
102. Vessally, E.; Saeidian, H.; Hosseinian, A.; Edjlali, L.; Bekhradnia, A. A review on synthetic applications of oxime esters. *Curr. Org. Chem.* **2017**, *21*, 3.
103. Dima A.; Boura, K.; Stergiou, P-Y.; Foukis, A.; Gkini, A.; Kandylis, P.; Pissaridi, K.; Kanellaki, M.; Papamichael, E.; Koutinas, A. Scale-up for esters production from straw whiskers for biofuel applications. *Bioresour. Technol.* **2017**, *242*, 109–112.
104. Phonsatta, N. Comparison of Antioxidant Evaluation Assays for Investigating Antioxidative Activity of Gallic Acid and Its Alkyl Esters in Different Food Matrices. *J. Agric. Food Chem.* **2017**, *65*, 7509–7518.

105. Pérez, B.; Anankanbil, S.; Guo, Z. Synthesis of Sugar Fatty Acid Esters and Their Industrial Utilizations. *Fat. Acids* **2017**, 329–354.
106. Sun, J.; Pan, L.; Tsang, D.; Li, Z.; Zhu, L.; Li, X. Phthalate esters and organochlorine pesticides in agricultural soils and vegetables from fast-growing regions: a case study from eastern China. *Environ. Sci. Pollut. Res.* **2018**, *25*, 34–42.
107. Muir, T. W. A Chemical Probe for Protein Crotonylation. **2018**, 7–10.
108. Zhao, H.; Pendri, A.; Greenwald, R. B. General procedure for acylation of 3° alcohols: Scandium triflate/DMAP reagent. *J. Org. Chem.* **1998**, *63*, 7559–7562.
109. Trabelsi, I.; Essid, K.; Frikha, M. H. Esterification of Mixed Carboxylic-fatty Anhydrides Using Amberlyst-15 as Heterogeneous Catalyst. *J. Oleo Sci.* **2017**, *66*, 667–676.
110. Phukan, P. Iodine as an extremely powerful catalyst for the acetylation of alcohols under solvent-free conditions. *Tetrahedron Lett.* **2004**, *45*, 4785–4787.
111. Torabinia, M.; Venkatesan, A.; Moon, H. Phase shift effect of double dielectric layers in electrowetting on dielectric microfluidic device. *Proceedings of the IEEE International Conference on Micro Electro Mechanical Systems (MEMS)*, **2018**, *2018*–Janua.
112. Ren, H.; Fair, R. B.; Pollack, M. G. Automated on-chip droplet dispensing with volume control by electro-wetting actuation and capacitance metering. *Sensors Actuators, B Chem.* **2004**, *98*, 319–327.
113. Guan, Y.; Tong, A. Y.; Nikapitiya, N.; Moon, H. Numerical modeling of microscale droplet dispensing in parallel-plate electrowetting-on-dielectric (EWOD) devices with various reservoir designs. *Microfluid. Nanofluidics*, **2016**, *20*, 1–21.
114. Krska, S. W.; DiRocco, D. A.; Dreher, S. D.; Shevlin, M. The Evolution of Chemical High-Throughput Experimentation to Address Challenging Problems in Pharmaceutical Synthesis. *Acc. Chem. Res.* **2017**, *50*, 2976–2985.
115. Santanilla, A. B. *et al.*, "Complex Molecules," *Science* **2015**, *347*, 443–448.
116. Collins, K. D.; Glorius, F. Intermolecular Reaction Screening as a Tool for Reaction Evaluation. *Acc. Chem. Res.* **2015**, *48*, 619–627.
117. Kaminski, T. S.; Garstecki, P. Controlled droplet microfluidic systems for multistep chemical and biological assays. *Chem. Soc. Rev.* **2017**, *46*, 6210–6226.
118. Klippenstein, S. J.; Pande, V. S.; Truhlar, D. G. Chemical kinetics and mechanisms of complex systems: A perspective on recent theoretical advances. *J. Am. Chem. Soc.* **2014**,

136, 528–546.

119. Khan, S.; He, X.; Khan, J. A.; Khan, H. M.; Boccelli, D. L.; Dionysiou, D. D. Kinetics and mechanism of sulfate radical- and hydroxyl radical-induced degradation of highly chlorinated pesticide lindane in UV/peroxymonosulfate system. *Chem. Eng. J.* **2017**, *318*, 135–142.
120. Procopiou, P. A.; Baugh, S. P.; Flack, S. S.; Inglis, G. G. An Extremely Powerful Acylation Reaction of Alcohols with Acid Anhydrides Catalyzed by Trimethylsilyl. **1998**, *12*, 2342–2347.
121. Nguyen, H. T.; Tran, P. H. RSC Advances acylation of secondary alcohols and phenols. **2016**, 98365–98368.
122. Snyder, L. R. Classification off the Solvent Properties of Common Liquids. *J. Chromatogr. Sci.* **1978**, *16*, 223–234.
123. Sakakura, A.; Kawajiri, K.; Ohkubo, T.; Kosugi, Y.; Ishihara, K. Widely Useful DMAP-Catalyzed Esterification under Auxiliary Base- and Solvent-Free Conditions. **2007**, *8*, 14775–14779.
124. Xu, S.; Held, I.; Kempf, B.; Mayr, H.; Steglich, W.; Zipse, H. The DMAP-catalyzed acetylation of alcohols - A mechanistic study (DMAP = 4-(dimethylamino)pyridine). *Chem. Eur.* **2005**, *11*, 4751–4757.
125. Valencia, P. M.; Pridgen, E. M.; Rhee, M.; Langer, R.; Farokhzad, O. C.; Al, V. Micro fl uidic Platform for Combinatorial Synthesis and Optimization of Targeted Nanoparticles for Cancer Therapy. **2013**, *12*, 10671–10680.
126. Zhang, X.; Xiang, Y. Combinatorial approaches for high-throughput characterization of mechanical properties. *J Mater.* **2017**, *3*, 209–220.
127. Nittis, V.; Fortt, R.; Legge, C. H.; De-Mello, A. J. A high-pressure interconnect for chemical microsystem applications. *Lab Chip*. **2001**, 1, 148–152.
128. Mitchell, M. C.; Spikmans, V.; Manz, A.; De-Mello, A. J. Microchip-based synthesis and total analysis systems (μSYNTAS): Chemical microprocessing for generation and analysis of compound libraries. *J. Chem. Soc. Perkin 1*, **2001**, 5, 514–518.
129. Kikutani, Y.; Horiuchi, T.; Uchiyama, K.; Hisamoto, H.; Tokeshi, M.; Kitamori, T. Glass microchip with three-dimensional microchannel network for 2 × 2 parallel synthesis. *Lab Chip* **2001**, *2*,. 188–192.

130. Theberge, A. B.; Mayot, E.; El Harrak, A.; Kleinschmidt, F.; Huck, W. T.; Griffiths, A. D. Microfluidic platform for combinatorial synthesis in picolitre droplets. *Lab Chip.* **2012**, *12*, 1320–1326.
131. Spivey, A. C.; Arseniyadis, S. Nucleophilic catalysis by 4-(dialkylamino)pyridines revisited - The search for optimal reactivity and selectivity. *Angew. Chem. Int. Ed.* **2004**, *43*, 5436–5441.
132. Anelli, P. L.; Biffi, C.; Montanari, F.; Quici, S. Fast and Selective Oxidation of Primary Alcohols to Aldehydes or to Carboxylic Acids and of Secondary Alcohols to Ketones Mediated by Oxoammonium Salts under Two-Phase Conditions. *J. Org. Chem.* **1987**, *52*, 2559–2562.
133. Sahoo, H. R.; Kralj, J. G.; Jensen, K. F., Multistep continuous-flow microchemical synthesis involving multiple reactions and separations. *Angew. Chem. Int. Ed.* **2007,** *46* (30), 5704-5708.
134. Aota, A.; Mawatari, K.; Takahashi, S.; Matsumoto, T.; Kanda, K.; Anraku, R.; Hibara, A.; Tokeshi, M.; Kitamori, T. Phase separation of gas–liquid and liquid–liquid microflows in microchips. *Microchim. Acta* **2009,** *164*, 249.
135. Peroni, D.; Van Egmond, W.; Kok, W. T.; Janssen, H.-G., Advancing liquid/liquid extraction through a novel microfluidic device: Theory, instrumentation and applications in gas chromatography. *J. Chromatogra. A* **2012,** *1226*, 77-86.
136. Cervera-Padrell, A. E.; Morthensen, S. T.; Lewandowski, D. J.; Skovby, T.; Kiil, S.; Gernaey, K. V. Continuous hydrolysis and liquid–liquid phase separation of an active pharmaceutical ingredient intermediate using a miniscale hydrophobic membrane separator. *Org. Process Res. Dev* **2012,** *16* (5), 888-900.
137. Mousa, N. A.; Jebrail, M. J.; Yang, H.; Abdelgawad, M.; Metalnikov, P.; Chen, J.; Wheeler, A. R.; Casper, R. F. Droplet-scale estrogen assays in breast tissue, blood, and serum. *Sci. Transl. Med.* **2009,** *1* (1), 1ra2-1ra2.
138. Wijethunga, P. A.; Nanayakkara, Y. S.; Kunchala, P.; Armstrong, D. W.; Moon, H., On-chip drop-to-drop liquid microextraction coupled with real-time concentration monitoring technique. *Anal. Chem.* **2011,** *83*, 1658-1664.
139. Paul, S.; Moon, H. In *Separation of binary solution by liquid-liquid microextraction on EWOD digital microfluidics*, 2017 IEEE 12th International Conference on Nano/Micro

Engineered and Molecular Systems (NEMS), IEEE: **2017**; 342-345.

140. Yang, H.; Mudrik, J. M.; Jebrail, M. J.; Wheeler, A. R. A digital microfluidic method for in situ formation of porous polymer monoliths with application to solid-phase extraction. *Anal. Chem.* **2011,** *83*, 3824-3830.
141. Moon, H.; Wheeler, A.; Garrell, R.; Loo, J.; Kim, C.-J. In *On-chip sample preparation by electrowetting-on-dielectric digital microfluidics for matrix assisted laser desorption/ionization mass spectrometry*, 18th IEEE International Conference on Micro Electro Mechanical Systems, **2005**. MEMS 2005, IEEE: 2005; 859-862.
142. Wu, B.; von der Ecken, S.; Swyer, I.; Li, C.; Jenne, A.; Vincent, F.; Schmidig, D.; Kuehn, T.; Busse, F.; Stronks, H. Rapid Chemical Reaction Monitoring by Digital Microfluidics-NMR: Proof of Principle Towards an Automated Synthetic Discovery Platform. *Angew. Chem. Int. Ed.* **2019**.
143. Dubois, P.; Marchand, G.; Fouillet, Y.; Berthier, J.; Douki, T.; Hassine, F.; Gmouh, S.; Vaultier, M. Ionic liquid droplet as e-microreactor. *Anal. Chem.* **2006,** *78*, 4909-4917.
144. Jebrail, M. J.; Ng, A. H.; Rai, V.; Hili, R.; Yudin, A. K.; Wheeler, A. R. Synchronized synthesis of peptide-based macrocycles by digital microfluidics. *Angew. Chem. Int. Ed.* **2010,** *49*, 8625-8629.
145. Torabinia, M.; Asgari, P.; Dakarapu, U. S.; Jeon, J.; Moon, H. On-chip organic synthesis enabled using an engine-and-cargo system in an electrowetting-on-dielectric digital microfluidic device. *Lab Chip.* **2019,** *19*, 3054-3064.
146. Keng, P. Y.; Chen, S.; Ding, H.; Sadeghi, S.; Shah, G. J.; Dooraghi, A.; Phelps, M. E.; Satyamurthy, N.; Chatziioannou, A. F.; van Dam, R. M. Micro-chemical synthesis of molecular probes on an electronic microfluidic device. *Proc. Natl. Acad. Sci.* **2012,** *109*, 690-695.
147. Lam, K.; Cao, E.; Sorensen, E.; Gavriilidis, A., Development of multistage distillation in a microfluidic chip. *Lab Chip.* **2011,** *11*, 1311-1317.
148. Ziogas, A.; Kolb, G.; Kost, H. J.; Hessel, V.; Hessel, V. Development of High Performance Micro Rectification Equipment for Analytical and Preparative Applications. *Chem. Ing. Tech.* **2011,** *83*, 465-478.
149. Cho, S. K.; Moon, H.; Kim, C.-J. Creating, transporting, cutting, and merging liquid droplets by electrowetting-based actuation for digital microfluidic circuits. *J.*

Microelectromech. s **2003,** *12*, 70-80.

150. Huang, H.-Y.; Shen, H.-H.; Tien, C.-H.; Li, C.-J.; Fan, S.-K.; Liu, C.-H.; Hsu, W.-S.; Yao, D.-J. Digital microfluidic dynamic culture of mammalian embryos on an electrowetting on dielectric (EWOD) chip. *PloS one* **2015,** *10* (5).
151. Zeng, Y.; Wang, T. Quantitative microfluidic biomolecular analysis for systems biology and medicine. *Anal. Bioanal. Chem.* **2013,** *405*, 5743-5758.
152. Liu, Y.-J.; Yao, D.-J.; Lin, H.-C.; Chang, W.-Y.; Chang, H.-Y. DNA ligation of ultramicro volume using an EWOD microfluidic system with coplanar electrodes. *J. Micromech. Microeng.* **2008,** *18*, 045017.
153. Torabinia, M.; Farzbod, A.; Moon, H. Electromechanical model to predict the movability of liquids in an electrowetting-on-dielectric microfluidic device. *J. Appl. Phys.* **2018,** *123*, 154902.
154. Chatterjee, D.; Hetayothin, B.; Wheeler, A. R.; King, D. J.; Garrell, R. L. Droplet-based microfluidics with nonaqueous solvents and solutions. *Lab Chip.* **2006,** *6*, 199-206.
155. Chen, C.-H.; Tsai, S.-L.; Chen, M.-K.; Jang, L.-S. Effects of gap height, applied frequency, and fluid conductivity on minimum actuation voltage of electrowetting-on-dielectric and liquid dielectrophoresis. *Sensors and Actuators B: Chemical* **2011,** *159* (1), 321-327.
156. Fowler, J.; Moon, H.; Kim, C.-J. In *Enhancement of mixing by droplet-based microfluidics*, Technical Digest. MEMS 2002 IEEE International Conference. Fifteenth IEEE International Conference on Micro Electro Mechanical Systems (Cat. No. 02CH37266), IEEE: **2002**, 97-100.
157. Nahar, M. M.; Moon, H., Phase separation of multiphase droplets in a digital microfluidic device. *Micro. Nano. Lett.* **2019,** *7*, 19.
158. Madikizela, L. M.; Zunngu, S. S.; Mlunguza, N. Y.; Tavengwa, N. T.; Mdluli, P. S.; Chimuka, L., Application of molecularly imprinted polymer designed for the selective extraction of ketoprofen from wastewater. *Water SA* **2018,** *44*, 406-418.
159. Erwa, I. Y.; Ibrahim, A. A., Removal of chromium (VI) ions from aqueous solution using wood sawdust as adsorbent. *J. Nat. Med.* **2016,** *17*, 112.
160. Aota, A.; Nonaka, M.; Hibara, A.; Kitamori, T. Countercurrent laminar microflow for highly efficient solvent extraction. *Angew. Chem. Int. Ed.* **2007,** *46*, 878-880.

161. Moore, F., Separation of zirconium from other elements by liquid-liquid extraction. *Anal. Chem.* **1956,** *28* (6), 997-1001.
162. Marsh, A.; Stuart, D.; Mitchell, D.; Howes, T. Characterizing mixing in a rotating drum bioreactor for solid-state fermentation. *Biotech. Lett.* **2000,** *22* (6), 473-477.
163. Martin, T.; Davies, G. The extraction of copper from dilute aqueous solutions using a liquid membrane process. *Hydrometallurgy* **1977,** *2* (4), 315-334.

Biographical Information

Udaya Sree Dakarapu was born and raised in India. She obtained her Bachelor of Science in chemistry from Nagarjuna University, India in 2005. She obtained her Master of Science in organic chemistry from Andhra University, India in 2007. She obtained a Masters in organic chemistry from University of Texas at Arlington in 2015. In 2015, Udaya Sree Dakarapu began her doctoral studies under the supervision of Dr. Junha Jeon at the Univeristy of Texas at Arlington (UTA). Udaya Sree Dakarapu worked on development of new strategies and methodologies to create building blocks for drug synthesis. Udaya Sree Dakarapu has worked on various projects with emphasis on new strategies for transition metal catalyzed hydrosilylation of propargyl alcohols. She was involved in the development of on-chip organic synthesis in an electrowetting-on-dielectric digital microfluidic device, LBCI-HAT olefin polymerization, aryne cycloaddition reactions and reductive arene ortho-silanolization. Udaya Sree Dakarapu plans to continue her career in academia after receiving her degree from UTA.